Contents of issue 3 vol. XLVII

Polish Academy of Sciences

Institute of Fundamental Technological Research

Archives of Mechanics

Archiwum Mechaniki Stosowanej

volume 47 issue 3

Polish Scientific Publishers PWN

Warszawa 1995

ARCHIVES OF MECHANICS IS DEVOTED TO
Theory of elasticity and plasticity • Theory of nonclassical continua • Physics of continuous media • Mechanics of discrete media • Nonlinear mechanics • Rheology • Fluid gas-mechanics • Rarefied gas • Thermodynamics

---

Printed in Poland, Editorial Office: Świętokrzyska 21,
00-049 Warszawa (Poland)

Arkuszy wydawniczych 17,25. Arkuszy drukarskich 14.25
Papier offset. kl. III 70 g. B1. Oddano do składania w maju 1995 r.
Druk ukończono w sierpniu 1995 r.
Druk i oprawa: Drukarnia Braci Grodzickich, Żabieniec ul. Przelotowa 7

Arch. Mech., 47, 3, pp. 419–420, Warszawa 1995

Preface

Polish Solid Mechanics Conferences have a long tradition going back to the first conference in 1953 at Karpacz. At the beginning, those conferences were of the summer school type, lasted 2 weeks and concentrated on classical problems of elasticity and structural mechanics. Until 1969 all conferences were organised by the late Professor Wacław Olszak. Afterwards, they turned into Polish Solid Mechanics Conferences held every year, and later every other year. Polish Solid Mechanics Conferences have always been organised by the Institute of Fundamental Technological Research of the Polish Academy of Sciences in co-operation with the Committee of Mechanics of the Academy of Sciences.

30th Polish Solid Mechanics Conference held in Zakopane, September 5–9, 1994, was organised by the Centre of Mechanics of the Institute of Fundamental Technological Research. Among 255 participants there were 147 scientists from Polish universities and research institutions and 78 participants from other countries. The conference scientific program included 11 invited general lectures, 4 sectional lectures, 113 oral presentations and 72 contributions presented during a poster session.

The main subject of the Conference concentrated on mechanics of materials and on the structural mechanics. Specific topics of the sessions were as follows:

- foundations of mechanics,
- mechanics of phase transformations,
- strain localisation and instability,
- mechanics of porous media and composites,
- fracture mechanics, damage and fatigue,
- inelastic materials and structures,
- dynamics of solids and structures,
- structural mechanics and optimisation,
- numerical methods.

The Conference provided the forum for presentation of new scientific results and ideas in all major areas of contemporary mechanics of solids and structures. The participants have enriched the Conference with excellent scientific contributions and with stimulating discussions during various sessions. High level of the presented papers and friendly atmosphere created by the participants certainly contributed to the success of the conference.

Though no conference proceedings volume was planned, all participants were encouraged to submit their contributions as full-length papers for publication in the Archives of Mechanics or Engineering Transactions. This proposal has evoked

a great response and resulted in submission of more than 60 papers. A great majority of them, after a regular reviewing procedure, have been accepted for publication and they are now printed in this and the forthcoming issues of the journal.

March 1995

W. K. Nowacki
Conference Chairman

Arch. Mech., 47, 3, pp. 421–435, Warszawa 1995

Functional approach in nonlinear dynamics (*)

C. STOLZ (PALAISEAU)

DETERMINATION of the evolution of a system is studied through the definition of functionals presented in nonlinear dynamics. After a short account of the notions necessary for the description of the motion and of the mechanical interactions, the paper is devoted to the Lagrangean, the Hamiltonian and the canonical equations of shock waves.

1. Thermodynamical frame of the constitutive equations

IN ORDER to explain and to predict the motion and the equilibrium of bodies or structures subjected to various physical interactions, a kinematical description of the motion is performed first. In the case of a continuum, this description must ensure the continuity of the body during its motion.

Usually one looks for the motion of a material point M from a reference configuration by describing its displacement $u(M,t)$.

After a kinematical description of the body, one has to deal with mechanical interactions. Many statements enable the description of these interactions; we can use for example the virtual power statement. This shows the manner to describe the mechanical interaction between each material point of the body with respect to a given loading distribution. For the sake of simplicity and conciseness of this presentation, a thermodynamical description of interaction is adopted.

First of all, the local state is defined by a set of state variables such as the strain $\varepsilon(u)$, a set of internal parameters α and the absolute temperature T.

The local interaction is defined by a thermodynamical potential or the free energy $w(\varepsilon,\alpha,T)$, from which the equations of state are deduced.

For example, in the case of linear thermoelasticity and a small perturbation near the natural state at the temperature T_0, this potential has the following form ($\tau = T - T_0$):

$$w(\varepsilon,\tau) = \frac{1}{2}\varepsilon\cdot C\cdot\varepsilon + k\cdot\varepsilon\tau + \frac{1}{2}s\tau^2,$$

and in the case of isothermal plasticity with linear hardening this potential can be given as

$$w(\varepsilon,\alpha) = \frac{1}{2}(\varepsilon-\alpha)\cdot C\cdot(\varepsilon-\alpha) + \frac{1}{2}\alpha\cdot H\cdot\alpha.$$

The thermodynamical forces are defined by the state equations:

$$\sigma_r = \frac{\partial w}{\partial\varepsilon}, \qquad A = -\frac{\partial w}{\partial\alpha}, \qquad s = -\frac{\partial w}{\partial T}.$$

(*) General paper presented at 30th Polish Solid Mechanics Conference, Zakopane, September 5–9, 1994.

In the case of reversibility, the knowledge of the free energy is sufficient to determine the local state of equilibrium. In linear thermoelasticity, the local reversible stresses $\sigma_r = C : \varepsilon$ are in equilibrium with the given loading.

In nonlinear mechanics, the internal states are generally associated with irreversibility. Then the fundamental inequality of thermodynamics implies that the internal production of entropy must be non-negative. The equations of state do not provide the full constitutive equations, some complementary laws are necessary to describe the evolution of irreversibility.

In the total dissipation, we distinguish the part due to the conduction and the part due to internal forces. The two parts are assumed to be separately non-negative. The mechanical part has the form:

$$D_m = \sigma : \dot{\varepsilon} - \left(\frac{dw}{dt} + s\dot{T}\right) = (\sigma - \sigma_r) : \dot{\varepsilon} + A \cdot \dot{\alpha} \geq 0.$$

To determine the evolution of the irreversibility, complementary laws must be given. Let us assume that the dissipation is normal or that the material is standard. This ensures the existence of a potential of dissipation ω, and the evolution of the internal state satisfies

$$\dot{\alpha} = \frac{\partial \omega}{\partial A}, \quad \text{or} \quad A = \frac{\partial d}{\partial \dot{\alpha}}.$$

The potentials d and ω are convex functions of the variables, with a minimum value at the origin.

For example, in the case of linear viscosity the potential of dissipation is $d(\dot{\varepsilon}) = \frac{1}{2}\dot{\varepsilon} : \eta : \dot{\varepsilon}$ with η being a positive definite operator, then $\sigma_{ir} = \partial d / \partial \dot{\varepsilon} = \eta : \dot{\varepsilon}$. The state of internal stresses during the evolution is $\sigma = \sigma_r + \sigma_{ir}$, and for linear viscoelasticity we have for example $\sigma = C : \varepsilon + \eta : \dot{\varepsilon}$; in this case we recognize the Kelvin–Voigt model.

The Maxwell description is obtained by choosing the thermodynamical potential in the following form: $w = \frac{1}{2}(\varepsilon - \alpha) : C : (\varepsilon - \alpha)$, and a pseudopotential of dissipation in a quadratic manner $d = \frac{1}{2}\dot{\alpha} : \eta : \dot{\alpha}$.

In the case of a regular and differentiable function, the hypothesis of convexity of the potential of dissipation gives us the characterization of the evolution of the internal state by the equalities:

$$\sigma_{ir} = \frac{\partial d}{\partial \dot{\varepsilon}}, \qquad A = \frac{\partial d}{\partial \dot{\alpha}}.$$

More generally, the definition of the gradient is replaced by the notion of subgradient as

$$(\sigma_{ir}, A) \in \partial d(\dot{\varepsilon}, \dot{\alpha}),$$

if

$$d(\dot{\varepsilon}, \dot{\alpha}) + \sigma_{ir} : (\varepsilon^* - \dot{\varepsilon}) + A : (\alpha^* - \dot{\alpha}) \leq d(\varepsilon^*, \alpha^*),$$

for all admissible fields ε^*, α^*.

We emphazise that the hypothesis of existence of a potential for the dissipation ensures the positiveness of the entropy production:

$$\sigma_{ir} : \dot{\varepsilon} + A : \dot{\alpha} = \langle \partial d(\dot{\varepsilon}, \dot{\alpha}), (\dot{\varepsilon}, \dot{\alpha}) \rangle \geq d(\dot{\varepsilon}, \dot{\alpha}) - d(0,0) \geq 0.$$

2. Equilibrium and quasi-static evolution

The quasi-static evolution is a solution of the local equations, the displacement field and the internal state must verify:

- the state equations

$$\sigma_r = \frac{\partial w}{\partial \varepsilon}, \qquad A = -\frac{\partial w}{\partial \alpha}, \qquad s = -\frac{\partial w}{\partial T},$$

- the conservation of the momentum

$$\operatorname{div} \sigma = 0, \qquad \sigma = \sigma_r + \sigma_{ir},$$

- the equations of evolution of the state variables.

For the overall system the rule of the free energy is replaced by the global free energy

$$W(\tilde{\varepsilon}, \tilde{\alpha}, \tilde{T}) = \int_{\Omega_t} w(\varepsilon, \alpha, T)\, d\omega.$$

In a global description the equations of state possess the same form as in the local one, but the state of the system is defined by fields of state variables. The equations of state are relationships between fields of state variables:

$$\widetilde{\sigma_r} = \frac{\partial W}{\partial \tilde{\varepsilon}}, \qquad \tilde{A} = -\frac{\partial W}{\partial \tilde{\alpha}}, \qquad \tilde{s} = -\frac{\partial W}{\partial \tilde{T}}.$$

These relations are obtained by the following definition:

$$\frac{\partial W}{\partial \tilde{q}} \cdot \tilde{q}^* = \int_{\Omega_t} \frac{\partial w}{\partial q} : q^*\, d\omega.$$

By using the properties of characterization of the evolution of the internal state and integration over the body, we can define the dissipative function

$$D(\tilde{\dot{\varepsilon}}, \tilde{\dot{\alpha}}) = \int_{\Omega_t} d(\dot{\varepsilon}, \dot{\alpha})\, d\omega,$$

for which the evolution is given in terms of fields of state variables:

$$(\tilde{\sigma}_{ir}, \tilde{A}) \in \partial D(\dot{\tilde{\varepsilon}}, \dot{\tilde{\alpha}}),$$

if

$$D(\dot{\tilde{\varepsilon}}, \dot{\tilde{\alpha}}) - D(\tilde{\varepsilon}^*, \tilde{\alpha}^*) + \tilde{\sigma}_{ir} \cdot (\tilde{\varepsilon}^* - \dot{\tilde{\varepsilon}}) + \tilde{A} \cdot (\tilde{\alpha}^* - \dot{\tilde{\alpha}}) \geq 0, \qquad \forall (\tilde{\varepsilon}^*, \tilde{\alpha}^*).$$

Then we have in the case of a regular function:

$$\frac{\partial D}{\partial \tilde{v}} \cdot \varepsilon(\delta \tilde{u}) = \int_{\Omega_t} \sigma_{ir} : \varepsilon(\delta u)\, d\omega,$$

$$\frac{\partial D}{\partial \dot{\tilde{\alpha}}} \cdot \delta \tilde{\alpha} = \int_{\Omega_t} A \cdot \delta \alpha\, d\omega.$$

Let us consider that the external loading derives from a potential given in terms of traction $\lambda \underline{T}^d$ applied to the external surface of the body. Then, the global free energy can be replaced by the potential energy of the system,

$$W(\tilde{u}, \tilde{\alpha}, \tilde{\lambda}) = \int_{\Omega_t} w(\varepsilon(u), \alpha)\, d\omega - \int_{\partial \Omega_t} \lambda \underline{T}^d \cdot u\, da.$$

By combining all the equations in terms of fields of state variables, the quasi-static evolution is then given in a global manner by the variational system

$$\frac{\partial W}{\partial \tilde{u}} \cdot \delta \tilde{u} + \frac{\partial D}{\partial \dot{\tilde{\varepsilon}}} \cdot \varepsilon(\delta \tilde{u}) = 0,$$

$$\frac{\partial W}{\partial \tilde{\alpha}} \cdot \delta \tilde{\alpha} + \frac{\partial D}{\partial \dot{\tilde{\alpha}}} \cdot (\delta \tilde{\alpha}) = 0.$$

These equations are defined on a set of admissible fields, the displacement is subjected to boundary conditions $u = u^d$ over $\partial \Omega_u$.

The preceeding equations are general, they contain the essential structure of the problem of quasi-static evolution.

The first equation of this system expresses the conservation of momentum, taking into account the constitutive law:

$$\operatorname{div} \sigma = 0; \qquad \sigma = \sigma_r + \sigma_{ir}, \quad \sigma \cdot n = \lambda \underline{T}^d \text{ over } \partial \Omega_\sigma;$$

the second one expresses the thermodynamic forces associated with the internal parameters.

3. The Lagrangean and the dynamical case

By definition, the Lagrangean is the difference between the kinetic energy and the potential of interaction applied to the system. For all kinematically admissible fields, the potential of interaction of the system is the potential energy

$$W(\tilde{u}, \tilde{\alpha}, \tilde{T}, \lambda) = \int_{\Omega_t} w(\varepsilon, \alpha, T)\varrho \, d\omega - \int_{\partial\Omega_t} \lambda \underline{T}^d \cdot u \, da.$$

The kinetic energy is given by

$$K(\tilde{v}) = \int_{\Omega_t} \frac{1}{2}\varrho v^2 \, d\omega,$$

and the Lagrange's functional is then

$$L = K - W.$$

If we denote the acceleration by $\gamma = \dot{v}$, we can compute some quantities:

$$\frac{\partial L}{\partial \tilde{u}} \cdot \delta\tilde{u} = -\int_{\Omega_t} \sigma_r : \delta\varepsilon \, d\omega + \int_{\partial\Omega_t} \lambda \underline{T}^d \cdot \delta u \, da,$$

$$\frac{\partial L}{\partial \tilde{v}} \cdot \delta\tilde{v} = \int_{\Omega_t} \varrho v \cdot \delta v \, d\omega,$$

$$\frac{d}{dt}\left(\frac{\partial L}{\partial \tilde{v}} \cdot \delta\tilde{u}\right) = \frac{\partial L}{\partial \tilde{v}} \cdot \delta\tilde{v} + \left(\frac{d}{dt}\frac{\partial L}{\partial \tilde{v}}\right) \cdot \delta\tilde{u}$$

$$= \int_{\Omega_t} (\varrho v \cdot \delta v + \varrho\gamma \cdot \delta u) \, d\omega + \int_{\Gamma} m[v] \cdot \delta u \, da.$$

The system is determined by the equation of the motion expressed in the law of conservation of the momentum,

$$\operatorname{div} \sigma = \varrho\gamma,$$

where the stress σ is decomposed as previously as $\sigma = \sigma_r + \sigma_{ir}$ taking the constitutive law into account.

In the dynamical case, strong discontinuities along the moving surfaces occur and the conservation of momentum is defined by the relation between the jumps of mechanical quantities: $[\sigma \cdot n] = m[v]$. Taking all these relations into account, the evolution of the system is governed by

$$-\left(\frac{d}{dt}\frac{\partial L}{\partial \tilde{v}} - \frac{\partial L}{\partial \tilde{u}}\right) \cdot \delta\tilde{u} = \frac{\partial D}{\partial \tilde{\dot{\varepsilon}}} \cdot \tilde{\varepsilon}(\delta u),$$

$$\frac{\partial L}{\partial \tilde{\alpha}} \cdot \delta\tilde{\alpha} = \frac{\partial D}{\partial \dot{\tilde{\alpha}}} \cdot \delta\tilde{\alpha},$$
$$\frac{\partial L}{\partial \tilde{T}} \cdot \delta\tilde{T} = \int_{\Omega_t} \varrho s \delta T \, d\omega.$$

These equations are a generalization of the classical Lagrange's formulation to nonlinear dynamics [15], they have the same form as the expression given by BIOT [1] in viscoelasticity. In this formulation we have defined, as previously, the dissipation function as

$$D = \int_{\Omega_t} d(\dot{\varepsilon}, \dot{\alpha}) \varrho \, d\omega.$$

The first equation is the equation of motion, the second one – the evolution law for the internal state, the last one defines the local entropy. To this set of equations we must add the conduction law and the condition of positivity of the entropy production,

$$\frac{d}{dt} \int_{\Omega_t} \varrho s \, d\omega + \int_{\partial\Omega_t} \frac{q \cdot n}{T} \, da \geq 0.$$

4. The Hamiltonian of the system

The Hamiltonian is a Legendre transformation of the Lagrangean, with respect to the velocity and temperature [13]:

$$H(\tilde{u}, \tilde{p}, \tilde{\alpha}, \tilde{s}, \lambda) = -L(\tilde{u}, \tilde{v}, \tilde{\alpha}, \tilde{T}, \lambda) + \int_{\Omega_t} p \cdot v \, d\omega + \int_{\Omega_t} T s \varrho \, d\omega.$$

The Hamiltonian assigns a stationary value to the right-hand side with respect to the velocity and the temperature. Therefore:

$$H = \int_{\Omega_t} \frac{1}{2} \frac{p^2}{\varrho} \, d\omega + \int_{\Omega_t} \varrho \, e(u, \alpha, s) \, d\omega - \int_{\partial\Omega_t} \lambda \underline{T}^d \cdot u \, da.$$

In this expression appears the density of internal energy, $e = w + Ts$.

In a global formulation, we obtain successively

$$\frac{\partial H}{\partial \tilde{p}} \cdot \delta\tilde{p} = \int_{\Omega_t} \frac{p}{\varrho} \delta p \, d\omega,$$
$$\frac{\partial H}{\partial \tilde{u}} \cdot \delta\tilde{u} = \int_{\Omega_t} \frac{\partial w}{\partial \varepsilon} : \varepsilon(\delta u) \, d\omega - \int_{\partial\Omega_t} \lambda \underline{T}^d \cdot \delta u \, da$$
$$= \int_{\Omega_t} (\sigma - \sigma_{ir}) : \varepsilon(\delta u) \, d\omega - \int_{\partial\Omega_t} \lambda \underline{T}^d \cdot \delta u \, da.$$

Taking into account the equation of dynamics, the boundary conditions and the jump conditions along strong discontinuities, the expressions are then modified to

$$\frac{\partial H}{\partial \tilde{u}} \cdot \delta \tilde{u} = -\int_{\Omega_t} \sigma_{ir} : \varepsilon(\delta u)\, d\omega - \int_{\Omega_t} \varrho\gamma \delta u\, d\omega + \int_{\Gamma} [\sigma \cdot n] \cdot \delta u\, da,$$

$$\frac{\partial H}{\partial \tilde{u}} \cdot \delta \tilde{u} = -\frac{\partial D}{\partial \tilde{\dot{\varepsilon}}} \cdot \tilde{\varepsilon}(\delta u) - \frac{d}{dt} \int_{\Omega_t} p \cdot \delta u\, d\omega,$$

$$\frac{d}{dt} \int_{\Omega_t} p \cdot \delta u\, d\omega = \int_{\Omega_t} \varrho\gamma \cdot \delta u\, d\omega + \int_{\Gamma} m[v] \cdot \delta u\, da.$$

Finally, the Hamiltonian formulation of the evolution of the system is obtained

$$\frac{\partial H}{\partial \tilde{p}} \cdot \delta \tilde{p} = \frac{d}{dt} \int_{\Omega_t} u \cdot \delta p\, d\omega,$$

$$\frac{\partial H}{\partial \tilde{u}} \cdot \delta \tilde{u} = -\frac{\partial D}{\partial \tilde{\dot{\varepsilon}}} \cdot \tilde{\varepsilon}(\delta u) - \frac{d}{dt} \int_{\Omega_t} p \cdot \delta u\, d\omega,$$

$$\frac{\partial H}{\partial \tilde{\alpha}} \cdot \delta \tilde{\alpha} = -\frac{\partial D}{\partial \tilde{\dot{\alpha}}} \cdot \delta \tilde{\alpha},$$

$$\frac{\partial H}{\partial \tilde{s}} \delta \tilde{s} = \int_{\Omega_t} \varrho T \delta s\, d\omega.$$

As previously, a conduction law must be given and the positivity of the entropy production must be verified to determine the evolution of the system.

5. Some properties

Generalization: the definition of the Lagrangean or of the Hamiltonian can be extended to generalized media. The proposed description can be performed in all the cases in which we can define the behaviour by the two potentials only: a global free energy and a dissipative function. If some particular internal constraints exist, this description must be repeated.

The conservation of energy: for the real motion, the value of the Hamiltonian is the sum of the kinetic energy, of the internal energy and of the potential energy of the external (given) load, then the conservation of the energy of the system can be easily rewritten as

$$\frac{dH}{dt} - \frac{\partial H}{\partial \lambda} \frac{d\lambda}{dt} = P_{\text{cal}}.$$

When the external load is kept fixed $d\lambda/dt = 0$, the exchange of energy is only due to the heat rate supply P_{cal}. Generally, this quantity has the form

$$P_{\text{cal}} = -\int_{\partial\Omega_t} q \cdot n \, da,$$

where q is the heat flux. This result is useful in fracture mechanics to discuss the heat generated by the propagation of the crack, as presented in the following section.

Conservation law: in the case of a conservative system, in an adiabatic evolution ($P_{\text{cal}} = 0$), the Hamiltonian is constant,

$$H(t) = H(0),$$

this property can be rewritten in terms of the Lagrangean

$$L - \tilde{v} \cdot \frac{\partial L}{\partial \tilde{v}} = H(0).$$

Property of stationarity: the Lagrangean has the properties of stationarity in elasticity or viscoelasticity: let us consider a variation of the Lagrangean in isothermal evolution:

$$\delta L = \frac{\partial L}{\partial \tilde{v}} \cdot \delta\tilde{v} + \frac{\partial L}{\partial \tilde{u}} \cdot \delta\tilde{u} = \frac{d}{dt}\left(\frac{\partial L}{\partial \tilde{v}} \cdot \delta\tilde{u}\right) + \frac{\partial D}{\partial \dot{\tilde{\varepsilon}}} \cdot \tilde{\varepsilon}(\delta u),$$

then

$$\delta \int_{t_1}^{t_2} L \, dt = \delta D,$$

where δD is the total viscous dissipation during the variation.

Finally let us note that the above results may be adapted to the case of other types of the boundary conditions, and they lead to a well-posed problem.

6. Application in fracture mechanics

In classical approach to rupture, the body can be decomposed into three domains: the first one, near the crack tip, is the process zone where the local mechanisms of rupture take place, the second one is a domain where all the mechanical fields are more or less singular and, finally, the third domain where all the fields satisfy the matching conditions with external loading.

Determination of the thermodynamical force associated with propagation of the crack is governed by the constitutive behaviour defined in the process zone.

In the classical approach, the process zone is assumed to be small and a global description of the propagation of the crack is then performed. Then, the thermodynamical force associated with the propagation is determined, some local hypothesis being assumed. We can admit the hypothesis of similarity and of continuity for the mechanical fields, then an asymptotical analysis can be performed to determine the singularities accompanying the propagation of the crack.

Many results have been obtained in the case of linear elasticity or in finite elasticity; the main result is the definition of the release rate of energy, which is the main characteristic of the crack [5].

But in the case of inelastic behaviour, such a complete discussion does not exist [2]. The main goal is the determination of some local dissipative process or structure accompanying the propagation of the crack.

Here we assume that the constitutive law is described in a thermodynamical manner, i.e. the potential energy and the dissipative function are given. The thermodynamical description of the propagation of the crack is then performed in a global manner to determine the equivalent heat source due to the crack propagation.

For the overall system the crack length is an internal variable, which defines the volume of sound material $\Omega_t = \Omega(l)$ and the body is decomposed into two domains Ω_Γ and V_Γ, separated by a curve or a surface Γ, the volume V_Γ rounding the crack tip and $\Omega(l) = \Omega_\Gamma + V_\Gamma$.

The Hamiltonian is the sum of two terms:

$$H_\Gamma = \int_{\Omega_\Gamma} \left(\frac{1}{2} \frac{p^2}{\varrho} + \varrho e(u, s) \right) d\omega - \int_{\partial\Omega(l)} \lambda \underline{T}^d \cdot u \, da,$$

$$H_V = \int_{V_\Gamma} \left(\frac{1}{2} \frac{p^2}{\varrho} + \varrho e(u, s) \right) d\omega.$$

Consider that the volume V_Γ is translated with the rate of propagation of the crack $\dot{l}$. The variations of all average quantities $F = \langle f \rangle_{\Omega_\Gamma} + \langle f \rangle_{V_\Gamma}$ during the propagation are easily derived:

$$\frac{d}{dt} F = \frac{d}{dt} \langle f \rangle_{\Omega_\Gamma} + \langle f^* \rangle_{V_\Gamma},$$

$$\frac{d}{dt} \langle f \rangle_{\Omega_\Gamma} = \left\langle \frac{df}{dt} \right\rangle_{\Omega_\Gamma} + \int_\Gamma f \dot{l} \, n \cdot e_x \, da.$$

The asterisk (*) denotes the derivative in the moving frame accompanying the crack in its motion in the direction e_x.

By integrating by parts, and assuming that all the quantities are regular, one obtains:

$$P_{\text{cal}} = -\int_{\Omega_\Gamma} \operatorname{div}|, q\, d\omega + \int_\Gamma q \cdot n\, da,$$

$$\frac{d}{dt} H_\Gamma = \frac{\partial H_\Gamma}{\partial p} \cdot \frac{dp}{dt} + \frac{\partial H_\Gamma}{\partial u} \cdot v + \frac{\partial H_\Gamma}{\partial s} \cdot \dot{s} + \int_\Gamma \left(\frac{1}{2}\varrho v^2 + e\right) \dot{l}\, da.$$

Then, if in the moving domain V the fields are regular, we have

$$\lim_{\Gamma\to 0}\left(H_V^* + \int_\Gamma \sigma \cdot n \cdot u^*\, da\right) + \lim_{\Gamma\to 0}\int_\Gamma \sigma \cdot n \cdot (v - u^*) + \left(\frac{1}{2}\varrho v^2 + e\right) \dot{l}\, da$$

$$= \lim_{\Gamma\to 0}\int_\Gamma q \cdot n\, da.$$

Along Γ, the continuity of the displacement is expressed as $v - u^* + \dot{l}\, u_{,x} = 0$.

This equation defines the heat source due to the crack; it is equal to the derivative of the Hamiltonian with respect to the crack length. The regularity hypothesis implies that the contributions defined in the volume V and on Γ vanish,

$$\frac{\partial H}{\partial l} = \lim_{\Gamma\to 0}\int_\Gamma -\sigma \cdot n \cdot u_{,x} + \left(\frac{1}{2}\varrho v^2 + e\right) da.$$

The derivative of the Hamiltonian with respect to the length of the crack plays the role of the release rate of energy. When some discontinuities exist in the volume V_Γ, on a line or on a surface Σ ($[u^*] + \dot{l}\,[u_{,x}] = 0$), we have a continuous line of heat sources defined by ($2\overline{\sigma} = \sigma^+ + \sigma^-$)

$$\frac{\partial H}{\partial l} = \lim_{\Gamma\to\Sigma}\int_\Gamma \left(-\sigma \cdot n \cdot u_{,x} + \frac{1}{2}\varrho v^2 + e\right) da = \int_\Sigma -\overline{\sigma} \cdot n \cdot [u_{,x}] + [e]\, da.$$

This result can be established by considering a Γ curve which tends to the line of discontinuities [5]. The same method can be applied to determine the part of the entropy production due to the moving crack; the result is then

$$\lim_{\Gamma\to 0}\int_\Gamma \left(-\sigma \cdot n \cdot u_{,x} + \frac{1}{2}\varrho v^2 + e\right)/T\, da\ \ \dot{l} \geq 0,$$

or in the case of discontinuities,

$$\int_\Sigma -\overline{\sigma} \cdot n \cdot \left[\frac{u_{,x}}{T}\right] + \left[\frac{e}{T}\right] da\ \ \dot{l} \geq 0.$$

7. The canonical equations of shock waves

The local equations of shock waves will be derived again from a thermodynamical potential and a pseudopotential of dissipations. The canonical equations rule the jump relations and the constitutive behaviour in a section of the shock [6]. Let us consider a shock wave, we proposed to study the evolution of the shock. Locally the surface of discontinuity is replaced by its tangent plane and consider a frame moving with a velocity ϕ which is the normal speed of the shock.

Along the line of discontinuities, some relationships between the jump of the quantities must be satisfied.

- For the momentum:

$$[\sigma \cdot n] - m[v] = 0.$$

- For the energy:

$$[q \cdot n] + m\left[\frac{1}{2}v^2 + w\right] - [\sigma \cdot n \cdot v] = 0.$$

- For the entropy production:

$$m[s] + \left[\frac{q \cdot n}{T}\right] \geq 0.$$

- Denoting by m the mass flux: $m = \varrho(v - \phi)$, this quantity expresses the mass conservation.

The shock is governed by the constants of the shock mT^d, mQ^d which are related respectively to the flux of momentum and to the flux of energy; then the jump conditions are rewritten as:

$$\sigma^+ \cdot n - mv^+ = \sigma^- \cdot n - mv^- = mT^d,$$

$$q^+ \cdot n + m\left(\frac{1}{2}v^2 + e\right)^+ - \sigma \cdot n \cdot v^+ = q^- \cdot n + m\left(\frac{1}{2}v^2 + e\right)^- - \sigma \cdot n \cdot v^- = mQ^d.$$

The main problem is to determine the state $(-)$ if the state $(+)$ and the constants mT^d, mQ^d are given with respect to the positivity of the entropy production in an inelastic material. The jump conditions give us only the jump of entropy, but no direct relation between this discontinuity and the jump of internal parameters. One must determine the loading path or the history of all the quantities inside the shock.

To solve this problem we can consider the discontinuity surface as a layer normal to the direction of the propagation of the shock; and one has to study the inner expansion of all the quantities in a continuous process in the frame moving with the shock surface, assuming that all quantities depend only of the local normal coordinate $X = x - \phi t$. For the inner expansion X varies from $-\infty$ to ∞. Then we are interested in a one-dimensional motion.

A constitutive law and a pseudo-potential of dissipation being given to describe the inner behaviour, the dissipation is known inside the shock and therefore the jump of entropy is given by

$$m[s] + \left[\frac{q \cdot n}{T}\right] = \int_{-\infty}^{\infty} \frac{D_m}{T} - \frac{q \cdot \operatorname{grad} T}{T^2} dx \geq 0.$$

Using the other jump conditions expressed in terms of the given constant of the shock, the jump of entropy is rewritten as

$$mQ\left[\frac{1}{T}\right] + mT^d\left[\frac{v}{T}\right] - m\left[\frac{\left(w - \frac{1}{2}v^2\right)}{T}\right] = \int_{-\infty}^{\infty} \frac{D_m}{T} - q \cdot \frac{\operatorname{grad} T}{T^2} d\omega.$$

This defines the shock generating function P,

$$P = \frac{mQ^d}{T} + mT^d\frac{v}{T} - m\frac{\left(w - \frac{1}{2}v^2\right)}{T},$$

in the steady state analysis: $\varrho \dot{f} = \phi f_{,x}$, and P has the following form:

$$P(v, \alpha, T) = \frac{mQ^d}{T} + mT^d\frac{v}{T} - m\frac{\left(w(v, \alpha, T) - \frac{1}{2}v^2\right)}{T}.$$

Properties of the functional P

The jump of P is the total dissipation:

$$P(x^+) - P(x^-) = \int_{-\infty}^{\infty} \frac{D_m}{T} - q \cdot \frac{\operatorname{grad} T}{T^2} dX.$$

Function P is supposed to be a continuous function of X and the value of P on a segment dX has the following form:

$$P\,dX = m\frac{Q^d}{T}dX + \frac{mT^d}{T} \cdot (v(X + dX) - v(X)) - \frac{1}{T}m\left(w - \frac{1}{2}v^2\right)dX;$$

then P is related to the Lagrangean defined on the segment dX:

$$L = \left(\frac{1}{2}v^2 - w\right) m\,dX + mT^d \cdot [v]_X^{X+dX}.$$

Defining the dissipative function D as previously, we have

$$D(\varepsilon(X), \alpha(X), T(X)) = \frac{1}{T}\left(d(\phi\varepsilon_{,x}, \phi\alpha_{,x}) + \frac{1}{2}\frac{K}{T}(T_{,x})^2\right),$$

where a Fourier law is adopted for the thermal conduction $q = -K \cdot \operatorname{grad} T$.

Then the shock structure is determined by the canonical equations:

$$\frac{\partial P}{\partial T} = \frac{\partial D}{\partial T_{,x}}, \qquad \frac{\partial P}{\partial u} = \frac{\partial D}{\partial u_{,x}}, \qquad \frac{\partial P}{\partial \alpha} = \frac{\partial D}{\partial \alpha_{,x}},$$

$$\frac{dP}{dX} = \frac{D_m}{T} - q \cdot \frac{\operatorname{grad} T}{T^2}.$$

Some comments

Let us consider a hyperbolic system

$$\frac{\partial g}{\partial t} + f'(g)\frac{\partial g}{\partial x} = 0.$$

The jump relation gives the speed of the discontinuity line:

$$-[g]\phi + [f(g)] = 0,$$

or

$$\phi = \frac{f(g_1) - f(g_2)}{g_1 - g_2}.$$

To study the shock structure, assuming some internal processes with viscosity, the equation are then modified to the form

$$\frac{\partial g}{\partial t} + f'(g)\frac{\partial g}{\partial x} = \nu\frac{\partial^2 g}{\partial x \partial t}.$$

In the moving frame $X = x - \phi t$, the function g is a regular function of X, and

$$(f' - \phi)\frac{\partial g}{\partial X} = \phi\nu\frac{\partial^2 g}{\partial X \partial X}.$$

Taking account of the matching conditions for the shock at infinity: in $-\infty$, g tends to g_2 and $\partial g/\partial X$ tends to 0; in a similar manner, in $+\infty$ g tends to g_1 and $\partial g/\partial X$ to 0. Then by integration, the initial jump condition is recovered:

$$-\phi(g_1 - g_2) + f(g_1) - f(g_2) = 0.$$

But this point of view allows us to study the stability of the shock discontinuity, when the internal structure exhibits some dissipative mechanisms. This simple example shows how the dissipative mechanism can be taken into account with the

constants of shock. In the first case we have only the relation of discontinuities, in the second case we make an inner expansion of the shock and the constants of the shock are recovered at ∞.

Consider a more complex system:

$$\frac{\partial}{\partial t}\frac{\partial A}{\partial q_i} + \frac{\partial}{\partial x}\frac{\partial B}{\partial q_i} = \eta L_{ij}\frac{\partial^2 q_j}{\partial t \partial x},$$

where A and B are scalar functions of the n parameters q_i, and η is a small positive scalar, L is a matrix of dissipation coefficients. We assume also that

$$\frac{\partial^2 A}{\partial q_i \partial q_j} Q_i Q_j > 0$$

for all state q and non-zero arbitrary Q. First we neglect the dissipation $\eta = 0$, the shock conditions are easily found; if ϕ is the shock speed, we obtain

$$\frac{\partial B}{\partial q_i}(q^+) - \phi\frac{\partial A}{\partial q_i}(q^+) = \frac{\partial B}{\partial q_i}(q^-) - \phi\frac{\partial A}{\partial q_i}(q^-) = C_i,$$

where C_i are the constants of the shock. For such a phenomenon, a shock generating function is obtained from

$$P = \phi A - B + C_i q_i.$$

Two points q which may be connected by a shock with a given shock constant are stationary points of P. Now if we take dissipative mechanism into account, $\eta = 1$, and we must write some inequalities corresponding to dissipative mechanisms. If we define a pseudopotential of dissipation $\frac{1}{2}\dot{q}_{,x} L \dot{q}_{,x}$, we obtain the canonical shock equations

$$\frac{\partial P}{\partial q_i} = \phi L_{ij} q_{j,x}$$

with the same constant C_i.

In plasticity, the determination of compatible state (+) and (−) is not easy to study, but in the case of propagation of longitudinal waves, if we assume that the loading process is monotonic, we obtain a curve, which gives the relation between the jump of the quantities. This curve is similar to the adiabatic Hugoniot curve known in gas dynamics [11]. This result is obtained by the assumption of a radial loading path during the shock. This is the structure of the shock. Some other approaches could also be employed [10].

References

1. M.A. BIOT, *On variational methods in the mechanics of solids*, IUTAM Evanston, 1978.
2. H.D. BUI, *Introduction aux problèmes inverses en mécanique des matériaux*, Eyrolles Collection DER EDF, 83, 1993.
3. H.D. BUI, *Mécanique de la rupture fragile*, Ed Masson, Paris 1978.
4. H.D. BUI and A. EHRLACHER, *Propagation dynamique d'une zone endommagée*, Comptes Rendus de l'Académie des Sciences de Paris, t. 298, Série B, pp. 873–876, 1980.
5. H.D. BUI, A. EHRLACHER and Q.S. NGUYEN, *Thermomechanical coupling in fracture mechanics*, [in:] Thermomechanical coupling in solids, H.D. BUI and Q.S. NGUYEN [Eds.], Elsevier Sci. Pub. (North Holland), 1987.
6. P. GERMAIN, *Shock waves, jump relations, and structure*, Advances in Applied Mechanics, **12**, pp. 131–194, Academic Press, Inc., New York and London 1972.
7. P. GERMAIN and E.H. LEE, *On shock waves in elastic-plastic solids*, J. Mech. Phys. Solids, **21**, pp. 359–382, 1973.
8. P. GERMAIN, Q.S. NGUYEN and P. SUQUET, *Continuum thermodynamics*, J. Appl. Mech, no 50, pp. 1010–1020, 1983.
9. B. HALPHEN and Q.S. NGUYEN, *Sur les matériaux standard généralisés*, J. de Mécanique, **14**, 1, pp. 254–259, 1975.
10. V.N. KUKUDJANOV, *Investigation of shock wave structure in elasto-visco-plastic bars using the asymptotic method*, Arch. Mech., **33**, 5, pp. 739–751, 1981.
11. J. MANDEL, *Ondes de choc longitudinales dans un milieu élastoplastique*, Mech. Res. Comm., **5**, 6, pp. 353–359, 1978.
12. Q.S. NGUYEN, *A thermodynamic description of a running crack problem*, IUTAM Symposium, "Three Dimensional Constitutive Relations and Ductile Fracture", Dourdan, Ed. North Holland Publ., pp. 315–330, 1981.
13. C. STOLZ, *Sur les équations générales de la dynamique des milieux anélastiques*, Comptes Rendus de l'Académie des Sciences de Paris, Série II, t. 307, pp. 1997–2000, 1988.
14. C. STOLZ, *Sur la propagation d'une ligne de discontinuité et la fonction génératrice de choc pour un solide anélastique*, Comptes Rendus de l'Académie des Sciences de Paris, Série II, t. 308, pp. 1–3, 1989.
15. C. STOLZ, *Dynamique des milieux continus anélastiques et discontinuités mobiles*, Calcul des Structures et Intelligence Artificielle, P. Ladevèze, R. Ohayon editors, Vol 3, Pluralis, 1989.
16. G.W. SWAN, G.E. DUVALL and C.K. THORNHILL, *On steady wave profiles in solids*, J. Mech. Phys. Solids, **21**, pp. 215–227, 1973.

ÉCOLE POLYTECHNIQUE
LABORATOIRE DE MÉCANIQUE DES SOLIDES, PALAISEAU, FRANCE.

Received November 28, 1994.

Arch. Mech., 47, 3, pp. 437–483, Warszawa 1995

Towards modelling of deformable ferromagnets and ferroelectrics (*)

A. TOURABI, P. GUELIN and D. FAVIER (GRENOBLE)

dedicated to the memory of Professor J. Kravtchenko

A ONE-DIMENSIONAL and isothermal discrete memory-type modelling of ferromagnetic properties has been introduced recently and is briefly recalled. This modelling has been performed through a simple and straightforward implementation of the three-dimensional patterns of elasticity and pure hysteresis, used previously in order to describe the thermomechanical properties of various materials ranging from shape memory alloys to granular media. The aim of this paper is twofold: firstly, the one-dimensional isothermal model is enlarged to the non-isothermal case in order to illustrate the ability of the scheme to model various hysteretic behaviours ranging from soft type to hard type; secondly, some hints are given on the three-dimensional generalization of the theory regarding magnetic, dielectric and mechanical phenomena, these phenomena being coupled or not, far from the thermodynamic equilibrium.

1. Introduction

i. THE PRESENT PAPER is an attempt to suggest a new approach to puzzling problems in the arena of hysteretic polarized systems. The proposed approach is founded on a thermomechanical pattern of pure hysteresis which is of material discrete memory-type: consequently, and in spite of the fact that this pattern is proved to be rather effective, its price may be considered to be quite excessive if the material discrete memory assumption cannot be justified further as physically meaningful, owing to the processes involved at the relevant microscopic level.

ii. Special attention will be devoted to the case where both reversible and always irreversible properties (of pure hysteresis) are simultaneously present as a global property under consideration. In this case the relevant pattern is that of elastohysteresis. Its differential form is:

$$dA = dA_{\text{rev}} + dA_{\text{hys}}, \tag{1.1}$$

where, following the method suggested by DUHEM [1], the external "action" (stress σ, magnetic field H, electric field E) is split into two partial contributions A_{rev} and A_{hys} of reversible and purely hysteretic type, respectively. Such modelling, obtained by modifying the well-established modelling of the physical behaviour of systems capable of reversible modifications, implies that the unusual term is

(*) Sectional paper presented at 30th Polish Solid Mechanics Conference, Zakopane, September 5–9, 1994, under the title: "From constitutive modelling of shape memory properties to that of magnetic hysteresis".

endowed with mathematical and physical features which are different from that of the reversible term. It is then obvious that special attention will be devoted to the definition of dA_{hys} without neglecting the interesting features which remain to be studied concerning non-trivial definitions of dA_{rev}. The splitting (1.1) is discussed at the beginning of the paper (Sec. 2.1).

iii. Owing to the material discrete memory form which is given to the hysteretic contribution dA_{hys} in (1.1), it is worthwhile to notice that the proposed phenomenological pattern cannot be connected with the classical works based on the switch concept. This type of approach is originally founded on the notion of "fictitious substance" suggested by P.Weiss and J. de Freudenreich in 1916, then studied by PREISACH [2] in order to describe some alloys [3]. Regarding the limitations and rules of careful implementation of such models, the remarks and method of NEEL remain to be of outstanding interest ([3] part 1 and 2). It is at least necessary to recall the introductory warning of Neel, avoiding any distortion through some imperfect translation ([1]):

Malheureusement, bien qu'il soit possible d'attribuer un sens physique aux quantités H_c et H_a, il est impossible de justifier a priori le choix des valeurs à donner à φ et à ψ pour obtenir les lois de Rayleigh; en fait, il ne s'agit pas là d'une théorie, mais d'une représentation purement formelle, difficile à concilier avec ce que nous savons aujourd'hui des processus d'aimantation dans les champs faibles, qui sont dus principalement aux déplacement réversibles ou irréversibles des parois de séparation entre les différents domaines élémentaires. Il ne se produit pas notamment de renversements, en bloc, de l'aimantation, domaine par domaine.

The fact is that the works founded on basic "up" and "down" switching operators have been extended by several authors [4,5] and recently mathematical tools have been proposed [6, 7].

iv. It is worthwhile to notice that the property (or "notion") of "spontaneous polarization" is not explicitly invoked, except in a short paragraph put at the end of the paper (Sec. 3.3). This choice cannot be entirely justified by a short comment. However, it may be useful to introduce immediately some hints on this method. Let us consider the form introduced by Rayleigh (in its "Notes on electricity and magnetism") following [3]:

$$(1.2) \qquad I - I_n = a(H - H_n) \pm \frac{b}{2}(H - H_n)^2, \qquad H \succ \text{ or } \prec H_n, \quad n = 1,2$$

in order to describe the ascending and the descending branches of a hysteresis cycle. In (1.2) the prominent role is that of the apex of the cycle which are located at (I_1, H_1) and (I_2, H_2): if one substitutes for I the usual difference: $B - \mu_0 H$ or some other difference such as: $B - \mu(0)H$, the main point is that the differences $B - B_n$ and $H - H_n$ are involved once more in the new functional form.

([1]) The notations of Neel are obvious as soon as one knows that c is for cohercitive and that φ is the probability associated with H_c.

Conversely, it is possible to consider a functional form between $H - H_n$ and $B - B_n$ without any use of the polarization notion. The proposed pattern is built following this method: a distinction is made between the intensive variable A_{hys} and what will be defined as its associated current reference value ${}_R A_{\text{hys}}$ dragged along from the relevant previous reference state at time t_R to the current state at time t. This reference value ${}_R A_{\text{hys}}$ may be considered as the generalisation of the field H_n and the distinction between A_{hys} and ${}_R A_{\text{hys}}$ is a basic feature which is introduced as early as the beginning of the paper (Sec. 2.2.2). In fact this method and the form (1.1) itself imply the distinction between *three-dimensional* intensive and extensive variables. If hysteresis is implied, this distinction is connected with that of cause and of effect. Consequently, the physical intuition may be less useful than in classical situations to which the remark of de Gennes may be almost always applied: "ce qu'on entend ici par cause et par effet ne prête pas à de grands discours philosophiques, mais se sent bien sur des exemples concrets ..." [8] (A translation may be tentatively: what one means here by cause and by effect is not an opportunity to deliver large philosophical speeches, but is intuitively well detected through actual examples... .). One will see that in the hysteretic, always irreversible, case under consideration through (1.1), a non-intuitive distinction is suggested between cause and effect and between extensive and intensive three-dimensional variables: energetic terms ($H\,dB$ and $(H - H_n)dB$, for example) and convexity ($\dfrac{\partial^2 H}{\partial B^2}$ for example) are indeed prominent features in order to describe the stationary process between the apex (B_1, H_1) and (B_2, H_2).

v. The basic limitations of the proposed phenomenological approach are implied in the always irreversible pattern (1.1): the properties are supposed to be *rate independent*. Non-viscous "standard" hysteresis (Fig. 1) is considered in "sufficiently" quasi-static situations. This assumption is compatible with the analysis of DUHEM [1]. Duhem considered that a study of equilibrium processes has to distinguish *three* types of systems; the systems capable of reversible modifications, the frictional systems and the systems with hysteresis. This classification rejects the common point of view that the only distinction between a non-quasi-static process and a hysteretic process is that of the time scale. As DUHEM concludes (p. 164 of [1]): "Such a loophole evidently has only one aim: to subject the whole of Physics to the laws of Statics and Dynamics which were formulated by Gibbs and Helmholtz. It would have a legitimacy of this goal if we had reasons to believe that all mass systems have to yield to the rules of this Statics and this Dynamics. But of such reasons, we have none".

Moreover, following the method implemented in [3] (part 2), one makes the assumption that it is possible to avoid "shape effects" and the associated effects of "depolarizing" fields.

vi. Some remarks are useful in order to avoid misunderstanding concerning the rate-independence assumption and the quasi-static assumption. The latter

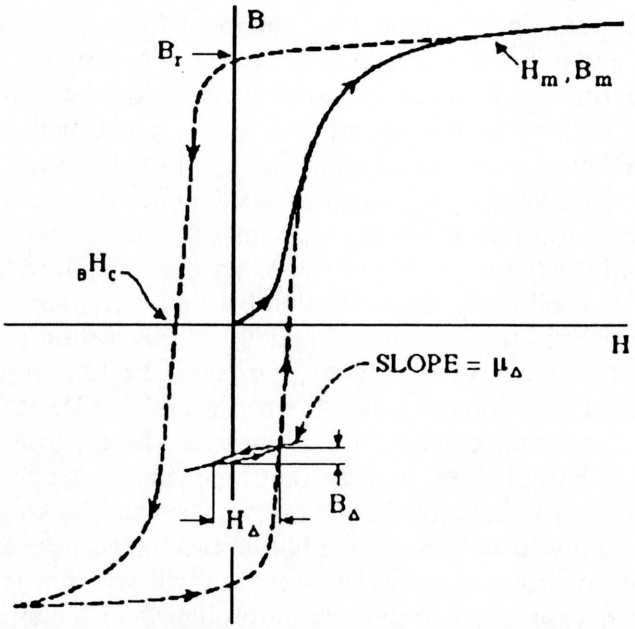

FIG. 1. Magnetisation curve and "standard-shaped" hysteresis loop [from R.M. BOZORTH, *Ferromagnetism*, Van Nostrand Comp., Princeton 1951].

may be considered as quite admissible, at least in a purely mechanical study restricted to the constitutive modelling of rate-independent properties. However, it is necessary to notice that the dynamic equation (the conservation of momentum equation) is nevertheless involved in the approach (see Sec. 2.2.3). The reason is as follows: on the one hand the Intrinsic Internal Power P_{ii} is implied (in any pattern of hysteresis) *both* at the level of the First Principle in implicit form *and* at the level of the *definition* of the Intrinsic Dissipation Φ in explicit form. On the other hand, the momentum equation is necessarily involved, even in the study of quasi-static cases, in order to substitute for the External Extrinsic Power P_{ee} (in explicit form in the First Principle) the power P_{ii}. Moreover, in the mechanical case, the assumption does not imply that the dynamic equation is not required to define the pattern in a comprehensive form resulting, for example, in well-posed boundary-value problems. We must have reasons to believe in the dynamic equation. Now let us return to the case of a polarized systems. The main lines of the above sketch are the same but the situation is not simple any more: it is necessary to fix on the approach of Minkowski or to fix on that of Abraham (and different definitions of the ponderomotive force are implied by this choice).

vii. These short remarks allow us to see that the quasi-static assumption is not "only" a technical assumption resulting in a gap eventually admissible for an introductory paper basically devoted to constitutive modelling. It may be also considered as a warning acting at the level of principles and methods. Accord-

ingly it may be useful to be aware of the heuristic features which are involved in a large amount of works devoted to open problems which are neither basically of a quasi-static type, nor devoted to phenomenological approaches: typical stimulating studies are for example those founded on the equations of Maxwell [9] or on the study of "classical" difficulties regarding ponderomotive forces [10]. On the other hand, pinning processes and possible gradual, continuous, upsetting are essential features in order to justify the discrete memory structure of some pattern implying that a "state" may be compared with others (still memorized) through levels of dissipated energy and implying also that the hysteretic property is understood as a "spontaneously" perfectly stationary process what subloop perturbations it may be encounter: accordingly, topic as "special" as the problem of the relationship between topological and energetic stability [11] may result in stimulating heuristic sketches.

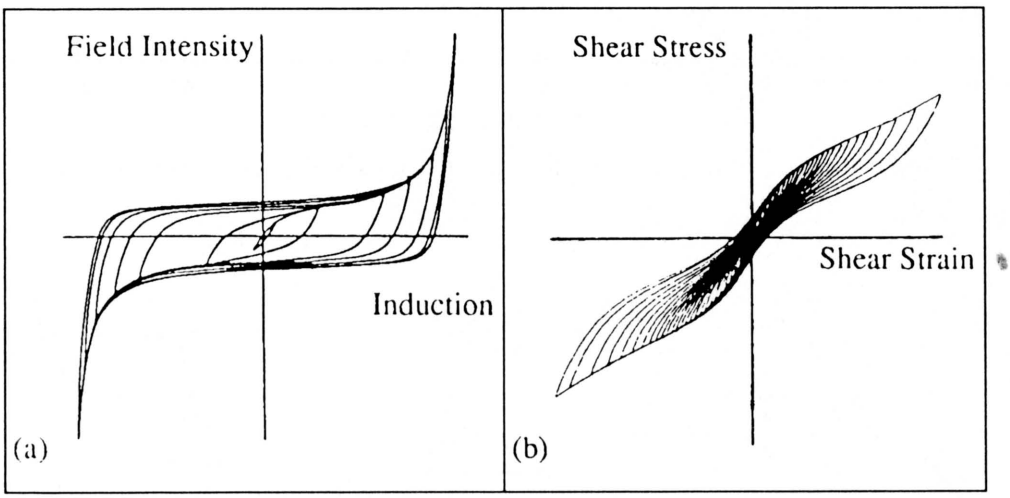

FIG. 2. A unified "thermodynamic" presentation of magnetisation of a ferromagnetic material (a) [BOZORTH] and of deformation of a shape memory alloy (b) (CuZnAl polycristalline alloy at $T > A_f$) [25].

Of outstanding interest are also the studies suggesting how the main common features of ferroelectrics and ferromagnets are combined with mechanical hysteresis in ferroelastic materials [12]. Such studies lead inevitably to a comparison (Fig. 2) between the shape memory properties (Fig. 3) and the ferromagnetic properties: it is then easier to implement (1.1) (Fig. 4) in the magnetic case, for example (Fig. 5), and to introduce at a micro-scale some relationships between mechanical and magnetic basic processes (Sec. 3.3 Fig. 14). Moreover, through these studies, *actual* cases are as many as the opportunities in order to improve the underlying principles and methods: the case of materials similar to a Nickel-Iodine Boracite [12] is a typical example in order to avoid the implementation of classical loophole (of first loading type).

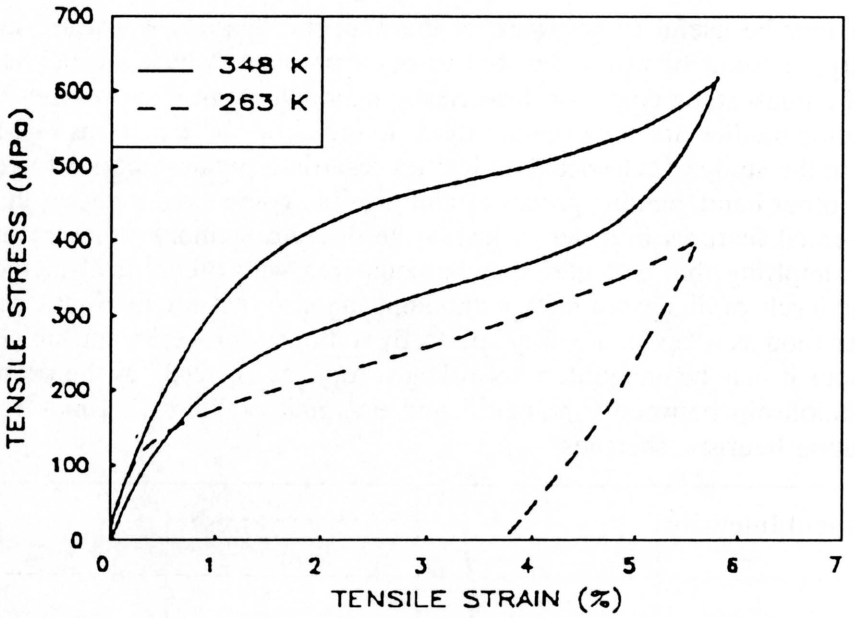

FIG. 3. Isothermal stress-strain tensile curves [27] for a NiTi shape memory alloy at $T = 348\,\mathrm{K} > A_f$ and at $T = 263\,\mathrm{K} < M_f$.

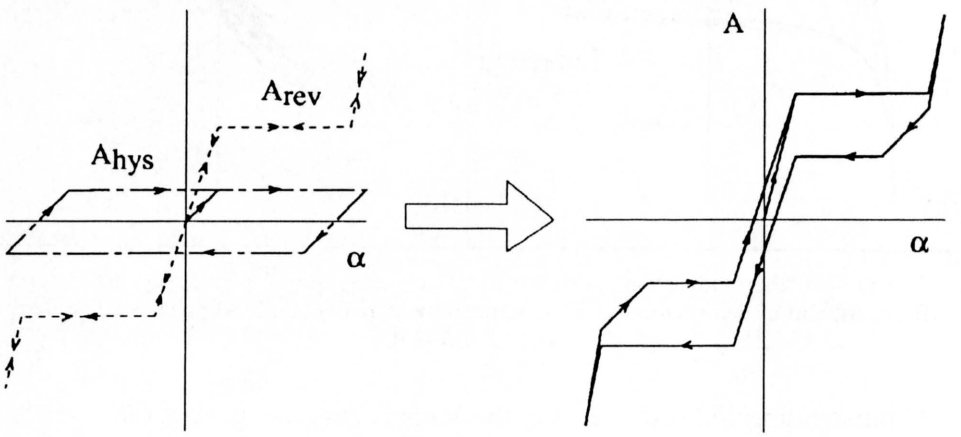

FIG. 4. Splitting of the intensive external "action".

viii. As suggested by the abstract, the aim of the paper is twofold. Firstly, a one-dimensional approach allows us to illustrate the sophisticated features associated with a (scalar) coupling effect between A_{hys} and A_{rev} (in the non-isothermal case). Secondly, the three-dimensional pattern is sketched allowing to show that the classification of the coupling effects which are *a priori* possible far from the equilibrium, cannot be obtained through a classical treatment using, for example, some principle of additive Lagrangian or the distinction between the order of

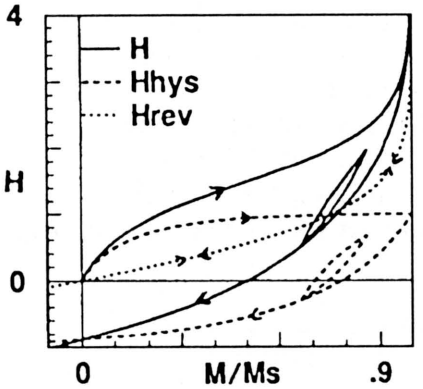

FIG. 5. The splitting of the magnetic field [from 21].

truncated series. It is however hardly useful to notice that the classical coupling effects are implicitly taken as a basic heuristic background, even if there is no explicit generalization in this introductory paper.

2. One-dimensional elastohysteretic model

2.1. From Duhem's analysis and Neel warning to the decomposition of the normal "action"

Introducing the Helmholtz free energy F as function of the normal variable α, the associated infinitesimal change of the external "action" A for a reversible isothermal phenomenon is simply given by:

$$dA = d\left(\frac{\partial F}{\partial \alpha}\right). \tag{2.1}$$

As Duhem emphasised, this relation is obviously not applicable for either frictional systems or systems capable of permanent deformations. For *the latter* he suggested therefore to modify Eq. (2.1) by incorporating another term to give

$$dA = d\left(\frac{\partial F}{\partial \alpha}\right) \pm h\, d\alpha\,, \tag{2.2}$$

where the sign + indicates when the normal variable increases, and the sign – when it decreases. The quantity h may depend upon the state of the system (through α) and also of the external "action" A. The splitting of the external "action" in the elastohysteresis theory which is expressed by Eq. (1.1) is thus similar to Duhem's proposal. Obviously this method of modelling the evolution of systems with hysteresis can be applied only if this evolution is macroscopically continuous, i.e. if a macroscopic equilibrium state can always be reached and also left by a modification of infinitesimal slowness. Phenomena of this type are common even if accurate observations reveal that microscopically the evolutions

proceed through a series of elementary processes [13, 14]. These implicit references concerning modern microstructural results should be supplemented by a short comment on the non-usual suggestion of Duhem. One notices that a single normal variable α has been considered and that, moreover, the same variable is used to introduce the modification (2.2) of Eq. (2.1). For sake of simplicity let us drop out the ambition to discuss the bearing of the "normal" notion for hysteretic system. Then one may wonder why Duhem did not suggest to study further some alternative method such as

$$dA = d\left(\frac{\partial F}{\partial \alpha_{\text{rev}}}\right) \pm h(\alpha_{\text{hys}}; \ldots)\, d\alpha_{\text{hys}}$$

implying the splitting: $\alpha = \alpha_{\text{rev}} + \alpha_{\text{hys}}$, still frequently encountered in classical plasticity theory regarding the strain or the strain rate: $D = D_{\text{elas}} + D_{\text{plas}}$.

As long as the fundamental question remains in the arena of continuum mechanics, it is well known (but not overpublished) that the role played by the strain rate D is of a dramatic mathematical importance. Accordingly it is not physically relevant to introduce an approach (or even to think of a method) implying the breakdown of such a fundamental variable without producing some decisive unquestionable physical argument. On the one hand, the results of isothermal classical mechanical tests do not allow to discern any opportunity: the only unquestionable physical notion is that of limit surface of plasticity.

On the other hand, it remains possible to search for a basic argument at some microscopic physical level and to introduce eventually some associated statistical argument. However it is worthwhile to underline that the negative result obtained at the macroscopic level is definitely ominous, owing to the status of the first principle and independently of any doctrinal argument. The fact is that it is now rather hopeless to find an opportunity at the level of microscopic physical processes. For nearly 20 years it has been possible, with the aid of transmission electron microscopy, to observe dislocations movements occurring during the deformation of small samples. The simplest case (a simple dislocation moving between two parallel walls) implies the elastic-perfectly plastic behaviour. Following the Neel warning, the basic feature is the *a priori* possible coexistence of reversible or irreversible displacements: the basic back and forth process is not possible through the "renversements en bloc" involved in the switching process (cf. Sec. 3.3). The case of a Frank-Read source operating between the walls is more complex but similar [15]. For such elementary mechanisms (of typical scale about $10^{-9}\,\text{mm}^3$) it is possible to search for a rather clear physical definition of the splitting of α. Unfortunately the essential result is as follows: the deformation of a real material is the result of the addition and interaction of a multitude of elementary mechanisms, the thresholds of which are continuously distributed. The splitting of α is no longer a convenient convention but a physically irrelevant assumption. Some remarks are given below regarding the magnetic case (Sec. 3.3 point ii).

2.2. Discrete memory scheme of the pure hysteresis contribution

2.2.1. The Masing model. The main feature of the pure hysteresis behaviour are its stationary properties during periodic cyclic loading. A one-dimensional model which behaves like a pure non-relaxation hysteretic system consists of a collection of elastic springs (perfectly elastic phenomena) and rigid plastic or slip elements (pure solid friction phenomena) arranged in either a series-parallel or a parallel-series combination. With respect to the physical property, these two combinations are identical. Owing to the remarks given above (cf. Sec. 2.1) and to the fact that one needs a R^1 model *which may be heuristic to built a* R^3 *pattern*, the relevant heuristic model is unique. The fact is that the model (Fig. 6) has

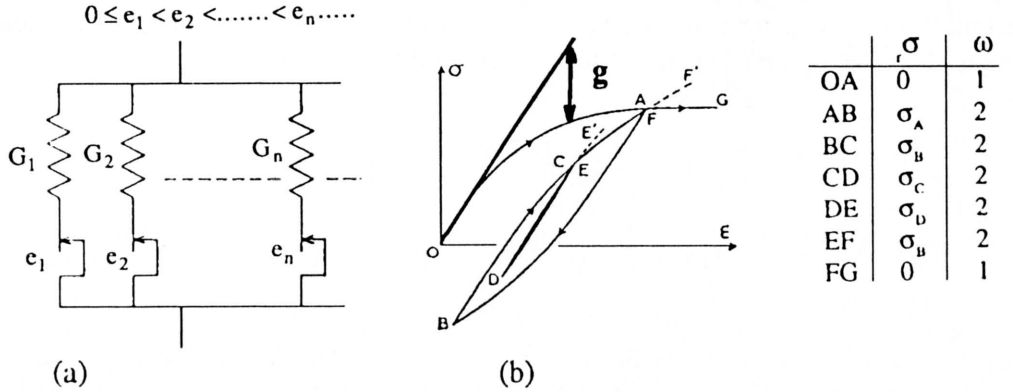

	σ_r	ω
OA	0	1
AB	σ_A	2
BC	σ_B	2
CD	σ_C	2
DE	σ_D	2
EF	σ_B	2
FG	0	1

FIG. 6. A pure hysteresis model and its behaviour.

been suggested by several authors as a simple model for the yielding behaviour of materials and was used as early as in 1926 by MASING [16]. We will recall the mechanical, energetic and thermodynamic analysis initiated by de CARBON [17] excluding the general random cyclic case and enlarged by one of the authors [18] through a radical departure of the classical approaches briefly recalled above (Sec. 1, iii). All along the following analysis of "Masing's model" (Sec. 2.2.2 to 2.2.4), the mechanical vocabulary is used, i.e. the external "action" A is the hysteresis stress (denoted by σ in this section) and the normal variable α is the deformation ε.

2.2.2. Mechanical analysis. The parallel-series model consists of a collection of linear elastic and slip elements arranged *by pairs* as indicated in Fig. 6a. G_i, S_i and e_i are respectively the spring rigidity coefficient, the critical slipping stress and the equivalent deformation limit e_i $(= S_i/G_i)$. If the number of elements becomes very large and because the pairs are necessarily arranged in increasing order of e_i, the rigidity coefficient G_i can be described in terms of a distribution function $g''(e)$ where $g''(e)\,de$ is the rigidity coefficient for the pairs having their deformation limit between e and $e + de$. The neutral initial assumption postulates that there is no strength in any branch before the first loading OA (Fig. 6b). Moreover,

there is no isolated spring (owing to (1.1) this requirement is trivial). Two features are at the roots of the heuristic meaning of the model. The first one is that it takes into account the warning of Neel. The second feature is that the order of the pairs is a strictly internal intrinsic property entirely independent of the details concerning the shape of g provided that $g'' \geq 0$, $g(0) = g'(0) = G_0 - g'(\infty) = 0$; in other words, this "absolute" or "universal" feature is at the origin of an inevitable algorithmic part of the pattern. Moreover, the whole structure of the R^3 enlargement will be necessarily dominated by the coexistence of "absolute" features and of invariant (dragged along) material properties "similar" to G_i and S_i. The mechanical analysis consists of distinguishing the pairs for which the slip element moves and which transmit a stress σ_s from the others that have not slipped and which transmit a stress σ_{ns}. The distribution function $g''(e)$ is then related to the shape $S(e)$ of the first loading curve as follows:

$$\sigma(\varepsilon) = S(\varepsilon) = \sigma_s + \sigma_{ns} = \int_0^{\varepsilon} e g''(e)\, de + \int_{\varepsilon}^{\infty} \varepsilon g''(e)\, de = G_0\varepsilon - g(\varepsilon),$$

(2.3)

$$\sigma''(\varepsilon) \leq 0, \qquad G_0 = \int_0^{\infty} g''(e)\, de, \qquad g(0) = g'(0) = G_0 - g'(\infty) = 0.$$

By performing identical mechanical analysis it can be shown that any branch (like AB) or arc of branch (like EF) of the path $OABCDEFG$ is described by a general functional form where piecewise constant functionals are involved:

$$\Delta_R^t\sigma = \sigma - {}_R\sigma = \omega S\left[(\Delta_R^t\varepsilon)/\omega\right], \qquad \omega = 1 \text{ or } 2,$$

(2.4)

$$\Delta_R^t x = x(t) - x(t_R),$$

$$\frac{d\Delta_R^t\sigma}{dt} \equiv \frac{d\sigma}{dt} = G_0\frac{d\varepsilon}{dt} - \frac{dg}{dt} = G_0\dot{\varepsilon} - f(\Delta_R^t\sigma, \omega)\dot{\varepsilon}\,.$$

${}_R\sigma$ and ${}_R\varepsilon$ are the reference state stress and strain defined as piecewise constant by branch or arc of branch (cf. table of Fig. 6). In this equation the coefficient ω generalizes the Masing rule [16] which postulates that the unloading curve AB is deduced from the first loading curve by a similarity of ratio -2. From the consideration of the internal closed subloops CDE inside the minor loop $ABCF$, it is clear that the reference state cannot be taken as the last inversion. The thermodynamic analysis below has to furnish at least (cf. Sec. 2.2.5) firstly a criterion in order to define the reference state in non-obvious R^3 cases, and then an algorithm which distinguishes the current reference state from all the previous inversion states.

2.2.3. Energetic analysis. At least in principle, the energetic analysis is straightforward because the internal energy change dE is stored in the springs and the

sliding of the slip elements leads to an energy dissipation (considered here as a heat loss) associated with the irreversibility. In fact there is no problem regarding the first loading studied by de CARBON [17]. The cyclic case is puzzling because of discrete memory form. It has been introduced by one of the authors [18] and results in

$$
\begin{aligned}
dE &= \sigma_{ns}\, d\varepsilon = \sigma\, d\varepsilon - d\varepsilon(\sigma - {}_R\sigma)/\omega + d\sigma(\varepsilon - {}_R\varepsilon)/\omega, \\
-dQ &= \sigma_s\, d\varepsilon = +d\varepsilon(\sigma - {}_R\sigma)/\omega - d\sigma(\varepsilon - {}_R\varepsilon)/\omega.
\end{aligned} \tag{2.5}
$$

In spite of the fact that the quasi-static form of the first law:

$$
dE = \partial W + \partial Q = -P_{\mathrm{ii}}dt + \dot{Q}_{\mathrm{ii}}dt, \qquad (0 = P_{\mathrm{ee}} + P_{\mathrm{ii}}),
$$

is trivially verified, such relations imply a conceptual breakdown prohibiting their introduction without, firstly, the proposal of an associated thermodynamics [18] and secondly, further physical justifications at some relevant microscopic scales [15]. Let us suppose that these problems are solved. It is then worthwhile to notice that (2.4) and (2.5) have the same status and that, consequently, in a general three-dimensional approach (2.4) and (2.5) are involved in the constitutive pattern. This point is important because it implies, for example, that a numerical technique must include the enlarged R^3 forms substituted for (2.5) as well as the enlarged R^3 form substituted for (2.4).

2.2.4. Thermodynamic analysis. Following the usual convention, a quantity received by the continuum is positive. The thermodynamic analysis must verify the fundamental properties of the rheological model, i.e. each possible path is irreversible, there is a quasi-reversibility after each inversion and it is always possible to return the model to its neutral initial state by a great number of almost symmetrical cycles whose amplitude decreases slowly, as it is well known. Let Π denote the reversible power, and let

$$
\Phi = -P_{\mathrm{ii}} - \Pi, \qquad \Phi \geq 0 \tag{2.6}
$$

be the usual definition of the intrinsic dissipation. The fact that the model is entirely irreversible must be expressed by the fact that Φ is *almost everywhere positive* along any possible evolution. The Gibbs equation is proposed to be written in the form:

$$
dE = \Pi\, dt + dI. \tag{2.7}
$$

The meaning of the introduced quantity I is outlined by deducing from (2.5), (2.6) and (2.7) the following relation between rates (of supply):

$$
dI + (-dQ) = \Phi\, dt. \tag{2.8}
$$

The quantity dI appears therefore to be the part of Φ which is not the energy dissipated as heat by the gliding of the friction sliders: the sum of the rate of supply of disorder and of the rate of internal intrinsic heat extracted and given to the surroundings is equal to Φ. Equations (2.6) and (2.8) have introduced 3 unknowns. One of the authors has suggested to complete the thermodynamic analysis of the pure hysteresis model by assuming that $\Pi\, dt$ is of discrete memory form: ${}_R\sigma\, d\varepsilon$. This assumption results in [18]

$$\Phi\, dt = (\sigma - {}_R\sigma)\, d\varepsilon, \qquad \Pi\, dt = {}_R\sigma\, d\varepsilon\,. \tag{2.9}$$

Firstly, the non-negative value of the intrinsic dissipation Φ allows one to determine the inversion criterion. For instance, it is not possible to keep the point O as the reference state along the branch AB (Fig. 6), for it would result in a negative value of Φ as soon as the loading is reversed at point A. Then A is an inversion state and this inversion state is the reference state at least for the path immediately following the inversion. Secondly, the quasi-reversible behaviour which occurs after each inversion is underlined at the inversion point by a zero value of the intrinsic dissipation and the equality of the external power P_e with the reversible power Π. The restoration of the model properties after an inversion state is associated with a final assumption. The model has to be considered as receiving a large flow of order at this inversion point which counterbalances exactly the disorder produced during the preceding branch: this notion of order is that of negentropy introduced by Brillouin (in "Science and information theory", p. 114, 1962). Then, after each inversion the value of I is always zero and the disorder quantity I is defined for each branch. During the fundamental process of demagnetization, the I value tends towards zero as does the stress supported by the model [18].

The result of the thermodynamic analysis is used to define the reference state from all the inversion states, and the reference state still memorized. Owing to $g'' \geq 0$ this is made possible by a rule of minimum increase of $d\Phi$. This rule states that, for instance, at the point F of the path EFG the reference state has to be changed, since

$$d\Phi \text{ (along } FG \text{ with } {}_R\sigma = \sigma(0)) < d\Phi \text{ (along } FF' \text{ with } {}_R\sigma = \sigma(B)). \tag{2.10}$$

The rule applies also at the point E of the path DEF. By using the Masing rule and the condition $g''(e) \geq 0$ it is shown [18] that an equivalent but more practical way to determine the current reference state is obtained by introducing a "help function" defined through the differential form $dW_L = \Phi dt$. An algorithm for the determination of the reference state is then built up from the piecewise continuous variations of an integral form and easily enlarged to the three-dimensional case [19, 20].

2.2.5. Remarks concerning the three-dimensional extension

i. The previous analyses have demonstrated the relevance of the concept of discrete memory of past inversion states in any hysteretic model. This ultimate model has to be at least composed: firstly of a constitutive set of differential-difference equations (2.4) and (2.5) involving piecewise constant functionals as arguments; secondly – of an inversion criterion based on a particular form of the intrinsic dissipation function, and lastly – of an algorithm determining at any time the relevant reference state and the Masing functional.

ii. This holds for the one-dimensional case. However it is worthwhile to underline three points concerning the three-dimensional theory. In this case the "action" A is defined implicitly through the definition of its rate dA. The constitutive set is then a set of differential-difference equations including not only the rate form of (2.4) but also nontrivial generalization of (2.5). Secondly, the definition of the rate operator under consideration implies a nontrivial generalization of the invariance ${}_R\sigma$ = constant (and thus $d_R\sigma = 0$) physically obvious and trivially expressed in the isothermal one-dimensional case. Owing to its underlying thermodynamics [18], the discrete memory pattern of hysteresis implies thirdly the existence of a unique neutral state of demagnetization which can be actually reached, at least asymptotically, through any of the fundamental processes pertaining to the set of relevant demagnetization strategies. It is then always possible to put back the model in the basic initial state and to achieve a continuous improvement of the intrinsic pattern.

iii. In the one-dimensional case, the existence and the uniqueness of both the basic demagnetization state and of the associated strategy are rather obvious. The strategy is two-fold; the initial state I_s is some unknown state; for the Masing's model there can exist some initial strengths in springs. Firstly, a sufficiently large loading-unloading is performed, the only assumption being there that the measurements are able to give the first and second derivatives of $A(\alpha)$ as accurately as required owing to the subsequent process: the points D_l and D_u of curvature discontinuities are then obtained. Owing to the unknown loading history preceding the initial state I_s, the apparent behaviour may be the path P_1 or the path P_2 as well. Both paths are nevertheless associated with the unique intrinsic behaviour: an identification process cannot be founded on the path P_1 nor on the path P_2. Secondly, it remains to perform the well-known cyclic loading, slowly decreasing, almost symmetrical and tending to the point $((\alpha_u + \alpha_l)/2, 0)$ (Fig. 7).

iv. In the three-dimensional case the problem is much less simple. It can be sketched briefly when the properties are described through a two-dimensional functional. This occurs for example in tensorial three-dimensional mechanical analysis of the isotropic elastic-plastic material when both the stress and strain paths remain in deviatoric planes. This occurs also for the vectorial pattern of rigid isotropic magnetic material when the field and magnetization vectors remain in the fixed planes passing through the origin of the fields spaces. In such

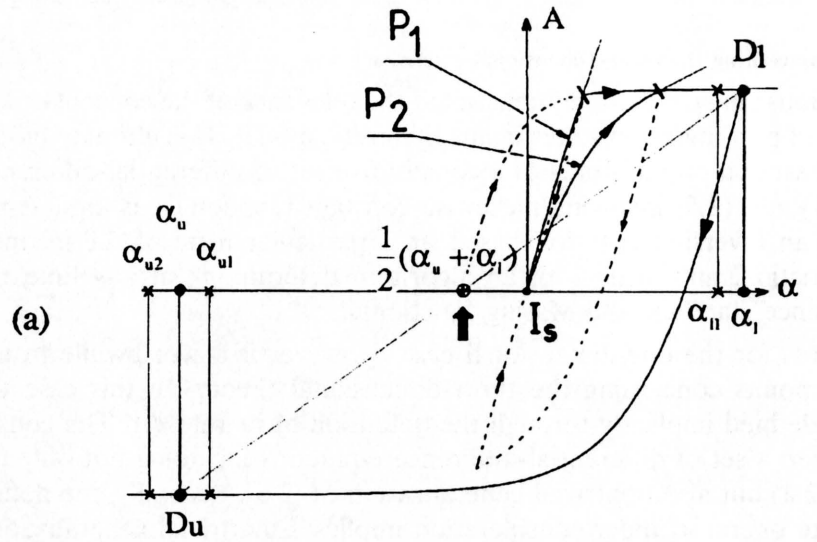

$$A'_{\alpha}|_{\alpha_u} = A'_{\alpha}|_{\alpha_l} \quad ; \quad -2\lim_{\alpha_{u1}\to\alpha_u} A''_{\alpha^2}|_{\alpha_{u1}} = A''_{\alpha^2}|_{\alpha_l} \left(= -A''_{\alpha^2}|_{\alpha_{u2}}\right)$$

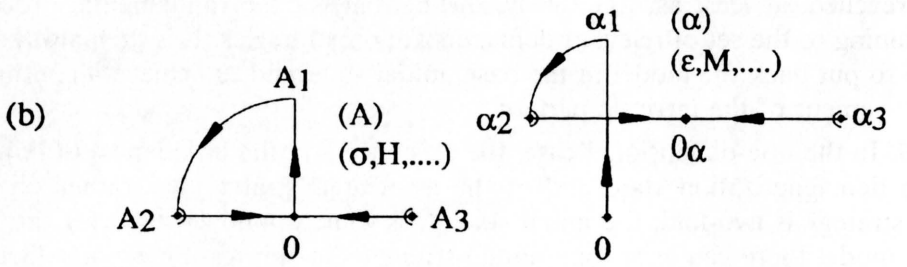

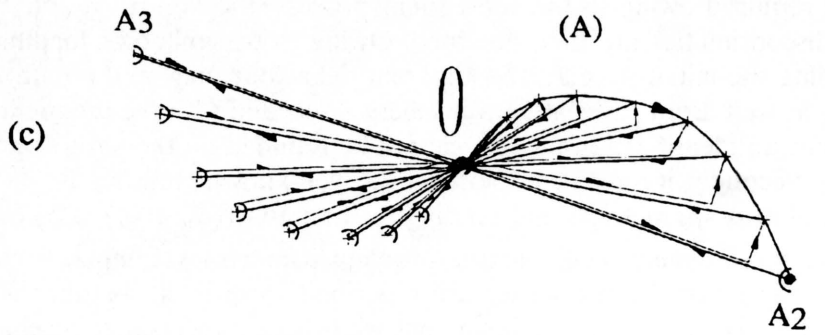

FIG. 7. Demagnetization process (a) in the one-dimensional case, (b) and (c) in the two-dimensional case.

situation an extensive path such as $O\ \alpha_1\ \alpha_2\ \alpha_3$ is associated to the intensive path (stress or field) $O\ A_1\ A_2\ A_3$. If O is the neutral state and if $O\ \alpha_1$ represents the unknown loading history leading to the initial state, any usual cyclic demagnetization on A_2A_3 tending to O gives, on $\alpha_2\alpha_3$, the final extensive location O_α, which is irrelevant (Fig. 7b). Owing to the definition of pattern, the relevant strategy for a generic path such as OA (Fig. 7c) is in fact of two-dimensional type because the polar angles must be covered back and forth, as well as the polar radius (Fig. 7c). However, owing to the current state of the theory, the special case of Fig. 7b must be studied further. It is worthwhile to underline that the solution may be useful for the improvement or the achievement of any continuum mechanics of "micro-structured" media endowed with pinning and upsetting processes allowing not only for reversible processes but also, in some sense, for "sliding" processes back and forth.

2.3. A first proposal of one-dimensional modelling of non-isothermal magnetisation

2.3.1. The heuristic isothermal case

i. The modelling recently introduced [21] may be recalled briefly as follows. Let α_s be a saturation bound of α, taken as a unit. The reversible contribution is taken to have the form:

$$\begin{aligned} A_{\text{rev}} &= \partial F/\partial x = a_{\text{rev}} \tanh^{-1} x, \\ dA_{\text{rev}} &= d(\partial F/\partial x) = a_{\text{rev}}/(1 - x^2)dx, \qquad \text{with} \quad x = \alpha/\alpha_s. \end{aligned} \tag{2.11}$$

Both forms are dependent on one parameter a_{rev}. A simple integral form for the hysteretic contribution along the first loading is

$$\begin{aligned} A_{\text{hys}} &= A_0 \tanh(a_{\text{hys}} x/A_0), \\ dA_{\text{hys}} &= a_{\text{hys}}[1 - (A_{\text{hys}}/A_0)^2]\, dx. \end{aligned} \tag{2.12}$$

By taking into account the discrete memory functional form (2.4) implying the Δ_R^t notion and the Masing functional ω, a generalized form of (2.12) is obtained,

$$d(\Delta_R^t A_{\text{hys}}) \equiv dA_{\text{hys}} = a_{\text{hys}}[1 - (A_{\text{hys}} - {}_R A_{\text{hys}})^c/(\omega A_0)^c]\, dx. \tag{2.13}$$

In this form, a physically useful parameter c ($c > 0$) has been introduced in order to improve the qualitative description. Then the model for the hysteretic contribution involves 3 parameters A_0, a_{hys} and c.

The derived form for the global scheme is identical to Duhem's proposal. The quantity h of (2.2) is now a function of the current state (through $A_{\text{hys}} = A - A_{\text{rev}}$) and is also a function of the history through the piecewise constant functional of reference state ${}_R A_{\text{hys}}$ and the Masing piecewise constant functional parameter ω. The model is used to generate the Fig. 8a which shows a calculated major

hysteresis loop, a minor hysteresis loop and an internal subloop inside a minor loop. Figure 8b shows a simulation of a demagnetization process. The parameters used were $a_{rev} = A_0 = 1$, $a_{hys} = 10$ and $c = 0.5$ and have no quantitative physical meaning.

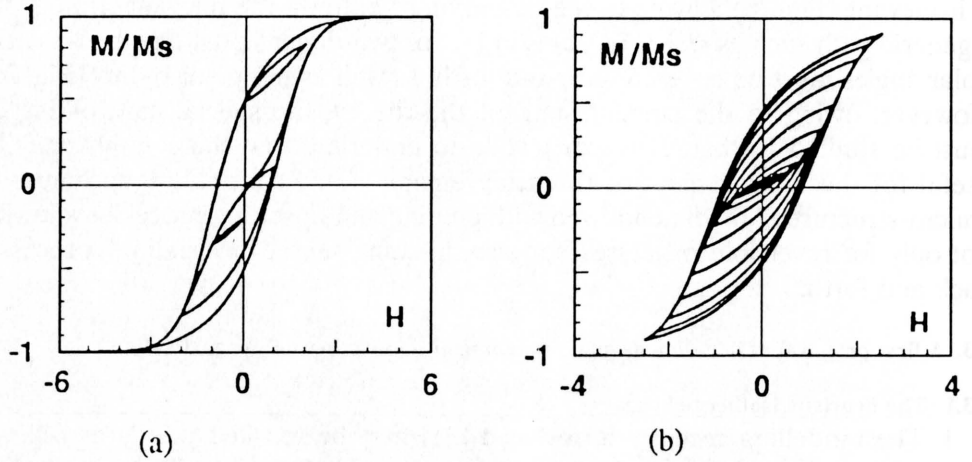

FIG. 8. Calculated hysteresis loops (arbitrary units).

ii. The elastohysteretic model is idealized and applies to materials with a "normal" structure leading to "standard-shaped" hysteresis loops (Fig. 1.). The modelling of the magnetization curves requires then the prior identification of 5 parameters. Two, α_s and A_0, are straightforwardly determined from the major hysteresis loop obtained with a field sufficient to magnetise the material to saturation. As long as the hysteresis width can then be considered as constant for low values of the magnetization α, A_0 is equal to the intrinsic coercivity ${}_{\alpha}A_c$. Secondly, from the equations (2.11) and (2.13) we deduce the following expression for the slope

$$dA/dx = a_{rev}/(1 - x^2) + a_{hys}[1 - (A_{hys} - {}_{R}A_{hys})^c/(\omega A_0)^c]. \tag{2.14}$$

In the case of a "standard" hysteresis loop, GANS [22] suggested that the reversible permeability μ_r (defined in Fig. 1 as μ_Δ with A_Δ vanishing) was determined by the biasing induction alone. BROWN [23] gave a theoretical justification to this rule but considered reversible susceptibility χ_r to be a function of magnetization alone. The reversible susceptibility is the slope $d\alpha/dA$ just after an inversion state where $A_{hys} = {}_{R}A_{hys}$. Then (2.14) can be written as

$$\alpha_s/\chi_r = a_{rev}/(1 - x^2) + a_{hys}, \tag{2.15}$$

which obeys the Gans rule. Conversely, far from the inversion state, the hysteretic contribution tends toward zero. Summarising, one can say that through the pattern (1.1), the Gans rule expresses the fact that the addition of the inverse of

a reversible susceptibility and of an almost everywhere constant or vanishing inverse of an irreversible susceptibility appears as an almost everywhere reversible inverse of a total susceptibility, in spite of the prominent hysteretic features of the properties.

The measured variation of χ_r with x can be fitted to any appropriate function. With the proposed choice (2.11), the initial value of the reversible susceptibility χ_0 is obtained by setting x to 0 in (2.15), and then

$$a_{\text{rev}} + a_{\text{hys}} = \alpha_s/\chi_0. \tag{2.16}$$

The value of the slope $d\alpha/dA$ for a zero magnetization ($A = {}_{\alpha}A_c$) is simply α_s/a_{rev}. Then a_{rev} and a_{hys} are determined. The last parameter c characterizes the squareness of the hysteresis curve which increases with increasing c. The value of B_r/B_m (Fig. 1) is then directly related to the value of this parameter.

2.3.2. The non-isothermal case. Such an adaptation has been previously introduced through the modelling of shape memory properties [24 to 27]. However, the theory is in tensorial form. As usual, this form is not convenient to give briefly the basic hints and to illustrate the modelling. Fortunately, the ferroelectric properties can be actually similar to that of shape memory alloys. This is an opportunity to sketch briefly the adaptation of the model in a convenient scalar case.

Let us therefore consider the properties of a lead Zirconate (Fig. 9b). A simple modelling (Fig. 10a) must be build as follows. Firstly the hysteresis contribution is taken as temperature-independent (Fig. 10b). Secondly, the reversible contribution is expressed as the sum of two terms, the first one A_{RS} being similar to that previously used in the magnetization case and temperature-independent (Fig. 10c), the second one A_{RT} (Fig. 10d) being

$$A_{RT}(T) = A_T(T) \cdot \tanh\left[a_t \frac{x}{A_T(T)}\right] \tag{2.17}$$

or, in differential notations,

$$dA_{RT}(T) = a_t \left[1 - \tanh^2\left(a_t \frac{x}{A_T(T)}\right)\right] \cdot dx \tag{2.18}$$

with, for the sake of simplicity,

$$A_T(T) = k(T - T_0)^3 \mathcal{H}(T - T_0), \tag{2.19}$$

where $\mathcal{H}(T - T_0)$ is the Heaviside function, and $T_0 = 132°\text{C}$, $k = 2 \cdot 10^{-3}$.

The qualitative result obtained with this very simple pattern (Fig. 9a) is sufficient to suggest that the adaptation of the modelling can be performed in order to take into account the main qualitative features of the hysteretic properties from the soft type to the hard type. The features of the cyclic behaviour with subloops and of the demagnetization path are illustrated (Fig. 11) by two sophisticated cases ($T = 132°\text{C}$, $146°\text{C}$). The parameters used for all the modelling were $a_{\text{hys}} = 45$, $A_0 = 1$, $c = 4$, $a_{\text{rev}} = 0.26$ and $a_t = 6$.

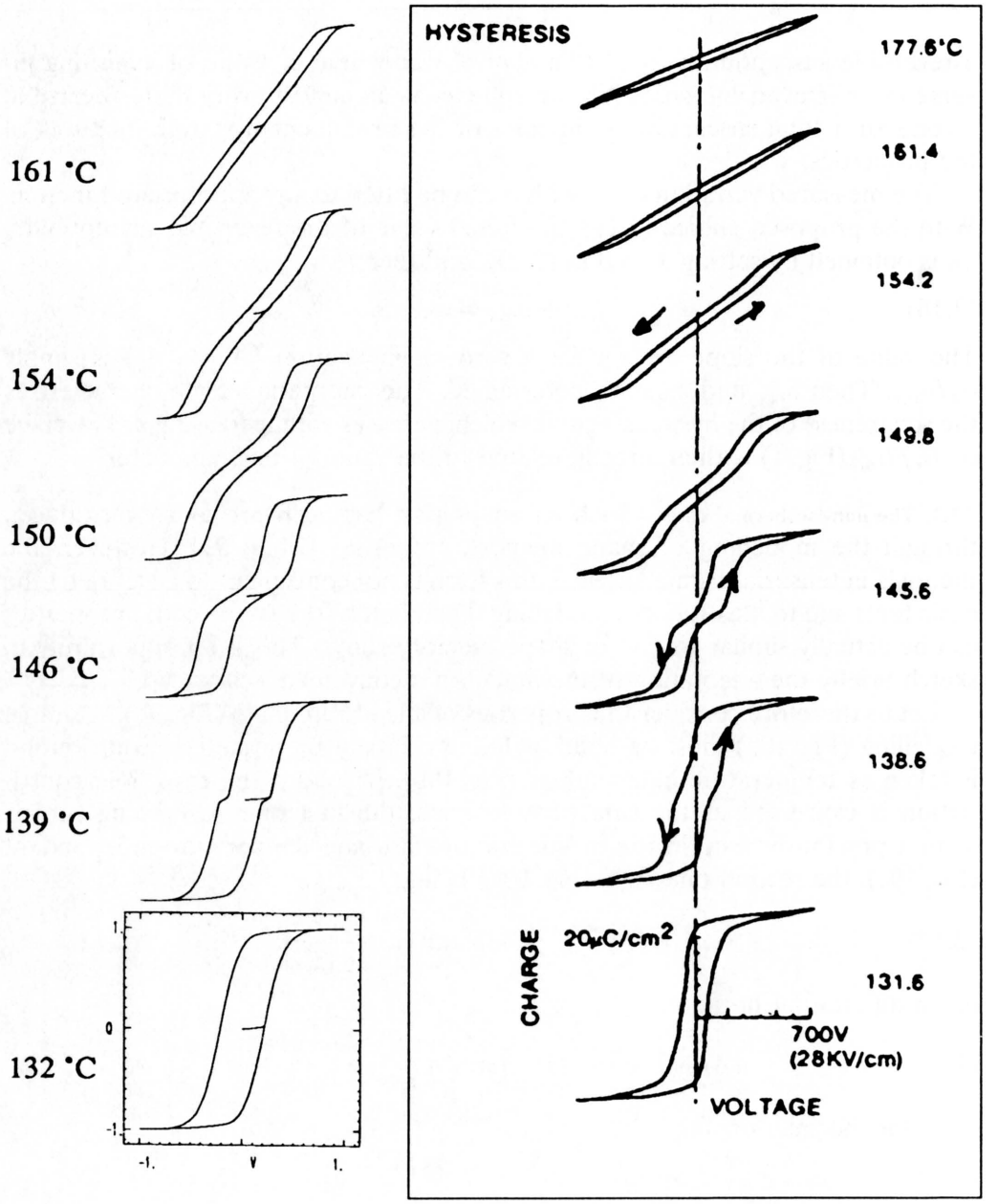

(a) (b)

FIG. 9. Qualitative modelling of the properties of lead Zirconate (a) modelling, (b) experimental results [28].

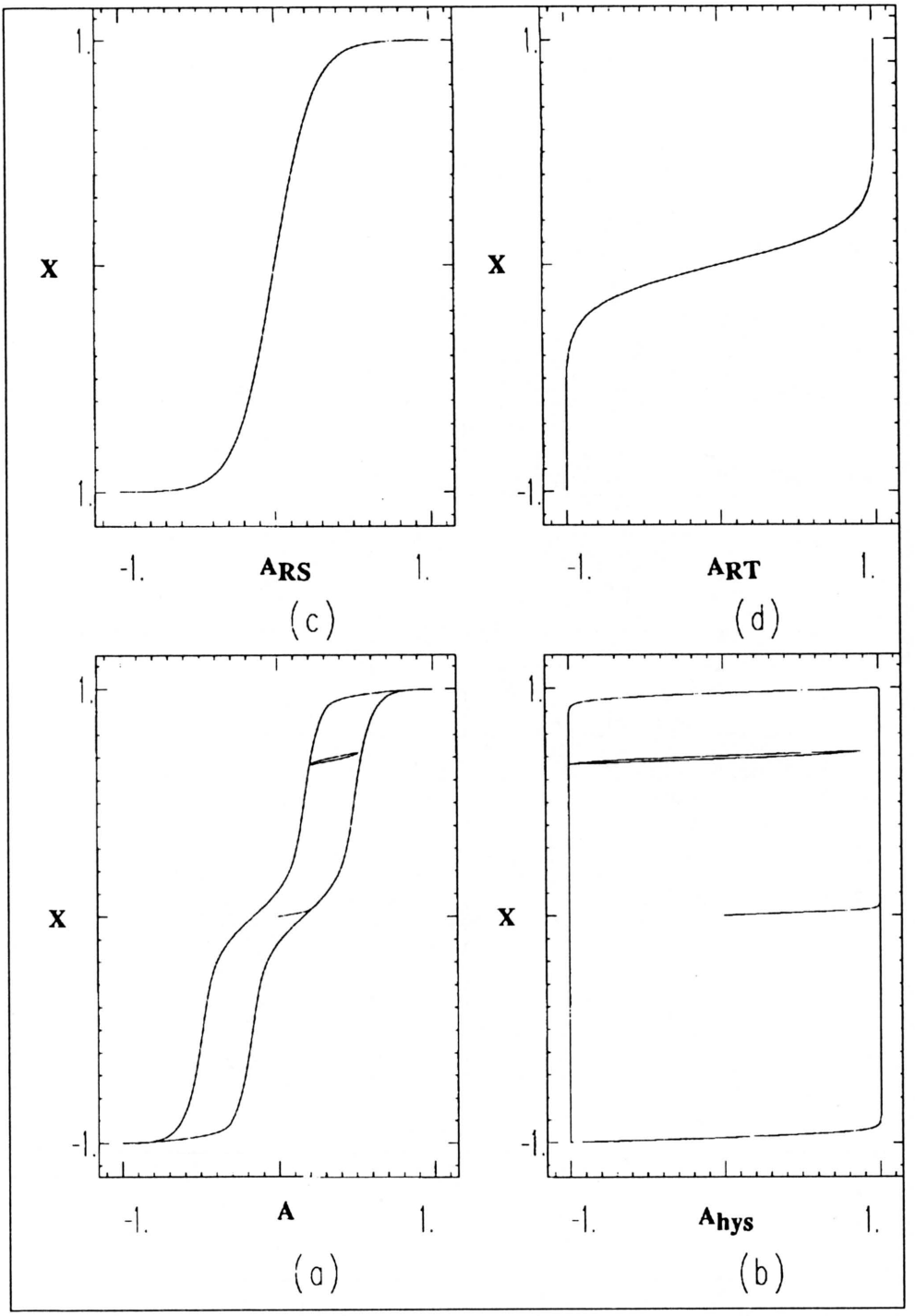

FIG. 10. Modelling of temperature-dependent properties ($A = A_{hys} + A_{RS} + A_{RT}$).

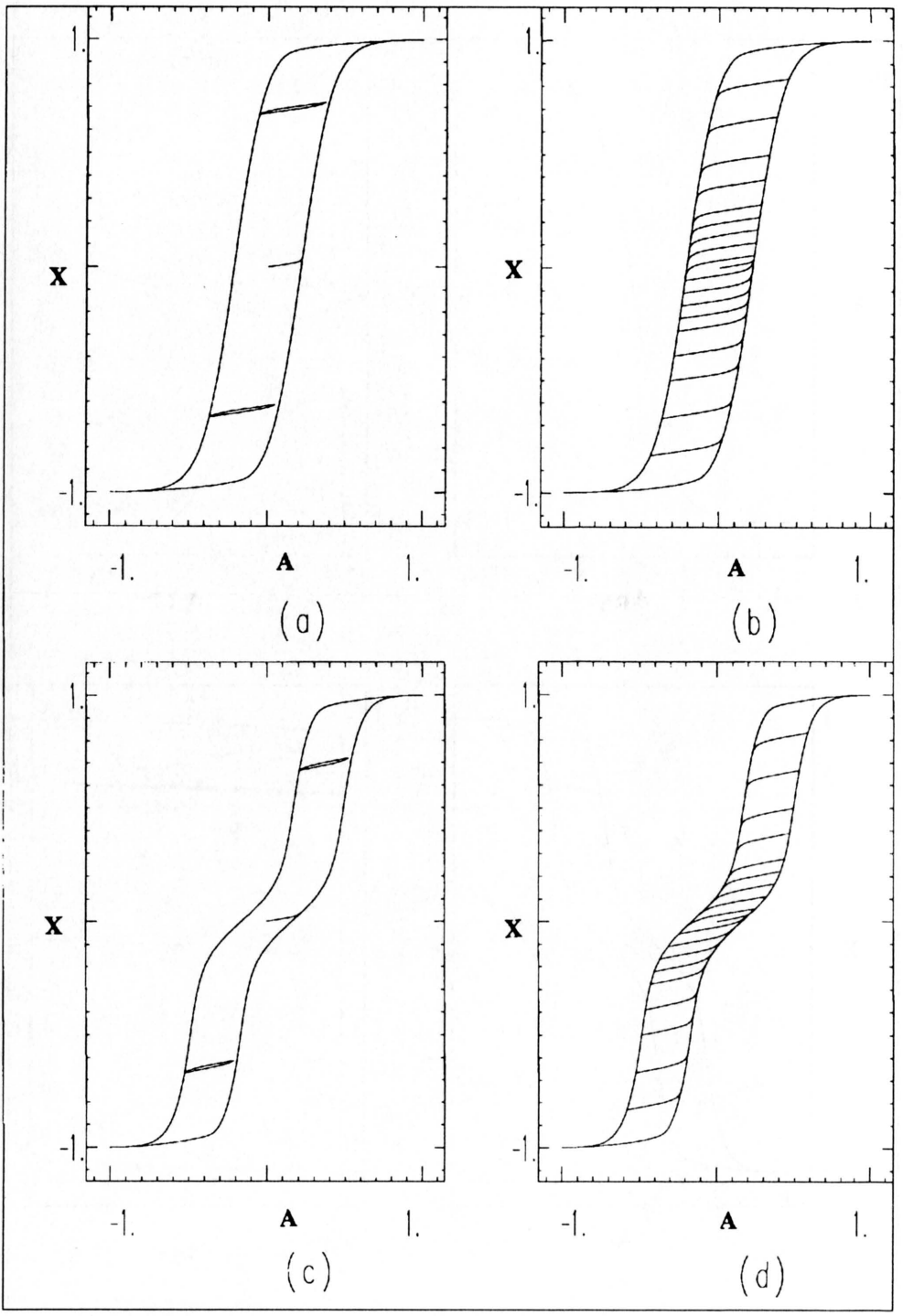

FIG. 11. Features of the cyclic behaviour (a,b) $T = 132°C$ and (c,d) $T = 146°C$.

3. On the vectorial generalization of the scalar models of pure hysteresis and elastohysteresis

3.1. Introduction of a quasi-linear vectorial form

Owing to the implicit definition of the "action" A through the general differential pattern

$$(1.1): \qquad dA = dA_{\text{rev}} + dA_{\text{hys}},$$

the attention must be in the first step focused on the contribution of hysteretic type in order to obtain a vectorial generalization under isothermal condition: at the level of principles and methods this contribution is indeed much more puzzling to define than the reversible one. Writing (2.13) in the form:

$$(3.1) \qquad d(\Delta_R^t A_{\text{hys}}) \equiv dA_{\text{hys}} = a_{\text{hys}} dx + \left[\frac{-a_{\text{hys}}}{(\Delta_R^t A_{\text{hys}})^2}\left(\frac{\Delta_R^t A_{\text{hys}}}{\omega A_0}\right)^c\right] \times (\Delta_R^t A_{\text{hys}} dx)\Delta_R^t A_{\text{hys}},$$

one notices that the scalar differential-difference pattern is

$$(3.2) \qquad \dot{A}_{\text{hys}} = a_1 \dot{\alpha} + a_2 \Delta_R^t A_{\text{hys}}, \qquad a_2 = \beta_{4A}\Phi_A, \qquad \Phi_A = \Delta_R^t A_{\text{hys}} \dot{\alpha},$$

where a_2 is a scalar functional associated with the limit A_0 of "plastic" type, and where Φ_A is the intrinsic dissipation. As well as in the case of the tensorial generalization [19, 20], one can make use of the quasi-linear vectorial form suggested by (3.2):

$$(3.3) \qquad \begin{aligned} &\dot{\mathbf{A}}_{\text{hys}} = a_1 \dot{\boldsymbol{\alpha}} + a_2 \Delta_R^t \mathbf{A}_{\text{hys}}, \qquad a_2 = \beta_{4A}\Phi_A, \\ &\Phi_A \overset{\text{Symb}}{=} \Delta_R^t \mathbf{A}_{\text{hys}} \cdot \dot{\boldsymbol{\alpha}}, \qquad \Delta_R^t \mathbf{A}_{\text{hys}} \overset{\text{Def}}{=} \mathbf{A}_{\text{hys}} - {}_R\mathbf{A}_{\text{hys}}. \end{aligned}$$

Then one knows [19, 20] that the main difficulties occur concerning the definitions of the rate operator, of the intrinsic dissipation Φ_A and of the scalar functional a_2. In order to introduce the solution brought by the proposed pattern it is convenient, firstly, to give a rather detailed analysis of some basic hints, and secondly to suggest the relationships between this first sketch and the usual qualitative features of the well-known experimental results obtained at macro or micro-scale (Sec. 3.2 and 3.3, respectively).

3.2. Basic hints concerning the Preferred Reference Frames, the dragged along material properties and the Ilyushin representation

In this paragraph the subscript "hys" is omitted for the sake of simplicity, but always implicit. When some hints must be given regarding the reversible features, the subscript "rev" is explicit.

3.2.1. Preferred Reference Frames (PRF) and dragged along material properties

i. Let us deal firstly with the difficulty concerning the rate operator. As well as in the tensorial (mechanical) case, the vectorial pattern will be *defined* introducing orthonormal PRF, where the reference external "actions" ${}_R\mathbf{A}$ and the tensorial material parameters are dragged along. The relevant rate of **A** is then the partial "time" derivative in the relevant PRF, which remains to be defined.

ii. The simplest case is that of a *rigid* material under isothermal condition and exhibiting a single hysteretic process. The relevant PRF is associated with the initial material direction of the usual (quasi-reversible) anisotropy of the initial "demagnetized" state (cf. Sec. 2.2.5 iii and iv).

Accordingly, the material parameters are defined once for all in this initial "demagnetized" state through two tensors: firstly, the second order tensor $\boldsymbol{\mu}$ of reversible linear behaviour, and secondly the second order tensor P associated with the (entirely) irreversible limit behaviour of "plastic" type. This definition results in the usual linear form describing infinitesimal evolutions in the vicinity of the demagnetized state:

$$\dot{A}_i = \mu_0 d_i, \qquad \mu_0 d_i = \mu_{ij}\,\dot{\alpha}_j, \qquad \dot{} \equiv \frac{\partial}{\partial t}, \tag{3.4}$$

and in the quadric of anisotropy of the limit irreversible behaviour:

$$P_{\lim_{ij}} A_i A_j = A_0^2. \tag{3.5}$$

The linear (infinitesimal) behaviour (3.4) is written under a form taking into account from now on the approach proposed in the case of the anisotropic deformable medium.

iii. Another simple case is that of a *rigid* isothermal material exhibiting two uncoupled or coupled hysteretic processes (denoted (**E**, **D**) and (**H**, **B**) or (**E**, **P**) and (**H**, **M**)). The approach is similar. The previous linear forms are now:

$$\begin{aligned} \dot{E}_i &= \mu_0 d_i^E, \qquad \mu_0 d_i^E = \begin{cases} \mu_{ij}^E\,\dot{D}_j \\ \text{or } \mu_{ij}^E\,\dot{P}_j \end{cases}, \\ \dot{H}_i &= \mu_0 d_i^H, \qquad \mu_0 d_i^H = \begin{cases} \mu_{ij}^H\,\dot{B}_j \\ \text{or } \mu_{ij}^H\,\dot{M}_j \end{cases}, \end{aligned} \tag{3.6}$$

where **D** and **B** are the displacement and induction vectors, respectively, and where $\underline{\boldsymbol{\mu}}^E$ and $\underline{\boldsymbol{\mu}}^H$ are the *inverse* of the dielectric permittivity (or susceptibility) tensor and of the magnetic permeability or susceptibility tensor, respectively. In the irreversible range the limit behaviour is defined by

$$P^E_{\lim_{ij}} E_i E_j = E_0^2, \qquad P^H_{\lim_{ij}} H_i H_j = H_0^2. \tag{3.7}$$

One recalls that **E** and **H** denote purely hysteretic fields and that, at this stage of the analysis, the relationship between these fields and the Applied External Extrinsic (AEE) fields in not conspicuous even if it may be foreseen through (2.3). This point is studied below (Sec. 3.3).

iv. The above presentation is supplemented considering now the case of a *deformable* material exhibiting both the elastic-plastic hysteresis and the previous couple of vectorial hysteresis. For the sake of simplicity, the analysis is restricted to a two-dimensional sketch.

In the initial demagnetised neutral state of the material element $M(0)$ the mechanical and non mechanical PRF are PRF_{m0} PRF_{E0} PRF_{H0}, respectively (Fig. 12a, where PRF_{H0} is omitted for the sake of simplicity). The directions of the PRF are associated with those of the mechanical and non-mechanical *initial* anisotropic directions. The relative orientations are O_m^E and O_m^H, respectively (Fig. 12a).

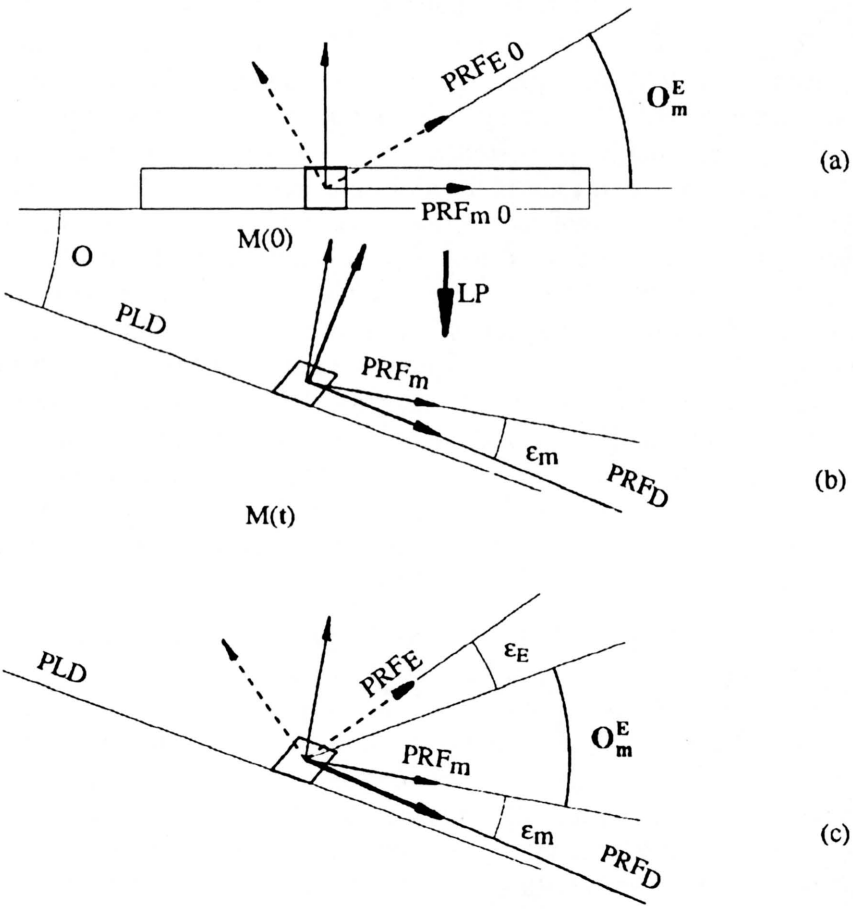

FIG. 12. Sketch of the evolution of the Preferred Reference Frame (PRF).

Due to the Loading Process (LP), the current configuration $M(t)$ of $M(0)$ is "rotated" and strained (by stretching and shearing). Let us denote by PRF_D (Fig. 12b) the reference frame defined by the rotation of the principal direction of strain rate D: the PRF_D is "almost in the strip" because the rotation of the PRF_D is approximately the rotation O of the Preferred Loading Direction (PLD) (cf. Fig. 12b where the current PRF_D is represented making implicitly the assumption that its initial orientation is that of PRF_{m0}).

The first basic assumption is: the initial and the limit properties introduced in (3.6) and (3.7) are dragged along in the relevant PRF (the "$\underline{\mu}$" and the "P_{lim}" are given once and for all in the initial state as well as in the rigid cases).

The second basic assumption is as follows: the actual rotation of the PRF_m is almost that of PRF_D, up to a "small" angle ε_m. Consequently, the rotation of the PRF_m is approximately the rotation of the PLD or of the PRF_D, such as suggested in Fig. 12b: the PRF_m are "almost in the strip". It remains obviously to define the "small" angle ε_m. This question is revisited below (Sec. 3.5.4).

The PRF_E and PRF_H being both almost dragged along by the matter, the *relative* orientation of this couple of PRF with respect to the current PRF_m is almost the same as that (O_m^E and O_m^H) in the initial configuration (up to $\varepsilon_m + \varepsilon_E$ and $\varepsilon_m + \varepsilon_H$). The situation is sketched in Fig. 12c, where the angles ε are magnified. Consequently, when each pattern of pure hysteresis is defined in its PRF, it appears only to be a small correction (associated with the ε effect) if the whole set of hysteretic pattern is *expressed* in only one of the PRF, for example the PRF_m or in the PRF_D, or in the frame of an observer. Moreover, the reversible contribution may be defined or expressed in a PRF_{rev} only slightly different from the PRF_D up to ε_{rev}, under the condition that ε_{rev} is a function of kinematics but not a functional: the functional form is indeed admissible for ε_m, ε_E and ε_H but not for ε_{rev}. Let us return to the hysteretic process saying that, finally, up to the rotation ε_n ($n = m, E, H$), the analysis results, with respect to an extrinsic observer, in the consideration, in the PRF_D, for example, of three sets of components associated with the three external "actions" of hysteretic type.

v. Once one is aware of these extrinsic features, one must face the turning point of the analysis. As suggested by the entirely intrinsic one-dimensional case, the intrinsic problems are indeed to define fields like σ, ${}_R\sigma$, $\Delta_R^t\sigma$ but *never* σ *alone, except* in the special case of the first loading along which the set of discrete memory is empty (cf. Sec. 2.2.2, implemented in the case $\omega = 1$). In the pattern the coexistence of A, ${}_RA$ and $\Delta_R^t A$ is inevitable. One knows that the behaviour of pure hysteresis implies a limit behaviour, as suggested by the R^1 model. Moreover, the limit behaviour is defined through a limit surface of the A space (a typical example is the limit surface of plasticity). The behaviour is therefore dependent on the direction of the path with respect to the limit surface and a geometrization

of the pattern is obviously interesting. However one needs a *geometrization* able to give A as a sum: ${}_RA + \Delta^t_R A$. It must be done in a unique space common to A, ${}_RA$ and $\Delta^t_R A$. Then, as well as in the purely mechanical case, it is now necessary to define angular parameters of the *intensive* fields in a space whose axes *are the same* regarding σ, ${}_R\sigma$, $\Delta^t_R\sigma$; E, ${}_RE$, $\Delta^t_R E$; H, ${}_RH$, $\Delta^t_R H$.

This point is immediately interesting in the mechanical case because, for example, it is indeed obvious that the principal directions of the tensors A ${}_RA$ and $\Delta^t_R A$ are not the same, so that the implementation of the associated orientations in a pattern of hysteresis leads to a set of drawbacks, the physical meanings of which are puzzling. In the purely mechanical case this condition has been previously fulfilled with the aid of the Ilyushin representation [19, 20]: the axis of the Ilyushin space are the same for σ, ${}_R\sigma$ and $\Delta^t_R\sigma$ and the principal directions of these tensors are indeed not involved. Moreover, the final expression of the pattern must be invariant with respect to the choice of the initial PRF.

vi. Now let us return to the case where three types of fields are simultaneously involved, one being tensorial and the others vectorial (distinction between polar and axial vectors may be provisionally omitted). The tensorial pattern being from now on outlined [19, 20], it is not necessary to introduce a specific formalism: it is sufficient to define a one-to-one invariant linear mapping between each vector **A** (in PRF_A) and its associated purely deviatoric tensor $\overline{\mathbf{A}}$ (in PRF_A): the definition of $\overline{\mathbf{A}}$ is chosen in order to obtain a three-parameter geometrical object with only one invariant. Finally, in this introductory paper one must face the definition of three similar tensorial patterns defined through the components in the three corresponding PRF_A (endowed with slightly different evolutions, due to the small rotations ε). From the three sets of components one can obtain the three Ilyushin representations in a *unique* space I^3 in spite of the fact that the *definition* of the pattern implies the process of dragging along by the matter through the *components* in the *three* PRF_A. No transformations of coordinates are implied at the level of the definition in the Ilyushin space associated to the three PRF_A, where the components are physically meaningful and reflecting the three discrete memory processes. On the contrary, an external extrinsic observer may record second order coupling effects in the special reference frame where he specifies the AEE fields. Moreover, some first order "absolute" coupling effect can be defined in the "absolute" I^3 space; for example, we can substitute for Φm in the mechanical pattern the total intrinsic dissipation $\Phi t = \Phi m + \Phi e + \Phi h$ or substitute for Φe and Φh the sum $\Phi em = \Phi e + \Phi h$. It remains to introduce the formal features of the basic tools (Sec. 3.2.2 below).

3.2.2. Basic hints concerning the Ilyushin representation. For reasons introduced below (Sec. 3.5) it is useful to implement a special representation of a polar vector: the features of this representation are given in this paragraph.

i. The Ilyushin representation of a *purely deviatoric* symmetric second order tensor $\overline{\mathrm{A}}$ is

$$
\begin{aligned}
\overline{A}^{11} &= \sqrt{\frac{2}{3}} Q_A (1 - \cos^2\theta_{A1} - \cos^2\theta_{A2} - \cos^2\theta_{A3})^{1/2} \cos\varphi_A^d, \\
\overline{A}^{22} &= \sqrt{\frac{2}{3}} Q_A (1 - \cos^2\theta_{A1} - \cos^2\theta_{A2} - \cos^2\theta_{A3})^{1/2} \cos\left(\varphi_A^d - \frac{2\pi}{3}\right), \\
\overline{A}^{33} &= \sqrt{\frac{2}{3}} Q_A (1 - \cos^2\theta_{A1} - \cos^2\theta_{A2} - \cos^2\theta_{A3})^{1/2} \cos\left(\varphi_A^d + \frac{2\pi}{3}\right), \\
\overline{A}^{23} &= \frac{1}{\sqrt{2}} Q_A \cos\theta_{A1}, \\
\overline{A}^{31} &= \frac{1}{\sqrt{2}} Q_A \cos\theta_{A2}, \\
\overline{A}^{12} &= \frac{1}{\sqrt{2}} Q_A \cos\theta_{A3}.
\end{aligned}
\tag{3.8}
$$

The five parameters of the geometrical object are Q_A, φ_A^d, θ_{A1}, θ_{A2}, θ_{A3}. Only the first one is invariant: the second invariant φ_A is a function of φ_A^d and $\theta_{A1,2,3}$ (see for example the simple form (3.11) associated to the special case (3.9)). Regarding the vectorial equivalence one considers only a three parameters case: Q_A, φ_A^d, θ. *A priori* θ may be such as $\theta = \theta_{A1} = \theta_{A2} = \theta_{A3}$ or $\theta = \theta_{A1}$, $\theta_{A2} = \theta_{A3} = 0$ or $\theta = \theta_{A2}$, $\theta_{A1} = \theta_{A3} = 0$ or $\theta = \theta_{A3}$, $\theta_{A1} = \theta_{A3} = 0$.

The distinction between the last cases is obviously irrelevant. The first one is unnecessarily superabundant regarding the θ_i angles. Then one considers the representation (3.8) reduced to the form

$$
\begin{aligned}
\overline{A}_{11} &= \sqrt{\frac{2}{3}} Q_A \sin\theta \cos\varphi_A^d, \\
\overline{A}_{22} &= \sqrt{\frac{2}{3}} Q_A \sin\theta \cos\left(\varphi_A^d - \frac{2\pi}{3}\right), \\
\overline{A}_{33} &= \sqrt{\frac{2}{3}} Q_A \sin\theta \cos\left(\varphi_A^d + \frac{2\pi}{3}\right), \\
\overline{A}.. &= \frac{1}{\sqrt{2}} Q_A \cos\theta \quad (.. \Leftrightarrow 23 \text{ or } 31 \text{ or } 12),
\end{aligned}
\tag{3.9}
$$

$$
\begin{aligned}
&\text{if}: \quad 23 \Leftrightarrow .. \quad \text{then}: \quad \overline{\mathrm{A}} = \overline{A}_{11}\mathbf{h}_1 \otimes \mathbf{h}_1 + \overline{\mathrm{A}}..; \\
&\overline{\mathrm{A}}.. = \overline{A}_{22}\mathbf{h}_2 \otimes \mathbf{h}_2 + \overline{A}_{33}\mathbf{h}_3 \otimes \mathbf{h}_3 + A..(\mathbf{h}_2 \otimes \mathbf{h}_3 + \mathbf{h}_3 \otimes \mathbf{h}_2),
\end{aligned}
$$

where $\mathbf{h}_i$ $(i = 1, 2, 3)$ denote the base vectors of the relevant PRF.

The case

$$\overline{A}_{11} = \sqrt{\frac{2}{3}} Q_A \sqrt{1 - 3\cos^2\theta}\cos\varphi_A^d; \quad \ldots$$

$$\overline{A} = \frac{1}{\sqrt{2}} Q_A \cos\theta = \overline{A}_{23} = \overline{A}_{31} = \overline{A}_{12}, \tag{3.10}$$

is not implemented (see (3.15)).

One knows that the phase φ_A of $\overline{A}$ defined following (3.9) is

$$\cos 3\varphi_A = f(4f^2 - 3), \qquad f = \sin\theta\cos\varphi_A^d = \cos\varphi_A \tag{3.11}$$

with, obviously,

$$\begin{aligned}
\cos 3\varphi_A^d &= \sqrt{6}\, 3\overline{\mathrm{III}}_A^d \big/ (2\overline{\mathrm{II}}_A^d)^{3/2}, \\
2\overline{\mathrm{II}}_A^d &= (q^d)^2 = Q_A^2 - 2A_{23}^2 = \sum_1^3 (\overline{A}_{ii})^2 = \mathrm{tr}\left[(\overline{A}^d)^2\right], \\
3\overline{\mathrm{III}}_A^d &= \sum_1^3 (\overline{A}_{ii})^3 = \mathrm{tr}\left[(\overline{A}^d)^3\right], \\
\cos 3\varphi_A &= \sqrt{6}\, 3\overline{\mathrm{III}}_A \big/ Q_A^3.
\end{aligned} \tag{3.12}$$

ii. Let us consider the following splitting of **A**:

$$\begin{aligned}
\mathbf{A} \equiv A^1\mathbf{h}_1 + A^2\mathbf{h}_2 + A^3\mathbf{h}_3 &= \mathbf{A}^{\|} + \mathbf{A}^d = q_{\mathbf{A}}^{\|}\mathbf{n} + \mathbf{A}^d \\
&= (\mathbf{h}_1 + \mathbf{h}_2 + \mathbf{h}_3) q_{\mathbf{A}}^{\|} \big/ \sqrt{3} + \sqrt{\frac{2}{3}} q_{\mathbf{A}}^d \left[\mathbf{h}_1 \cos\varphi_{\mathbf{A}} + \mathbf{h}_2 \cos\left(\varphi_{\mathbf{A}} - \frac{2\pi}{3}\right)\right. \\
&\qquad \left. + \mathbf{h}_3 \cos\left(\varphi_{\mathbf{A}} + \frac{2\pi}{3}\right)\right].
\end{aligned} \tag{3.13}$$

The role played by the direction of **n** ("out" of the direction $\mathbf{h}_1$, $\mathbf{h}_2$, $\mathbf{h}_3$) is then similar to that played by the Ilyushin direction associated with θ and $\overline{A}..$, which is also "out" of the directions 1, 2, 3 of the "deviatoric" Ilyushin plane. One has obviously

$$\mathbf{A}^{\|}\cdot\mathbf{A}^d = 0, \qquad Q_{\mathbf{A}}^2 = (q^{\|})^2 + (q^d)^2, \qquad \tan\theta_{\mathbf{A}} = \frac{q^d}{q^{\|}} \equiv \frac{Q_{\mathbf{A}}\sin\theta_{\mathbf{A}}}{Q_{\mathbf{A}}\cos\theta_{\mathbf{A}}}$$

and consequently,

$$
\begin{aligned}
Q_{\mathbf{A}} &= \left(\sum_1^3 (A^n)^2\right)^{1/2}, \qquad \cos\theta_{\mathbf{A}} = \left(\sum_1^3 A^n\right) \Big/ (\sqrt{3} Q_{\mathbf{A}}), \\
q^{\|} &= Q_{\mathbf{A}} \cos\theta_{\mathbf{A}}, \qquad q^d = Q_{\mathbf{A}} \sin\theta_{\mathbf{A}}, \\
q^d &= \sqrt{\frac{2}{3}} \left[(A^1)^2 + (A^2)^2 + (A^3)^2 - A^2A^3 - A^3A^1 - A^1A^2\right]^{1/2}, \\
\cos 3\varphi_{\mathbf{A}} &= \sqrt{6}\, 3\overline{\mathrm{III}}^d_{\mathbf{A}} \big/ (q^d)^3, \\
3\overline{\mathrm{III}}^d &= \sum_1^3 (\overline{A}^n)^3, \qquad \overline{A}^n = A^n - q^{\|}/\sqrt{3}.
\end{aligned}
\tag{3.14}
$$

The splitting (3.13) results in the purely deviatoric tensor $\overline{\mathsf{A}}$ which is "Ilyushin equivalent" to **A** because it is defined following the formulae

$$
\begin{aligned}
Q_A &\equiv Q_{\mathbf{A}}, \qquad \varphi^d_A \equiv \varphi_{\mathbf{A}}, \qquad \theta_A \equiv \theta_{\mathbf{A}}, \\
3\overline{A}_{22} &= -A_1 + 2A_2 - A_3, \qquad A_1 = \overline{A}_{11} + \sqrt{\frac{2}{3}} A.., \\
3\overline{A}_{33} &= -A_1 - A_2 + 2A_3, \qquad A_2 = \overline{A}_{22} + \sqrt{\frac{2}{3}} A.., \\
\sqrt{6}\overline{A}.. &= A_1 + A_2 + A_3, \qquad A_3 = \overline{A}_{33} + \sqrt{\frac{2}{3}} A.., \\
3\dot{A}_{22} &= -\dot{A}_1 + 2\dot{A}_2 - \dot{A}_3, \qquad \dot{A}_1 = \dot{\overline{A}}_{11} + \sqrt{\frac{2}{3}} \dot{A}.., \\
&\vdots
\end{aligned}
\tag{3.15}
$$

Each path $\dot{A}_i(t)$ in the PRF_A is associated with a path in the space I^3: with the aid of the angles φ^d and θ the geometrical sketches are obvious. It is possible to substitute for a direct vectorial approach $\dot{\mathbf{A}}_{\mathrm{hys}} \Leftrightarrow \dot{\boldsymbol{\alpha}}$ a tensorial pattern $[\ ]_I$ (which is from now on outlined [19, 20]), following the formula

$$
\dot{\mathbf{A}}_{\mathrm{hys}} \Leftrightarrow \dot{\mathsf{A}} \Leftrightarrow \left[\dot{\mathsf{A}} \Leftrightarrow \mathsf{D}\right]_I \Leftrightarrow \mathsf{D} \Leftrightarrow \mathbf{d} \Leftrightarrow \dot{\boldsymbol{\alpha}}. \tag{3.16}
$$

It is also clear that (3.15) is useful in the anisotropic case in order to substitute for a property such as P_{lim} (Eqs. (3.5) and (3.7)) acting on **A**, a property acting on A. In the isotropic case, for example, one substitutes for the (matricial) form

$$
|A_1 \ A_2 \ A_3| \left|1\right| \left|\begin{matrix} A_1 \\ A_2 \\ A_3 \end{matrix}\right| = A_1^2 + A_2^2 + A_3^2 = A_0^2
$$

the form

$$|\overline{A}_{11}\ \overline{A}_{22}\ \overline{A}_{33}\ \overline{A}_{..}|\left|1\right|\left|\begin{matrix}\overline{A}_{11}\\ \overline{A}_{22}\\ \overline{A}_{33}\\ \overline{A}_{..}\end{matrix}\right| = \overline{A}_{11}^2 + \overline{A}_{22}^2 + \overline{A}_{33}^2 + 3\frac{2}{3}A^2$$

$$= \sum_1^3 \left(\overline{A}_{nn} + \sqrt{\frac{2}{3}}A\right)^2 = Q_A^2 = A_0^2,$$

which is a similar (matricial) form. The Mises-like triclinic case, where

$$|A_1\ A_2\ A_3|\left|\begin{matrix}a & f & e\\ f & b & d\\ e & d & c\end{matrix}\right|\left|\begin{matrix}A_1\\ A_2\\ A_3\end{matrix}\right| = A_0^2$$

results in

$$|\overline{A}_{11}\ \overline{A}_{22}\ \overline{A}_{33}\ \overline{A}_{..}|\left|\mathsf{P}\right|\left|\begin{matrix}\overline{A}_{11}\\ \overline{A}_{22}\\ \overline{A}_{33}\\ \overline{A}_{..}\end{matrix}\right| = A_0^2,$$

$$\left|\mathsf{P}\right| = \left|\begin{matrix} a & f & e & \sqrt{\frac{2}{3}}(a-d)\\ & b & d & \sqrt{\frac{2}{3}}(b-e)\\ \text{sym} & & c & \sqrt{\frac{2}{3}}(c-f)\\ & & & P_{44}\end{matrix}\right|, \qquad P_{44} = \frac{2}{3}[a+b+c+2(d+e+f)].$$

A preliminary remark is as follows: even in the isotropic case and when the limit condition is defined in the PRF_A through $\mathsf{A}^2 = A_0^2$ (resp $\mathbf{A}^2 = A_0^2$), the shape of the limit surface in I^3 is not obvious (see (3.11)). A short hint is obtained through the case defined with (3.9): $\overline{\mathsf{A}} = \overline{A}_{11}\mathbf{h}_1 \otimes \mathbf{h}_1 + \overline{\mathsf{A}}_{..}$ ($23 \Leftrightarrow \cdot\cdot$) because the form may suggest the result (the surface in I^3 is of revolution with respect to the axis 1).

The meaningful remarks are as follows: The substitution (3.15) is permitted regarding scalar, non-directional properties, but not in order to express the properties of material symmetry. In other words, it does not hold for the anisotropic parts of the relations (3.4) or (3.6). Consequently, the use of (3.16) implies that the directional properties act on the relation between $\mathbf{d}$ and $\dot{\boldsymbol{\alpha}}$ but not in the

constitutive scheme $[\ ]_I$ of the I^3 space: this remark is relevant regarding the classical coupling effects. It remains now to give some hints concerning the *physical* meaning of the fields A which are neither the AEE fields nor the usual depolarization fields, nor the spontaneous polarization field.

3.3. One-dimensional sketch of the physical roots of the principles and methods introduced above (Sec. 3.2)

The present paragraph may be regarded as an attempt to *bring nearer* two different approaches: the mechanical approach suggested by one of the authors and the classical treatment of polarized system. The latter starts from Maxwell's equations and implements a multipolar analysis resulting in densities: ϱ, P, Q... ; M, ... of electric charge, polarization ... (as spatial averages of multipole moments) and the series

$$\mathcal{P} = D - \varepsilon_0 E = P - \operatorname{div} Q + \dots ,$$
$$\mathcal{M} = (1/\mu_0)B - H = M + \dots$$

generally taken as sufficiently relevant under the usual truncated forms:

$$\varepsilon_0 E + P = D, \qquad \mu_0(H + M) = B.$$

i. In order to modify the sketch of the mechanical approach, the first step may be to consider not only the material itself but also an ideal, very rigid, pianowire-like continuum, the methodological role of which is similar to that of the vacuum: it is obviously endowed with large elastic limit (10^3 times that of the actual material under consideration). The second step is to make use of the electromagnetic convention to sketch the qualitative features of the materials: the "actions" are taken as abscissae. The third step is to distinguish reversible and irreversible behaviours (Fig. 13a, b).

The mechanical polarization is therefore P_m. The features of the "new" or "unusual" mechanical sketch so obtained are as follows. Firstly the reversible (linear or not) behaviour may be studied through P_m as well as through $\sigma(\varepsilon)$ or $\varepsilon(\sigma)$, without introducing basic drawbacks. Obviously such convention is much more reasonable if the initial actual compliance $s(0)$ is taken as a reference ($\mu(0)$ instead of μ_0, $\varepsilon(0)$ instead of ε_0). Secondly, P_m is endowed with the usual property: it is a positive polarization except in the irreversible case where it may change the sign (P_{m1} and P_{m3}). The third point is that P_m is not necessarily *a priori* interesting in the hysteretic case. It may be misleading if the relevant intensive variable is $\Delta^t_R\sigma$, if the relevant rate is the strain rate $\dot{\varepsilon}$, and if the relevant power is the internal intrinsic power: $-\sigma\dot{\varepsilon}$. The consequence is simple: it is at least interesting to study the spontaneous polarization through: σ, $\Delta^t_R\sigma$, $\dot{\varepsilon}$ instead of P_m. Following this last approach σ_g is a *result*, of discrete memory form, referred to the initial compliance. Obviously P_m is a similar result, but referred

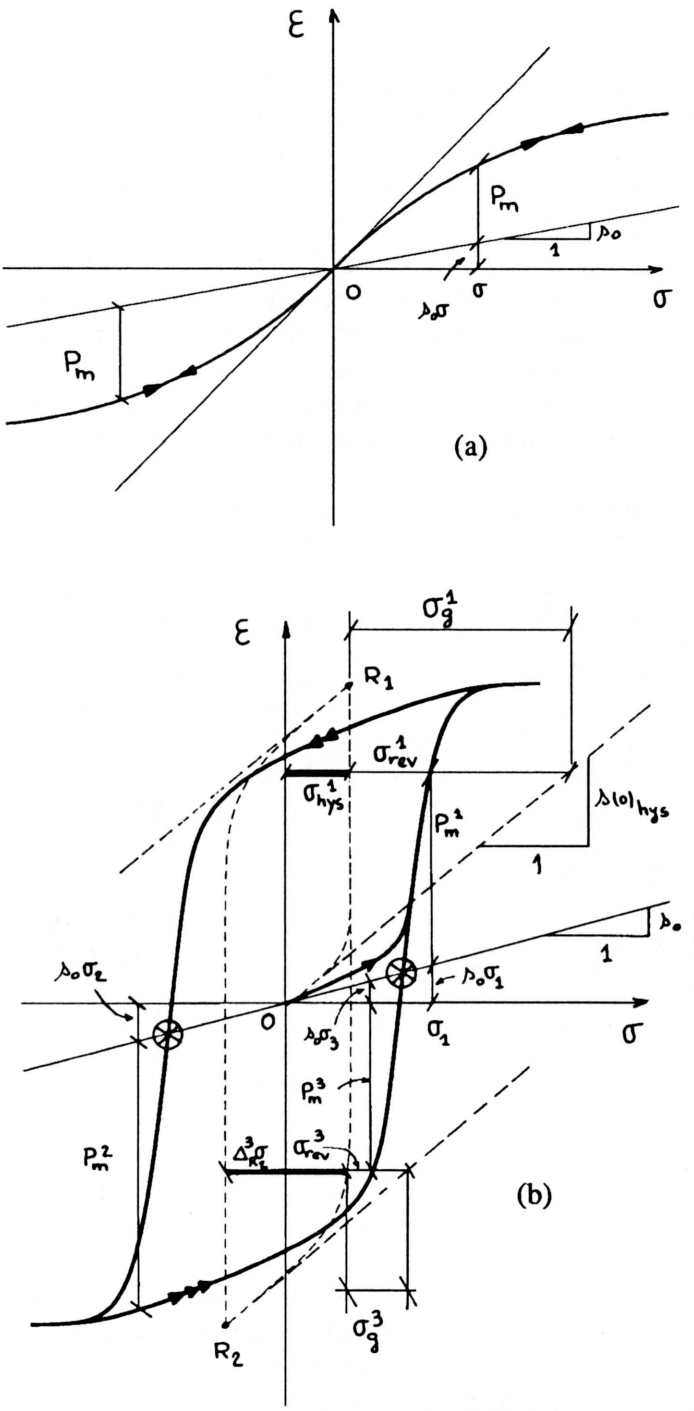

FIG. 13. Mechanical constitutive properties presented with the convention of the polarized materials theory (a) case of reversible properties (b) case of hysteretic properties.

to a fictitious continuum, and therefore less interesting. Under the assumption regarding the depolarizing shape effects, the fields E and H which have been involved are similar to σ. A constitutive definition concerning σ, E and H may be *expressed* through σ_g and P_m or through $\Delta_0^t H - \mu_0$ (vacuum) $\Delta_0^t B$, if it is necessary to exhibit a display compatible with the standard presentation of polarization.

ii. It is hardly necessary to add that the approach using P_m is associated with a splitting process of the extensive variable (cf. Sec. 2.1). However, it remains necessary to give some hints regarding the compatibility with the microscopic processes of an approach involving A, ${}_R A$, $\dot{\alpha}$. Let us consider for example the magnetic case. The comparison of the basic mechanical and magnetic processes are sketched in Fig. 14a, b. The analogy is made conspicuous between the strip

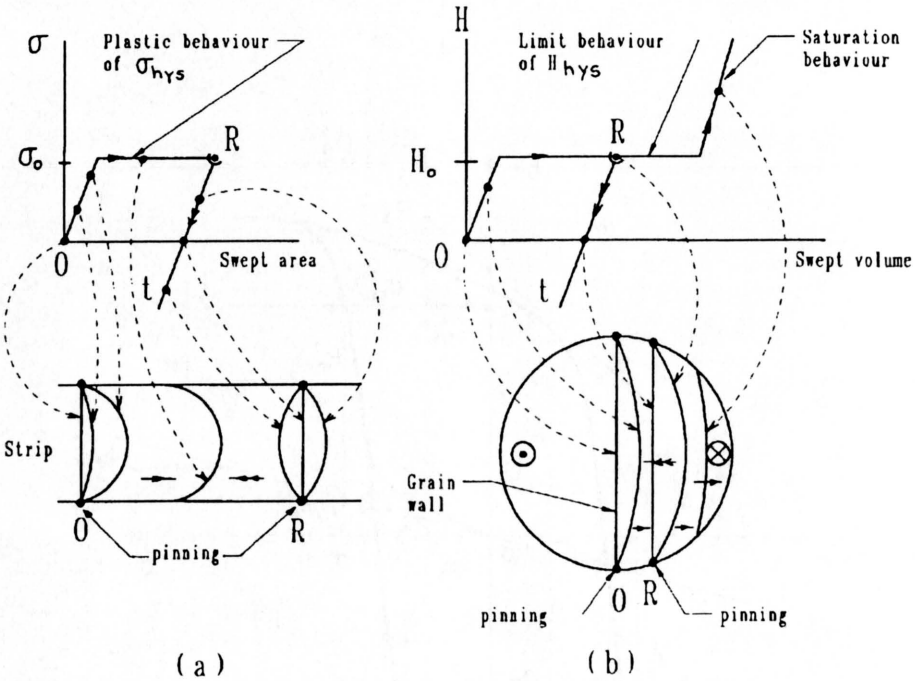

FIG. 14. Sketch of the Neel process. Dragging along of ${}_R\sigma$ (resp. ${}_R H$) from the state R to the current state at t: the process associated with the pinning at R acting as a reference for the process at $t > t_R$. The previous reference was O acting for $t \in]0, t_R]$: ${}_R A$ is piecewise constant.

free of defects and the spherical grain; the dislocation and the walls; the swept area and the swept volume; the internal stress field σ and the field H; the critical pinning stress σ_0 and the field H_0; the reversible displacement under σ smaller than σ_0 and under the field H smaller than H_0; the irreversible sliding for σ and H equal to σ_0 and H_0, respectively. However, the magnetic process is more sophisticated, resulting in the saturation property: when the wall is sufficiently far from the center of the grain, a strong field is necessary to obtain a decreasing surface of the wall, a process "almost" reversible which is associated with a very

small increase of the swept volume: the process is the addition of a reversible process and of a pure hysteretic process. The former needs a strong field; the latter needs not a stronger field than previously to be (slightly) activated under the form of (small) additional swept volume. It is now possible to justify the fact that the polarization notion is not introduced in the first part of the paper (Sec. 2.2.2 relations (2.3) and (2.4)). The associated thermodynamics, the basic hints of the three-dimensional enlargement and the relevance at microlevel are involved in order to introduce some heuristic sketch similar to that given above.

3.4. Formal aspect concerning the vectorial generalization of the reversible contribution

In this paragraph the subscript rev is omitted.

3.4.1. Some hints regarding the nonlinear isotropic case

i. In spite of the fact that the general pattern (1.1) is founded on the addition of reversible and hysteretic *rates* it is interesting, regarding the reversible part, to study the elastic-like approach. If such an approach is convenient, the rate form of the reversible contribution of the whole pattern will be obtained through a "time" derivative. In the isothermal isotropic case some hints must be introduced briefly regarding the *nonlinear* behaviours such as those of limit type or saturation type previously introduced in the one-dimensional analysis through (2.12) and (2.11), respectively. Finally, it is possible (although not necessary in a covariant derivation) to make use of the components in the $\mathrm{PRF}_{\mathrm{rev}}$ (base vectors $\mathbf{h}_i$).

ii. The geometrical relations are:

$$\begin{aligned} \mathbf{n}_\alpha &= n_{\alpha i}\mathbf{h}_i, & n_{\alpha i} &= \alpha_i/Q_{\boldsymbol{\alpha}}, & \mathbf{n}_\alpha\cdot\mathbf{n}_\alpha &= 1, \\ \mathbf{n}_A &= n_{Ai}\mathbf{h}_i, & n_{Ai} &= A_i/Q_{\mathbf{A}}, & \mathbf{n}_A\cdot\mathbf{n}_A &= 1. \end{aligned}$$

In the isotropic case one must obtain

$$\mathbf{n}_A = \mathbf{n}_\alpha, \qquad \frac{A_i}{Q_{\mathbf{A}}} = \frac{\alpha_i}{Q_{\boldsymbol{\alpha}}}, \qquad \mathbf{A}\cdot\boldsymbol{\alpha} = Q_A Q_\alpha .$$

It remains to define the relation between Q_A and Q_α. The approach is founded on the relation

$$\frac{d}{dt}F(Q_\alpha) \equiv \frac{dF}{dQ_\alpha}\frac{dQ_\alpha}{d\alpha_i}\frac{d\alpha_i}{dt} = A_{\mathrm{revi}}\frac{d\alpha_i}{dt},$$

$$Q_\alpha^2 = \sum_1^3 (\alpha_i)^2, \qquad \frac{Q_\alpha}{d\alpha_i} = \frac{\alpha_i}{Q_\alpha}.$$

The linear case:

$$A_i = \mu\alpha_i, \qquad Q_A = \mu Q_\alpha$$

is obtained with $F_L = \mu Q_\alpha^2/2$, and the genealizations of (2.12) and (2.11) are

$$A_i = \left(Q_{0r} \tanh \frac{Q_\alpha}{Q_{0r}} a_r\right) \frac{\alpha_i}{Q_\alpha}, \qquad Q_A = Q_0 \tanh \frac{Q_\alpha}{Q_0} a_r,$$

and

$$A_i = \left(\mu Q_S \operatorname{arctanh} \frac{Q_\alpha}{Q_S}\right) \frac{\alpha_i}{Q_\alpha}, \qquad Q_A = \mu Q_S \operatorname{arctanh} \frac{Q_\alpha}{Q_S},$$

respectively. They are obtained with:

$$F_T = \frac{Q_{0r}}{a_r} \ln \coh \frac{Q_\alpha}{Q_0} a_r,$$

and

$$F_S = \mu Q_S \left[\operatorname{arctanh} \frac{Q_\alpha}{Q_S} + \frac{Q_\alpha}{2} \ln(Q_S^2 - Q_\alpha^2)\right],$$

respectively. Potential functions similar to $F_L + F_T$ are also heuristic.

It may be interesting to substitute for F_S a potential G_v (G for Gibbs, v for vacuum) "dual" of $F_L + F_T$, in order to substitute for the saturated behaviour

$$\lim_{Q_A \to \infty} Q_\alpha = Q_S + \frac{Q_A}{\mu_0}.$$

From

$$\begin{aligned}
G_v(Q_A) &= \frac{Q_A^2}{2\mu_0} + \mu Q_S^2 \ln \cosh \left(\frac{Q_A}{\mu Q_S}\right), \\
\frac{dG_v}{dQ_A} &= Q_S \tanh \left(\frac{Q_A}{\mu Q_S}\right) + \frac{Q_A}{\mu_0}, \\
Q_\alpha dQ_A &= dG_v = \alpha_i dA_i, \\
0 &= d(Q_A Q_\alpha) - Q_A(dQ_\alpha) - (dQ_A)Q_\alpha = d(Q_A Q_\alpha) - dF_v - dG_v
\end{aligned}$$

one obtains

$$\begin{aligned}
\alpha_i &= \left(Q_S \tanh \left(\frac{Q_A}{\mu Q_S}\right) + \frac{Q_A}{\mu_0}\right) \frac{A_i}{Q_A}, \\
Q_\alpha &= Q_S \tanh \left(\frac{Q_A}{\mu Q_S}\right) + \frac{Q_A}{\mu_0}.
\end{aligned}$$

iii. It is not interesting to discuss the rate forms starting from the relation:

$$\left(Q_A Q_\alpha^2\right) \dot{A}_i - (Q_\alpha \alpha_i)\left(\sum A_n \dot{A}_n\right) = (Q_\alpha Q_A^2)\dot{\alpha}_i - (Q_A A_i)\left(\sum \alpha_n \dot{\alpha}_n\right).$$

One must, at first, study the nonlinear anisotropy case.

3.4.2. Some hints regarding the nonlinear anisotropic case

i. The constitutive problem is now much more complicated than in the isotropic case. The aim is not to enter into a detailed physical discussion of each possible case of spontaneous electric polarization of ferroelectrics or of magnetization of ferromagnetics above their transition temperature. Consequently, magnetic and electric cases are once more not distinguished.

ii. In the (well known) linear case, the number of independent coefficients is 6, 4, 3 or 2 for the triclinic, monoclinic, orthorhombic and T-T-H (Trigonal, Tetragonal, Hexagonal) systems, respectively. The generic potential function is

$$F_{LT}(\alpha_1^2, \alpha_2^2, \alpha_3^2, \alpha_2\alpha_3, \alpha_3\alpha_1, \alpha_1\alpha_2) = \sum_1^3 \frac{1}{2}\mu_{nn}\alpha_n^2 + \mu_{23}\alpha_2\alpha_3 + \mu_{31}\alpha_3\alpha_1 + \mu_{12}\alpha_1\alpha_2,$$

and $A_{\text{rev}i} = \mu_{ij}\alpha_j$ is obtained from

$$A_i\,\dot{\alpha}_i = \dot{F}_{LT} = (\mu_{11}\alpha_1 + \mu_{12}\alpha_2 + \mu_{13}\alpha_3)\,\dot{\alpha}_1 + (\mu_{21}\alpha_1 + \mu_{22}\alpha_2 + \mu_{23}\alpha_3)\,\dot{\alpha}_2 + (\mu_{31}\alpha_1 + \mu_{32}\alpha_2 + \mu_{33}\alpha_3)\,\dot{\alpha}_3.$$

The form associated with the other systems are easily obtained. For example the TTH case is given by the potential:

$$F_{LTTH} = \frac{1}{2}\mu_1\left(\alpha_1^2 + \alpha_2^2\right) + \frac{1}{2}\mu_3\alpha_3^2$$

written here with the usual convention (principal symmetry axis parallel to the coordinate axis 3).

In the linear case it is simple and straightforward to substitute for an isotropic form an anisotropic property μ_{ij}. The aim is now to perform the same explicit generalization ([2]) starting from closed forms such as $\ln\cosh(x)$ or $x\cdot\operatorname{arctanh}(x)$, and excluding the use of infinite series or some trivial approximation using piecewise continuous functions.

iii. Let us firstly consider the case of the potential function based on the $\ln\cosh(Q_\alpha)$ function. A potential function immediately suggested by the linear case is:

$$F_{TT} = \frac{Q_0^2}{\mu_0}\ln\cosh\left(\frac{\mu_0 L}{Q_0}\right),$$

$$L^2 = \varepsilon_{11}\alpha_1\alpha_1 + \varepsilon_{12}\alpha_1\alpha_2 + \varepsilon_{13}\alpha_1\alpha_3 + \varepsilon_{21}\alpha_2\alpha_1 + \varepsilon_{22}\alpha_2\alpha_2 + \varepsilon_{23}\alpha_2\alpha_3 + \varepsilon_{31}\alpha_3\alpha_1 + \varepsilon_{32}\alpha_3\alpha_2 + \varepsilon_{33}\alpha_3\alpha_3 = \varepsilon_{ij}\alpha_i\alpha_j,$$

$$\dim\varepsilon_{ij} = 1, \qquad \varepsilon_{ij} = \varepsilon_{ji};$$

([2]) Explicit forms of the potential function are not frequently encountered in the theory of finite elasticity [24].

one obtains

$$A_i = \left[\frac{Q_0}{L}\tanh\left(\frac{\mu_0 L}{Q_0}\right)\right]\varepsilon_{ij}\alpha_j,$$

resulting in

$$A_i^0 = \mu_0\varepsilon_{ij}\alpha_j, \qquad n_{Ai}^0 = \frac{Q_\alpha}{Q_A}\mu_0\varepsilon_{ij}n_{\alpha j}, \qquad \dot{Q}_A = \mu_0(\varepsilon_{ji}\varepsilon_{ik}\alpha_j\alpha_k)^{1/2}$$

for weak fields ($\mu_0 L \ll Q_0$), and in

$$A_i^\infty = \frac{Q_0}{L}\varepsilon_{ij}\alpha_j, \qquad n_{Ai}^\infty = \frac{Q_\alpha}{Q_A}\frac{Q_0}{L}\varepsilon_{ij}n_{\alpha j}, \qquad Q_A^\infty = Q_0\left(\frac{\varepsilon_{ji}\varepsilon_{ik}\alpha_j\alpha_k}{\varepsilon_{jk}\alpha_j\alpha_k}\right)^{1/2}$$

for strong fields ($\mu_0 L \gg Q_0$).

Owing to the feature of the asymptotic behaviour that the pattern $dA_{\text{hys}} + dA_{\text{rev}}$ must be eventually able to take into account, it is important that Q_A^∞ tends toward a bounded limit under strong field $\boldsymbol{\alpha}$: this condition is fulfilled.

The case of a potential function based on the function $Q_\alpha \text{arctanh}\, Q_\alpha + \ln(Q_S^2 - Q_\alpha^2)$ is similar. One substitutes for Q_α the form L. Starting from

$$F_{ST} = \mu_0 Q_S L \text{arctanh}\left(\frac{L}{Q_S}\right) + \frac{Q_S}{2}\text{Ln}\,(Q_S^2 - L^2),$$

this simple approach of the saturation behaviour results in:

$$A_i = \left[\mu_0\frac{Q_S}{L}\text{arctanh}\left(\frac{L}{Q_S}\right)\right]\varepsilon_{ij}\alpha_j \qquad \text{and} \qquad A_i^0 = \mu_0\varepsilon_{ij}\alpha_j\,.$$

The saturation limit is defined by $L^2 = Q_S^2$.

iv. If the implementation of truncated series or piecewise continuous approximations are avoided, the approach sketched above implies two similar drawbacks: firstly, it is not easy to define a weak modification of the potential function in order to improve the modelling in the transition range between weak and strong fields; secondly, the shape of the limit surface associated with the asymptotic behaviour cannot be easily specified *a priori* or slightly modified. Such difficulties are well known in the classical theory of finite elasticity and have been underlined (as well as others which are more basic) in a comprehensive study of isotropic finite thermoelasticity [24]. A differential definition in the PRF_{rev} may avoid these drawbacks and is therefore revisited below (Sec. 3.5.2)

3.5. Formal aspects concerning the vectorial generalization of the hysteretic contribution

In this paragraph the suffix "hys" is omitted. It is worthwhile to recall that, in this introductory paper, polar and axial vectors are not distinguished. Moreover, in order to make conspicuous the geometrical properties of the Ilyushin

representation, one makes use of the linear transformation (3.15), substituting for polar vectors a special deviatoric symmetric absolute second order tensor. Such a treatment may appear unskilful in order to deal with the vectorial case. In fact the derivations are not more cumbersome than those obtained through a direct treatment and, moreover, the Ilyushin representation is the only one which is able to give unified treatment, *including the mechanical case when a unified discrete memory pattern is implemented.*

3.5.1. Some hints regarding the isotropic case. Regarding the needs of experiments, the hints given below are almost equivalent to a comprehensive study. However it is not always possible to let the mechanical part of the pattern be restricted by the assumption (3.9) if the aim is to perform a general numerical analysis.

i. Owing to (1.1), (3.3), (3.15) and (3.16), and under relevant provisional assumptions introduced for the sake of simplicity (cf. Sec. 3.2.1, iv, v, vi), it remains to define the pattern of pure hysteresis denoted $\left[\dot{\mathsf{A}} \Leftrightarrow \mathsf{D}\right]_I$ in (3.16).

For the sake of simplicity let us suppose that the irreversible limit behaviour is Mises-like:

$$Q_A^2 = \operatorname{tr}\mathbf{A}^2 = A_0^2,$$

and that the mechanical process is restricted to the simple particular form (3.9) (3.12) concerning purely deviatoric symmetric second-order tensors. If the vectorial constitutive problem $(\dot{\mathbf{A}}, \dot{\boldsymbol{\alpha}})$ is solved in a deviatoric form following (3.15), then the constitutive patterns regarding $(\dot{\underline{\sigma}}, \dot{\overline{\mathsf{D}}})$, $(\dot{\mathbf{H}}, \dot{\mathbf{B}})$, $(\dot{\mathbf{E}}, \dot{\mathbf{D}})$ are similar and will be denoted by a generic single one $(\dot{\overline{A}}, \dot{\overline{D}})$. Accordingly, the forms recalled below are not new for the reader knowing all about the current state of the theory [19, 20]. The generic form which is Ilyushin-equivalent to $(3.3)_1$ is then, in the PRF_A:

$$\frac{\partial}{\partial t}\Delta_R^t \overline{A}^{ij} = \dot{\overline{A}}^{ij} = a_1 \dot{\overline{D}}^{ij} + a_2 \Delta\overline{A}^{ij} \qquad (A \equiv \overline{\sigma}, E, H), \quad \mathbf{A} = a_1\mathbf{d} + a_2\Delta\mathbf{A}. \tag{3.17}$$

ii. The rate-independence of (3.17) is defined in a linear form by

$$\begin{aligned} a_1 &= 2\mu_A, \qquad \dim \mu_A = \dim A, \\ a_2 &= \alpha_4 \overline{M} + \alpha_6 \overline{N}^d + \alpha_8 \overline{P}, \qquad \dim a_2 = \dim t^{-1}, \\ \overline{M} &= \Delta\overline{A}_{ij}\overline{D}_{ij}, \qquad \overline{N}^d = \Delta\overline{A}^d_{nn}\Delta\overline{A}^d_{nn}\overline{D}_{nn}, \qquad \overline{P} = \Delta\overline{A}..\overline{D}.. . \end{aligned}$$

The quasi-linearity of (3.17) gives then three constitutive identities:

$$\frac{\dot{\overline{\mathrm{II}}}_{\Delta\overline{A}}}{2\overline{\mathrm{II}}_{\Delta\overline{A}}} - \frac{\dot{\overline{\mathrm{III}}}^{\,d}_{\Delta\overline{A}}}{3\overline{\mathrm{III}}^d_{\Delta\overline{A}}} = 2\mu_A\left(\frac{\overline{M}}{2\overline{\mathrm{II}}_{\Delta\overline{A}}} - \frac{\overline{N}^d}{3\overline{\mathrm{III}}^d_{\Delta\overline{A}}}\right) = \operatorname{tg} 3\varphi^d_\Delta\, \dot{\varphi}^d_\Delta, \tag{3.18}$$

$$\frac{\dot{\overline{\mathrm{II}}}_{\Delta\overline{A}}}{2\overline{\mathrm{II}}_{\Delta\overline{A}}} - \frac{\dot{X}}{2X} = 2\mu_A\left(\frac{\overline{M}}{\overline{\mathrm{II}}_{\Delta\overline{A}}} - \frac{\overline{P}}{2X}\right) = \mathrm{tg}\,\theta_\Delta\,\dot{\theta}_\Delta\,, \tag{3.18}$$

$$\frac{\dot{\overline{\mathrm{III}}}^{\,d}_{\Delta\overline{A}}}{3\overline{\mathrm{III}}^{d}_{\Delta\overline{A}}} - \frac{\dot{X}}{2X} = 2\mu_A\left(\frac{\overline{N}^d}{3\overline{\mathrm{III}}^{d}_{\Delta\overline{A}}} - \frac{\overline{P}}{2X}\right),$$

with:

$$Q^2_{\Delta A} = 2\overline{\mathrm{II}}_{\Delta\overline{A}} = \mathrm{tr}\,(\Delta\overline{A})^2, \qquad Q_\Delta\,\dot{Q}_\Delta = \dot{\overline{\mathrm{II}}}_{\Delta\overline{A}},$$

$$3\overline{\mathrm{III}}^{d}_{\Delta\overline{A}} = \mathrm{tr}\,(\Delta\overline{A}^d)^3 = \sum_1^3 (\Delta\overline{A}^{nn})^3,$$

$$X = \Delta\overline{A}^2_{..}, \qquad \dot{X} = 2\Delta\overline{A}..\Delta\dot{\overline{A}}.., \qquad 6X = (\Delta A_1 + \Delta A_2 + \Delta A_3)^2.$$

The scalar forms associated with (3.17) are

$$\begin{aligned}
\dot{\overline{\mathrm{II}}}_{\Delta\overline{A}} &= 2\mu_A\overline{M} + (\alpha_4\overline{M} + \alpha_6\overline{N}^d + \alpha_8\overline{P})2\overline{\mathrm{II}}_{\Delta\overline{A}},\\
\dot{\overline{\mathrm{III}}}^{\,d}_{\Delta\overline{A}} &= 2\mu_A\overline{N} + (\alpha_4\overline{M} + \alpha_6\overline{N}^d + \alpha_8\overline{P})3\overline{\mathrm{III}}^{d}_{\Delta\overline{A}},\\
\dot{X} &= 2\mu_A P + (\alpha_4\overline{M} + \alpha_6\overline{N}^d + \alpha_8\overline{P})2X.
\end{aligned} \tag{3.19}$$

The behaviour is quasi-reversible in the vicinity to the right of a loading-unloading "inversion" point, for (3.17) is reduced to

$$\Delta\dot{\overline{A}}^{ij} = 2\mu_A\overline{D}^{ij}, \qquad \dot{\mathbf{A}} = 2\mu_A\mathbf{d}. \tag{3.20}$$

iii. The generic path is split into "radial" and "neutral" infinitesimal paths along which:

$$\begin{aligned}
\dot{\varphi}^{\,d}_\Delta &\equiv \dot{\varphi}_{\boldsymbol{\Delta}} = 0\\
\dot{\theta}_\Delta &\equiv \dot{\theta}_{\boldsymbol{\Delta}} = 0
\end{aligned} \qquad \text{and} \qquad \overline{\Phi}_A \equiv \overline{\Phi}_{\mathbf{A}} = 0, \tag{3.21}$$

respectively (in-phase paths are such as: $\dot{\varphi}^{\,d}_{\overline{A}} = \dot{\theta}_{\overline{A}} = 0$, $\dot{\varphi}_{\mathbf{A}} = \dot{\theta}_{\mathbf{A}} = 0$).

The radial paths are defined through

$$Q^2_{\Delta A} = A_0^2\Omega_A^2 q_A(W_A), \qquad W_A = \int_R^t \frac{2}{\Omega_A^2}\overline{\Phi}_A\,d\tau,$$

$$\begin{aligned}
\Omega_A &= \omega\omega'(\omega, \varphi^d_A, \varphi^d_{\varrho R}, \theta_A, \theta_{\varrho R}),\\
\varphi_{\varrho R} &= \theta_{\varrho R} = 0, \qquad \varphi_{\Delta A} = \varphi_A, \qquad \theta_{\Delta A} = \theta_A \quad \text{if } \omega = 1,
\end{aligned} \tag{3.22}$$

(3.22) [cont.]
$$\alpha_6 = \alpha_8 = 0,$$
$$\alpha_4 = \frac{1}{2\overline{\Pi}_{\Delta\overline{A}}}\left(q_1\left(\frac{2\overline{\Pi}_{\Delta\overline{A}}}{\Omega_A^2}\right) - 2\mu_A\right), \qquad q_1 \equiv q_A'(q_A^{-1}),$$
$$q_1(1) = 0, \qquad q_1 \downarrow \text{ on } [0,1],$$

where the symbol ϱR denotes the reference state (ϱ) prior to the current one R along the current branch Δ_R^t. One takes generally (cf. Eq. (3.1)):

$$q_1 = 2\mu_A(1 - x^{c/2}) \quad c \geq 0 \quad (c = 2 \Rightarrow \text{Prager model}).$$

Then

$$\alpha_4 = -2\mu_A \big/ (\Omega Q_0)^c Q_{\Delta A}^{2-c}.$$

Moreover, one notices that

(3.23)
$$\varphi_\Delta^d = \varphi_{\overline{D}}^d = \varphi_{\dot{\overline{A}}}^d,$$
$$\theta_\Delta = \theta_{\overline{D}} = \theta_{\dot{A}}.$$

Owing to (3.15),

$$\varphi_{\Delta\mathbf{A}} = \varphi_{\mathbf{D}}, \qquad \theta_{\Delta\mathbf{A}} = \theta_{\mathbf{D}}.$$

The infinitesimal intensive and extensive radial paths of isotropic pure hysteresis process have the same orientation in the relevant mechanical, electrical and magnetic PRF, respectively.

The neutral paths are such as $\overline{\Phi}_A = 0$ and deduced by similarity from the (Mises-like) limit irreversible behaviour. Then

(3.24)
$$\Delta\dot{\overline{A}}_{ij} = 2\mu_A \overline{D}_{ij}, \qquad \overline{\Phi} = 0,$$
$$N = \frac{Q_\Delta}{\Omega_A} = \frac{Q_\Delta}{\omega\omega'(\omega, \varphi_A^d, \varphi_{\varrho R}^d, \theta_A, \theta_{\varrho R})} = cte,$$
$$2\dot{Q}_\Delta \big/ Q_\Delta + A_N \dot{\varphi}^d + B_N \dot{\theta} = 0.$$

The two-fold identification process of PEGON [20], founded on (3.18) and (3.24), results in the model:

(3.25)
$$\dot{\overline{A}}^{ij} = 2\mu_A \overline{D}^{ij} + \beta_4 \overline{\Phi}_A \Delta\overline{A}^{ij}, \qquad \dot{\mathbf{A}} = 2\mu_A \mathbf{d} + \beta_4 \overline{\Phi}_A \Delta\mathbf{A},$$
$$\overline{\Phi}_A \equiv \overline{M} + \gamma_4 \dot{\varphi}_\Delta^d + \delta_4 \dot{\theta}_\Delta, \qquad \gamma_4 = A_N \overline{\Pi}_\Delta / 2\mu_A,$$
$$\beta_4 \overline{\Phi}_A \equiv \alpha_4 \overline{M} + \alpha_6 \overline{N}^d + \alpha_8 \overline{P}, \qquad \delta_4 = B_N \overline{\Pi}_\Delta / 2\mu_A,$$

(3.25) [cont.]
$$\alpha_4 = \beta_4 \left(1 + \frac{\gamma_4}{2\overline{\mathrm{II}}_\Delta} \frac{2\mu_A}{\mathrm{tg}\, 3\varphi^d_\Delta} \frac{1}{\sin^2\theta} + \frac{\delta_4}{2\overline{\mathrm{II}}_\Delta} \frac{2\mu_A}{\mathrm{tg}\,\theta}\right),$$
$$\alpha_6 = -\beta_4 \frac{\gamma_4}{2\overline{\mathrm{III}}^d_\Delta} \frac{2\mu_A}{\mathrm{tg}\, 3\varphi^d_\Delta}, \qquad \alpha_8 = -\beta_4 \frac{2\mu_A}{2X} \left(\frac{\delta_4}{\mathrm{tg}\,\theta} - \frac{1}{\mathrm{tg}^2\theta \mathrm{tg}\, 3\varphi^d_\Delta}\right).$$

In the isotropic Mises-like case under consideration one obtains [20]

$$A_N = -\frac{2}{\cos\alpha}\left[\sin\left(\varphi^d_{\Delta\overline{A}} - \varphi^d_{\varrho R}\right)\sin\theta_\Delta \sin\theta_{\varrho R}\right],$$
$$B_N = \frac{2}{\cos\alpha}\left[\cos\left(\varphi^d_{\Delta\overline{A}} - \varphi^d_{\varrho R}\right)\cos\theta_\Delta \sin\theta_{\varrho R} - \sin\theta_\Delta \cos\theta_{\varrho R}\right],$$
$$-\cos\alpha = \cos\left(\varphi^d_{\Delta\overline{A}} - \varphi^d_{\varrho R}\right)\sin\theta_\Delta \sin\theta_{\varrho R} + \cos\theta_\Delta \cos\theta_{\varrho R},$$
$$\Omega = \omega\omega' = 2\cos\alpha.$$

It is worthwhile to notice that the model can be implemented in the Coulomb-like case: there exist actual experimental results suggesting the interest of this theoretical feature regarding ferromagnetic polycrystals [29].

3.5.2. The two-fold feature of the first loading process

i. It has been previously underlined that the Preisach model and the proposed pattern was associated with basically different types of microprocesses ("en bloc" switching and "pure hysteresis pinning", respectively, cf. Sec. 1 iii) and Sec. 3.3 ii)). Accordingly, there exist also several "associated" differences between the phenomenological features of the two sketches. For example, the proposed pattern is able to take into account, in three-dimensional situations, the cyclic processes implying *exactly closed* cycles and *exactly closed* sharp-ended subloops, symmetrical or not, giving in a simple and straightforward way the rate of internal intrinsic heat at each current state of the evolution. However, the aim of the current remark is in fact to warn against the trap made up of set of analogies which may appear when one deals only with the first loading processes. For example, if one considers only the first loading ($\omega = 1$), spiral-like process starting from the demagnetized unique initial neutral state, then the functional mapping between A and α may appear as described in similar ways by the proposed pattern and by the Mayergoyz's vectorial model [30] which is a vectorial generalization of the Preisach model (cf. Fig. 15). This analogy is founded on the fact that, for $\omega = 1$, the proposed differential-difference pattern is reduced to a purely differential sketch. The trap consists in the fact that the situation of the first loading type is either unable to reflect the foundation of the pattern, or able to restrict the analysis in such a way that basic difficulties are avoided.

ii. On the contrary, scarcely ambiguity remains if the purely differential first-loading form of the hysteretic pattern is implemented in order to describe a property explicitly defined as intrinsically reversible. Let us consider, for example,

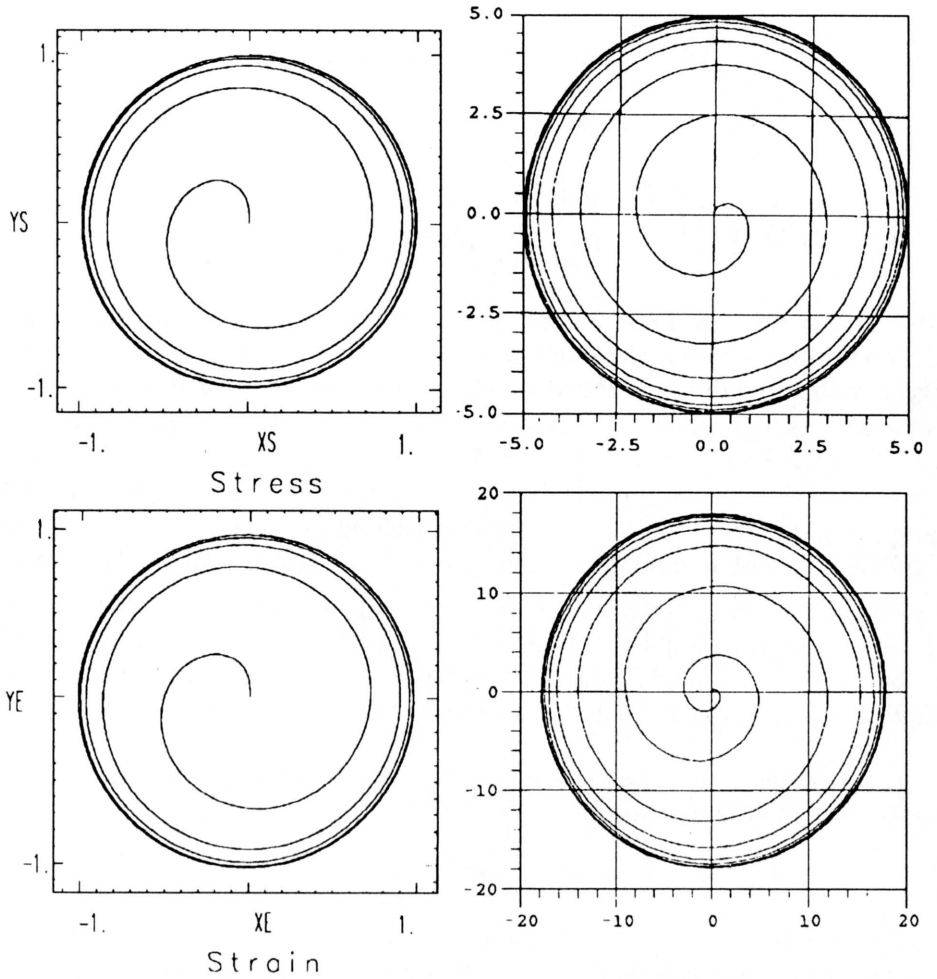

FIG. 15. The first-loading trap: on the right – the Mayergoyz model [30]; on the left – the discrete memory model in the corresponding "two-dimensional" mechanical case.

the case where a relevant modelling involves an asymptotic behaviour of limit type, previously studied through the ln cosh function (Sec. 3.4.1 ii); Sec. 3.4.2 iii)). A modelling endowed with a convenient compliance is obtained through (3.4), (3.5), (3.15), (3.16) and (3.22), (3.25). The pattern is

$$\dot{\mathbf{A}}^{\text{rev}} \Leftrightarrow \dot{\mathsf{A}}^{\text{rev}} \Leftrightarrow \left[\dot{\mathsf{A}}^{\text{rev}} \Leftrightarrow \overline{\mathsf{D}}\right]_I \Leftrightarrow \overline{\mathsf{D}} \Leftrightarrow \mathbf{d} \Leftrightarrow \dot{\boldsymbol{\alpha}}.$$

Input and output forms are given under explicit form by

$$d_i = \left(\mu_{ij}^{\text{rev}}/\mu_0^{\text{rev}}\right) \dot{\alpha}_j, \qquad 3\overline{D}_{11} = 2d_1 - d_2 - d_3, \quad \ldots, \quad \sqrt{6}\overline{D}_{..} = d_1 + d_2 + d_3,$$

$$\dot{A}_n^{\text{rev}} = \dot{\overline{A}}_{nn} + \sqrt{\frac{2}{3}}\,\dot{\overline{A}}.. \quad (n = 1,2,3).$$

The constitutive kernel is (cf. (3.22), (3.25)).

$$\dot{\overline{A}}_{ij}^{\text{rev}} = 2\mu_0^{\text{rev}}\overline{D}_{ij} + \beta_4\overline{\Phi}\overline{A}_{ij} \quad \text{in } \text{PRF}_{\text{rev}},$$
$$\beta_4\overline{\Phi} = -\left[2\mu_0 \Big/ (A^c_{0\text{rev}} Q^{2-c}_{\text{rev}})\right](\overline{A}_{ij}\overline{D}_{ij}), \qquad Q^2_{\text{rev}} = \text{tr}(\overline{\mathbf{A}}^2)$$

in the case where the limit behaviour is isotropic and of Mises-like type. The quasi-reversible behaviour is defined by μ_{ij} and the modelling of the transition range may be slightly modified through c. The derivation of the forms is much more cumbersome when the isotropic limit behaviour is Coulomb-like ($Q_0 = Q_{00}/(1 + \gamma\cos 3\varphi_A)^n$, $n \approx 1/4$, $\gamma = 1/2$ for example, see [19, 20]), and when the limit behaviour is *anisotropic* (see (3.24) which must be implemented under a slightly simplified form because Q_Δ is identical with Q and $\varphi^d_{\varrho R}$, $\theta_{\varrho R}$ are dropped out). The differential modelling of $\mathbf{A}_{\text{rev}}$ is not only compliant but also effective because the rate $\dot{\mathbf{A}}_{\text{rev}}$ is defined directly introducing only one more parameter c and, for example, two more parameters concerning the definition of the PRF_{rev} (See Sec. 3.5.4 and Eq. (3.29)): only three parameters are added to the tensorial parameters $(\mu_{ij}^{\text{rev}}; P^{\text{rev}}_{\text{lim}_{ij}})$ which are necessarily involved.

3.5.3. Associated thermodynamics. One knows that an important consequence of the quasi-linearity is the relation:

$$\overline{\Phi}_A = Q_{\Delta\overline{A}} Q_{\overline{D}} = Q_{\Delta\mathbf{A}} \cdot Q_{\mathbf{d}} \tag{3.26}$$

along radial paths. On the other hand, the pattern is founded on a unique discrete memory thermodynamics which holds for the mechanical, electrical and magnetic processes.

For each phenomenon the rates of reversible power, internal intrinsic received heat supply, internal energy supply and order supply are such as [19, 20]:

$$\left|\begin{matrix} \overline{\pi} \\ -\dot{\overline{Q}}_{ii} \\ \dot{\overline{E}} \\ \dot{\overline{I}} \end{matrix}\right|_{(m,E,H)} = \left|\begin{matrix} -1 & -1 & 0 \\ 0 & 1/\omega & -1/\omega \\ -1 & -1/\omega & 1/\omega \\ 0 & 1-1/\omega & 1/\omega \end{matrix}\right| \cdot \left|\begin{matrix} \overline{P}_{ii} \\ \overline{\Phi} \\ \overline{c} \end{matrix}\right|_{(m,E,H)}, \tag{3.27}$$

where $\overline{\Phi}$ is given by (3.25), and

$$-\overline{P}_{ii} = \overline{A}^{ij}\overline{D}^{ij}$$

$\left(\equiv \overline{\Phi}\right.$ for in-phase paths $\dot{\varphi}^d_{\mathbf{A}} = \dot{\theta}_{\mathbf{A}} = 0$ or for radial paths : $\left.\dot{\varphi}^d_\Delta = \dot{\theta}_\Delta = 0\right)$

Owing to (3.26) and to the splitting of any actual path, one obtains

$$\overline{c'} = \frac{\overline{c}}{(\omega')^2} = \frac{1}{\omega'}\left[\dot{Q}_{\Delta\overline{A}} - \frac{\dot{\omega}'}{\omega'}Q_{\Delta\overline{A}}\right]\left[\int_R^t \frac{\overline{\Phi}}{\omega' Q_{\Delta\overline{A}}}d\tau\right], \qquad \overline{\Phi'} = \overline{\Phi}/(\omega')^2,$$

(3.28)

$$\overline{c'} = \dot{Q}'_{\Delta} Q'_{\Delta'\alpha}, \qquad \overline{\Phi'} = Q'_{\Delta}\dot{Q}'_{\Delta'\alpha}.$$

Consequently the pattern is of one-dimensional type along radial paths. One notices that the one-dimensional form of (3.28) is $\dot{A}\,\Delta\alpha$ and that, consequently, (3.27) gives (2.5), as required.

Regarding the electrical and magnetic hysteretic properties, of intrinsic dissipation $\overline{\Phi}_{EH} = \overline{\Phi}_E + \overline{\Phi}_H$, the relations (3.27) result in the following explicit forms:

a) hysteretic form of Prigogine-like criterion: $(\partial\overline{\Phi'}/\partial Q'_{\Delta'\alpha})\cdot(\partial^2\overline{\Phi'}/\partial Q'^2_{\Delta'\alpha}) \leq 0$, [18, 19];

b) Second Principle: $\overline{\Phi}_{EH} \succ 0$ almost everywhere;

c) anenergetic form of the First Principle:

$$\begin{aligned}
\dot{\overline{I}}_{\mathrm{EM}} &= \dot{\overline{Q}}_{\mathrm{EM}} + \dot{\overline{\Phi}}_{\mathrm{EM}},\\
\omega\dot{\overline{I}}_{\mathrm{EM}} &= \frac{\partial}{\partial t}(\Delta\mathbf{E}\cdot\Delta\mathbf{D} + \Delta\mathbf{H}\cdot\Delta\mathbf{B}),\\
-\omega\dot{\overline{Q}}_{\mathrm{EM}} &= (\Delta\mathbf{E}\cdot\Delta\dot{\mathbf{D}} + \Delta\mathbf{H}\cdot\Delta\dot{\mathbf{B}}) - (\Delta\dot{\mathbf{E}}\cdot\Delta\mathbf{D} + \Delta\dot{\mathbf{H}}\cdot\Delta\mathbf{B}),\\
\overline{\Phi}_{\mathrm{EM}} &= \Delta\mathbf{E}\cdot\Delta\dot{\mathbf{D}} + \Delta\mathbf{H}\cdot\Delta\dot{\mathbf{B}} \equiv \Delta\mathbf{E}\cdot\dot{\mathbf{D}} + \Delta\mathbf{H}\cdot\mathbf{B};
\end{aligned}$$

d) Gibbs-like relation:

$$\begin{aligned}
\dot{\overline{E}}_{\mathrm{EM}} &= \dot{\overline{I}}_{\mathrm{EM}} + \overline{\Pi}_{\mathrm{EM}},\\
\overline{\Pi}_{\mathrm{EM}} &= {}^t_R\mathbf{E}\cdot\dot{\mathbf{D}} + {}^t_R\mathbf{H}\cdot\dot{\mathbf{B}};
\end{aligned}$$

e) First Principle:

$$\dot{\overline{E}}_{\mathrm{EM}} = \dot{\overline{Q}}_{\mathrm{EM}} - \overline{P_{ii}}_{\mathrm{EM}}.$$

The internal intrinsic powers are:

$$\begin{aligned}
-\overline{P_{ii}}^{\mathrm{hys}}_{\mathrm{meca}} &= \overline{\underline{\sigma}}^{\mathrm{hys}}\cdot\overline{\mathsf{D}},\\
-\overline{P_{ii}}^{\mathrm{hys}}_{\mathrm{EM}} &= \mathbf{E}^{\mathrm{hys}}\cdot\dot{\mathbf{D}} + \mathbf{H}^{\mathrm{hys}}\cdot\dot{\mathbf{B}}.
\end{aligned}$$

In this introductory paper the dissipative process of conduction is not introduced (nor the Poynting equation).

3.5.4. Some hints regarding the coupling effects. Finally, some hints can be introduced regarding the second order effects and the coupling effects.

In order to obtain the second order effect in a fixed frame chosen for convenience, three relevant constitutive laws have to be defined regarding ε_m, ε_e and ε_h, under the form of differential-difference equations. A simple modelling of the mechanical second order effect is such as [19, 32]:

$$\varepsilon_m - \varepsilon_{mR} = \omega\varepsilon_{ml}\left[1 - \exp\left(-\left(\frac{\Delta\Omega^{\text{kin}}}{\omega\Omega_c}\right)^2\right)\right]\tanh\left(\frac{\Delta\Omega^{\text{kin}}}{\omega\Omega_c}\right), \tag{3.29}$$

$$\dot{\varepsilon}_m\,\dot{\Omega}^{\text{kin}} \leq 0$$

introducing two physical parameters ε_{ml} and Ω_c (Fig. 16). In (3.29) the rotation Ω^{kin} ($0 \leq \Omega^{\text{kin}} \leq \pi/4$) is associated with the kinematics following the form [32]

$$\tan 2\Omega^{\text{kin}} = 2(2\tau J_3)/(J_2^2 - J_3^2 + 4\tau^2) \tag{3.30}$$

in the special "two-dimensional" case under consideration, where τ is the shear and J_i ($i = 1, 2, 3$) are the stretches associated with the transformation: $z^1 = J_1 Z$, $z^2 = J_2 Z^2 + 2\tau Z^3$, $z^3 = J_3 Z^3$.

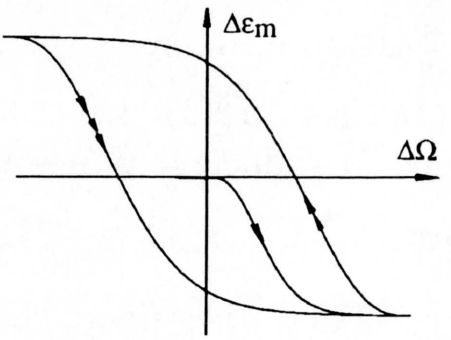

FIG. 16. Small correcting rotation of the Preferred Reference Frame (PRF).

Similar model of ε_e and ε_h can be studied in a first step. Concerning the case where the reversible contribution is defined through differential equations, one remembers that ε_{rev} must be defined through a reversible form ((3.29) is suggestive).

Regarding the coupling effect, the situation may be sketched as follows:

a. In this introductory paper the generalisation of the classical treatment is not performed: for example, the features of the components $\partial E_i/\partial D_j$ are not studied in a comprehensive form in order to generalise the classical photoelastic sketch founded on the study of the small changes of $\partial E_i/\partial D_j$ as a linear function the strain components $\Delta_0^t \varepsilon_{kl}$.

b. The pattern (3.25) is basically uncoupled. However, strong coupling effects may be introduced in the irreversible range if, for example, one substitutes for $\overline{\Phi}_E$ (resp. $\overline{\Phi}_H$) in the first equation (3.25) the total electromagnetic intrinsic dissipation:

$$\overline{\Phi}_{EM} = \overline{\Phi}_E + \overline{\Phi}_H.$$

c. To the scalar, internal intrinsic strong coupling effects introduced above, classical scalar coupling effects can be obtained through the pressure or the temperature-dependence of the properties (both in the quasi-reversible and irreversible ranges). This feature of the pattern is interesting in spite of the fact that little theoretical and experimental work has been devoted to the pressure and stress-dependence of magnetization [31].

4. Concluding remarks

For the benefit of engineers, some hints have been given in order to derive the hysteretic losses and the associated polarizations. However, the constitutive study is restricted to quasi-static nonviscous situations and no hints are explicitly given regarding the problem of *forces* and *torques*.

Regarding the boundary value problems, the proposed pattern may be implemented as a rather effective ingredient regarding materials exhibiting permanent irreversible behaviour. However a second gap must be underlined: in this introductory paper there are no hints regarding *conduction* and concerning the distinction between *short and long range interactions*.

Concerning the fundamental questions, one notices firstly that only elementary mathematical skills are required to suggest the basic forms of the current state of the pattern. However the demagnetization problem must be studied further. Secondly, from the continuum mechanics viewpoint, the situation may be summarized as follows: through the notion of a dragged along material process expressing the material discrete memory concept, one has substituted for the polarization the notion of "internal intrinsic proper field", of pure hysteretic type or of elastohysteretic type, both being associated with *always irreversible* properties: however, the cumbersome derivation of the formal features of the anisotropic pure hysteresis has not been introduced [32]. It is also worthwhile to notice that, in order to define both the specific properties and the universal features, both the Prefered Reference Frame and the couple: Ilyushin space – pure hysteretic algorithm, are involved. The pattern is sensitive to the relevant microstructural processes and is therefore both heuristic and of a rather good testability. Thirdly, the two gaps underlined above (points i and ii) interfere with some possible improvement of our approach. For example, it is not yet possible to take into account some microstructural results involving mechanical measurements [33]. At the present time it may be only suggested that the classical conservation principles, the typical stationary feature of the hysteretic properties and the prominent

role of short range interactions, if considered together, can be at the origin of the fact that the discrete memory pattern is rather effective regarding the constitutive modelling. Anyway, much more sophisticated cases are also interesting [34].

References

1. P.M. DUHEM, *The evolution of mechanics*, Sijthoff & Noordhoff, (English translation of "L'evolution de la mécanique", Paris 1903), chap. XIV, 1980.
2. F. PREISACH, *On magnetic aftereffect*, Z. Phys., **94**, pp. 277–302, 1935.
3. L. NEEL, *Théorie des lois d'aimantation de Lord Rayleigh*, Cahiers de Physique, **12**, pp. 1–20, 1942 and **13**, pp. 19–30, 1943.
4. D.L. ATHERTHON, B. SZPUNAR and J.A. SZPUNAR, *A new approach to Preisach diagrams*, IEEE Trans. Magn., **MAG.23**, pp. 1856–1867, 1987.
5. I.D. MAYERGOYZ, G. FRIEDMAN and C. SALLING, *Comparison of the classical and generalized Preisach hysteresis models with experiments*, IEEE Trans. Magn., **MAG.25**, pp. 3925–3927, 1989.
6. M.A. KRASNOSEL'SKII and A.V. POKROVSKII, *Systems with hysteresis*, Springer-Verlag, Berlin 1989, pp. 384–396, and Nauka, Moscow 1983.
7. V.V. CHERNORUTSKII and M.A. KRASNOSEL'SKII, *Hysteresis systems with variable characteristics*, Nonlinear Analysis, Theory, Methods and Application, **18**, 6, pp. 543–557, 1992.
8. P.G. DEGENNES, *Pierre Curie et le rôle de la symétrie dans les lois physiques*, [in:] Symmetries and Broken Symmetries in Condensed Matter Physics, N. BOCCARA [Ed.], I.D.S.E.T., Paris, pp. 1–9, 1981.
9. H.A.M. Van den BERG, *Self-consistent domain theory in soft ferromagnetic media*, J. Applied Physics, **57**, pp. 2168–2173, 1985 and **60**, pp. 1104–1123, 1986.
10. O. COSTA de BEAUREGARD, *Une nouvelle classe de forces électromagnétiques d'ordre* c^{-2}, Cahiers de Physique, 206, pp. 1–16, 1967.
11. J. FRIEDEL, *Concluding remarks*, [in:] Symmetries and Broken Symmetries in Condensed Matter Physics, ibid [8], pp. 197–209, 1981.
12. J-C. TOLEDANO, *La ferroélasticité*, A. Téléc, 29, 7–8, pp. 249–270, 1974.
13. A. AMENGUAL, F. GARCIAS, F. MARCO, C. SEGUI and V. TORRA, *Acoustic emission of the interface motion in the Martensitic Transformation of Cu-Zn-Al shape memory alloys*, Acta Met., **36**, 8, pp. 2329–2334, 1988.
14. R. VERGNE, J.C. COTILLARD and J.L. PORTESEIL, *Quelques aspect statistiques des processus d'aimantation dans les corps ferromagnetiques. Cas du déplacement d'une seule paroi de Bloch à 180° dans un milieu monocristallin aléatoirement perturbé.*, Rev. Phys. Appl., **169**, pp. 449–476, 1981.
15. A. TOURABI, *Contribution à l'étude de l'hystérésis élastoplastique et de l'écrouissage de métaux et alliages réels*, Thesis, Grenoble 1988.
16. G. MASING, Proc. 2nd Int. Congress Applied Mech., pp. 332–335, 1926.
17. C. de CARBON, *Déformation des solides*, C. R. Acad. Sc., Paris, t. 215, pp. 241–244, 1942.
18. P. GUELIN, *Remarques sur l'hystérésis mécanique – Les bases d'un schéma thermomécanique à structure héréditaire*, J. de Meca., **19**, 2, pp. 217–247, 1980.
19. P. PEGON, *Contribution à l'étude de l'hystérésis élastoplastique*, Thesis, Grenoble 1988.
20. P. PEGON, P. GUELIN, D. FAVIER, B. WACK and W.K. NOWACKI, *Constitutive scheme of discrete memory form for granular materials*, Arch. Mech., **43**, 1, pp. 3–27, 1991.
21. D. FAVIER, P. GUELIN and R. CAMMARANO, *Application of a phenomenological elastohysteresis theory to the modelling of magnetisation*, Trans. 7th Int. Symp. on Magnetic Anisotropy and Coercivity in RE-TM alloy, Univ. of Western Australia, Section 2, pp. 137–150, Canberra 1992.
22. R. GANS, *Magnetisch korrespondierende Zustande*, Physikalishe Zeitschrift, 11, pp. 988–991, 1910.
23. W.F. BROWN, *Domains theory of ferromagnetics under stress; Part III. The reversible susceptibility*, Phys. Rev., **54**, pp. 279–287, 1938.
24. D. FAVIER, *Contribution à l'étude théorique de l'élastohystérésis à température variable – application aux propriétés de mémoire de forme*, Thesis, 1988.
25. A. TOURABI, B. WACK and D. FAVIER, *Experimental determination of the hysteretic properties in shape memory alloys*, Mat. Sci. Forum, 56–58, pp. 493–498, 1990.

26. D. FAVIER, P. GUELIN and P. PEGON, *Thermomechanics of hysteresis effects in shape memory alloys*, Mat. Sci. Forum, 56–58, pp. 559–564, 1990.

27. P.Y. MANACH and D. FAVIER, *Comparison of homogeneous shear and tensile tests on a NiTi shape memory alloy*, Proc. Int. Conf. On Mart. Transformations, Monterey, C.M. WAYMAN and J. PERKINS [Eds.], pp. 941–946, 1992.

28. R.B. OLSEN and D.D. BROWN, *High effiency direct conversion of heat to electrical energy – Related pyroelectric measurements*, Ferroelectrics, **40**, pp. 17–27, 1982.

29. J.L. PORTESEIL and R. VERGNE, *Evolution des propriétés magnétiques d'une substance polycristalline soumise à des cycles d'hystérésis dissymétriques successifs*, Rev. Phys. Appl., 12–8, pp. 1077–1093, 1977.

30. J.D. MAYERGOYZ, *Mathematical models of hysteresis*, IEEE Trans. on Mag., **MAG-22**, 5, pp. 603–608, 1986.

31. J.L. PORTESEIL, *Two general features of the hysteresis behaviour of ferromagnets: anisotropy of demagnetisation and reptation*, Physica, **93B**, pp. 201–211, 1978.

32. D. FAVIER, P. GUELIN, B. WACK, P. PEGON and W.K. NOWACKI, *Constitutive scheme of anisotropic elastic-plastic hysteresis*, Trans. SMIRT 11, L23/4, pp. 533–538, 1991 and Proc. of Mecamat 91, Paris, France, 1991.

33. J. ZBROSZCZYK, J. DRABECKI and B. WYSLOCKI, *Angular distribution of rotational hysteresis losses in Fe-3.25% Si single crystal with orientations (001) and (011)*, IEEE Trans. Mag., **17**, 3, pp. 1275–1282, 1981.

34. S. SENOUSSI, *Revue of the critical current densities and magnetic irreversibilities in high-Tc superconductors*, J. de Physique III, 2, pp. 1041–1257, 1992.

UNIVERSITÉ JOSEPH FOURIER, GRENOBLE, FRANCE.

Received January 16, 1995.

Arch. Mech., 47, 3, pp. 485–498, Warszawa 1995

Effect of prior quasi-static loading on the initiation and growth of dynamic adiabatic shear bands (*)

R. C. BATRA (BLACKSBURG) and C. ADULLA (TROY)

WE STUDY the initiation and growth of adiabatic shear bands in a thin-walled steel tube deformed first quasi-statically either in simple compression or simple tension or by a pressure applied to the inner surface of the tube, and then by equal and opposite tangential speeds applied to the end surfaces of the tube. The objective is to see how prior quasi-static deformations of the tube affect the nominal shear strain at which a shear band initiates in the tube. The first set of numerical experiments simulates the tests recently conducted by Murphy who found that the nominal strain at the initiation of the shear bands decreased with an increase in the axial static compressive stress induced in the tube.

1. Introduction

ADIABATIC SHEAR BANDS are narrow regions, usually a few microns wide, of intense plastic deformation that form during high strain-rate plastic deformation of most metals. TRESCA [1] seems to be the first to observe these during the hot forging of platinum and he termed these "hot lines". Subsequently MASSEY [2] also noticed these during the hot forging process. However, the research activity in this area appears to be influenced strongly by the work of ZENER and HOLLOMON [3] who observed 32 μm wide shear bands during the punching of a hole in a steel plate. They also pointed out that the intense plastic deformations of the steel heated it up significantly, and that it became unstable when the thermal softening equalled the hardening caused by strain and strain-rate effects. The reader is referred to ROGERS [4], CLIFTON [5], OLSON *et al.* [6], and to recent issues of the Applied Mechanics Reviews [7] and the Mechanics of Materials Journal [8] for a review of the work in this area.

The experimental work under controlled conditions has been performed on tubular specimens using a Kolsky bar by DUFFY *et al.* [9, 10] and GIOVANOLA [11]. These tests have involved the twisting of a thin tube, observing deformations of a grid pasted on the outer surface of the tube and using infrared lamps to measure the temperature rise of a small region either included in or enclosing the shear band. Such observations have enhanced significantly our understanding of the mechanism of the shear band formation. Recently MURPHY [12] conducted a series of tests in which a steel tube was loaded quasi-statically in simple compression and then twisted dynamically. He found that an increase in the prior compressive load increased the nominal strain at which a shear band initiated.

(*) Paper presented at 30th Polish Solid Mechanics Conference, Zakopane, September 5–9, 1994.

Here we study the dynamic twisting of a steel tube preloaded quasi-statically either in simple compression or simple tension, or by an internal pressure. The maximum preload applied is such as not to cause plastic deformations of the tube. It is found that the nominal shear strain at which a shear band initiates increases with an increase in the value of the internal pressure, and with an increase in the tensile load applied, but decreases with an increase in the magnitude of the compressive stress. The last result contradicts test observations of MURPHY [12]. We had to increase the thickness of the tube in order to avoid its buckling. However, we observed that for the tube preloaded in either simple tension or compression, the material particles underwent significant displacements in the radial direction when the tube was twisted; these displacements were virtually zero when there was no preload applied. This change in the radial dimensions probably affects noticeably the nominal shear strain at which a shear band initiates.

2. Formulation of the problem

We use rectangular Cartesian coordinates and the referential description of motion to describe the dynamic deformations of an elastic-thermoviscoplastic body. The balance laws governing the deformations of a body are given, for example, in TRUESDELL and NOLL [13] and are omitted here. However, in the balance of internal energy, we assume that the deformations are locally adiabatic and that all of the plastic working rather than 90–95% of it, as asserted by FARREN and TAYLOR [14] and SULIJOADIKUSUMO and DILLON [15], is converted into heating. We note that for a thermoviscoplastic body deformed in simple shear, BATRA and KIM [16] have shown that realistic values of thermal conductivity do not affect the value of the nominal strain at which a shear band initiates. A similar result was obtained by BATRA and PENG [17] for depleted uranium and tungsten blocks deformed in plane strain compression. However, the post-localization response is influenced by heat conduction.

We make the following constitutive assumptions for the material of the tube.

$$\sigma_{ij} = -p\delta_{ij} + s_{ij}, \qquad p = K(\varrho/\varrho_0 - 1), \tag{2.1}$$

$$s_{ij}^{\Delta} = 2\mu(\overline{D}_{ij} - D_{ij}^{p}), \qquad \overline{D}_{ij} = D_{ij} - \frac{1}{3}D_{kk}\delta_{ij}, \tag{2.2}$$

$$2D_{ij} = v_{i,j} + v_{j,i}, \qquad \sigma_{ij}^{\Delta} = \dot{\sigma}_{ij} + \sigma_{ik}W_{kj} - \sigma_{jk}W_{ki}, \tag{2.3}$$

$$2W_{ij} = v_{i,j} - v_{j,i}, \qquad \varrho_0\dot{e} = \varrho c\dot{\theta} + p\frac{\dot{\varrho}}{\varrho^2}, \qquad D_{ii}^{p} = 0, \tag{2.4}$$

$$D_{ij}^{p} = \Lambda s_{ij}, \qquad \sigma_m = (A + B(\varepsilon_p)^n)\left(1 + D\ln\left(\frac{\dot{\varepsilon}_p}{\dot{\varepsilon}_0}\right)\right)(1 - \nu\theta), \tag{2.5}$$

$$\Lambda = 0 \quad \text{if either} \quad J_2 < \sigma_m \quad \text{or} \quad J_2 = \sigma_m \quad \text{and} \quad s_{ij}D_{ij}^{p} < 0, \tag{2.6}$$

otherwise, Λ is a solution of

$$J_2 = \sigma_m, \qquad J_2 = \left(\frac{3}{2}s_{ij}s_{ij}\right)^{1/2}, \tag{2.7}$$

$$\dot{\varepsilon}_p = \left(\frac{2}{3}D^p_{ij}D^p_{ij}\right)^{1/2}, \qquad \varepsilon_p = \int \dot{\varepsilon}_p\, dt. \tag{2.8}$$

Here σ_{ij} is the Cauchy stress tensor, p the hydrostatic pressure, δ_{ij} the Kronecker delta, K the bulk modulus, μ the shear modulus, a superimposed triangle indicates the Jaumann derivative, $\overline{D}_{ij}$ is the deviatoric part of the strain-rate tensor D_{ij}, W_{ij} is the spin tensor, q_i the heat flux per unit area, c the specific heat and θ equals the temperature rise. Equation $(2.5)_1$ implies that the plastic strain-rate is directed along the normal to the instantaneous yield surface $J_2 = \sigma_m$, and the "radius" of the yield surface depends upon the strain-hardening, strain-rate hardening and thermal softening of the material point. The plastic strain-rate D^p_{ij} equals zero when the deformations are elastic; otherwise, its value depends upon the state of deformation at the material point. The relation $(2.5)_2$ giving the dependence of σ_m upon the plastic strain, plastic strain-rate and the temperature has been proposed by JOHNSON and COOK [18]; symbols A, B, D, n and ν denote material parameters and $\dot{\varepsilon}_0 = 1/\text{sec}$.

We take the body to be initially stress-free, and at rest at uniform temperature θ_0. It is first loaded quasi-statically and then twisted dynamically. Here the quasi-static load is simulated by applying it slowly till it reaches the desired value and subsequently holding it steady. Boundary conditions for the three loadings considered (with axial compression and tension counted as two separate loadings) are:

a. Simple compression/tension of the tube (see Fig. 1 for the choice of axes)

$$\sigma_{33}(x_1, x_2, 0, t) = -\sigma_{33}(x_1, x_2, \ell, t) = \begin{cases} \pm\sigma t/t_{rs}, & 0 \le t \le t_{rs}, \\ \pm\sigma, & t > t_{rs}, \end{cases} \tag{2.9}$$

$$\sigma_{ij}(x_1, x_2, x_3, t)n_j = 0 \tag{2.10}$$

on the inner and outer surfaces of the tube,

$$\begin{aligned} v_1(x_1, x_2, 0, t) &= \begin{cases} \varepsilon_{i3j}x_j\omega < t - t_s > /t_{rd}, & |t - t_s| \le t_{rd}, \\ \varepsilon_{i3j}x_j\omega, & (t - t_s) \ge t_{rd}, \end{cases} \\ v_i(x_1, x_2, \ell, t) &= -v_i(x_1, x_2, 0, t). \end{aligned} \tag{2.11}$$

b. Tube pressured from inside

On the inner surface of the tube

$$\begin{aligned} \sigma_{ij}n_j &= -pn_i t/t_{rs}, \qquad 0 \le t \le t_{rs}, \\ &= -pn_i, \qquad t \ge t_{rs}, \end{aligned} \tag{2.12}$$

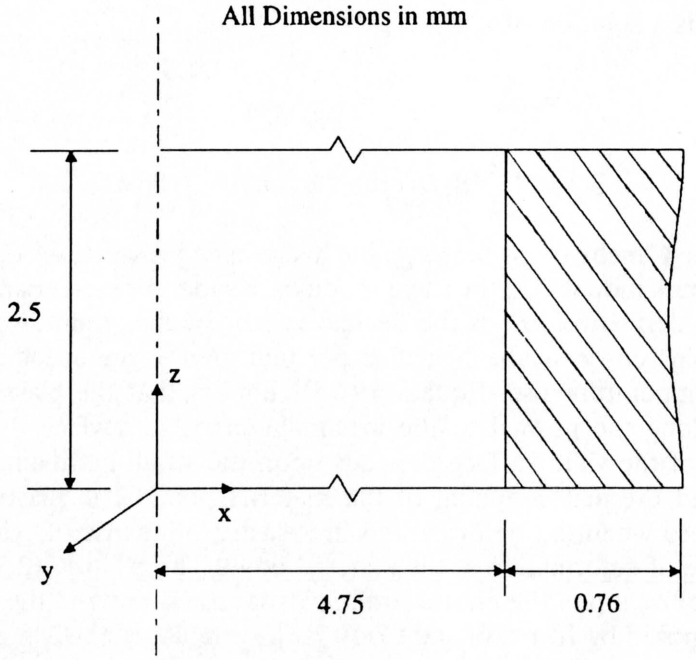

FIG. 1. Tube geometry.

and on the outer surface of the tube

$$
\begin{aligned}
\sigma_{ij}n_j &= 0, \qquad t \geq 0, \\
v_3(x_1, x_2, 0, t) &= v_3(x_1, x_2, \ell, t) = 0, \qquad 0 \leq t \leq t_s, \\
v_i(x_1, x_2, 0, t) &= \begin{cases} \varepsilon_{i3j} x j \omega < t - t_s > / t_{rd}, & |t - t_s| \leq t_{rd}, \\ \varepsilon_{i3j} x_j \omega, & (t - t_s) \geq t_{rd}, \end{cases} \\
v_i(x_1, x_2, \ell, t) &= -v_i(x_1, x_2, 0, t).
\end{aligned} \tag{2.13}
$$

That is, the tube is first loaded axially either in compression or tension from zero to an axial stress of σ in time t_{rs}, the axial load is held constant for time $(t_s - t_{rs})$ so that the elastic waves can attenuate somewhat, and then the tube is twisted by applying equal and opposite tangential velocities at the ends of the tube. The angular speed increases linearly from 0 to the steady value ω in time t_{rd}; the quantity $< t - t_s >$ equals 0 for $t \leq t_s$, and equals $(t - t_s)$ otherwise. Equations (2.11) imply that the ends $x_3 = 0$ and $x_3 = \ell$ of the tube are subjected to equal and opposite tangential speeds. The nominal strain-rate at a point equals $2\omega r/L$, where r is the radial coordinate of a point and L is the initial length of the tubular specimen. Because of the small thickness of the tube, the nominal shear strain-rate varies only a little through the thickness of the tube. Henceforth, $2\omega r_m/L$ is referred to as the average shear strain-rate; r_m equals the mean radius of an end-surface of the tube. The axial stress σ and the internal pressure p are

limited to a small fraction of the yield stress of the material. Thus the preload causes only elastic deformations of the tube. In Eqs. (2.11) and (2.13), ε_{ijk} is the permutation symbol and equals 1 or -1 accordingly as i, j, k form an even or an odd permutation of 1, 2, and 3; and equals 0 when any two indices are equal. Even though the pressure applied to the inner surface of the tube equals a fraction of the yield stress of the material, the state of stress at a point is biaxial and some material points may yield.

3. Results and discussion

In order to compute numerical results, we assigned following values to various material and geometric parameters.

$$\varrho = 7860\,\text{kg/m}^3, \qquad G = 76\,\text{GPa}, \qquad \theta_m = 1520^\circ\,\text{C},$$

$$c = 473\,\text{J/kg}^\circ\,\text{C}, \qquad \theta_0 = 25^\circ\,\text{C}, \qquad A = 792.2\,\text{MPa},$$

$$B = 509.5\,\text{MPa}, \qquad D = 0.014, \qquad n = 0.26, \qquad m = 1.03,$$

maximum tube thickness = 0.76 mm, inner radius of the tube = 4.75 mm, L = 2.5 mm,

$$t_{rs} = 20\,\mu\text{s}, \qquad t_s = 50\,\mu\text{s}, \qquad t_{rd} = 20\,\mu\text{s}. \tag{3.1}$$

The values of material parameters taken from RAJENDRAN'S report [18] are for 4340 steel. The thickness of the tube was assumed to vary sinusoidally:

$$\frac{w(x_3)}{w_A} = 1 + \frac{\varepsilon}{2}\left(\cos\frac{2\pi x_3}{L} - 1\right), \tag{3.2}$$

where ε can be viewed as the defect parameter, $w(x_3)$ is the wall thickness at a point x_3 along the gage section, w_A is the maximum wall thickness, and L is the initial length of the tube; the thickness variation given by Eq. (3.2) is depicted in Fig. 1 for $\varepsilon = 0.08$. The thickness of the tubular specimens employed by MURPHY [12] was also given by Eq. (3.2). However, the value of w_A in our simulations is twice that used by Murphy, since computations with the tube employed by Murphy indicated buckling of the tube prior to the initiation of a shear band. Also, the tubes tested by Murphy were made of HY-100 steel but parameters given in (3.1) are for a 4340 steel. It is because values of material parameters for HY-100 steel for the Johnson-Cook model are not available. Also, there are not enough test data available for HY-100 steel to determine the values of A, B, D etc. for it. We should note that because of the nonlinearities involved, the determination of material parameters from the test data is not unique.

The problems formulated in the previous section were solved numerically by using the large scale explicit finite element code DYNA3D [19]. The code uses

8-noded brick elements with one-point quadrature rule to evaluate various integrals. It employs hour-glass control to eliminate the spurious modes and artificial viscosity to smear out the shocks. The time step size is computed suitably so as to satisfy the Courant condition, thereby ensuring the stability of the computed solution.

Even though the specimen geometry and the loading conditions are such as to cause axisymmetric deformations of the tube, the problem is solved as three-dimensional because of the way the boundary conditions are applied in the code. Also antisymmetry of the velocity field about the midplane suggests that deformations of only half of the tube should be studied. Since the code DYNA3D employs Cartesian coordinates, the imposition of the constraint that points on the midplane move only radially required a major modification of the code. It was done and accordingly deformations of the entire tube were analyzed.

In order to assess the effect of the finite element mesh on the solution of the problem, two different meshes were tried, one containing nearly four times the number of elements as the other; these are depicted in the insert of Fig. 2. It

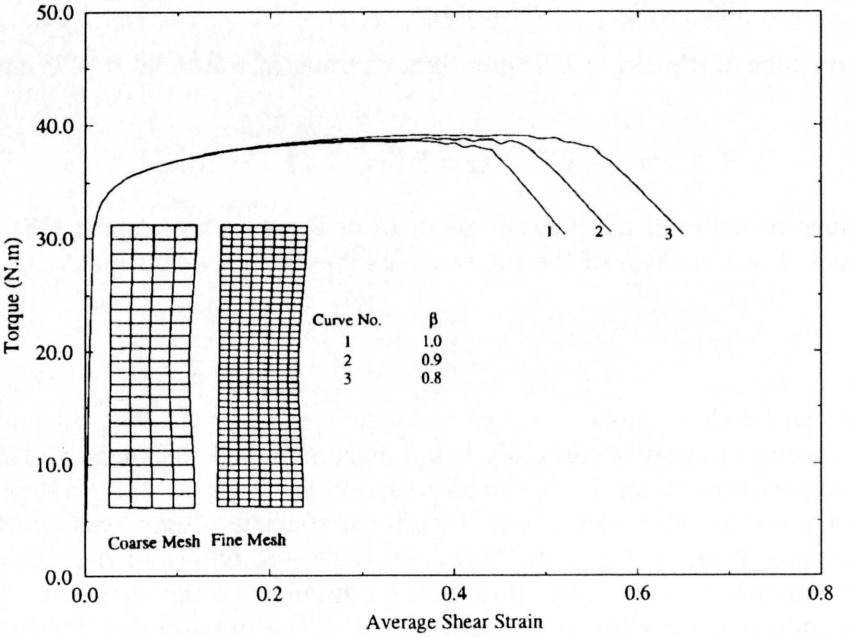

FIG. 2. Torque vs. average shear strain curves for three different values of the fraction β of plastic work converted into heat. The insert shows the coarse and fine meshes used.

was found that the torque required to deform the tube versus the average shear strain curve was unaffected by the mesh used. However, the rate of drop of the torque is considerably more for the fine mesh as compared to that for the coarse mesh, since once a shear band initiates, the fine mesh is capable of delineating the sharp gradients of the deformation fields better than the coarse mesh. Also,

the axisymmetric deformations are essentially concentrated in one central row of elements which, for the fine mesh, is of smaller size. The CPU time required to analyze the problem with the fine mesh is nearly 4 times that required for the coarse mesh. Thus, if the objective is to find the value of the nominal shear strain when a shear band initiates, it is sufficient to use a coarse mesh.

In DYNA3D artificial bulk viscosity is added to smear out the shocks. One of its consequences can be that the initiation of a shear band is either delayed or is totally suppressed. In applying the artificial viscosity method, the pressure in elements being compressed is augmented by an artificial viscous term, q, before evaluating the stress divergence. In expanding elements $q = 0$, otherwise

$$q = \varrho\hat{\ell}|D_{kk}(|Q_1\hat{\ell}|D_{kk}| + Q_2\hat{c}), \tag{3.3}$$

where Q_1 and Q_2 are dimensionless constants which default to 1.5 and 0.06, respectively, $\hat{\ell}$ is the cube root of the volume of the element, and $\hat{c}$ is the speed of sound in the material and equals $((K + (4/3)G)/\varrho_0)^{1/2}$. For a fixed mesh, we computed results for $Q_1 = 1.0$, 1.25 and 1.5, and for each value of Q_1, Q_2 was assigned values 0.02, 0.04 and 0.06. The time-history of the torque required to deform the tube was found to be virtually identical for the nine cases signifying that the average shear strain at which a shear band initiates is unaffected by the value of the artificial viscosity. Results presented below are for $Q_1 = 1.5$ and $Q_2 = 0.06$.

3.1. Effect of the fraction of plastic work converted into heat

Because the deformations have been assumed to be locally adiabatic, i.e., the effect of heat conduction has been neglected, the temperatue rise at a material point is directly proportional to the total plastic work done there. A lower fraction, β, of the plastic work converted into heat will delay the rise in the temperature of a material particle and hence, the shear band will initiate at a higher value of the average strain. That this indeed is the case is clear from the torque versus the average shear strain curves depicted in Fig. 2 for the three cases, namely, when 100%, 90%, or 80% of the plastic work is converted into heat. Because of the nonlinearities in the problem, the incremental changes in the value of the average shear strain are unequal for the same incremental changes in the value of β. Henceforth, we assume that all of the plastic work is converted into heat.

3.2. Effect of initial axial load

For the case when the tube is first axially loaded quasi-statically either in compression or in tension and then twisted with the load curves defined by Eq. (2.11), Figs. 3 and 4 illustrate the torque versus average shear strain curves for four different values of the axial load. Note that the maximum axial stress applied equals 45% of the value of the material parameters A appearing in Eq. (2.5). Because of the prestress, the shear stress and hence the torque required to initiate yielding

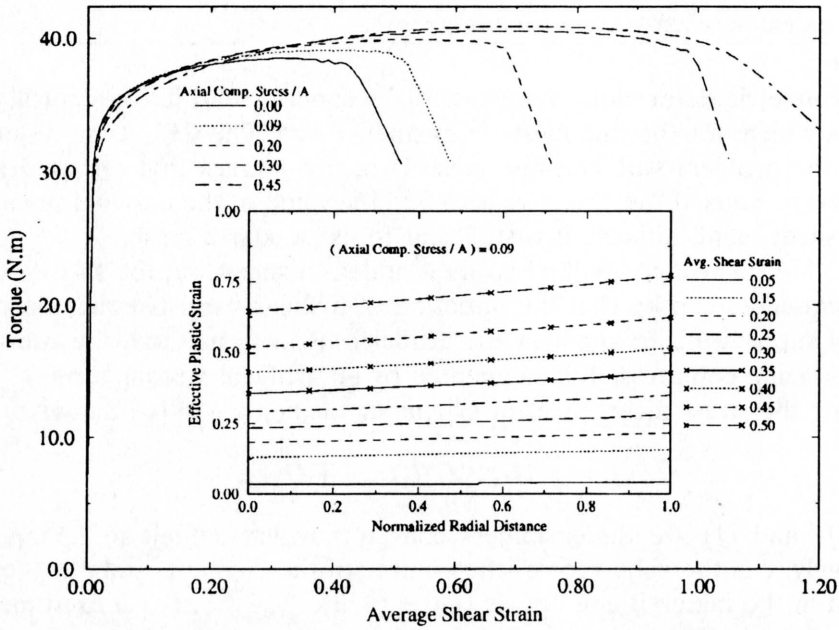

FIG. 3. Torque vs. average shear strain curves for five different values of the initial axial compressive stress. The insert shows the distribution of the effective plastic strain, at different times, on a radial line in the thinnest cross-section.

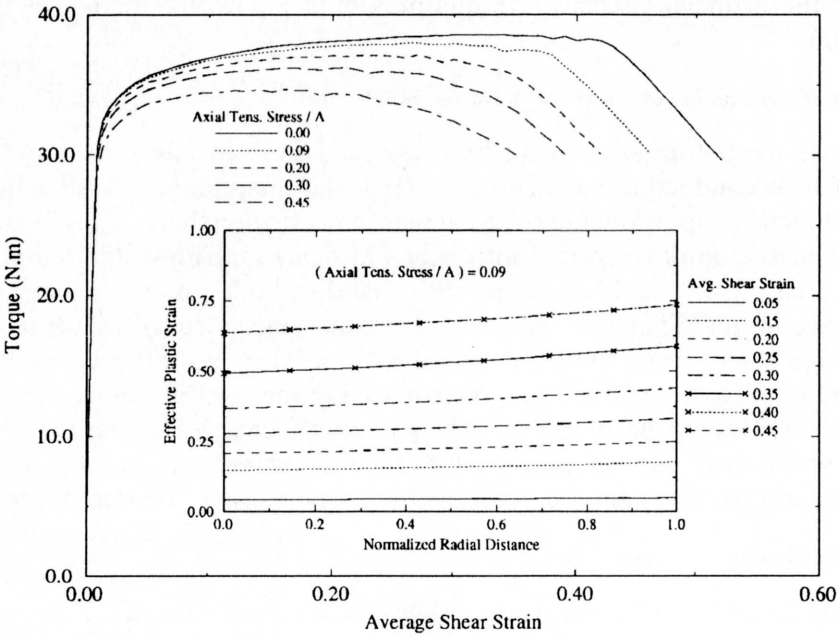

FIG. 4. Torque vs. average shear strain curves for four different values of the initial axial tensile stress. The insert depicts the distribution of the effective plastic strain, at different times, on a radial line in the thinnest cross-section.

should be less than that necessary when there is no prestress applied. Results plotted in Figs. 2 and 3 confirm this. The average shear strain at which a shear band initiates, as indicated by the drop in the torque required to deform the tube, increases with an increase in the magnitude of the axial compressive prestress and the reverse happens when the prestress is tensile. This trend contradicts the experimental observations of MURPHY [12] who reported that the average shear strain at the instant of the initiation of a shear band decreased with an increase in the magnitude of the axial compressive prestress. A close examination of the deformed shape of the tube indicated significant radial displacements of points on the central cross-section; for example, see Fig. 5. The inserts in Figs. 3 and 4 depict distribution of the effective plastic strain on a radial line in the thinnest section of the tube. It is clear that deformations of the tube along the radial line are nonhomogeneous, with the largest effective plastic strain occurring at points on the outermost surface of the tube. For axial prestress equal to $0.09A$, the shear band initiates at average shear strains of 0.48 and 0.37 for the compressive and tensile cases; however, the distribution of the effective plastic strain along the radial direction is essentially the same in the two cases. The severe deformations of the central cross-section result in an increase of the cross-sectional area for tubes prestressed in compression, and in a decrease of the cross-sectional area for tubes preloaded in tension. This change in the cross-sectional area delays the initiation of the shear band for the tube prestressed in compression and enhances the initiation of the shear band in the tube prestressed in tension. We note that the axial length of the tube decreases (increases) for the tube prestressed in compression (tension). It is not clear whether Murphy's experimental set-up allowed for this change in the axial length of the specimen. For the case of no preload, the tube length, the inner radius, and the outer radius remained unchanged.

We simulated a case when one end of the tube was held fixed and at the other end the axial component of velocity was first increased linearly from zero to the desired value in $20\,\mu s$, so as to induce an axial compressive stress in the tube by the desired amount. Subsequently, the axial component of velocity was decreased to zero and a tangential component of velocity was prescribed. This type of boundary data resulted in a gradual decrease of the axial compressive stress to zero. Analysis of the quasi-static problem involving a cylinder subjected to compressive and torsional loads given in CHAKRABARTY'S book [20] suggests that this trend is consistent with the predictions of the Prandtl-Reuss theory of plasticity.

Figure 6 depicts the evolution of the effective plastic strain on an axial line on the outer surface of the tube obtained by using a fine mesh. It is evident that deformations are nonhomogeneous even at an average shear strain of 0.05, and this nonhomogeneity in the deformations increases as the tube continues to be twisted. Eventually the deformations localize in the central element. Once it happens, the material outside this element does not undergo any more plastic deformations, and some parts may even unload. The width of the region of localization cannot be deciphered accurately since the mesh used is not fine enough.

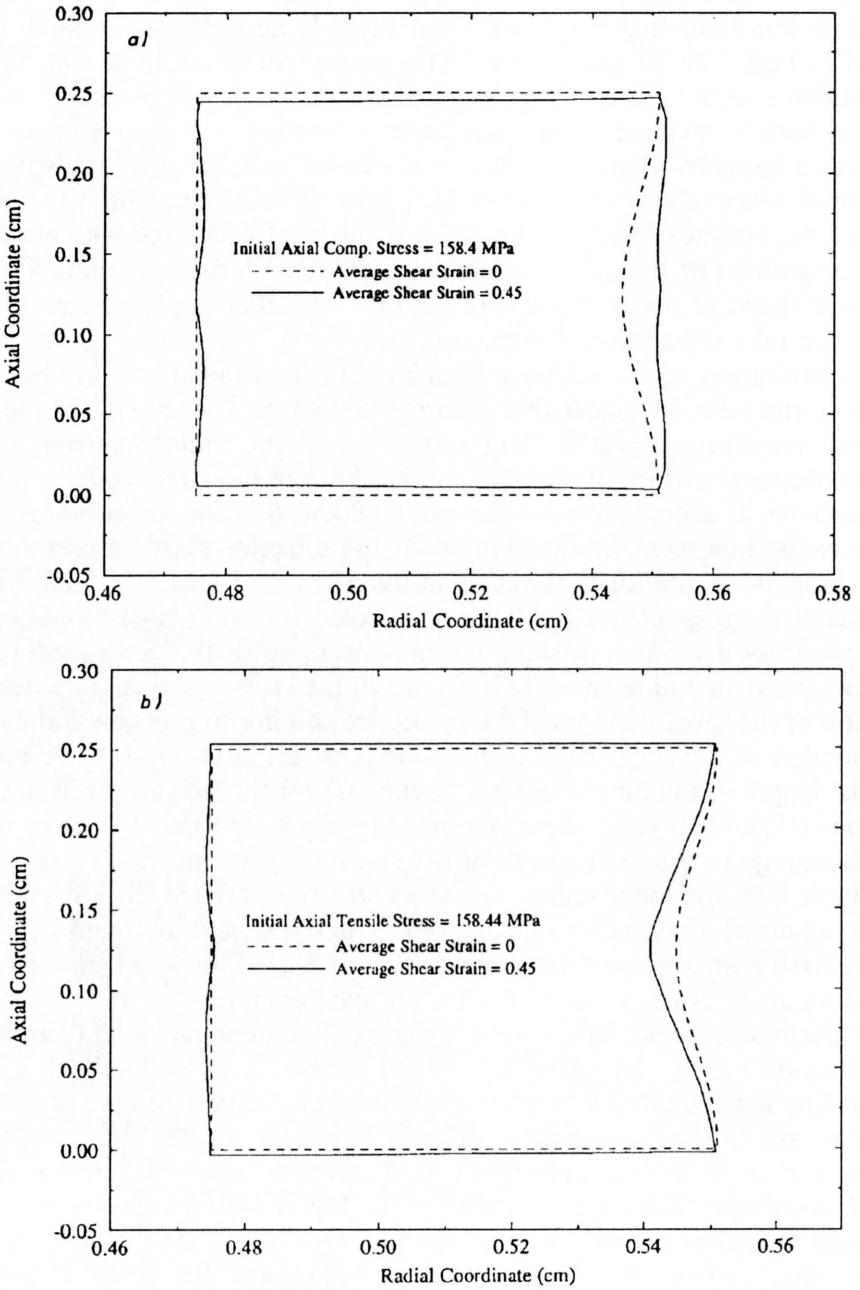

FIG. 5. Sections of the deformed tubes initially prestressed in (a) compression and (b) tension.

For this reason, the computations were stopped soon after the torque required to deform the tube began to drop. We note that in the code effective plastic strains are computed at the centroids of the elements.

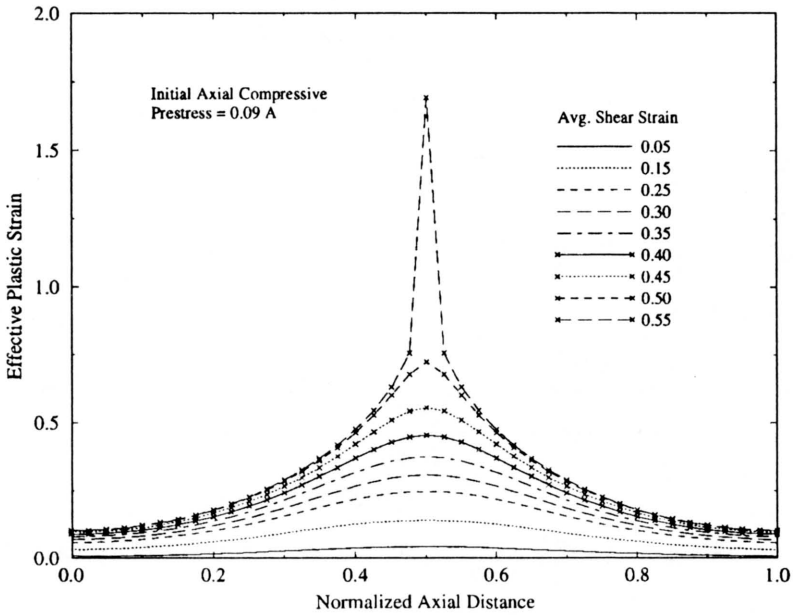

FIG. 6. Distribution of the effective plastic strain at different times on a line parallel to the axis of the tube and passing through the outermost point of the thinnest cross-section.

3.3. Effect of initial internal pressure

We assume that the end surfaces are held fixed in the axial direction and an internal pressure is applied slowly to the tubular specimen. Even when the internal pressure applied was 71.3 MPa, the stress state at a point was such as to cause no yielding of the material. Subsequently, with the internal pressure held steady, the end surfaces are twisted in equal and opposite directions by applying tangential velocity on them so as to induce an average shear strain-rate of $5000\,s^{-1}$. In Fig. 7 we have plotted the torque required to deform the tube versus the average shear strain. As expected, with an increase of the internal pressure the shear stress and hence the torque when the tube begins to deform, plastically decrease. However, the average shear strain at which a shear band initiates increases with an increase in the value of the internal pressure because of an increase in the inner and outer radii of the tube. Figure 8 illustrates the distribution, on a radial line, of the effective plastic strain at different times. Whereas initially the effective plastic strain is a little higher at points on the outermost surface than that at points on the innermost surface, the reverse happens after the shear band has initiated. Also, the variation of the effective plastic strain in the radial direction is not linear as was the case for the tube prestressed in axial tension or compression. Figure 9 depicts a longitudinal section of the tube just before the torque is applied and also when the average strain equals 0.45. It is clear that significant radial displacements of material points occur during the time the tube is being twisted.

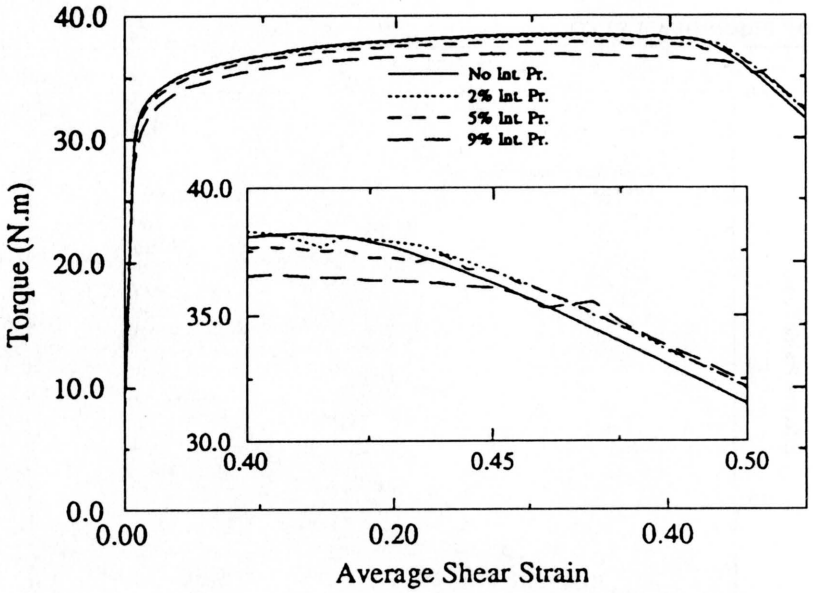

FIG. 7. Torque vs. average shear strain curves for four different values of the internal pressure.

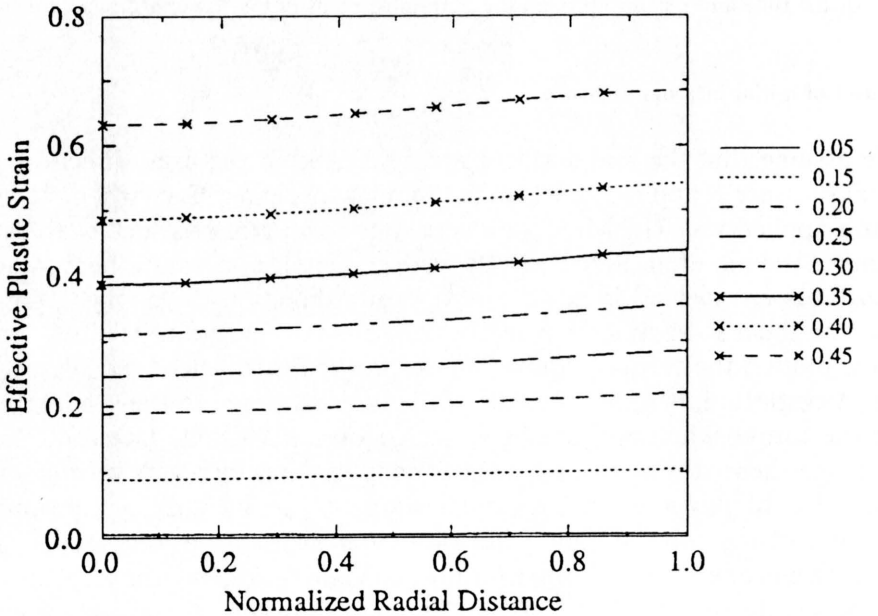

FIG. 8. The distribution of effective plastic strain, at different times, on a radial line in the thinnest cross-section.

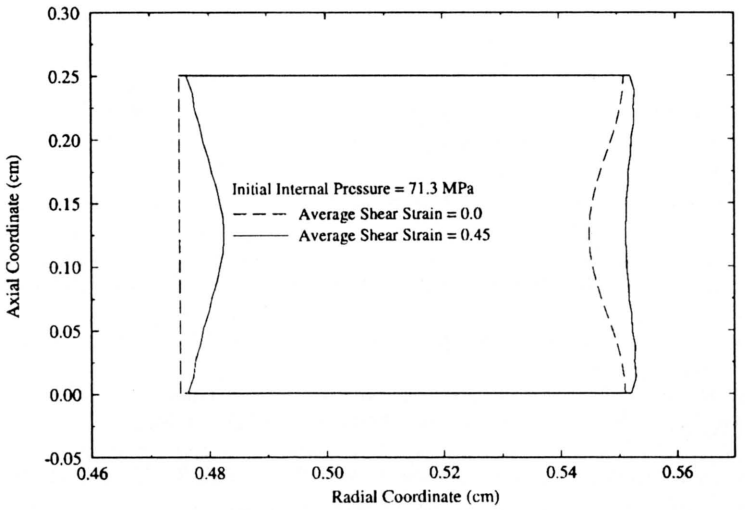

FIG. 9. A longitudinal section of the deformed tube.

4. Conclusions

We have studied the effects of the prior axial load and internal pressure applied quasi-statically on tubular specimens which are subsequently deformed dynamically in torsion. The thickness of the tube varies sinusoidally. It is accomplished by keeping the inner radius fixed but varying the outer radius, so as to obtain minimum thickness at the central cross-section of the tube. The thermomechanical response of the material of the tube is modeled by the Johnson-Cook law. For a tube with no preload, the inner radius and the axial length of the tube remained unchanged during its torsional deformations. However, for a preloaded tube, these dimensions changed noticeably. The average shear strain, γ_c, at the instant of the initiation of the shear band, as signified by a sudden drop in the torque required to deform the tube, is found to increase with an increase in the magnitude of the axial compressive stress or the internal pressure, and decrease with an increase in the value of the tensile stress. The main reason for the difference in the response of the tube prestressed in compression and tension is due to the deformations of the central section of the tube.

5. Acknowledgements

This work was supported by the U.S. National Science Foundation grant CMS9411383 to the Virginia Polytechnic Institute and State University. Some of the computations were performed on the NSF sponsored supercomputer center at the Cornell University, Ithaca, NY.

References

1. H. TRESCA, *On further application of the flow of solids*, Proc. Inst. Mech. Engng., **30**, 301–345, 1878.
2. H.F. MASSEY, *The flow of metal during forging*, Proc. Manchester Assoc. Engng., 21–26, 1926.
3. C. ZENER and J.H. HOLLOMON, *Effect of strain rate on plastic flow of steel*, J. Appl. Phys., **14**, 22–32, 1944.
4. H.C. ROGERS, *Adiabatic plastic deformation*, Ann. Rev. Mat. Sci., 299–311, 1979.
5. R.J. CLIFTON, *Adiabatic shear banding*, Material Response to Ultra-High Loading Rates, NRC Report NMAB-356, 129–142, 1980.
6. G.B. OLSON, J.F. MESCALL and M. AZRIN, *Adiabatic deformation and strain localization*, [in:] Shock Waves and High Strain-Rate Phenomenon in Metals, M.A. MEYERS and L.E. MURR [Eds.], Plenum Press, NY, 221–247, 1980.
7. H.M. ZBIB, T. SHAWKI and R.C. BATRA [Eds.], *Material Instabilities*, Special Issue of Applied Mechanics Reviews, **45**, 3, March 1992.
8. R.C. ARMSTRONG, R.C. BATRA, M.A. MEYERS and T.W. WRIGHT [guest editors], *Special Issue on Shear Instabilities and Viscoplasticity Theories*, Mech. Materials, **17**, 83–327, 1994.
9. K.A. HARTLEY, J. DUFFY and R.H. HAWLEY, *Measurement of the temperature profile during shear band formation in steels deforming at high strain rates*, J. Mech. Phys. Solids, **35**, 283–301, 1987.
10. A. MARCHAND and J. DUFFY, *An experimental study of the formation process of adiabatic shear bands in a structural steel*, J. Mech. Phys. Solids, **36**, 251–283, 1988.
11. J.H. GIOVANOLA, *Adiabatic shear banding under pure shear loading. Part I. Direct observation of strain localization and energy dissipation measurements*, Mech. Materials, 7, 59–72, 1988.
12. B.P. MURPHY, *Shear band formation in a structural steel under a combined state of stress*, M. Sc. Thesis, Brown University, Providence 1990.
13. C.A. TRUESDELL and W. NOLL, *Nonlinear field theories of mechanics*, Handbuch der Physik, III/3, S. FLÜGGE [Ed.], Springer Verlag, Berlin 1965.
14. W.S. FARREN and G.I. TAYLOR, *The heat developed during plastic extrusion of metal*, Proc. Roy. Soc., **A107**, 422, 1925.
15. A.U. SULJOADIKUSUMO and O.W. DILLON, Jr., *Temperature distribution for steady axisymmetric extrusion with an application to Ti-6A1-4V. Part 1*, J. Thermal Stresses, **2**, 97–112, 1979.
16. R.C. BATRA and C.H. KIM, *Effect of heat conduction on the initation and growth of shear bands*, Int. J. Engng. Sci., **29**, 949–960, 1991.
17. R.C. BATRA and Z. PENG, *Development of shear bands in dynamic plane strain compression of depleted uranium and tungsten blocks*, Int. J. Impact Engng., 1995 [to appear].
18. G.R. JOHNSON and W.H. COOK, *Constiutive model and data for metals subjected to large strains, high strain rates and high temperatures*, Proc. 7th Int. Symp. Ballistics, pp. 541–548, The Hague, The Netherlands 1983.
19. A.M. RAJENDRAN, *High strain rate behavior of metals, ceramics and concrete*, Report # WL-TR-92-4006, Wright Patterson Air Force Base, 1992.
20. R.G. WHIRLEY and J.O. HALLQUIST, *DYNA3D user's manual (A nonlinear "Explicit", three-dimensional finite element code for solid and structural mechanics)*, UCRL-MA-107254, Univ. California, Lawrence Livermore National Laboratory, 1991.
21. J. CHAKRABARTY, *Theory of plasticity*, McGraw Hill Book Co., 1987.

DEPARTMENT OF ENGINEERING SCIENCE AND MECHANICS
VIRGINIA POLYTECHNIC INSTITUTE AND STATE UNIVERSITY, BLACKSBURG, USA.

Received February 27, 1995.

Arch. Mech., 47, 3, pp. 499–512, Warszawa 1995

Some remarks on domain-transition problems (*)

Z. CHEN (ALBUQUERQUE) and T. CLARK (LOS ALAMOS)

DOMAIN-TRANSITION PROBLEMS are characterized by an evolving local change of deformation mechanisms from a macroscopically uniform deformation field. Localization and turbulence are two of the examples of current interest. One of the important features associated with the domain-transition is the formation and propagation of a material boundary between two sub-domains of different deformation mechanisms. Since various approaches have been proposed to model specific domain-transition phenomena in specific fields of continuum mechanics without mutual communications, an attempt is made here, based on the moving jump forms of conservation laws, to explore the common feature behind these different approaches. With an emphasis on localized creep damage, the possibility of simplifying existing modeling procedures is investigated, which might yield a unified simple approach to analyze different domain-transition problems.

1. Introduction

INTERDISCIPLINARY RESEARCH provides a mutual benefit in the evolution of modern science and technology. Different physical phenomena often resemble each other in certain forms. Better results may be achieved with less efforts if researchers in diverse fields communicate with each other. To facilitate interdisciplinary research, domain-transition problems in continuum mechanics are considerd here due to their importance in environmental- and manufacturing-related applications.

Domain-transition problems are characterized by an evolving local change of deformation mechanisms from a macroscopically uniform deformation field. Localization and turbulence are the examples of current interest in solid mechanics and fluid mechanics, respectively. The similarity in modeling these two physical phenomena has been briefly discussed by CHEN and CLARK [1]. For localization problems, there exists a change in the type of governing equations corresponding to a local change in deformation mechanisms, if local constitutive models are used. For turbulence modeling, the Reynolds stress tensor has non-zero elements, in particular, a non-zero trace, inside the turbulent region, while the trace of the Reynolds stress tensor is taken to be zero outside the turbulent region. One of the important features associated with the domain-transition is the formation and propagation of a material boundary between two sub-domains of different material properties. Across the moving material boundary, there might exist some jumps in field variables such as mass density, stress, strain, velocity or internal state variables. The information from one sub-domain can be transferred to

(*) Paper presented at 30th Polish Solid Mechanics Conference, Zakopane, September 5–9, 1994.

another one via a certain type of continuity conditions. Since every physical phenomenon must follow the conservation laws, the moving jump forms of conservation laws are employed here to explore the common feature of domain-transition problems. With an emphasis on localized creep damage, the possibility of simplifying existing modeling procedures is investigated. As a result, a unified simple approach might be available to analyze different domain-transition problems.

An outline of the remainder of this paper is as follows. Section 2 reviews some basic concepts, and modeling issues in localization and turbulence. Based on the moving jump forms of conservation laws, both a deterministic and a stochastic way are taken in Sec. 3 to show how the evolution of localized creep damage can be predicted in a proposed simple manner. Finally, some concluding remarks are given in Sec. 4.

2. Background

Since a significant amount of energy dissipation is associated with the evolution of localization, much research has been conducted in experimental, theoretical and computational aspects of localization problems, as reviewed recently by CHEN and SCHREYER [2]. Although various promising analytical and numerical approaches exist in the current literature, there are still some pressing limitations that prohibit the successful prediction of localization phenomena in a general case. Among the continuum models proposed, for instance, the experimental means to identify model parameters and the physics behind boundary conditions is not sufficient for a higher-order models; Mode-I failures can not be properly regularized by the Cosserat approach; and the slow loading rates as in the cases of creep and relaxation can not be well-specified by rate-dependent local models. And also, the transition between different failure modes is not well-known.

In fact, the key component of various modeling approaches for localization is nothing but controlling the evolution of inhomogenous interactions among material particles. In a macro-mechanical sense, however, the evolution process might be equally well characterized by the formation and propagation of a material surface discontinuity associated with a local change in terms of material properties. Based on the essential feature of localization phenomena observed, hence, a partitioned-modeling approach has been proposed with the introduction of moving boundaries [3]. The basic ideas of the approach are that different local constitutive models are used inside and outside the localized deformation zone with a moving material boundary being defined between two sub-domains, and that the constitutive law governing the moving boundary depends on localization mechanisms. As a result, simplified governing differential equations can be formulated in the partitioned domains for given boundary and initial conditions. To establish a sound mathemathical foundation for the partitioned-modeling approach, an attempt has been made to investigate the use of moving jump conditions in

defining the moving boundary [4]. By taking the initial point of localization as that point where the type of the governing equations changes, i.e., a hyperbolic to an elliptic type for dynamic problems and elliptic to another elliptic type for static problems, a moving material boundary between localized and non-localized deformation zones can be defined through the moving jump forms of conservation laws across the boundary. Jumps in density, velocity, strain and stress can be accommodated on this moving surface of discontinuity between two sub-domains of different deformation mechanisms. Thus, localization problems might be considered in the same category as shock and solidification phenomena. Analytical solutions for one-dimensional rate-independent problems have been obtained to illustrate the proposed procedure [4]. However, analytical solutions might not be available in general, and instead, a simple approach must be developed to accommodate different constitutive models. To this end, the moving jump forms of conservation laws in mass density and linear momentum are reviewed next with an emphasis on their implication to different failure modes. For convenience but with no loss of generality, it is assumed that no energy sources or sinks occur in the purely mechanical problems so that the conservation in mass and linear momentum implies that in energy.

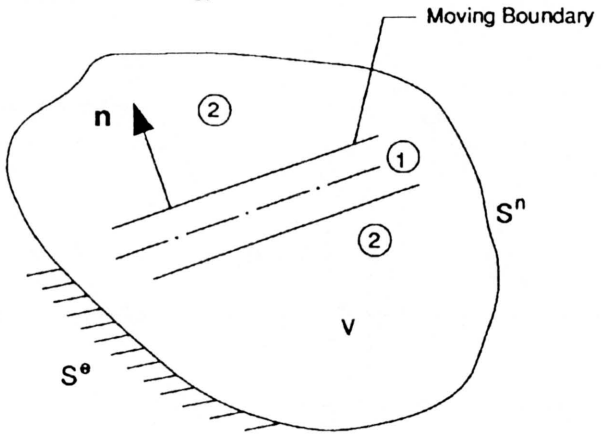

FIG. 1. Continuum body with discontinuous failure.

Consider a continuum body V subjected to essential and natural boundary conditions S^e and S^n, as shown in Fig. 1. With bold-faced letters denoting tensors of first or higher orders, a direct notation is employed to describe equations. In a three-dimensional framework, the spatial forms of conservation in mass and linear momentum can be written as

$$\dot{\varrho} + \varrho(\nabla \cdot \mathbf{v}) = 0 \tag{2.1}$$

and

$$\varrho \mathbf{a} - \nabla \cdot \boldsymbol{\sigma} = \mathbf{0}, \tag{2.2}$$

respectively. In Eqs. (2.1) and (2.2), ϱ denotes the mass density, ∇ gradient operator, $\mathbf{v}$ particle velocity vector, $\mathbf{a}$ particle acceleration vector, and $\boldsymbol{\sigma}$ Cauchy stress tensor, with body forces omitted. If there exist jumps in certain field variables across a boundary moving with a velocity $\mathbf{v}_b$ in the space, the jump conditions corresponding to (2.1) and (2.2) take the forms of

$$\varrho_1(\mathbf{v}_1 - \mathbf{v}_b)\cdot\mathbf{n} = \varrho_2(\mathbf{v}_2 - \mathbf{v}_b)\cdot\mathbf{n} \tag{2.3}$$

and

$$\varrho_1[(\mathbf{v}_1 - \mathbf{v}_b)\cdot\mathbf{n}]\mathbf{v}_1 - \varrho_2[(\mathbf{v}_2 - \mathbf{v}_b)\cdot\mathbf{n}]\mathbf{v}_2 = (\boldsymbol{\sigma}_1 - \boldsymbol{\sigma}_2)\cdot\mathbf{n}, \tag{2.4}$$

in which the subscripts 1 and 2 denote field variables on the two sides of the moving boundary, and $\mathbf{n}$ the unit normal to the boundary.

Introduce a local coordinate system with coordinate x_3' parallel to $\mathbf{n}$. For the purpose of simplicity, consider the jumps in the $x_1'x_3'$-plane with the unit vector $\mathbf{t}$ being along the x_1'-axis, as depicted in Fig. 2. The normal speed of the moving

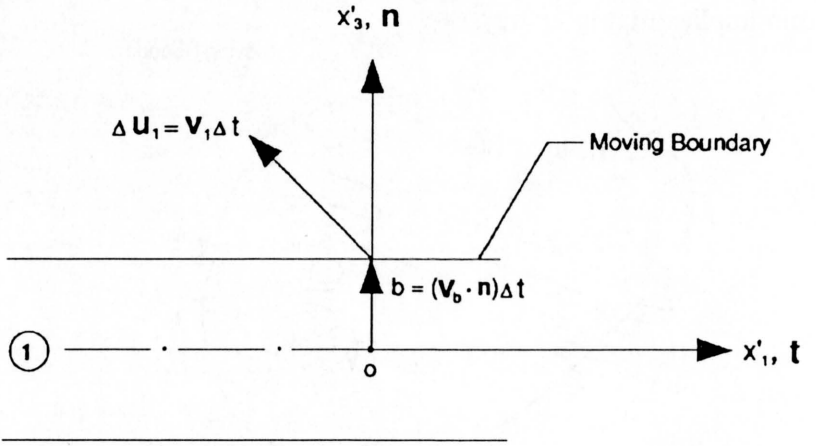

FIG. 2. A local coordinate system.

boundary, $\mathbf{v}_b\cdot\mathbf{n}$, represents the trend of expansion, and the tangential speed, $\mathbf{v}_b\cdot\mathbf{t}$, the trend of shearing. As a result, the trace of the moving boundary reflects the effect of different failure modes, as illustrated later. Suppose that the origin of the coordinate system is the point from which localization evolves, and that the half-band width, b, of side 1 increases as manifested by the outward movement of the boundary. To identify different failure modes, let us first write down the following conventional definitions:

$$\begin{aligned}
&\text{Diffuse Failure} \Rightarrow && \mathbf{v}_1 = \mathbf{v}_2 && \text{and} && \dot{\boldsymbol{\varepsilon}}_1 = \dot{\boldsymbol{\varepsilon}}_2;\\
&\text{Localized Failure} \Rightarrow && \mathbf{v}_1 = \mathbf{v}_2 && \text{and} && \dot{\boldsymbol{\varepsilon}}_1 \neq \dot{\boldsymbol{\varepsilon}}_2;\\
&\text{Discrete Failure} \Rightarrow && \mathbf{v}_1 \neq \mathbf{v}_2 && \text{and} && \dot{\boldsymbol{\varepsilon}}_1 \neq \dot{\boldsymbol{\varepsilon}}_2,
\end{aligned}$$

with $\dot{\boldsymbol{\varepsilon}}_1$ and $\dot{\boldsymbol{\varepsilon}}_2$ being the total strain rates on the side 1 and 2, respectively. As can be seen, the transition between continuous and discontinuous failure modes is characterized by the condition of localized failure.

The mechanisms involved in different failure modes can be made clear by invoking the moving jump form of conservation laws. The substitution of the condition for diffuse failure into Eqs. (2.3) and (2.4) results in no jumps in any field variables across the moving boundary. In other words, the moving boundary is meaningless. However, the case for localized failure is not simple. A careful reasoning must be performed. Since the condition of $\mathbf{v}_1 = \mathbf{v}_2$ still holds for localized failure, the result similar to the case of diffuse failure, except for $\dot{\boldsymbol{\varepsilon}}_1 \neq \dot{\boldsymbol{\varepsilon}}_2$, follows if there is no jump in mass density. However, the occurrence of a jump in mass density would yield

$$\mathbf{v}_1 \cdot \mathbf{n} = \mathbf{v}_2 \cdot \mathbf{n} = \mathbf{v}_b \cdot \mathbf{n} \tag{2.5}$$

based on Eq. (2.3). The substitution of Eq. (2.5) into Eq. (2.4) would then result in the continuity of the traction across the moving boundary, i.e.,

$$(\boldsymbol{\sigma}_1 - \boldsymbol{\sigma}_2) \cdot \mathbf{n} = \mathbf{0} \tag{2.6}$$

for $\dot{\boldsymbol{\varepsilon}}_1 \neq \dot{\boldsymbol{\varepsilon}}_2$. Because there is a jump in the strain rate for localized failure, it makes sense to claim that a corresponding jump must exist in mass density. Thus, Eqs. (2.5) and (2.6) together with a jump in mass density represent the essential feature of localized failure.

To examine how the jump in the strain rate is derivable from Eq. (2.6), assume the stress tensor in side 1 is related to that in side 2 by

$$\boldsymbol{\sigma}_1 = \boldsymbol{\sigma}_2 + \mathbf{T}_1 : \dot{\boldsymbol{\varepsilon}}_1^k \tag{2.7}$$

in which $\mathbf{T}_1$ denotes a fourth-order tangent stiffness tensor with minor symmetries, and $\dot{\boldsymbol{\varepsilon}}_1^k$ the jump in the strain rate field. For rate-dependent problems such as creep and relaxation, a tangent tensor can be derived if it is assumed that the total strain rate is equal to the inelastic strain rate whenever the inelastic state is activated during the loading process. According to Maxwell's compatibility conditions, the jump $\dot{\boldsymbol{\varepsilon}}_1^k$ must be a rank-one tensor of the form

$$\dot{\boldsymbol{\varepsilon}}_1^k = \frac{1}{2b}(\dot{\mathbf{m}} \otimes \mathbf{n} + \mathbf{n} \otimes \dot{\mathbf{m}}). \tag{2.8}$$

To be consistent with the definition of localized failure, the vector $\dot{\mathbf{m}}$ in Eq. (2.8) is taken to be $\mathbf{v}_1$ that is equal to $\mathbf{v}_b$ according to Eq. (2.5). Thus, it follows that $\mathbf{n} \cdot \dot{\boldsymbol{\varepsilon}}_1^k \cdot \mathbf{n} = \dfrac{\mathbf{v}_1 \cdot \mathbf{n}}{b}$ represents Mode I failure, and $\mathbf{n} \cdot \dot{\boldsymbol{\varepsilon}}_1^k \cdot \mathbf{t} = \dfrac{\mathbf{v}_1 \cdot \mathbf{t}}{2b}$ Mode II failure. During a time increment Δt, the total displacement at the material point of

concern is given by $\Delta \mathbf{u}_1 = \mathbf{v}_1 \Delta t$, as shown in Fig. 2. The use of Eqs. (2.6) – (2.8) then yields the classical necessary condition for a discontinuous bifurcation:

$$\mathbf{Q} \cdot \dot{\mathbf{m}} = \mathbf{0} \tag{2.9}$$

with $\mathbf{Q} = \mathbf{n} \cdot \mathbf{T}_1 \cdot \mathbf{n}$ being the acoustic tensor. In other words, the arguments based on the moving jump forms of conservation laws produce the same condition (2.9) as derived from classical approaches based on certain assumptions. An eigen-analysis can be performed to find out the orientation of the localized failure mode. However, the magnitude of failure is undetermined by Eq. (2.9). A suitable procedure must be developed to predict the evolution of the localized failure, for which the research in turbulence modeling [5, 6] might provide a heuristic hint.

As can be found from the comparison of nonlocal investigations in solids and fluids [1], the initiation and subsequent evolution of a turbulent zone from a laminar flow field resembles the localization phenomenon, based on the viewpoint of interactions among material particles. Historically, two different kinds of modeling procedures have been followed in the fluid mechanics and solid mechanics fields, respectively. Usually, a single model, the Reynolds-averaged Navier – Stokes equations with non-zero Reynolds stresses, is used to predict the evolution of turbulent region only, while in solid mechanics a single enhanced constitutive model is invoked to handle both localized and nonlocalized deformation fields. As a result, two different sets of governing equations hold inside and outside the turbulent region, whereas a single set of enhanced governing equations strives to be well-posed in a continuum domain containing localized deformations. However, the small size of the localization zone and limitations of existing experimental techniques might not justify the expense of a detailed modeling of localization.

Recent work by SIMO and OLIVER [7] illustrates that strain softening models must lead to the appearance of strong discontinuities (discrete failure modes), and the discontinuous solutions for rate-independent softening solids can be obtained based on the kinematics of strong discontinuities. In the next section, two methods are employed to illustrate a simple approach for predicting localized failure modes (weak discontinuities) based on the moving jump forms of conservation laws and on analogies to turbulence modeling.

3. Proposed approach

The basic idea of the proposed approach is that the essential feature of localization might be predicted without a detailed modeling effort as long as the equation governing the moving boundary is determined between two sub-domains of different mechanisms.

To illustrate the approach, a one-dimensional creep problem is considered, through which the applicability of the solution procedure to a general case can be made clear. For a bar of length L, which is fixed at one end and loaded at

other end by a constant tensile force f, the transition between the secondary and tertiary stages of creep is often characterized by the formation and evolution of localized creep damage [8].

To predict the essential feature of creep damage, it is assumed in the first method that a moving material boundary is initiated and two local rate-dependent models hold to the left and right of the boundary, if a critical state is reached. Inside the damage zone, i.e., in zone 1, the total strain rate is given by

$$\dot{\varepsilon}_1 = f_1(s_1, T, \psi, \varphi), \tag{3.1}$$

and outside the damage zone, i.e., in zone 2, the total strain rate takes the form of

$$\dot{\varepsilon}_2 = f_2(s_2, T, \psi), \tag{3.2}$$

with T being the absolute temperature, and ψ and φ denoting the measure of plasticity and damage, respectively. The plasticity and damage evolution equations can be formulated based on the work by CHAN *et al.* [9] which assumes a uniform damage across a material sample. The true stress s reflects the damage effect. Because the damage term is active only inside the damage zone, the true stress s_1 will accelerate $\dot{\varepsilon}_1$, while $\dot{\varepsilon}_2$ is only due to the dislocation flow. As a result, the evolution of localized creep damage can be predicted whithout invoking enhanced constitutive models, as long as the moving boundary is determined. It should be pointed out that conventional rate-dependent models do not introduce a length scale into creep problems, and hence, do not yield mesh-independent solutions.

With b^0 denoting the length of initial imperfection, and with the strain inside the damage zone, ε_1, being known at the critical state, the moving boundary can be determined based on the results in Sec. 2. Assuming that the fixed end initiates damage and the strain inside the damage zone is constant, the solution procedure for given total strain increments $\Delta\varepsilon^n$ is summarized as below with the superscript n denoting the loading step:

Step 1. $\varepsilon_1^n = \varepsilon_1^{n-1} + \Delta\varepsilon_1^n$.

Step 2. $u_b^n = \varepsilon_1^n b^{n-1}$.

Step 3. $b^n = b^{n-1} + u_b^n$.

By using the condition of localized failure, the deformation response outside the damage zone can be easily calculated at any time because the condition of $u_1 = u_2 = u_b$ holds and $\dot{\varepsilon}_2$ is known. As can be seen from the above analysis, the moving material boundary can be derived from the moving jump forms of conservation laws as long as the constitutive models in both sides of the boundary are known. An alternative method will then be a direct formulation of the equation governing the boundary. As long as the boundary is known, simple local models can also be derived according to the jump conditions.

Based on turbulence modeling, a stochastic method is used here to derive the equation governing the moving boundary. According to the recent studies on the failure wave [10], it is assumed that the evolution of creep damage φ is of wave type. For Mode I damage along the normal to the boundary after a critical state is reached, the "exact" evolution equation is then defined to be

$$\frac{\partial^2 \varphi}{\partial x_n \partial x_n} = A(\varphi) \frac{\partial^2 \varphi}{\partial t^2} \tag{3.3}$$

with the subscript n emphasizing the normal component of localized damage. Equation (3.3) is hyperbolic through the whole damage process. Although a creep damage wave has not been conclusively demonstrated, the propagation of a delayed front of cracking following the initial elastic compression wave has been observed in some dynamic experiments, which might be due to the sudden release of the large strain energy stored behind the large-amplitude elastic wave [10]. Further study is required to understand how a critical energy state can drive a damage wave.

We introduce the average over ensembles of samples of the damage, and decompose the variables into a mean part, denoted by an overbar, and a fluctuating part with zero mean, denoted by a prime, as follows:

$$\varphi = \overline{\varphi} + \varphi' \tag{3.4}$$

and

$$A(\varphi) = \overline{A(\varphi)} + [A(\varphi)]'. \tag{3.5}$$

For convenience, we will assume a simple linear relation for $A(\varphi)$, namely,

$$A(\varphi) = \alpha_0 + \alpha_1(\overline{\varphi} + \varphi') \tag{3.6}$$

with α_0 and α_1 being material parameters. For an elasto-damage process, α_0 corresponds to the inverse of the square of elastic wave speed. Substituting (3.4) and (3.6) into (3.3) yields

$$\frac{\partial^2(\overline{\varphi} + \varphi')}{\partial x_n \partial x_n} = \{\alpha_0 + \alpha_1(\overline{\varphi} + \varphi')\} \frac{\partial^2(\overline{\varphi} + \varphi')}{\partial t^2}. \tag{3.7}$$

Averaging Eq. (3.7) over ensembles and exploiting the zero-mean property of the fluctuating quantities give

$$\frac{\partial^2 \overline{\varphi}}{\partial x_n \partial x_n} = \{\alpha_0 + \alpha_1 \overline{\varphi}\} \frac{\partial^2 \overline{\varphi}}{\partial t^2} + \alpha_1 \overline{\varphi' \frac{\partial^2 \varphi'}{\partial t^2}}. \tag{3.8}$$

Equation (3.8) is "exact" for $\overline{\varphi}$, but involves the unknown correlation, $\overline{\varphi'\varphi'_{,tt}}$. Subtracting (3.8) from (3.7) results in an evolution equation for the fluctuations, i.e.,

$$\frac{\partial^2\varphi'}{\partial x_n \partial x_n} = (\alpha_0 + \alpha_1\overline{\varphi})\frac{\partial^2\varphi'}{\partial t^2} + \alpha_1\varphi'\frac{\partial^2\overline{\varphi}}{\partial t^2} + \alpha_1\left\{\varphi'\frac{\partial^2\varphi'}{\partial t^2} - \overline{\varphi'\frac{\partial^2\varphi'}{\partial t^2}}\right\}. \tag{3.9}$$

Multiplying (3.9) by φ' gives

$$\varphi'\frac{\partial^2\varphi'}{\partial x_n \partial x_n} = (\alpha_0 + \alpha_1\overline{\varphi})\varphi'\frac{\partial^2\varphi'}{\partial t^2} + \alpha_1\varphi'\varphi'\frac{\partial^2\overline{\varphi}}{\partial t^2} + \alpha_1\varphi'\left\{\varphi'\frac{\partial^2\varphi'}{\partial t^2} - \overline{\varphi'\frac{\partial^2\varphi'}{\partial t^2}}\right\}, \tag{3.10}$$

and averaging over ensembles of Eq. (3.10) then yields

$$\overline{\varphi'\frac{\partial^2\varphi'}{\partial x_n \partial x_n}} = (\alpha_0 + \alpha_1\overline{\varphi})\overline{\varphi'\frac{\partial^2\varphi'}{\partial t^2}} + \alpha_1\overline{\varphi'\varphi'}\frac{\partial^2\overline{\varphi}}{\partial t^2} + \alpha_1\overline{\varphi'\varphi'\frac{\partial^2\varphi'}{\partial t^2}}. \tag{3.11}$$

Equation (3.11) relates the unknown statistical quantity, $\overline{\varphi'\varphi'_{,xx}}$, to other statistical quantities, known and unknown.

At this point, the unknown correlations appearing in (3.11) will be modeled in terms of the "known" (i.e., to be computed) quantities by choosing the simplest dimensionally correct terms. First, we recast the derivatives as conservative terms to whatever degree is possible, as follows:

$$\overline{\varphi'\frac{\partial^2\varphi'}{\partial x_n \partial x_n}} = \frac{1}{2}\frac{\partial^2\overline{\varphi'\varphi'}}{\partial x_n \partial x_n} - \overline{\frac{\partial\varphi'}{\partial x_n}\frac{\partial\varphi'}{\partial x_n}}. \tag{3.12}$$

Note that $\overline{\varphi'_{,x}\varphi'_{,x}}$ is non-negative definite, and is, in some sense, a measure of the steepness of gradients of the damage. A simple model for this term may be

$$\overline{\frac{\partial\varphi'}{\partial x_n}\frac{\partial\varphi'}{\partial x_n}} \propto \frac{\overline{\varphi'\varphi'}}{\ell^2}, \tag{3.13}$$

where ℓ is a characteristic length scale for the damage. If the rate of growth of the length scale is proportional to the rate of change of the fluctuating damage, it follows that

$$\overline{\frac{\partial\varphi'}{\partial x_n}\frac{\partial\varphi'}{\partial x_n}} = c_0\frac{\overline{\varphi'\varphi'}}{\ell} \tag{3.14}$$

and

$$\frac{\partial\ell}{\partial t} = c_{\ell 0}\ell\left|\frac{\partial\overline{\varphi'\varphi'}}{\partial t}\right|, \tag{3.15}$$

where $c_{\ell 0}$ and c_0 are dimensionless constants. We follow an analogous route for the time derivative. With the assumption that the rate of change of the fluctuating damage parameter is proportional to the rate of change of the average damage, we get

$$\overline{\varphi' \frac{\partial^2 \varphi'}{\partial t^2}} = \frac{1}{2} \frac{\partial^2 \overline{\varphi' \varphi'}}{\partial t^2} - \overline{\frac{\partial \varphi'}{\partial t} \frac{\partial \varphi'}{\partial t}} \approx \frac{1}{2} \frac{\partial^2 \overline{\varphi' \varphi'}}{\partial t^2} - c_1 \frac{\partial \overline{\varphi}}{\partial t} \frac{\partial \overline{\varphi}}{\partial t}. \tag{3.16}$$

Again, c_1 is dimensionless constant. The last correlation on the right-hand side of (3.11) is third-order in the fluctuation, and is assumed to be zero. We recognize that the assumptions used here might appear unjustified, but we seek to merely demonstrate a possible approach to closure of the equations. Letting $\theta = \overline{\varphi' \varphi'}$ for convenience, the resulting system of equations, for the three quantities to be computed, is

$$\frac{1}{2} \frac{\partial^2 \theta}{\partial x_n \partial x_n} - c_0 \frac{\theta}{\ell^2} = (\alpha_0 + \alpha_1 \overline{\varphi}) \left\{ \frac{1}{2} \frac{\partial^2 \theta}{\partial t^2} - c_1 \left(\frac{\partial \overline{\varphi}}{\partial t} \right)^2 \right\} + \alpha_1 \theta \frac{\partial^2 \overline{\varphi}}{\partial t^2}, \tag{3.17}$$

$$\frac{\partial^2 \overline{\varphi}}{\partial x_n \partial x_n} = (\alpha_0 + \alpha_1 \overline{\varphi}) \frac{\partial^2 \overline{\varphi}}{\partial t^2} + \alpha_1 \left\{ \frac{1}{2} \frac{\partial^2 \theta}{\partial t^2} - c_1 \left(\frac{\partial \overline{\varphi}}{\partial t} \right)^2 \right\}, \tag{3.18}$$

and

$$\frac{\partial \ell}{\partial t} = c_{\ell 0} \ell \left| \frac{\partial \theta}{\partial t} \right|. \tag{3.19}$$

The above set of equations is closed, and thus, in principle, solvable. After rearranging the terms, we have

$$F(\theta, \overline{\varphi}, x_n) = \left\{ \frac{1}{\alpha_1^2 \theta - (\alpha_0 + \alpha_1 \overline{\varphi})^2} \right\} \left\{ \alpha_1 \left(\frac{1}{2} \frac{\partial^2 \theta}{\partial x_n \partial x_n} - c_0 \frac{\theta}{\ell^2} \right) - (\alpha_0 + \alpha_1 \overline{\varphi}) \frac{\partial^2 \overline{\varphi}}{\partial x_n \partial x_n} \right\},$$

$$G(\theta, \omega, \overline{\varphi}, x_n) = 2c_1 \omega^2 + \left\{ \frac{2}{(\alpha_0 + \alpha_1 \overline{\varphi})^2 - \alpha_1^2 \theta} \right\} \left\{ (\alpha_0 + \alpha_1 \overline{\varphi}) \left(\frac{1}{2} \frac{\partial^2 \theta}{\partial x_n \partial x_n} - c_0 \frac{\theta}{\ell^2} \right) - 2\alpha_1 \theta \frac{\partial^2 \overline{\varphi}}{\partial x_n \partial x_n} \right\},$$

and a first-order system of equations in t as below:

$$\frac{\partial \overline{\varphi}}{\partial t} = \omega, \tag{3.20}$$

$$\frac{\partial \omega}{\partial t} = F(\theta, \overline{\varphi}, x_n), \tag{3.21}$$

$$\frac{\partial \theta}{\partial t} = \sigma, \tag{3.22}$$

$$\frac{\partial \sigma}{\partial t} = G(\theta, \omega, \overline{\varphi}, x_n), \tag{3.23}$$

and

$$\frac{\partial \ell}{\partial t} = c_{\ell 0} \left| \frac{\partial \theta}{\partial t} \right|, \tag{3.24}$$

which can be solved via standard numerical schemes.

To illustrate the features of the model, Eqs. (3.20) – (3.24) are solved by using a fourth-order accurate Runge – Kutta – Fehlberg algorithm for the time advancement, and second-order finite-difference approximations for the spatial derivatives. The following values are chosen for the model parameters:

$$\alpha_0 = 1.0, \qquad \alpha_1 = 1.0, \qquad c_0 = 0.5, \qquad c_1 = 0.1, \qquad c_{\ell 0} = 0.5.$$

The initial conditions are assumed to be Gaussian as follows:

$$\overline{\varphi}(x,t) = 0.1,$$
$$\theta(x,t) = 0.05 \exp\left\{ - \left[10 \left(x - \frac{1}{2} \right) \right]^2 \right\}$$

and

$$\ell(x,t) = 10^{-3} + 10^{-1} \exp\left\{ - \left[10 \left(x - \frac{1}{2} \right) \right]^2 \right\}.$$

The numerical grid spacing is $\Delta_x = 0.01$, and the error criterion for the time advancement scheme is $\varepsilon = 10^{-7}$. It should be noted that a parametric study has not been performed for the model parameters. The calculations presented here are for illustrative purposes only.

Figure 3 shows the evolution of the average damage parameter. Note that the average damage appears to be evolving at an increasingly rapid rate, and is quite localized, showing very little spreading, or smearing. This sharp change of the function appears to cause some degree of oscillation in the numerical solution. This oscillation also appears in Fig. 4, which shows the evolution of the fluctuating damage self-correlation. We have not determined to what degree these oscillations are due to the numerical algorithm. It is important to know that $\overline{\varphi'\varphi'}$ should, by definition, never be negative. The model presented above, however, does not impose this condition. As can be observed from the figures, the damage wave front identifies the moving boundary, and the average damage measure reflects the overall damage effect on the creep bar. And also, it is interesting to see that the fluctuating damage self-correlation decreases in time as the fluctuations serve to drive the average damage. This indicates that the various fluctuations in the damage zone tend to coalesce in some sense to form an average damage (a macrocrack), and that this coalesced damage shows less statistical variation as time progresses. Hence, the coalesced damage seems to be characteristic of this type of models.

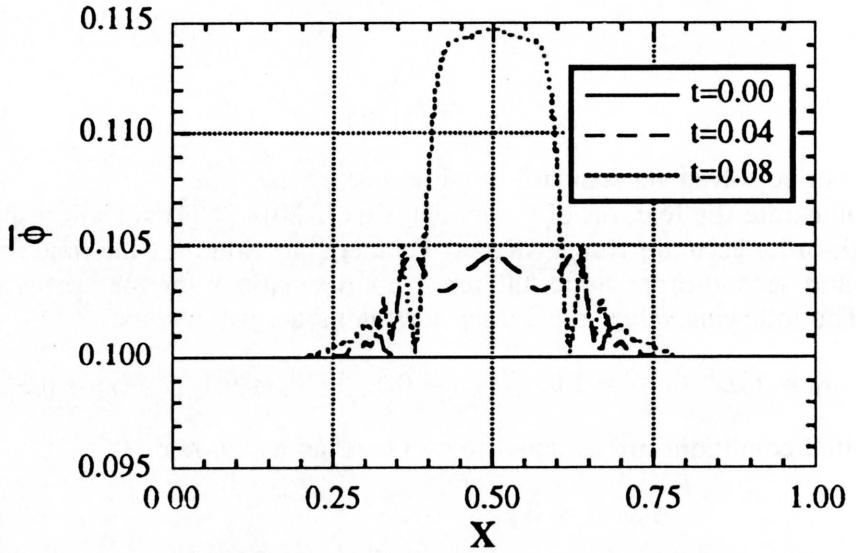

FIG. 3. Evolution of the averaged damage parameter.

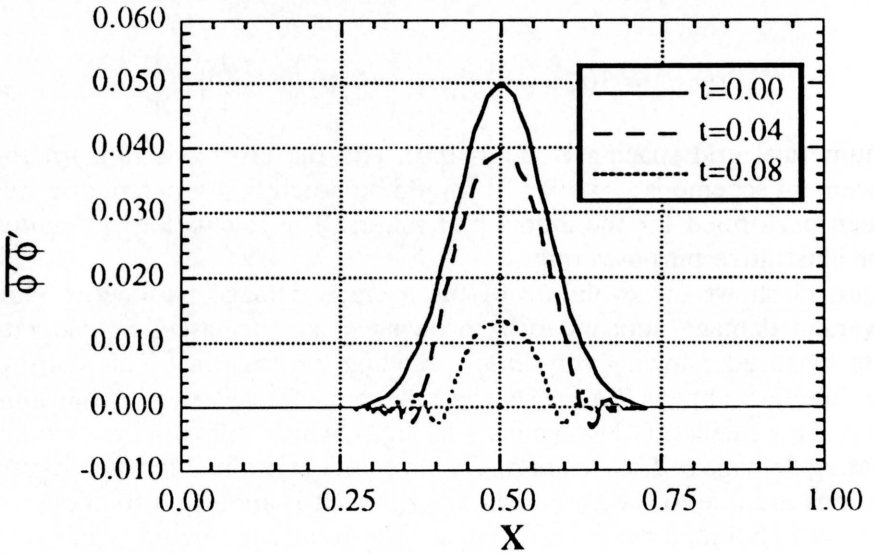

FIG. 4. Evolution of the fluctuating damage self-correlation.

As shown by de BORST *et al.* [11], a local stochastic model without an evolving internal structure can not predict the evolution of localization. The stochastic model presented here provides an alternative for localization problems, without invoking nonlocal terms. Because an evolving structure for the internal damage variable is constructed only inside the damage zone, the material boundary between damaged and undamaged zones can be easily determined. With the use of

moving jump forms of conservation laws, the overall response of localized creep damage can then be found.

4. Conclusion

As characterized by an evolving local change of deformation mechanisms from a macroscopically uniform deformation field, the common feature of domain-transition problems has been explored based on the moving jump forms of conservation laws. Without considering too much detail within a small zone, the evolution process might be predicted by a simple approach, i.e., the use of a moving material boundary between two sub-domains of different material properties. Future research is required to verify and improve the adequacy of the proposed simple constitutive models.

Acknowledgment

This work was partially supported by the US-DOE through Sandia National Laboratories (SNL), Los Alamos National Laboratory (LANL) and New Mexico Waste-Management Education and Research Consortium (WERC). The interest shown by Dr. M. Marietta and Dr. D.E. Munson of SNL is gratefully acknowledged.

References

1. Z. CHEN and T. CLARK, *A comparison of nonlocal investigations in solids and fluids: An introduction*, Engng. Science Preprints, **28**, ESP28.91036, 1991.
2. Z. CHEN and H.L. SCHREYER, *On nonlocal damage models for interface problems*, Intern. J. Solids and Struc., **31**, 9, pp. 1241–1261, 1994.
3. Z. CHEN, *A partitioned-solution method with moving boundaries for nonlocal plasticity*, Modern Approaches to Plasticity, D. KOLYMBAS [Ed.], Elsevier, New York, NY, USA, pp. 449–468, 1993.
4. Z. CHEN and D. SULSKY, *A partitioned-modeling approach with moving jump conditions for localization*, Intern. J. Solids and Struct., **32**, 13, pp. 1893–1905, 1995.
5. N.C. MARKATOS, *The mathematical modelling of turbulent flows*, Appl. Math. Modelling, **10**, pp. 190–220, 1986.
6. J.L. LUMLEY, *Computational modeling of turbulent flows*, Advances in Appl. Mech., **18**, pp. 123–176, 1978.
7. J.C. SIMO and J. OLIVER, *A new approach to the analysis and simulation of strain softening in solids*, [in:] Fracture and Damage in Quasibrittle Structures: Experiment, Modeling and Computer Analysis, Z.P. BAZANT, Z. BITTNAR, M. JIRASEK and J. MAZARS [Eds.], E & FN Spon, New York, NY, USA, pp. 25–39, 1994.
8. Z. CHEN and M.L. WANG, *A micro- and macro-mechanical modeling of creep mechanisms for the WIPP rock salt*, Proc. of 3rd Annual WERC Technology Development Conference, DOE/WERC, USA, pp. 23–33, 1993.
9. K.S. CHAN, S.R. BODNER, A.F. FOSSUM and D.E. MUNSON, *A constitutive model for inelastic flow and damage evolution in solids under triaxial compression*, Mech. Mat., **14**, pp. 1–14, 1992.
10. D.E. GRADY, *Dynamic failure of brittle solids*, [in:] Fracture and Damage in Quasibrittle Structures: Experiment, Modeling and Computer Analysis, Z.P. BAZANT, Z. BITTNAR, M. JIRASEK and J. MAZARS [Eds.], E & FN Spon, New York, NY, USA, pp. 259–272, 1994.

11. R.de BORST, J. CARMELIET, J. PAMIN and L.J. SLUYS, *New horizonts in computer analysis of damage and fracture in quasi-brittle materials*, [in:] Fracture and Damage in Quasibrittle Structures: Experiment, Modeling and Compute Analysis, Z.P. BAZANT, Z. BITTNAR, M. JIRASEK and J. MAZARS [Eds.], E & FN Spon, New York, NY, USA, pp. 359–372, 1994.

NEW MEXICO ENGINEERING RESEARCH INSTITUTE
UNIVERSITY OF NEW MEXICO, ALBUQUERQUE NM
and
THEORETICAL DIVISION
LOS ALAMOS NATIONAL LABORATORY, LOS ALAMOS, NM, USA.

Received November 4, 1994.

Arch. Mech., 47, 3, pp. 513–521, Warszawa 1995

Fatigue damage modelling of elastic-plastic materials (*)

J. JACKIEWICZ (BYDGOSZCZ) and W. OSTACHOWICZ (GDAŃSK)

IN THIS PAPER a simple damage model is proposed to take into account the nature of fatigue damage processes in certain materials. The model can be used to determine the effect of material deterioration during high-strain low cycling. The definition of the damage state is related to an irrecoverable plastic conversion rate of the volume element. Furthermore, this volume element is representative in the sense of the mechanics of continuous media. Emphasis is focused on the unified constitutive equation, which is expected to provide the applicability to evaluate the damage growth of the process zone in the widespread plastic zone. The special form of the constitutive damage evolution equation has been checked by the experimental results.

1. Introduction

FATIGUE is a damaging process, which occurs when stresses vary between maximum and minimum values due to periodic cycles. The process of fatigue damage of metals (see [9]) consists of:

- formation of intrusions or initiation of micro-cracks in active slip bands in favourably oriented grains, because of irreversible dislocation glide process,
- crack growth along slip bands, which form angles of about 45° with the maximum tensile stress direction (stage I),
- crack growth normal to the direction of maximum tensile stress (stage II).

In the high cycle fatigue case, because of the small amplitudes of the plastic strains, the formation of intrusions occurs only on slip planes of adequately oriented grains, and distributes sparsely in the material. Thus, a major part of the fatigue life is spent in the formation of these intrusions. On the other hand, low cycle fatigue is considered when the plastic strain is high enough to be measured. In low cycle fatigue, numerous active slip bands appear in many grains, and a large number of distributed micro-cracks develop in the material. Here, most of the fatigue life is occupied by the crack growth of stage I. Therefore, low cycle fatigue in metals must be considered separately from high cycle fatigue when the irreversible strains are only micro-plastic. Micro-plastic strains are not measurable and difficult to calculate.

The problem of crack initiation is quite complicated since it involves the crack nucleation at the micro-scale level. It is difficult to describe the small and short cracks growth in detail. Despite these complexities, fatigue damage assessments must be made for structures and components. The objective of this work is to further develop a mathematical model for the prediction of the fatigue life satisfying two conflicting requirements: simplicity and accuracy. Owing to the inherent

(*) Paper presented at 30th Polish Solid Mechanics Conference, Zakopane, September 5–9, 1994.

complexity of the problem, resulting from the random distribution of interacting defects, analytical expressions of the fatigue damage process may be described by global criteria only under some restrictive conditions emphasizing modest levels of defect concentrations.

2. Modelling of cyclic deformations and calculations of plastic strain energy

Fatigue damage is a process always associated with deformation and which also involves dissipation. The general constitutive equations describing the complete material behaviour are obtained by appropriate couplings of the damage evolution law with the evolution laws for the other internal variables and the elastic-plastic stress-strain laws. Cyclic deformations have important significance as a precursor to fracture. Because of their widespread significance, there was a considerable interest in the modelling of deformations. Complete understanding of the deformational behaviour of a particular material would require detailed knowledge of the atomic structure of that material. Therefore, the deformational properties are described by constitutive equations, which are derived from micromechanical and statistical considerations. In general, constitutive equations relate to the material modelled as a continuum, i.e. a material without atomic structure. The deformation is described by a field variable, the strain. Modelling of cyclic deformation under simple proportional loading can be accomplished with existing deformation models by replacing the axial strain with the equivalent strain. Extension to non-proportional loading is more difficult. Much of the early work in low cycle fatigue centred on the study of the transient behaviour of cyclic hardening and softening. In non-proportional loading, a path-dependent hardening often occurs and must be incorporated into the models for cyclic stress and strain. The ORNL model proposed by EISENBERG [4] and the INTERATOM model originally proposed by BRUHNS [2] belong to this type of constitutive relations, and this kind of models, which are considered to be the most promising constitutive laws.

The irrecoverable plastic strain energy is dissipated during a high-strain low cycle fatigue test when primary and subsequent prestrain fields are formed. Hence, the plastic strain energy per cycle is the area of the hysteresis loop and the total dissipated energy is the sum of the areas of these loops. In some cases the hysteresis loops stabilize after a few cycles and thus the strain energy per cycle may be assumed to be constant during the fatigue life. The uniaxial relation between the stress range $\Delta\sigma$ and the strain range $\Delta\varepsilon$ may be derived from the Ramberg–Osgood strain hardening law and from Masing's rule (symmetry with a ratio of 2 between tension and compression curves).

Fatigue lives of specimens are determined from constant amplitude tests. Real structures seldom experience constant amplitude loading. Therefore, some type of cycle counting schemes must be employed to reduce a complex irregular loading

history to a series of constant amplitude events. The most accurate fatigue life estimates are obtained using an analysis based on the strain at the most highly strained/stressed location. The rain flow method (see [3]) is usually used to define cycles as closed stress-strain hysteresis loops for damage analysis. Moreover, the rain flow method is treated as a special, uniaxial form of a hardening rule for elastic-plastic solids based on yield and memory surfaces.

3. Formulation of the cumulative damage model

The simplified physical model for ductile porous materials (aggregates of voids and a ductile matrix) has been employed, with the matrix material obeying the Huber-von Mises yield criterion. In predominantly ductile materials, material damage (see [1, 10]) is characterized by the development of distributed microscopic cavities (more generally by the microscopic internal structural changes) leading to the deteriorations of their mechanical properties. From a physical point of view, damage develops because of the initiation, growth and the coalescence of micro-cracks or micro-cavities. The initiation of these micro-defects occurs through a decohesion process at the interface between the defects (such as inclusions) and the matrix. During that process, in the plastic zones the incompressibility condition (i.e. $\varepsilon_{kk} = 0$) is in force but not in the highly localized process zone. When voids are present in ductile materials, the hydrostatic component of stress can cause macroscopic dilatation and influence the plastic yield. Because the material surrounding the voids is idealized as incompressible, the dilatation is completely caused by void growth.

The evolution of the void volume fraction (the material damage) results from the growth of existing voids and nucleation of new voids

$$\dot{D}^* = \dot{D}^*_{\text{nucleation}} + \dot{D}^*_{\text{growth}} . \tag{3.1}$$

In general, the damage state (see [8]) takes on the form

$$D^* = \beta \frac{\Delta dV^{*p}}{\Delta W^{*p}} , \tag{3.2}$$

where β denotes the coefficient of the energy dissipation in the material, ΔdV^{*p} and ΔW^{*p} are the volume of the damage zone in the widespread plastic zone and the plastic strain energy dissipated in the damage zone, respectively. This follows from the equivalence of plastic work dissipated in the continuum and in the matrix material

$$\int \sigma_{ij}\, d\varepsilon^p_{ij} = (1 - D^*) \int \sigma_\kappa\, d\varepsilon^p_\kappa \qquad \text{for} \quad D^* = \text{const.} \tag{3.3}$$

A volume element damaged may be geometrically modelled by a cube with defects inside it. The damage is very localized which is not always compatible with

continuum mechanics for which the damage is uniformly distributed in a volume element of a finite size. On the other hand, the constitutive damage evolution equations must characterize the behaviour of the volume element, which is representative in the sense of the mechanics of continuous media. The constitutive equations at the macro-scale may be derived from:

- the constitutive equations of the material matrix and the geometry of defects using a structural calculation at the micro-scale, and
- the homogenization technique using some mean values of the variables at the micro-scales.

The homogenization technique (see [10, 12]) is used to find the strain properties of the volume element or to derive the constitutive equations for the damage evolution. This technique refers to a method by which it is possible and reasonable to substitute for a heterogeneous medium (at a microscopic level) a homogeneous continuum model (at the macroscopic level). It is essential to define a volume element that is small enough to allow to distinguish the microscopic heterogeneities, which are large enough to represent the overall behaviour of the heterogeneous medium. Such a volume element V is called the representative volume element. Most of the macroscopic quantities are the averages over the representative volume element of the microscopic quantities. More precisely, the macroscopic quantity $\overline{f}$ is associated with the microscopic quantity f and defined by

$$\overline{f} = \langle f \rangle, \tag{3.4}$$

where

$$\langle f \rangle = \frac{1}{|V|} \int_V f(y)\, dy \tag{3.5}$$

and y refers to the microscopic set of coordinates (local coordinates in the representative volume element V).

Within the general framework of the thermodynamics of irreversible processes, the definition of the damage state is related to an irrecoverable plastic conversion rate of the representative volume. It is assumed that damage is accumulated during a given duty cycle. Therefore, the damage state D_n^* (see [7, 8]) after n reversals can be given as

$$D_n^* = \sum_{i=1}^{n} D_i^* = \beta \sum_{i=1}^{n} \frac{\Delta dV_i^{*p}}{\Delta W_i^{*p}}, \tag{3.6}$$

where ΔdV_i^{*p} and ΔW_i^{*p} are caused by the i-th load reversal.

The macroscopic measurable size of the fatigue defect is supposed to be present if the damage summation expressed in Eq. (3.6) approaches one, i.e.

$$\sum D_i^* = 1. \tag{3.7}$$

In the damage rule (3.6), the macroscopic effects of the microscopic defects are assumed to be isotropic, so that the damage variable D^* is a scalar, which takes values within the range zero (for the virgin material) to one (corresponding to the complete failure of the elementary volume element). Moreover, the irreversible microscopic deteriorations of the material can be described by a variable D^* just as the movements of dislocations are represented by the plastic strain tensor.

The following assumptions were made for calculations of the damage zone growth:

- limitation to isothermal and quasi-static processes;
- limitation to a small coupling between micro-plasticity and elasticity;
- during any increment of stress the changes of the strain tensor $d\varepsilon$ can be decomposed into a sum of the elastic component $d\varepsilon^e$ and plastic component $d\varepsilon^p$, thus

$$d\varepsilon = d\varepsilon^e + d\varepsilon^p ; \tag{3.8}$$

- the nucleation of micro-voids occurs by a decohesion process of the ductile matrix material from the rigid inclusions and carbides (it may be controlled by the accumulated plastic strain in the matrix material);
- in the nucleation case, during a given loading cycle the relative volume increment of the damage zone (see [8]) in the widespread plastic zone is proportional to the change of the third invariant of the plastic strain increment, i.e.

$$\frac{\Delta dV^{*p}}{dV} = \zeta I_3^*(\Delta\varepsilon_{ij}^p) = \zeta \Delta\varepsilon_1^p \Delta\varepsilon_2^p \Delta\varepsilon_3^p , \tag{3.9}$$

where ζ is constant;

- fatigue failure depends upon the mean stress σ_m;
- because the cavities on the grain boundary facets can coalesce to form open micro-cracks, the elasticity modulus has two different values in cyclic tension and compression loads close to fracture.

The phenomena of the distinguishable differences of the damage behaviour in tension and compression are associated with crack closure. This means that the effective stress must be a different function of the variable D^* in tension and compression loads close to fracture.

Notice that the plastic strain energy dissipated per unit volume during a given loading reversal is determined directly by the following equation

$$\frac{\Delta W^{*p}}{dV} = \int \sigma_{ij}(\varepsilon_{ij}^p)\, d\varepsilon_{ij}^p , \tag{3.10}$$

where σ_{ij} is the stress tensor.

By substituting from Eqs. (3.9) and (3.10) into Eq. (3.6), the fatigue damage increment of the Masing behaviour material can be expressed as follows

$$D_i^* = 4\beta\zeta \frac{(1+n')\Delta\sigma_i^{2/n'-1}}{(2K')^{2/n'}}, \tag{3.11}$$

where n' denotes the cyclic strain hardening coefficient and K' represents the cyclic strength coefficient of the Ramberg-Osgood relationship. Equation (3.11) defines the fatigue damage increment caused by the i-th load reversal corresponding to the stress range $\Delta\sigma_i$. On the ground of Eq. (3.11), the relationship between the cyclic stress range $\Delta\sigma_i$ and the number of cycles to failure, N_{fi}, for uniaxial symmetrical loading (i.e. $\sigma_{mi} = 0$) may be established. Thus at the end, the number of constant amplitude reversals to failure, $2N_{fi}$, is given by

$$2N_{fi} = \frac{1}{D_i^*} = \frac{(2K')^{2/n'}}{4\beta\zeta(1+n')\Delta\sigma_i^{2/n'-1}}. \tag{3.12}$$

4. Comparison with experimental results

The special form (3.12) of the damage rule (3.6) has been checked by the experimental results. A set of fatigue properties has been proposed by Morrow, which describes the empirical relationships found between stress, strain and fatigue life. The Morrow relationships may be expressed mathematically as

$$\begin{aligned} \frac{\Delta\sigma}{2} &= \sigma_f'(2N_f)^b, \\ \frac{\Delta\varepsilon^p}{2} &= \varepsilon_f'(2N_f)^c, \\ \frac{\Delta\varepsilon}{2} &= \frac{\Delta\varepsilon^e}{2} + \frac{\Delta\varepsilon^p}{2} = \frac{\sigma_f'}{E}(2N_f)^b + \varepsilon_f'(2N_f)^c, \end{aligned} \tag{4.1}$$

where σ_f'/E and ε_f' are the strain amplitudes corresponding to the elastic and plastic intercept for one cycle, respectively. The coefficients ε_f', σ_f' and the exponents b, c were fitted by the method of least squares. The coefficients describing the fatigue properties of the examined materials are taken from references [5, 6, 11] and summarized in Table 1. Furthermore, the theoretical high-strain fatigue results are reported and compared with the experimental results in Table 2 and Figs. 2, 4. It is seen that the damage rule (3.6) exhibits the same general tendency as the experimental data. The results obtained by means of the special form (3.12) of the damage rule (3.6) are very close to the experimental results.

Table 1. Properties of the examined materials.

	SAE 0030 [6]	E 36 [5]	SAE CMn [6]	A – 516 Gr 70 [11]
n'	0.136	0.21	0.141	0.193
K' [MPa]	738	1255	896	1067
ε'_f	0.28	0.6	0.15	0.204
σ'_f [MPa]	655	1194	869	842
b	−0.083	−0.124	−0.101	−0.102
c	−0.552	−0.57	−0.514	−0.499
$\beta\zeta$ [MPa]	4537	1515	9389	3394

Table 2. Comparison of experimental and theoretical high-strain fatigue results.

$2N_f$	SAE 0030		E 36		SAE CMn		A – 516 Gr 70	
	$\Delta\varepsilon/2$ [%] from equations		$\Delta\varepsilon/2$ [%] from equations		$\Delta\varepsilon/2$ [%] from equations		$\Delta\varepsilon/2$ [%] from equations	
	(4.1)	(3.12)	(4.1)	(3.12)	(4.1)	(3.12)	(4.1)	(3.12)
1000	0.794	0.772	1.416	1.398	0.637	0.640	0.854	0.914
2000	0.588	0.578	1.014	1.007	0.494	0.492	0.650	0.672
4000	0.444	0.442	0.738	0.737	0.390	0.388	0.502	0.504
7000	0.361	0.362	0.579	0.581	0.328	0.326	0.413	0.406
10000	0.319	0.322	0.500	0.502	0.295	0.295	0.367	0.357
20000	0.255	0.261	0.382	0.385	0.245	0.246	0.296	0.282
40000	0.210	0.216	0.299	0.303	0.207	0.211	0.243	0.228
70000	0.183	0.190	0.249	0.253	0.183	0.189	0.210	0.196
100000	0.169	0.176	0.224	0.228	0.170	0.177	0.193	0.179

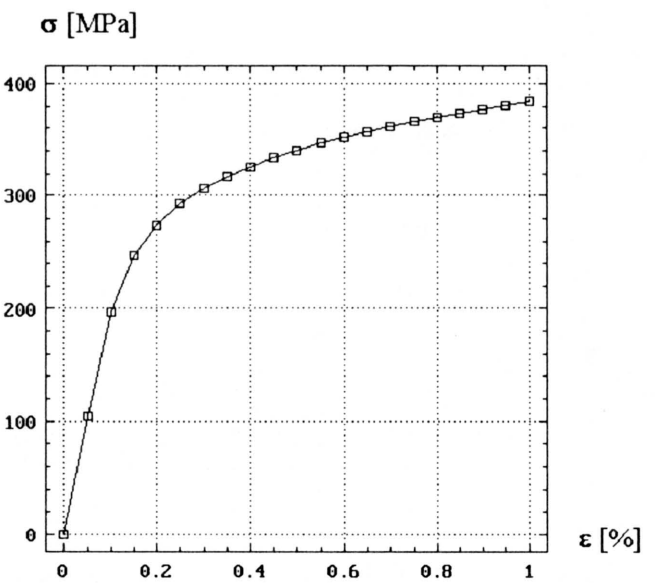

FIG.1. The cyclic stress-strain curve for the SAE 0030 steel.

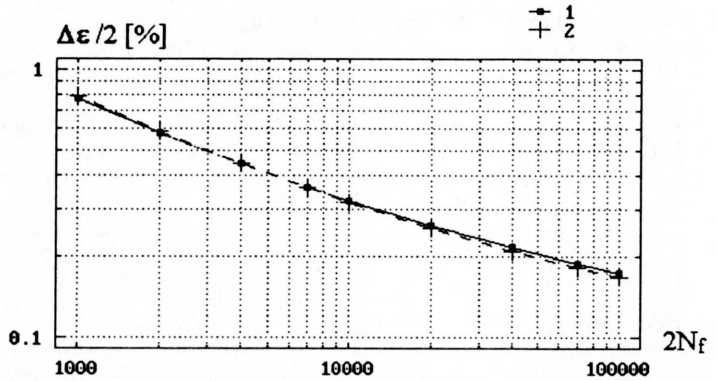

FIG. 2. The fatigue curves for the SAE 0030 steel: 1) theoretical data from equation (3.12), 2) experimental data from equation (4.1).

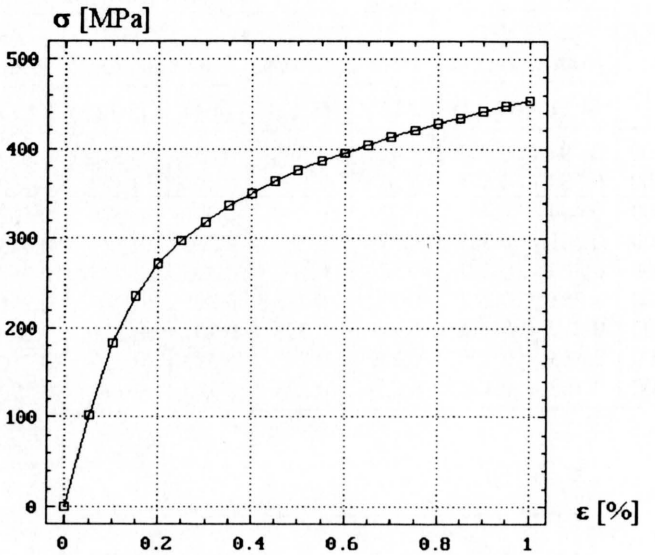

FIG. 3. The cyclic stress-strain curve for the E 36 steel.

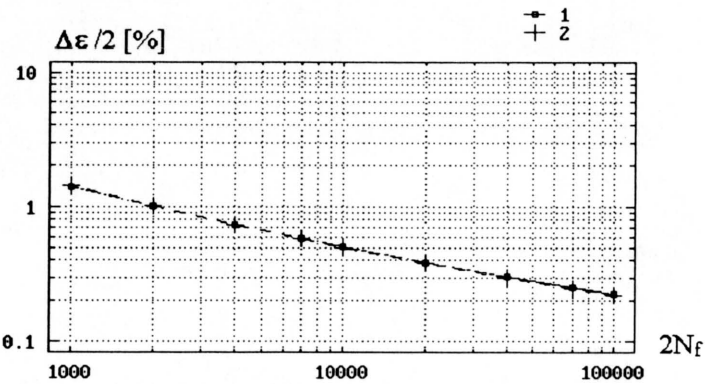

FIG. 4. The fatigue curves for the E 36 steel: 1) theoretical data from equation (3.12), 2) experimental data from equation (4.1).

5. Conclusions

From the analysis of the formulated theory and the experimental results of the examined materials the following conclusions may be drawn:

1. The theoretical model is formulated as some means to analyse the effect of distributed fatigue defects in certain materials, which correspond to the Masing hypothesis.

2. The fatigue failure condition (3.7) has the property of cumulation, which is known as Palmgren - Miner's rule.

3. If the plastic strain range $\Delta\varepsilon_i^p \to 0$, then because of Eq. (3.6), the increment of the damage D_i^* may be assumed to be zero.

4. The proposed approach considers the mechanics of continuous media in which the crack at the structure scale is such set of points (see [7]) for which the critical damage condition of macro-crack initiation has already been reached (i.e. $D^* = 1$). Application of this approach to current FEM or BEM structures codes can be straightforward.

References

1. M. BASISTA, *Damage mechanics experimental background*, Rozpr. Inż., **36**, 707–737, 1988.
2. O. BRUHNS, *Constitutive modelling in the range of inelastic deformations – a state of arts report*, INTERATOM – Report RAP-055-D(b), 1984.
3. S.D. DOWNING and D.F. SOCIE, *Simple rainflow counting algorithms*, Intern. J. Fatigue, **4**, 31–40, 1982.
4. M.A. EISENBERG, *A generalization of plastic flow theory with application to cyclic hardening and softening phenomena*, J. Engng. Materials and Technology, **98**, 221–228, 1976.
5. G. GLINKA, C. ROBIN, G. PLUVINAGE and C. CHEHIMI, *A cumulative model of fatigue crack growth and the crack closure effect*, Intern. J. Fatigue, **6**, 37–47, 1984.
6. G. GLINKA and A. NEWPORT, *Effects of notch-tip stress-strain calculation method on the prediction of fatigue crack initiation life*, Low Cycle Fatigue and Elasto-Plastic Behaviour of Materials, T.K. RIE [Ed.], Elsevier Applied Science, 1987.
7. J. JACKIEWICZ, *Incremental damage evaluation procedure*, Proc. of the 5th International Conference on Numerical Methods in Fracture Mechanics, A.R. LUXMOORE, D.R.J. OWEN [Eds.], Pineridge Press Limited, Swansea, 313–320, 1990.
8. J. JACKIEWICZ, *Evaluation and modelling of the fatigue damage evolution in steel structural components*, PhD Thesis, Polish Academy of Sciences, Institute of Fluid Flow Machinery, Gdańsk 1994.
9. J.F. KNOTT, *Fundamentals of fracture mechanics*, Butterworths, London 1973.
10. D. KRAJCINOVIC and J. LEMAITRE, *Continuum damage mechanics – theory and applications*, Springer-Verlag, Berlin 1987.
11. D. LEFEBVRE and F. ELLYIN, *Cyclic response and inelastic strain energy in low cycle fatigue*, Intern. J. Fatigue, **6**, 9–15, 1984.
12. J. MAZARS and Z.P. BAŻANT, *Cracking and damage – strain localization and size effect*, Elsevier Applied Science, London – New York 1989.

ACADEMY OF TECHNOLOGY AND AGRICULTURE IN BYDGOSZCZ
and
POLISH ACADEMY OF SCIENCES
INSTITUTE OF FLUID FLOW MACHINERY, GDAŃSK.

Received April 13, 1995.

Arch. Mech., 47, 3, pp. 523–536, Warszawa 1995

Gradient generalization to internal state variable approach (*)

W. KOSIŃSKI and W. WOJNO (WARSZAWA)

A THERMODYNAMIC THEORY of a rigid conductor is developed in which the response of a typical material point is influenced by information from its infinitesimal neighbourhood: the conservative state variable vector is enlarged by adding an internal state variable and its spatial gradient. The theory leads to a modified Fourier law of heat conduction governed by a system of quasi-linear equations. The type of the system is discussed under particular forms of the heat flux constitutive law. Analysis of weak discontinuity thermal waves is performed. A short discussion of relations between the present model and some previously developed ones is made.

1. Introduction

THEORIES OF MATERIALS with memory make use of different approaches. Some of them are based on the concept of constitutive functionals, which are defined on a Banach space of infinite histories of the thermo-mechanical configuration. Other formulations are based on rate-type equations, in which time-derivative of deformation and temperature appear. In all those approaches, infinite or finite histories of deformation measure and temperature at a typical material point appear as a final result. Then in most cases, the memory of the temporal type is only present, and no information from the infinitesimal neighbourhood of the configuration at the point influences its response.

There are, however, situations in which the necessity of such information is crucial for the appropriate description of the material behaviour and its dissipation. Thus in this paper we enlarge the set of state variables by adding to this set the spatial gradient of internal state variables. Consequently, the response of the material under consideration at the typical point will depend on the previous history and on its infinitesimal neighbourhood as well. In this approach, however, no higher gradients of temperature appear.

In the so-called gradient theories, on the other hand, additionally to higher gradients of temperature, also the higher order heat fluxes have to appear in order to express the power at a material point. This is not our case. Here the evolution equations for internal state variables themselves are rather postulated in the form compatible with the concept of internal state variables, that are quantities not-controllable from the exterior, while their initial values have to be specified.

(*) Paper presented at 30th Polish Solid Mechanics Conference, Zakopane, September 5–9, 1994.

In the course of derivation of the consequences of the thermodynamic laws, some particular examples of the constitutive dependences are considered. In the first one, a scalar internal variable has the meaning of a semi-empirical temperature scale, introduced by the first author in a series of papers. This case gives a modified Fourier-type heat conduction. Then, if the heat flux depends on the gradients of both the temperatures, absolute and semi-empirical, the theory leads to a parabolic system of equations. However, if additionally the dependence on the gradient of the absolute temperature is neglected, then the system of equations becomes hyperbolic, under mild assumptions concerning the signs of material functions. In this way one ends up with a wave-type heat conduction of thermodynamic model.

The classical theory of the heat conduction rests upon Fourier's law, in which the heat flux is proportional to the gradient of temperature. This hypothesis does not permit thermal disturbances to propagate with finite speeds. In the literature one can find many proposals modifying the proportionality law: MAXWELL [34], CATTANEO [5, 6], VERNOTTE [44], KALISKI [20], MÜLLER [41], LORD and SHULMAN [33], ACHENBACH [1], GURTIN and PIPKIN [18], FOX [15], BOGY and NAGHDI [4], MEIXNER [37], KOSIŃSKI and PERZYNA [26], LEBON [32], MAZILU [35], MORRO and RUGGERI [40], LARECKI and PIEKARSKI [31], and LARECKI [30].

Due to those proposals one can observe that additional memory effects are necessary to get a finite speed of propagation of thermal waves.

In the present paper the history of the spatial gradient of a thermal internal state variable is taken into account in the description of the material response.

In a series of papers of KOSIŃSKI [23], and CIMMELLI and KOSIŃSKI [8–10], the scalar internal variable has been called by the authors a *new* or *semi-empirical temperature*, for the heat flux vector is proportional to its spatial gradient. Such a proportionality law is of the Fourier type, however, in the case of deformable continuum it can lead to a modified thermoelasticity with a wave-type heat conduction governed by a system of quasi-linear hyperbolic equations. It was recently shown by KOSIŃSKI [24].

The aim of this paper is to derive the heat conduction law in a general case of an anisotropic heat conductor. We propose a rigorous procedure of derivation in the framework of a gradient generalization of the theory with internal state variables.

The organization of the paper is as follows: in Sec. 2 we shall present a general framework of the theory including universal balance laws of thermodynamics in local forms, together with constitutive assumptions that relate the response of a typical material point to an actual value of a state variable vector. Moreover, the evolution equation for the internal state variable will be postulated. In Sec. 3 we shall derive consequences of the thermodynamic laws for the constructed model of heat conducting solid. In Sec. 4 a particular case of an isotropic medium will be considered. In Sec. 5 the analysis of the type of the governing system of equations will be made, together with the derivation of expressions for weak discontinuity.

The thermal (so-called second sound) waves will be investigated under a particular set of assumptions. A short discussion relating the present model to the model developed previously and to a model developed in the framework of extended thermodynamics is included in the final section.

2. General framework

In 1954 BIOT [3] and MEIXNER [36] for the first time applied the internal state variable formalism in continuum mechanics. This formalism, called also the hidden variable approach, was already known in physical chemistry and quantum mechanics. In 1972 KOSIŃSKI and PERZYNA [26] (and later in KOSIŃSKI [21]) working in the framework of a thermodynamic theory with internal state variables derived, for the first time, expressions for finite speeds of thermal (and thermomechanical) waves. The results of those derivations were used later by MIHAILESCU and SULICIU [38], and MORRO [39]. Some generalizations of the thermoelastic model of KOSIŃSKI and PERZYNA [26] for more complex materials were developed by KOSIŃSKI and SZMIT [29], and WOŁOSZYŃSKA [45], and then partially reported by KOSIŃSKI [22].

Later on COLEMAN *et al.*, [13] repeated the first results of KOSIŃSKI and PERZYNA [26] in a slightly different setup, without referring to the internal state variable approach and to the original paper.

In 1989 the first author introduced, for the first time, a (material) gradient of a scalar internal state variable as a state variable in response functions of a thermoelastic material. In the course of derivation of consequences of the laws of thermodynamics he obtained a modified Fourier's type law and finite speeds of propagation of thermal and thermomechanical waves. That new model differs from the corresponding model of 1972. The new scalar internal state variable has been related to the absolute temperature by a suitable evolution equation. Later on a statistical interpretation for the variable has been given (CIMMELLI and KOSIŃSKI, [8]). The model has been mostly applied to rigid heat conductors in 1D and 3D cases, and to thermoelastic solids in 1D case (CIMMELLI and KOSIŃSKI, [8, 9], KOSIŃSKI and SAXTON, [27, 28], CIMMELLI *et al.*, [11], FRISCHMUTH and CIMMELLI, [16, 17], KOSIŃSKI, [24]).

There are some open problems related to the new model with the internal state variable gradient. One of them is the question of the absence of the internal state variable from the constitutive function for free energy. Moreover, in that model the gradient of the absolute temperature does not influence the response of the material. There were some reasons of constructing such a model, namely, to keep the generalization as simple as possible. The aim of this paper is to answer some of those questions.

2.1. Formulation of basic equations

Consider a motionless rigid heat conductor $\mathcal{B}$ that undergoes a thermodynamic process restricted by the two thermodynamic laws

$$\begin{aligned} \partial(\varrho\varepsilon)/\partial t + \operatorname{div}\mathbf{q} &= \varrho r, \\ \partial(\varrho\eta)/\partial t + \operatorname{div}(\mathbf{q}/\vartheta) &\geq \varrho r/\vartheta. \end{aligned} \tag{2.1}$$

Here ϱ is the mass density, $\mathbf{q}$ – the heat flux vector, ε – the specific internal energy per unit mass, r – the body heat supply, η – the specific entropy, ϑ – the absolute temperature.

Consider the material body $\mathcal{B}$ to be a heat conductor with the internal structure described by an influence of the history of the spatial gradient of absolute temperature on the response of a typical material point X of $\mathcal{B}$. In particular, it means that for the internal energy we are postulating the following constitutive equation

$$\varepsilon = \varepsilon^*(\eta, \operatorname{grad}\vartheta, \beta, \operatorname{grad}\beta). \tag{2.2}$$

The variable $\operatorname{grad}\beta$ will represent the history of the spatial gradient of ϑ if the internal state variable β, having the dimension of ϑ, will satisfy an evolution equation, i.e. it will be regarded as a solution of an initial value problem

$$\dot{\beta} = F(\vartheta, \operatorname{grad}\vartheta, \beta, \operatorname{grad}\beta), \qquad \beta(t_0) = \beta_0, \tag{2.3}$$

where t_0 is an initial instant and β_0 is an initial distribution of β, assumed to be given at t_0 for each X of $\mathcal{B}$. Let us notice that at this stage of considerations the variable β can be either a scalar-valued or a vector-valued quantity.

Assuming that the partial derivative of ε^* with respect to the entropy is equal to the absolute temperature, one can use the Legendre transformation to introduce the free energy ψ as $\psi = \varepsilon - \eta\vartheta$, and to regard the latter as a function of ϑ. Then the constitutive equation for ψ will take the form

$$\psi = \psi^*(\vartheta, \nabla\vartheta, \beta, \nabla\beta). \tag{2.4}$$

To get a more compact form we have used the standard symbol ∇ for denoting the grad operator. For the remaining thermal fields characterizing the response of the material we are postulating the following set of constitutive equations

$$\eta = \eta^*(\vartheta, \nabla\vartheta, \beta, \nabla\beta), \qquad \mathbf{q} = \mathbf{q}^*(\vartheta, \nabla\vartheta, \beta, \nabla\beta). \tag{2.5}$$

With the help of the notion of free energy, the laws (2.1) can be written as

$$\begin{aligned} \varrho(\dot{\psi} + \vartheta\dot{\eta} + \dot{\vartheta}\eta) + \operatorname{div}\mathbf{q} &= \varrho r, \\ -\varrho(\dot{\psi} + \dot{\vartheta}\eta) - \vartheta^{-1}\mathbf{q}\cdot\operatorname{grad}\vartheta &\geq 0, \end{aligned} \tag{2.6}$$

where a dot $\cdot$ denotes the scalar product operation, while the superimposed dot denotes the time partial derivative.

3. Thermodynamic restrictions

Now we are ready to derive the necessary and sufficient conditions under which the second law of thermodynamics will be satisfied at any thermodynamic process consistent with (2.4), (2.5), (2.3). To this end let us perform the time differentiation in (2.4), use the chain rule property and finally insert the result of these operations in (2.6). After grouping the terms standing in front of the appropriate time derivatives of the components of the state variable vector $(\vartheta, \nabla\vartheta, \beta, \nabla\beta)$, we get

$$\varrho(\partial_\vartheta\psi^* + \eta^*)\dot{\vartheta} + \varrho\partial_{\nabla\vartheta}\psi^*\cdot\dot{\overline{\nabla\vartheta}} + \varrho\partial_\beta\psi^* F + \varrho\partial_{\nabla\beta}\psi^*\cdot\dot{\overline{\nabla\beta}} + \mathbf{q}\cdot\nabla\vartheta/\vartheta \leq 0. \tag{3.1}$$

Now, taking the gradient of (2.3) we arrive at

$$\dot{\overline{\nabla\beta}} = \partial_\vartheta F\nabla\vartheta + \partial_{\nabla\vartheta}F\nabla\nabla\vartheta\partial_\beta F\nabla\beta + \partial_{\nabla\beta}F\nabla\nabla\beta. \tag{3.2}$$

Hence, the last inequality can be represented as

$$\begin{aligned}\varrho(\partial_\vartheta\psi^* + \eta)\dot{\vartheta} + \varrho\partial_{\nabla\vartheta}\psi^*\cdot\dot{\overline{\nabla\vartheta}} + \varrho\partial_{\nabla\beta}\psi^*\cdot\partial_{\nabla\vartheta}F\nabla\nabla\vartheta \\ + \varrho\partial_{\nabla\beta}\psi^*\cdot\partial_{\nabla\beta}F\nabla\nabla\beta + \varrho\partial_{\nabla\beta}\psi^*\cdot\partial_\beta F\nabla\beta \\ + \varrho\partial_\beta\psi^* F + \varrho(\partial_{\nabla\beta}\psi^*\partial_\vartheta F + (\varrho\vartheta)^{-1}\mathbf{q})\cdot\nabla\vartheta \leq 0,\end{aligned} \tag{3.3}$$

where ∂_c denotes the partial derivative with respect to c. Since the time derivatives of $\nabla\vartheta$, as well as the second gradients of ϑ and β, do not depend of the other variables and its derivatives, the inequality (3.3) leads to the identities

$$\partial_{\nabla\vartheta}\psi^* = 0, \qquad \eta = -\partial_\vartheta\psi^*, \tag{3.4}$$

then to the conditions

$$\partial_{\nabla\beta}\psi^*\cdot\partial_{\nabla\vartheta}F = 0, \qquad \partial_{\nabla\beta}\psi^*\cdot\partial_{\nabla\beta}F = 0, \tag{3.5}$$

and, at last, to the inequality

$$-\varrho\partial_{\nabla\beta}\psi^*\cdot\partial_\beta F\nabla\beta - \varrho\partial_\beta\psi^* F - \varrho(\partial_{\nabla\beta}\psi^*\partial_\vartheta F + (\varrho\vartheta)^{-1}\mathbf{q})\cdot\nabla\vartheta \geq 0. \tag{3.6}$$

In view of the restrictions (3.4), the constitutive equations (2.4)–(2.5) take the form

$$\begin{gathered}\psi = \psi^*(\vartheta, \beta, \nabla\beta), \qquad \eta = -\partial_\vartheta\psi^*(\vartheta, \beta, \nabla\beta), \\ \mathbf{q} = \mathbf{q}^*(\vartheta, \nabla\vartheta, \beta, \nabla\beta).\end{gathered} \tag{3.7}$$

These equations are still constrained by the orthogonality conditions (3.5) and the dissipation inequality (3.6).

3.1. Orthogonality conditions

The orthogonality conditions (3.5) can be fulfilled trivially in four ways:

A. When $\partial_{\nabla\beta}\psi^* = \mathbf{0}$, then the constitutive equations (3.7) are simplified to

$$\psi = \psi^*(\vartheta, \beta), \qquad \eta = -\partial_\vartheta \psi^*(\vartheta, \beta), \qquad \mathbf{q} = \mathbf{q}^*(\vartheta, \nabla\vartheta, \beta, \nabla\beta), \tag{3.8}$$

and the inequality (3.6) – to

$$-\varrho\partial_\beta\psi^* F - \vartheta^{-1}\mathbf{q}\cdot\nabla\vartheta \geq 0, \tag{3.9}$$

leaving the evolution equation (2.3) unchanged.

B. When $\partial_{\nabla\beta}\psi^* = \mathbf{0}$ and $\partial_{\nabla\beta}F = \mathbf{0}$, then the constitutive equations (3.7) and the dissipation inequality (3.6) have the same form as relations (3.8) and (3.9), while the evolution equation (2.3) simplifies to

$$\dot{\beta} = F(\vartheta, \nabla\vartheta, \beta). \tag{3.10}$$

C. When $\partial_{\nabla\beta}\psi^* = \mathbf{0}$ and $\partial_{\nabla\vartheta}F = \mathbf{0}$ then, similarly to the previous case, the constitutive equations and the dissipation inequality are also the same as in (3.8) and (3.9), however, with the evolution equation in the form

$$\dot{\beta} = F(\vartheta, \beta, \nabla\beta). \tag{3.11}$$

D. When at last $\partial_{\nabla\vartheta}F = \mathbf{0}$ and $\partial_{\nabla\beta}F = \mathbf{0}$, the constitutive equations (3.7) simplify to

$$\psi = \psi^*(\vartheta, \beta, \nabla\beta), \qquad \eta = -\partial_\vartheta\psi^*(\vartheta, \beta, \nabla\beta), \qquad \mathbf{q} = \mathbf{q}^*(\vartheta, \nabla\vartheta, \beta, \nabla\beta), \tag{3.12}$$

and the inequality (3.6) takes the form

$$-\varrho\partial_{\nabla\beta}\psi^*\cdot\partial_\beta F\nabla\beta - \varrho\partial_\beta\psi^* F - \varrho(\partial_{\nabla\beta}\psi^*\partial_\vartheta F + (\varrho\vartheta)^{-1}\mathbf{q})\cdot\nabla\vartheta \geq 0, \tag{3.13}$$

while the evolution equation (2.3) becomes

$$\dot{\beta} = F(\vartheta, \beta). \tag{3.14}$$

This is the only case of the general theory in which ψ^* may depend on $\nabla\beta$, and F must be independent of $\nabla\vartheta$ and $\nabla\beta$. This is the most interesting case of the general theory and, as it will be shown below.

In general, when fulfilled nontrivially, the orthogonality conditions (3.5) introduce constraints between β and ϑ and their derivatives. In the isotropic case these constraints are always of a differential type; meanwhile, in some anisotropic

cases they can be of a function type. Excellent example is given by the semi-linear constitutive equations, with a scalar-valued β,

$$\begin{aligned} \psi &= \psi_1^*(\vartheta,\beta) + \mathbf{a}(\vartheta,\beta)\cdot\nabla\beta, \\ F(\vartheta,\nabla\vartheta,\beta,\nabla\beta) &= F_1(\vartheta,\beta) + \mathbf{b}(\vartheta,\beta)\cdot\nabla\vartheta + \mathbf{c}(\vartheta,\beta)\cdot\nabla\beta, \end{aligned} \tag{3.15}$$

then the orthogonality conditions (3.5) take the form

$$\mathbf{a}(\vartheta,\beta)\cdot\mathbf{b}(\vartheta,\beta) = 0, \qquad \mathbf{a}(\vartheta,\beta)\cdot\mathbf{c}(\vartheta,\beta) = 0, \tag{3.16}$$

of the function type.

When for every ϑ and β

$$\mathbf{a} \perp \mathbf{b} \quad \text{and} \quad \mathbf{a} \perp \mathbf{c}, \tag{3.17}$$

then the orthogonality conditions (3.5), though satisfied nontrivially, do not yield any relationships between ϑ and β.

Let us consider an isotropic conductor governed by

$$\psi = \psi^*(\vartheta,\beta,|\nabla\beta|), \tag{3.18}$$

with β as a scalar-valued internal state variable, and with F depending on ϑ, $|\nabla\vartheta|$, β, $|\nabla\beta|$ and $\nabla\vartheta\cdot\nabla\beta$. Now the orthogonality conditions (3.5) lead to the constraints

$$\mathbf{A}_1\nabla\vartheta\cdot\nabla\beta + B_1|\nabla\beta| = 0, \qquad \mathbf{A}_2\nabla\vartheta\cdot\nabla\beta + B_2 = 0, \tag{3.19}$$

of the differential type, where $\mathbf{A}_1$, $\mathbf{A}_2$, B_1, B_2 are expressed by partial derivatives of ψ^* and F, that do not vanish identically. Hence there exist always relationships between ϑ and β.

4. Isotropic case

Let us assume that the conductor described in the case **D** by Eqs. (3.12), (3.14) is isotropic. If so, then the constitutive equations (3.12) take now the form

$$\begin{aligned} &\psi = \psi^*(\vartheta,\beta,|\nabla\beta|), \qquad \eta = -\partial_\vartheta\psi^*(\vartheta,\beta,|\nabla\beta|), \\ &\mathbf{q} = q_1(\vartheta,|\nabla\vartheta|,\beta,|\nabla\beta|,\nabla\vartheta\cdot\nabla\beta)\nabla\vartheta + q_2(\vartheta,|\nabla\vartheta|,\beta,|\nabla\beta|,\nabla\vartheta\cdot\nabla\beta)\nabla\beta, \end{aligned} \tag{4.1}$$

with the evolution equation (3.14), and restricted by the reduced inequality (3.13), that consequently can be written as

$$\begin{aligned} &-\varrho\partial_{\nabla\beta}\psi^*\cdot\partial_\beta F\nabla\beta - \varrho\partial_\beta\psi^* F - \vartheta^{-1}q_2\nabla\vartheta\cdot\nabla\beta \\ &\qquad -\varrho(\partial_{\nabla\beta}\psi^*\partial_\vartheta F + (\varrho\vartheta)^{-1}q_1\nabla\vartheta)\cdot\nabla\vartheta \geq 0. \end{aligned} \tag{4.2}$$

This set of equations form a most general system for an isotropic heat conductor.

Now we consider $\mathbf{q}$ as being independent of $\nabla\vartheta$

$$\mathbf{q} = q(\vartheta, \beta, |\nabla\beta|)\nabla\beta. \tag{4.3}$$

Then (4.2) will lead to extra potential relation. Since q_1 vanishes, then we have

$$-\varrho\partial_{\nabla\beta}\psi^*\cdot\partial_\beta F\nabla\beta - \varrho\partial_\beta\psi^* F - \varrho(\partial_{\nabla\beta}\psi^*\partial_\vartheta F + (\varrho\vartheta)^{-1}q\nabla\beta)\cdot\nabla\vartheta \geq 0. \tag{4.4}$$

In (4.4) the coefficient of $\nabla\vartheta$ and the rest of terms are independent of $\nabla\vartheta$. Moreover, due to prolonged evolution equation (3.2), that now reduces to

$$\dot{\overline{\nabla\beta}} = \partial_\vartheta F\nabla\vartheta + \partial_\beta F\nabla\beta, \tag{4.5}$$

we can see that the coefficient of $\nabla\vartheta$ has to vanish. This requires

$$\mathbf{q} = -\alpha^*\nabla\beta, \tag{4.6}$$

and

$$-(\vartheta\partial_\vartheta F)^{-1}\partial_\beta F\alpha^*|\nabla\beta|^2 - \varrho\partial_\beta\psi^* F \geq 0, \tag{4.7}$$

where

$$\alpha^*(\vartheta, \beta, |\nabla\beta|) := \varrho\vartheta|\nabla\beta|^{-1}\partial_\vartheta F\ \partial_{|\nabla\beta|}\psi^*. \tag{4.8}$$

The law (4.6) is of the Fourier type for $\mathbf{q}$ in terms of $\nabla\beta$ with the coefficient α^* defined by the thermodynamic potential.

This constitutes a generalization of the existing heat conduction theory with the so-called semi-empirical temperature, developed recently by W. Kosiński and his co-workers: V.A. Cimmelli, K. Saxton, K. Frischmuth, and already applied to thermal wave propagation problems in several papers.

If we require the linearity of (4.6) in $\nabla\beta$, then the coefficient α^* will be independent of $\nabla\beta$. Simple integration shows that the last requirement will be reached iff the free energy function is of the form

$$\psi = \psi_1^*(\vartheta, \beta) + 0.5\psi_2^*(\vartheta, \beta)|\nabla\beta|^2, \tag{4.9}$$

where the factor 0.5 has been assumed for the convenience only. Then

$$\alpha^*(\varrho\vartheta\partial_\vartheta F)^{-1} = \psi_2^*, \tag{4.10}$$

and

$$-\{(\vartheta\partial_\vartheta F)^{-1}\partial_\beta F\alpha^* + 0.5\varrho\partial_\beta\psi_2^* F\}|\nabla\beta|^2 - \varrho\partial_\beta\psi_1^* F \geq 0. \tag{4.11}$$

Since the last term as well as the coefficient of $|\nabla\beta|^2$ are independent of the latter, the last inequality can be split into two inequalities

$$(\vartheta\partial_\vartheta F)^{-1}\partial_\beta F\alpha^* \leq -0.5\varrho\partial_\beta\psi_2^* F, \tag{4.12}$$

and

$$\partial_\beta \psi_1^* F \leq 0. \tag{4.13}$$

When, however, the free energy is independent of β, then instead of (4.12) we get

$$(\vartheta \partial_\vartheta F)^{-1} \partial_\beta F \alpha^* \leq 0. \tag{4.14}$$

If for the stability reasons, as far as solutions of evolution equation (3.14) are concerned, we assume that $\partial_\beta F$ is non-positive, then (4.14) requires

$$\partial_\vartheta F \alpha^* \geq 0, \tag{4.15}$$

and no more inequalities will be present in this case. Inequality (4.15) gives the restriction on the *generalized* heat conduction coefficient α^*. If the present constitutive model is regarded as a first order generalization of the classical heat conduction model with the Fourier law, then the partial derivative $\partial_\vartheta F$ should be of a fixed sign. Assuming it to be positive, as we have done in our previous papers (cf. KOSIŃSKI [25]), we get from (4.15) the restriction on the positiveness of α^* only.

In ARCISZ and KOSIŃSKI [2] and KOSIŃSKI [25] papers, in the course of developing a generalized thermoelasticity with a wave-type heat conduction, three requirements have been formulated. One of them requires the evolution equation to have the same form as that discussed here in the isotropic case (3.14). The next property is:

- as a zero order approximation of the evolution equation, the Fourier law should be recovered, that is a proportionality (linear) law between the actual heat flux vector $\mathbf{q}$ and the spatial temperature gradient grad ϑ, i.e.

$$\mathbf{q} = -k \operatorname{grad} \vartheta.$$

The form of the right-hand side (RHS) of (3.14) will be compatible with this requirements if a control parameter exists, on which F depends, such that if the parameter tends to zero, the state variable β becomes a function of the absolute temperature. If τ_0 is that parameter, we define a new function f as $f = \tau_0 F$, where now f is independent of the control parameter τ_0. Then the evolution equation (3.14) will be rewritten in the form

$$\tau_0 \dot{\beta} = f(\vartheta, \beta). \tag{4.16}$$

Taking the limit of LHS in (4.16) in τ_0 and confining ourselves to bounded solutions for $\dot{\beta}$, and to such evolution equations for which the function f possesses nonvanishing partial derivatives $\partial f / \partial \beta$, and at least one null point, we get

$$\text{if} \quad \tau_0 \to 0 \quad \text{then} \quad \beta \to B(\vartheta), \tag{4.17}$$

where a function $B(\vartheta)$ satisfies the identity

$$f(\vartheta, B(\vartheta)) \equiv 0. \tag{4.18}$$

5. Parabolic and hyperbolic heat conduction models

In this section we shall analyse the equations that follow from the energy balance and the evolution equation when the constitutive assumptions made in the previous section are included. First the case of the heat flux depending on $\nabla\vartheta$ will be considered, then the simpler dependence (4.6) will be investigated.

Let us notice that in the most general case described by (4.1) the governing system of equations, composed of (2.6) and (3.14) leads to two equations: the first one is of the second order in ϑ and β, while the second equation is of the first order in β. However, if the second gradient of ϑ is expressed with the help of the (second order) prolonged equation of (3.14) in terms of the derivatives of β, then in the first equation the third mixed derivative $\nabla\nabla\dot{\beta}$ appears. This third order derivative is a singleton: no more third order derivatives appear, only lower order ones are present after that substitution. Moreover, provided the nonvanishing partial derivative of F with respect to ϑ does not vanish, the evolution equation can be regarded as an equation for ϑ, that allows to solve (independently of ϑ) the energy equation in terms of β.

The appearence of $\nabla\nabla\dot{\beta}$ as a singleton in the resulting system shows, that the resulting system is not hyperbolic, provided the energy equation is written as a first order quasi-linear system of four equations in terms of: β, $v = \dot{\beta}$, $\mathbf{p} = \nabla\beta$, $\mathbf{z} = \nabla v$. In the 1D case the system possesses only a double characteristic eigenvalue $\lambda^2 = 0$. This means that the system is of parabolic type. We will see in a moment that the second simpler case leads to a quasi-linear hyperbolic equations, under mild assumptions concerning the signs of material functions.

Let us pass to the second case described by (4.6), i.e. the heat flux independent of $\nabla\vartheta$. Performing the differentiation in (2.6) we get

$$
\begin{aligned}
(5.1)\qquad & \varrho c_v(\vartheta,\beta,\nabla\beta)\dot{\vartheta} - \varrho\partial_\beta\varepsilon^*\dot{\beta} + \varrho\partial_{\nabla\beta}\varepsilon^*\cdot\nabla\dot{\beta} \\
& -\partial_\beta\alpha^*(\vartheta,\beta,\nabla\beta)\nabla\beta\cdot\nabla\beta - \partial_\vartheta\alpha^*(\vartheta,\beta,\nabla\beta)\nabla\beta\cdot\nabla\vartheta \\
& -\partial_{\nabla\beta}\alpha^*(\vartheta,\beta,\nabla\beta)\otimes\nabla\beta\cdot\nabla\nabla\beta - \alpha^*(\vartheta,\beta,\nabla\beta)\triangle\beta = \varrho r,
\end{aligned}
$$

where $c_v(\vartheta,\beta,\nabla\beta) := \partial_\vartheta\varepsilon^*$ denotes the specific heat. If we apply to this energy equation the first two prolongations (i.e. spatial gradient and time derivative) of (3.14) in order to express the first derivatives of ϑ in the forms

$$
(5.2)\qquad \dot{\vartheta} = \tau^*(\vartheta,\beta)(\ddot{\beta} - \partial_\beta F\dot{\beta}), \qquad \nabla\vartheta = \tau^*(\vartheta,\beta)(\nabla\dot{\beta} - \partial_\beta F\nabla\beta),
$$

then we obtain one equation of the second order in β, similar to that derived already in previous papers (KOSIŃSKI [23, 24], DOMAŃSKI and KOSIŃSKI [14]),

$$
\begin{aligned}
(5.3)\qquad & \varrho c_v(\vartheta,\beta,\nabla\beta)\tau^*\ddot{\beta} - \varrho\partial_\beta\varepsilon^*\dot{\beta} + \varrho\partial_{\nabla\beta}\varepsilon^*\cdot\nabla\dot{\beta} - \partial_\beta\alpha^*(\vartheta,\beta,\nabla\beta)\nabla\beta\cdot\nabla\beta \\
& -\partial_\vartheta\alpha^*(\vartheta,\beta,\nabla\beta)\tau^*\nabla\beta\cdot\nabla\dot{\beta} - \partial_{\nabla\beta}\alpha^*(\vartheta,\beta,\nabla\beta)\otimes\nabla\beta\cdot\nabla\nabla\beta \\
& -\alpha^*(\vartheta,\beta,\nabla\beta)\triangle\beta + \partial_\vartheta\alpha^*(\vartheta,\beta,\nabla\beta)\tau^*\partial_\beta\nabla\beta\cdot\nabla\beta - \varrho c_v(\vartheta,\beta,\nabla\beta)\tau^*\partial_\beta\dot{\beta} = \varrho r.
\end{aligned}
$$

This equation is more complex than the corresponding one derived in KOSIŃSKI [24] for 3D thermal weak discontinuity waves. There it was shown, for example, that in the rigid case the governing system of equations for determining β and ϑ is composed of (4.16) with f given as a sum $f = f_1(\vartheta) + f_2(\beta)$, and

$$\tau_0 \varrho c_v(\vartheta)\ddot{\beta} - \tau_0 \alpha^{*\prime}(\vartheta)\nabla\dot{\beta}\cdot\nabla\beta - \alpha^*(\vartheta)f_1'(\vartheta)\triangle\beta - \varrho c_v(\vartheta)f_2'(\beta)\dot{\beta} + \alpha^{*\prime}(\vartheta)f_2'(\beta)\nabla\beta\cdot\nabla\beta = rf_1'(\vartheta). \tag{5.4}$$

Since ϑ can be expressed in terms of β and $\dot{\beta}$ from (4.16), Eq. (5.4) can be solved independently for β. The speed λ of a purely thermal wave is given here by

$$\tau_0 \varrho c_v(\vartheta)\lambda^2 - \tau_0 \alpha^{*\prime}(\vartheta)\nabla\beta\cdot\mathbf{n}\lambda - \alpha^*(\vartheta)f_1'(\vartheta) = 0. \tag{5.5}$$

We can see that the wave propagation is not symmetric if $\nabla\beta$ differs from zero, and the hyperbolicity condition is $c_v(\vartheta)\alpha^*(\vartheta)f_1'(\vartheta)\tau_0 > 0$.

Here, in the general case governed by (5.3), the speed is given by the equation

$$\varrho c_v(\vartheta,\beta,\nabla\beta)\tau^*\lambda^2 - \varrho\partial_{\nabla\beta}\varepsilon^*\cdot\mathbf{n}\lambda + \partial_\vartheta\alpha^*(\vartheta,\beta,\nabla\beta)\tau^*\nabla\beta\cdot\mathbf{n}\lambda - \partial_{\nabla\beta}\alpha^*(\vartheta,\beta,\nabla\beta)\otimes\nabla\beta\cdot\mathbf{n}\otimes\mathbf{n} - \alpha^*(\vartheta,\beta,\nabla\beta)\mathbf{n}\cdot\mathbf{n} = 0, \tag{5.6}$$

where $\mathbf{n}$ is a unit normal to a wave front. As previously, the propagation is nonsymmetric in general.

6. Concluding remarks

We want to close our paper with the final remarks concerning the role of our general derivation in the framework of gradient theory. The rigorously derived general first gradient theory with internal state variables supplies the previously developed model with the semi-empirical temperature, with new methods of analysis of singular solutions in the thermodynamics of heat conductors. Now, for the model we have at our disposal the natural viscosity method, given by the parabolic system, if the heat flux depends on the both gradients: $\nabla\vartheta$ and $\nabla\beta$. This can have a particular importance, when developing appropriate numerical schemes for finding solutions of the quasi-linear hyperbolic system.

The last but not least remark concerns the applicability of the hyperbolic model. In FRISCHMUTH and CIMMELLI [16, 17] the semi-empirical model has been elaborated from the numerical point of view. The numerical solutions to the governing system of equations in the case of a rigid conductor were reported and compared with the results of experiments obtained for several materials at low temperatures (cf. NARAYANAMURTI and DYNES [42], JACKSON and WALKER [19], and PAO and BANERJEE [43]). The results of those comparisons show that the model can reproduce sufficiently well the existing experimental results. We can point out, that the modification of the classical Fourier law developed in

the framework of a simplified gradient theory with internal state variables, when β does not appear in the constitutive laws, has been already compared with another one, developed for a rigid conductor in the framework of an extended thermodynamic approach (MORRO and RUGGERI, [40]). The results of the analysis have been reported in CIMMELLI *et al.* [12], and they show the conditions under which both models lead to the same system of equations, when a rigid conductor is discussed.

Acknowledgement

The present studies have been undertaken under the grant sponsored by KBN-Project No. 0645/P4/93/05.

References

1. J.D. ACHENBACH, *The influence of heat conduction on propagating stress jumps*, J. Mech. Phys. Sol., **16**, 273–282, 1968.
2. M. ARCISZ and W. KOSIŃSKI, *Hugoniot relations and heat conduction laws*, [submitted for publication, 1994].
3. M.A. BIOT, *Theory of stress-strain relations in anisotropic viscoelasticity and relaxation phenomena*, J. Appl. Phys., . **25**, 1385–1391, 1954.
4. D.B. BOGY and P.M. NAGHDI, *On heat conduction and waves propagation in rigid solids*, J. Math. Phys., **11**, 3, 917–923, 1970.
5. C. CATTANEO, *Sulla conduzione del calore*, Atti Sem. Mat. Fis. Univ. Modena, **3**, 83–101, 1948.
6. C. CATTANEO, *Sur une forme de l'equation de la chaleur, éliminant le paradoxe d'une propagation instantanée*, Comp. Rend. Sci., **247**, 431–433, 1958.
7. M. CHESTER, *Second sound in solids*, Phys. Rev., **131**, 2013–2015, 1963.
8. V.A. CIMMELLI and W. KOSIŃSKI, *Nonequilibrium semi-empirical temperature in materials with thermal relaxation*, Arch. Mech., **43**, 6, 753–767, 1991.
9. V.A. CIMMELLI and W. KOSIŃSKI, *Evolution hyperbolic equations for heat conduction*, Proc. 5-th Bilateral Polish-Italian Meeting, Thermodynamics and Kinetic Theory, W. KOSIŃSKI *et al.*, [Eds.], World Scientific Series on Advances in Math. Appl. Sci., Singapore, New Jersey, London, Hong Kong, Vol. 12, pp. 11–22, 1992.
10. V.A. CIMMELLI and W. KOSIŃSKI, *Well-posedness results for a nonlinear hyperbolic heat equation*, Ricerche di Matematica, **42**, 1–21, 1993.
11. V.A. CIMMELLI, W. KOSIŃSKI and and K. SAXTON, *A new approach to the theory of heat conduction with finite wave speeds*, Proc. VI Intern. Conference on Waves and Stability in Continuous Media, Acireale, May 27 – June 1, S. RIONERO, G. MULONE and F. SALEMI [Eds.], Le Matematiche, **46**, 1, 95–105, 1991.
12. V.A. CIMMELLI, W. KOSIŃSKI and and K. SAXTON, *Modified Fourier law – comparison of two approaches*, Arch. Mech., **44**, 4, 409–415, 1992.
13. B.D. COLEMAN, M. FABRIZIO and R. OWEN, *On the thermodynamics of second sound in dielectric crystals*, Arch. Rat. Mech. Anal., **80**, 2, 135–158, 1982.
14. W. DOMAŃSKI and W. KOSIŃSKI, *Asymptotic equations of geometrical optics for two models of hyperbolic heat waves*, [submitted to Arch. Mech., 1995].
15. N. FOX, *Generalized thermoelasticity*, Int. J. Engng. Sci., **57**, 1, 437–445, 1969.
16. K. FRISCHMUTH and V.A. CIMMELLI, *Numerical reconstruction of heat pulse experiments*, Int. J. Engng. Sci., **33**, 2, 209, 1995.

17. K. FRISCHMUTH and V.A. CIMMELLI, *Identification of constitutive functions and verification of model assumptions in semi-empirical heat conduction theory*, [under preparation].

18. M.E. GURTIN and A.C. PIPKIN, *A general theory of heat conduction with finite wave speeds*, Arch. Rat. Mech. Anal., **31**, 113–126, 1968.

19. H.E. JACKSON and C.T. WALKER, *Thermal conductivity, second sound, and phonon-phonon interactions in NaF*, Phys. Rev. Letters, **3**, 4, 1428–1439, 1971.

20. S. KALISKI, *Wave equation of heat conduction*, Bull. Acad. Polon. Sci., Série Sci.Tech., **13**, 4, 211–219, 1965.

21. W. KOSIŃSKI, *Thermal waves in inelastic bodies*, Arch. Mech., **23**, 733–748, 1975.

22. W. KOSIŃSKI, *Field singularities and wave analysis in continuum mechanics*, Ellis Horwood Series: Mathematics and Its Applications, Ellis Horwood Ltd., Chichester, Halsted Press: a Division of John Wiley & Sons, New York Chichester Brisbane Toronto, PWN – Polish Scientific Publishers, Warszawa 1986.

23. W. KOSIŃSKI, *Elastic waves in the presence of a new temperature scale*, [in:] Elastic Wave Propagation, M.F. MCCARTHY and M. HAYES [Eds.], Elsevier Science (North Holland), pp. 629–634, 1989.

24. W. KOSIŃSKI, *Thermal waves in the kinematic theory*, Proc. IUTAM Symposium on Nonlinear Waves in Solids, August 15-20, 1993, Victoria, B.C., Canada, Part of Nonlinear Waves in Solids, J. WAGNER and F. NORWOOD [Eds.], Appl. Mech. Review – ASME, Book No AMR 137, Fairfield, New Jersay, pp. 247–252, 1995.

25. W. KOSIŃSKI, *Thermodynamics of continua with heat waves*, Proc. 1995 ASME Joint Applied Mechanics and Materials Summer Meeting, 28-30 June, UCLA, Applied Mechanics Review, 1995, [in print].

26. W. KOSIŃSKI and P. PERZYNA, *Analysis of accelaration waves in materials with internal parameters*, Arch. Mech., **24**, 4, 629–643, 1972.

27. W. KOSIŃSKI and K. SAXTON, *Weak discontinuity waves in materials with semi-empirical temperature scale*, Arch. Mech., **43**, 4, 547–559, 1991.

28. W. KOSIŃSKI and K. SAXTON, *The effect on finite time breakdown due to modified Fourier laws*, Quart. Appl. Math., **51**, 1, 55–68, 1993.

29. W. KOSIŃSKI and K. SZMIT, *On waves in elastic materials at low temperature. Part I. Hyperbolicity in thermoelasticity, Part II. Principal waves*, Bull. Acad. Polon. Sci., Sér. Sci. Techn., **25**, 1, 17–32, 1977.

30. W. LARECKI, *Equations of heat transport based on approximate kinetic description of phonon processes*, Proc. 5-th Bilateral Polish-Italian Meeting, Thermodynamics and Kinetic Theory, W. KOSIŃSKI *et al.*, [Eds.], World Scientific Series on Advances in Math. Appl. Sci., Singapore, New Jersay, London, Hong Kong, Vol. 12, pp. 79–92, 1992.

31. W. LARECKI and S. PIEKARSKI, *Symmetric conservative form of low-temperature phonon gas hydrodynamics, I. Kinetic aspects of the theory*, Il Nuovo Cimento, D, **13**, 31–53, 1991.

32. G. LEBON, *Derivation of generalized Fourier and Navier–Stokes equations based on thermodynamics of irreversible processes*, Bull. Acad. Roy. Sci. Belgique, **64**, 45, 1978.

33. H.W. LORD and Y. SHULMAN, *A generalized dynamical theory of thermoelasticity*, J. Mech. Phys. Solids, **15**, 299–309, 1967.

34. J.C. MAXWELL, *On the dynamical theory of gases*, Phil. Trans. Royal. Soc. London, **157**, 49–101, 1867.

35. P. MAZILU, *The equation of heat conduction*, Rev. Roum. Math. Pures et Appl., **23**, 3, 419–435, 1978.

36. J. MEIXNER, *Thermodynamische Theorie der elastischen Relaxation*, Zeitschrift Naturforschung, **9a**, 654–665, 1954.

37. J. MEIXNER, *On the linear theory of heat conduction*, Arch. Rat. Mech. Anal., **39**, 1–36, 1970.

38. M. MIHAILESCU and I. SULICIU, *Finite and symmetric thermomechanical waves in materials with internal state variables*, Int. J. Solids Struct., **12**, 559–575, 1976.

39. A. MORRO, *Wave propagation in thermo-viscous materials with hidden variables*, Arch. Mech., **32**, 145–161, 1980.

40. A. MORRO and T. RUGGERI, *Second sound and internal energy in solids*, Int. J.Non Linear Mech., **22**, 27–36, 1987.

41. I. MÜLLER, *Zum Paradoxen der Wärmeleitungstheorie*, Z. Phys., **198**, 329, 1967.

42. V. NARAYANAMURTI and R.C. DYNES, *Observation of second sound in bismuth*, Phys. Rev. Letters, **28**, 22, 1461–1465, 1972.

43. Y.M. PAO and D.K. BANERJEE, *Thermal pulses in dielectric crystals*, Lett. Appl. Engng. Sci., **1**, 33–41, 1973.

44. M.P. VERNOTTE, *Les paradoxes de la theorie continue de l'equation de la chaleur*, Comp. Rend. Sci., **246**, 3154-3155, 1958.

45. K. WOŁOSZYŃSKA, *On coupling acceleration and shock waves in a thermoviscoplastic medium, Part I. Symmetry and hyperbolicity conditions, Part II. One-dimensional waves*, Arch. Mech., **33**, 261–272, 451–468, 1981.

POLISH ACADEMY OF SCIENCES
INSTITUTE OF FUNDAMENTAL TECHNOLOGICAL RESEARCH

Received November 18, 1994.

Arch. Mech., 47, 3, pp. 537–556, Warszawa 1995

Finite element simulation of 3D mechanical behaviour of NiTi shape memory alloys (*)

G. RIO, P. Y. MANACH (GUIDEL) and D. FAVIER (GRENOBLE)

A THREE-DEVELOPED finite element model of the isothermal deformation of shape memory alloys has been used in order to analyze and predict the mechanical behaviour of NiTi alloys. A general 3D kinematics has been studied. The constitutive behaviour is written using an elastohysteresis tensorial scheme; it is based on the splitting of the Cauchy stress tensor into two fundamental stress contributions of hyperelastic and pure hysteresis types, respectively. The equilibrium equations are then discretized by the finite element method. The validity of this formulation is established in the case of three-dimensional plate bending behaviour of NiTi shape memory alloys.

Notations

$(O, \mathbf{I}_a)$ orthonormal fixed reference frame ($a = 1,2,3$),
t absolute time,
$\partial/\partial t$ partial derivative with respect to time,
M material point,
θ^i curvilinear convected material coordinates ($i = 1,2,3$),
$\mathbf{M}$ position of point M,
$\mathbf{G}_i$ initial reference frame associated with the θ^i,
G_{ij} initial covariant components of the metric tensor $\mathbf{G}$,
$\mathbf{g}_i$ current reference frame associated with the θ^i,
g_{ij} current covariant components of the metric tensor $\mathbf{G}$,
$\sqrt{g}$ current density of metric volume per unit of material volume with $g = \det|g_{ij}|$,
$\mathbf{D}$ strain rate tensor ($2D_{ij} = \partial g_{ij}/\partial t$),
$\overline{\mathbf{D}}$ deviatoric part of the strain rate tensor,
t_r inversion time associated with an inversion point,
${}^t_r..\mathbf{G}$ Cauchy strain tensor ${}^t_r..\mathbf{G} = G_{ij}(t_r)\,\mathbf{g}^i \otimes \mathbf{g}^j$,
$\Delta^t_r..\boldsymbol{\varepsilon}$ Almansi strain tensor $\Delta^t_r..\boldsymbol{\varepsilon} = \Delta\boldsymbol{\varepsilon} = 1/2\,(\mathbf{G} - ..\,{}^t_r\mathbf{G})$,
$\overline{\boldsymbol{\varepsilon}}$ deviatoric part of the Almansi strain tensor,
$\boldsymbol{\sigma}$ Cauchy stress tensor,
$\mathbf{S}, \Delta^t_r\mathbf{S}$ deviatoric part of $\boldsymbol{\sigma}$ and of its variation,
$\mathrm{I}_\varepsilon, \overline{\mathrm{II}}_{\overline{\varepsilon}}, \overline{\mathrm{III}}_{\overline{\varepsilon}}$ invariants used for strain tensors: ε^i_i, $1/2\,\overline{\varepsilon}^i_j\overline{\varepsilon}^j_i$, $1/3\,\overline{\varepsilon}^i_j\overline{\varepsilon}^j_k\overline{\varepsilon}^k_i$, respectively,
E internal energy density,
$\overline{\phi}$ intrinsic dissipation rate,
W help function,
S_0, Q_0 von Mises parameters (limit shear stress S_0 and radius $Q_0 = \sqrt{2}S_0$, of the von Mises cylinder),
φ_r interpolation functions,
δ Kronecker symbol,
ω Masing functional ($\omega = 1$ or 2).

(*) Paper presented at 30th Polish Solid Mechanics Conference, Zakopane, September 5–9, 1994.

1. Introduction

THE SHAPE MEMORY ALLOY (SMA) specific properties lead to many projects of industrial applications such as, for example, electrical and mechanical connections or thermal regulation [1, 2]. However, most of these projects did not succeed due to several metallurgical and mechanical reasons. Among these reasons, the fact that no numerical tool (such as Computer Assisted Design (CAD) programs) adapted to these materials exists is an important obstacle to their industrial development. Thus, even if SMA crystallographic structure and microscopic properties (i.e. the martensitic transformation and related phenomena) have been extensively studied, it becomes essential to deepen the modelling of their thermomechanical behaviour and then to propose a numerical formulation of this behaviour adapted to an integration into CAD programs.

Up to now several authors have intended to model the thermomechanical behaviour of SMA. Some of these models are monodimensional ones [3–6] and are indeed devoided of interest to model the deformation behaviour of three-dimensional bodies. At the same time several theoretical tensorial schemes have also been developed [7–9] but as far as we know, none of these constitutive laws resulted in industrial programs or applications; for example, the program recently developed by BRINSON *et al.* [10] takes into account only monodimensional effects.

This paper is devoted to a three-dimensional finite element model of the isothermal deformation of SMA, in order to analyze and predict the mechanical behaviour of NiTi alloys. The formulation of this model is developed for large geometrical transformations including large deformations. In this context, a general 3D kinematics has been studied. The constitutive behaviour is defined using an elastohysteresis tensorial scheme which is based on the splitting of the Cauchy stress tensor into two fundamental stress contributions of hyperelastic and pure hysteresis types, respectively. Such a constitutive law has already shown its applicability for SMA [11–13]. The equilibrium equations are then deduced using the principle of virtual power, the system of nonlinear algebraic equations being solved by the Newton–Raphson method.

In a second part, the modelling ability of this formulation is presented in the case of three-dimensional plate made of NiTi shape memory alloys under bending. We focus at first on the influence of several boundary conditions on the simulation of NiTi plate bending. A set of numerical data is then displayed and compared with some simple elastic theoretical results found in the literature. Secondly, a simulation of the typical isothermal behaviours of shape memory alloys (i.e. pseudoelasticity and rubber-like behaviour) of a simple 3D body subjected to bending is proposed. This gives the first approach to the thermomechanical behaviour modelling of industrial shape memory alloy bodies.

2. Theoretical formulation

The theoretical formulation of the model is written considering large geometrical transformations including large deformations. As it was previously mentioned, a general 3D kinematics has been studied, no particular direction being favoured. Such a formulation allows for example the study of mechanical cylindric connections made of NiTi SMA. The definition of this kinematics in terms of involvements in the finite element program is briefly detailed in this paper.

2.1. Three-dimensional kinematics

Due to the incremental character of plastic constitutive laws, the description of elastoplastic deformation process is performed using an updated Lagrangian scheme, i.e. the configuration of the material at time t is taken as reference configuration for the time interval $[t, t + \Delta t]$. At the end of the increment Δt, the configuration of the material and the boundary conditions are updated, the new configuration being chosen as reference configuration for the next time increment. Let us consider a body Ω, its configuration at time t being the reference configuration. The equilibrium conditions are written in the final configuration, i.e. at

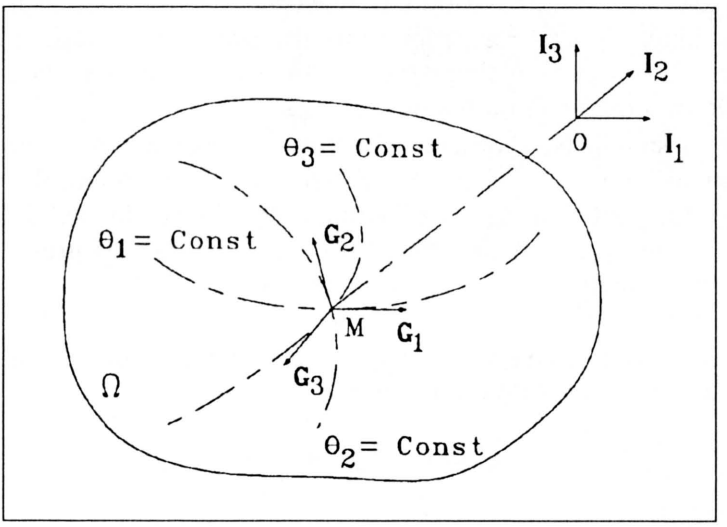

FIG. 1. Three-dimensional kinematics: definition of the convected material coordinates and of the local natural frame $\mathbf{G}_i$.

time $t + \Delta t$. The position of the body Ω, see Fig. 1, is defined using convected material coordinates θ^i, so that at time t, its position can be written as

$$\mathbf{M}(\theta^i, t) = z^a(\theta^i, t)\,\mathbf{I}_a, \tag{2.1}$$

where the $\mathbf{I}_a$ vectors denote a fixed reference frame. The local frame $(M, \mathbf{G}_i)$,

also called natural frame, is defined by the relation:

$$\mathbf{G}_i = \left(\frac{\partial \mathbf{M}}{\partial \theta^i}\right)_t = \left(\frac{\partial z^a}{\partial \theta^i}\right)_t \mathbf{I}_a . \tag{2.2}$$

In the final configuration, the position of the body Ω at time $t + \Delta t$ can be written in the form $\mathbf{M}(\theta^i, t + \Delta t) = z^a(\theta^i, t + \Delta t)\,\mathbf{I}_a$, the local frame $\mathbf{g}_i$ being then defined by

$$\mathbf{g}_i = \left(\frac{\partial \mathbf{M}}{\partial \theta^i}\right)_{t+\Delta t} = \left(\frac{\partial z^a}{\partial \theta^i}\right)_{t+\Delta t} \mathbf{I}_a . \tag{2.3}$$

From these definitions, the Almansi strain tensor is written as [14, 15]

$$\Delta_t^{t+\Delta t}\varepsilon_{ij}\, \mathbf{g}^i \otimes \mathbf{g}^j = \frac{1}{2}\left(\mathbf{G} - {}_t^{t+\Delta t}..\,\mathbf{G}\right) . \tag{2.4}$$

${}_t^{t+\Delta t}..\,\mathbf{G}$ represents a tensor, the components of which are those of the metric tensor $\mathbf{G}$ in the natural frame at time t, convected without modification until the time $t + \Delta t$. Similarly, $\Delta_t^{t+\Delta t}\varepsilon_{ij}$ represents the two times covariant components of the strain tensor between times t and $t + \Delta t$. For the remaining part of this study, the strain tensor will be denoted by $\Delta\boldsymbol{\varepsilon}$.

For sake of simplicity, the map of material coordinate is taken as the map of coordinate of the finite element discretization [16]. Practically, this choice imposes that the global integrals of volume should be divided into a sum of integrals performed on each element; this choice is in fact natural in the case of the finite element method.

Discretization of the kinematic fields. Let M be a material point of the body Ω. Its current position is defined by the relation:

$$\mathbf{M} = z^a\, \mathbf{I}_a = z^{ar}\, \varphi_r\, \mathbf{I}_a , \tag{2.5}$$

where the interpolation functions φ_r depend on a coordinate map ξ_i on the reference element, i.e. $\varphi_r = \varphi_r(\xi_i)$. Since the elements are assumed to be isoparametric $\varphi_r = \psi_r$ (ψ_r represents the interpolation of the functions), the displacement field $\Delta\mathbf{u}$ between times t and $t + \Delta t$ may be written as:

$$\Delta\mathbf{u} = \Delta u^a\, \mathbf{I}_a = \Delta u^{as}\, \psi_s\, \mathbf{I}_a . \tag{2.6}$$

The choice $\xi_i = \theta_i$ implies that ξ_i corresponds to the material coordinate of each element.

2.2. Constitutive behaviour

The thermomechanical behaviour of the alloys with shape-memory properties is the result of the action at a microscopical scale of reversible phenomena in association with irreversible phenomena; the observable effect of irreversible phenomena is the hysteresis loop [17] which can be universally spotted in many fields of physics [18]. Such an observation is the starting point to elaborate a class of thermomechanical schemes called elastohysteresis [11].

For SMA, the permanence of the simultaneous existence of reversible processes and hysteresis suggests to express the Cauchy stress tensor $\boldsymbol{\sigma}$ as the addition of two partial stresses, the first one being hyperelastic $\boldsymbol{\sigma}_r$ [11], while the second one is related to hysteresis of elastoplastic type $\boldsymbol{\sigma}_h$ [19, 20, 21]. This approach leads to the studies of two tensorial schemes of isothermal hyperelasticity and hysteresic behaviour, respectively. The last one which may be pure hysteresis (periodic under periodic loading) or evolutional hysteresis is non-standard and belongs to the discrete memory type [19, 22]. Both hyperelastic and hysteresis schemes allow the introduction of a particular formalism, the choice of which is driven by the physical processes involved in the thermomechanical behaviour of SMA. The pure elastohysteresis scheme allows the description of isothermal effects (i.e. superelasticity and pseudoelasticity) as well as shape memory effect [11].

2.2.1. Hyperelastic behaviour. For an isotropic body the hyperelastic stress is determined if one defines a density of elastic energy depending on three variables, i.e. three strain invariants. The thermomechanical properties of shape memory alloys are related to the thermoelastic martensitic transformation which occurs mainly by a shear-like mechanism. Macroscopically, if the material is assumed isotropic, the choice of the intensity of the deviatoric strain $\overline{\mathrm{II}}_{\bar{\varepsilon}}$ as the first variable of the density of elastic energy, is thus physically meaningful [11, 12]. The set of variables is completed by the ratio of elementary material volumes v and by the phase of the deviatoric strain tensor $\varphi_{\bar{\varepsilon}}$. Let us denote by $g = \det |\, g_{ij} \,|$ and $G = \det |\, G_{ij} \,|$, the ratio of elementary volumes is then defined by the relation $v = (g/G)^{1/2}$. Denoting by $\bar{\varepsilon}$ the deviatoric part of the Almansi strain tensor defined between the initial neutral state and the current state, the last variable can be expressed as:

$$\cos 3\varphi_{\bar{\varepsilon}} = 3\sqrt{6}\,\frac{\overline{\mathrm{III}}_{\bar{\varepsilon}}}{2\overline{\mathrm{II}}_{\bar{\varepsilon}}^{3/2}}\,, \tag{2.7}$$

where $\overline{\mathrm{III}}_{\bar{\varepsilon}}$ denotes the third invariant of the deviatoric strain tensor.

Let E be the density of elastic energy. The reversible stress contribution $\boldsymbol{\sigma}_r$ is defined, for an isothermal evolution, by the rate form

$$\frac{\partial E}{\partial t} = \sigma_r^{ij}\, D_{ji}\,. \tag{2.8}$$

D denotes the strain rate tensor for which $2D_{ij} = \partial g_{ij}/\partial t$ and in the isothermal case, E is simply the Helmholtz free energy. One obtains then by identifying all terms [11]:

$$\boldsymbol{\sigma}_r = \alpha_0 \mathbf{g} + \alpha_1 \Delta_0^t \boldsymbol{\varepsilon} + \alpha_2 \Delta_0^t \boldsymbol{\varepsilon} \cdot \Delta_0^t \boldsymbol{\varepsilon}\,, \tag{2.9}$$

where the coefficients α_i are functions of v, $\overline{\Pi}_{\bar{\varepsilon}}$, $\varphi_{\bar{\varepsilon}}$, $\partial E/\partial v$, $\partial E/\partial \overline{\Pi}_{\bar{\varepsilon}}$ and $\partial E/\partial \varphi_{\bar{\varepsilon}}$. In the case of shape memory alloys, a simple form for E is chosen as follows [11, 12]:

$$E = \frac{k_r \ln^2 v}{6} + \frac{Q_r^2}{2\mu_r} \ln\left[\cosh\left(\frac{2\mu_r}{Q_r}\sqrt{2\overline{\Pi}_{\bar{\varepsilon}}}\right)\right] + 2\mu_\infty \overline{\Pi}_{\bar{\varepsilon}}\,, \tag{2.10}$$

where k_r, Q_r, μ_r and μ_∞ are the parameters of this law and depend on the alloy and on the temperature. At this step, the variation of the hyperelastic constitutive law is needed to calculate the stiffness matrix; but for sake of clarity, the variation of strain and metric tensors, natural frame vectors as well as the variation of this law with respect to the degrees of freedom will not be detailed in this paper.

2.2.2. Pure hysteresis behaviour. The hysteresis contribution has the property of being always irreversible as it is related to the intervention of microstructural phenomena of dry friction type (strain rate-independent). It is different from a purely frictional stress due to the presence of some physical phenomena which are also able to store elastic energy. Rheological models containing elastic and slip elements have been considered to establish general pure hysteresis model [19]. From this analysis it has been shown that the internal energy and other thermomechanical quantities associated with the pure hysteresis contribution depends on the current state but also on the previous thermodynamical history through the memorisation of some discrete memory states. The material is assumed isotropic and the hysteresis contribution is only deviatoric. The basic hypotheses are the non-coupling volumetric-deviatoric behaviour and the isotropic plasticity evolution limited by the von Mises criterion which is directly included in the rate-form formulation of **S**; such hypotheses can be easily justified in the case of metallic materials. The constitutive law is then written in the form:

$$\frac{\partial}{\partial t}\left[\Delta_r^t S'^i_j\right] = 2\mu_h \overline{D}^i_j + \beta_4 \overline{\phi}\, \Delta_r^t S'^i_j\,. \tag{2.11}$$

The term $\mathbf{S}'$ is related to the deviatoric stress tensor **S** through the relation (2.14) and $\overline{\mathbf{D}}$ denotes the deviatoric strain rate tensor. The subscript r represents a reference situation which corresponds to the initial state for the first loading and to the last inversion state for the other cases, as long as any crossing point is not detected as it will be described in the next section [20]. The variable t, analogous to the time, is used to describe an evolution, and the parameter μ_h corresponds

to the Lamé's coefficient, while for a radial path, β_4 is defined by:

$$\beta_4 = -\frac{\mu_h}{\omega^2 S_0^2}, \tag{2.12}$$

where the similarity function of Masing ω is equal to 1 for the first loading and to 2 for the others. S_0 denotes the limit shear stress for the pure hysteresis contribution. The main advantage of this definition is that the identification of the parameters can be easily performed with only a tensile and a simple shear test [23]. The term $\overline{\phi}$ represents the intrinsic dissipation rate during an evolution and is defined on a radial path by the relation:

$$\overline{\phi} = \Delta_r^t S'^i_j \, \overline{D}^j_i . \tag{2.13}$$

The definition of the constitutive equation (2.11) is performed by using a mixed transportation scheme. The symmetrical components of S are obtained from those of S' by the relation:

$$S^{ij} = \frac{1}{2}\left(S'^i_k \, g^{kj} + S'^j_k \, g^{ki}\right) . \tag{2.14}$$

It can be noticed that the constitutive equation (2.11) defines the Lie derivative one time contravariant and one time covariant of the tensor S, while the previous relation can be interpreted as the integration of the Jaumann derivative of this tensor.

Resolution of the constitutive equation. The constitutive equation is a first order partial differential equation, the values of which are known at time t. It is then necessary to integrate this equation between times t and $t + \Delta t$ and two simple integration methods can be used. On the one hand, the equation can be linearized and then directly integrated by an implicit Newton method; on the other hand, it can be integrated by a Runge–Kutta explicit method [15]. In this last case, it implies that the calculation of all different values is made at several intermediate points while the first method necessitates only a calculation at time $t + \Delta t$. For the sake of simplicity and in order to be consistent with the resolution of other numerical problems (e.g. determination of inversion points), the first method has been retained here.

From these hypotheses, the derivative of S' with respect to time is linearized; denoting $\tau = t + \Delta t$, one obtains the constitutive equation in the form:

$$\frac{1}{2}\beta_4 \left[\Delta_r^\tau S'^l_k \, g^{km} + \Delta_r^\tau S'^m_k \, g^{kl}\right] \overline{D}_{lm} \, \Delta_r^\tau S'^i_j - \Delta_t^\tau S'^i_j + 2\mu_h \, \overline{D}^i_j = 0 \tag{2.15}$$

with

$$\Delta_t^\tau S'^i_k = \Delta_r^\tau S'^i_k - \Delta_r^t S'^i_k . \tag{2.16}$$

This equation, quadratic in $\Delta_r^\tau S'^i_j$, is then solved by a first order Newton method.

Determination of inversion and crossing points. The necessity of introducing discrete memory concept can be observed in the mono-dimensional case such as the one presented in Fig. 2. It can be seen in this figure that the third branch BC can not be continued along the path CD′ but along the path CD which is the continuation of the first loading branch. This shows that along the path ABC, it is necessary to keep the memory of point A, memory which is erased along the path CD for after C, the behaviour is identical as if the path ABC has not been performed. Along the paths OA, then AB, BC and CD, one must keep successively the memory of points O, then O and A, then O, A and B and finally O only. Points such as A and B are called inversion points while points such as C are called crossing points.

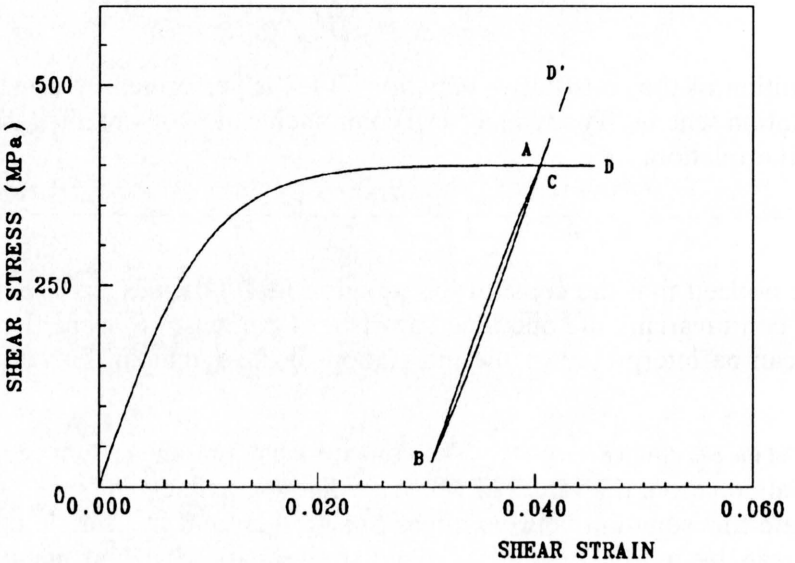

FIG. 2. Quasi-monodimensional simple shear test: definition of a pure hysteresis behaviour and of the inversion and crossing points.

The management of inversion points is performed by using the intrinsic dissipation rate function $\overline{\phi}$ presented in equation (2.13). This value is related to a volume element and must always be positive. The state at time t is an inversion point when the function $\overline{\phi}$ becomes negative. Furthermore the management of crossing points is performed by using an associate function W called help function and defined on a radial path by the relation [19, 21]:

$$W = \frac{2}{\omega^2} \int_{t_r}^{t} \overline{\phi}(\tau)\, d\tau \,. \tag{2.17}$$

After each inversion point, the level reached by the W function is memorized and W is set to zero for the next evolution. This function represents a measurement of dissipated energy along the path between two inversion points. A crossing

point is then observed when the current level of exchanged energy reaches a previously memorized level of W, reached on a previous branch. The crossing point represents the closure of a cycle which can then be erased. For non-radial path, the expression of relation (2.17) is rather more complicated [21]. It can be noticed that the crossing point has to be determined accurately, in order to avoid a numerical drift when performing a succession of centred cycles or loading-unloading loops.

2.3. Variational formulation

Let Ω be the region occupied by the material and Σ its boundary. The weak formulation of the boundary-value problem defined by the boundary conditions and by the equilibrium equations is obtained by using the principle of virtual power. In fact, it may be shown that this boundary-value problem is satisfied at time $t + \Delta t$ if and only if the following condition:

$$\int_{\Omega} \sigma^{ij} \; \overset{*}{v}_i \,|_j \; d\Omega = \int_{\Sigma} T^i \; \overset{*}{v}_i \; d\Sigma \tag{2.18}$$

is fulfilled for virtual velocity field $\overset{*}{\mathbf{v}}$ resulting from kinematically admissible displacement field. Here $\boldsymbol{\sigma}$ and $\mathbf{T}$ represent the Cauchy stress tensor and the surface external force, respectively. The region Ω as well as the surface Σ correspond to the material positions of the body at time $t + \Delta t$. From the finite element discretization and taking into account that the virtual velocity field is arbitrary in Ω and on Σ, this leads with (2.6) in a standard way to the system of algebraic nonlinear equations:

$$R_{bs}(\Delta u^{ar}) = 0 \qquad \forall bs, \tag{2.19}$$

where $\Delta\mathbf{u}$ denotes the displacement between time t and $t + \Delta t$, and

$$R_{bs}(\Delta u^{ar}) = \int_{\Omega(t)} \sigma^{ij} \; (\Delta u^{ar}) \; \overset{*}{v}_i \,|_j \; (\overset{*}{v}^{bs} = 1) \; d\Omega - \int_{\Sigma(t)} T^i \; \overset{*}{v}_i \; (\overset{*}{v}^{bs} = 1) \; d\Sigma \,. \tag{2.20}$$

$\overset{*}{v}^{bs}$ corresponds to the virtual velocity of a degree of freedom, $\overset{*}{\mathbf{v}}$ being chosen under the same form as the displacement field. The previous system is then solved by using the Newton–Raphson method.

3. Numerical results

This section is devoted to the numerical study of the bending behaviour of a NiTi square plate under several boundary conditions. The aim is to analyze the convergence and the ability of the elastohysteresis constitutive law to model the

pseudoelastic and the rubber-like behaviour of such shape memory alloys. The first part deals with the influence of the boundary conditions on the mechanical behaviour of a plate loaded by an uniform pressure on its upper side; then the second part deals with the influence of the mesh on the numerical results. Finally the last part is devoted to the description of the behaviour of a NiTi SMA plate in the austenitic as well as in the martensitic state.

3.1. Plate under several boundary conditions

The square plate which is studied here has the following dimensions: $40 \times 40 \times 2.6$ mm. For symmetry reasons, only the quarter of the plate, presented in Fig. 3, has been used for all tests. Therefore on faces BCGF and EFGH, the boundary conditions are symmetry type conditions, i.e. $v = 0$ on BCGF and $u = 0$ on EFGH. Three types of edge boundary conditions are used; a clamped plate (Case 1), a simply supported plate (Case 2) and a sliding simply supported plate (Case 3). For the first case, the boundary conditions are $u = v = w = 0$ on ADCB and AEHD. For the second case $w = u = 0$ on CD and $w = v = 0$ on DH, while for the last case, $w = 0$ on CD and DH. The plate is subjected to uniform pressure on the upper side ABFE. The mesh used for all these cases has 10 elements on each lateral side and 2 elements in the thickness, the elements being quadratic hexahedrons.

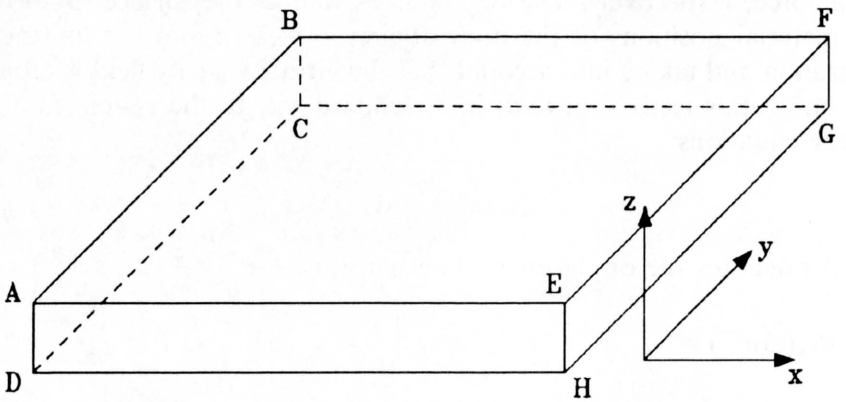

FIG. 3. Square plate used for the numerical results. u, v and w are the displacements along the x, y and z directions, respectively.

The pressure-deflection loading curves obtained for these three cases are presented in Fig. 4. The parameters of the elastohysteresis constitutive law are those determined from experimental results and given in Table 1 of the subsection 3.3. The curves drawn in dashed lines represent the simulation of respective problems with particular boundary conditions for a linear elastic material, with the Young modulus $E = 83000$ MPa and the Poisson's ratio $\nu = 0.393$; these parameters have been determined from those in Table 1 so that the associated linear

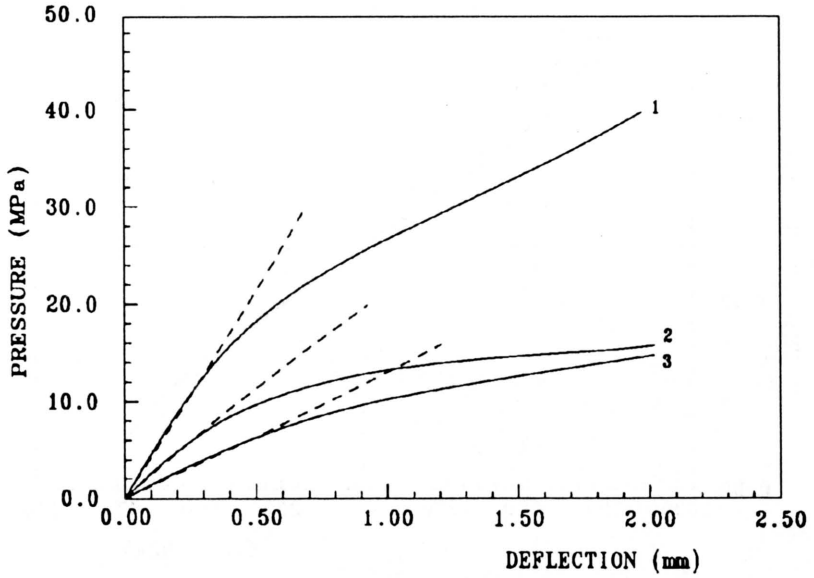

FIG. 4. Pressure-deflection loading curves obtained for a clamped plate (1), a simply supported plate (2), and a sliding simply supported plate (3). The curves in dashed line represent the elastic results associated to each case of boundary conditions with the parameters $E = 83000$ MPa and $\nu = 0.393$.

behaviour coincides with the initial quasi-linear stress-strain relation of the elastohysteresis behaviour. These elastic results have been compared to the analytical solutions given by TIMOSHENKO [24] and, despite the fact that these analytical results are given for thin plates, there is a good agreement between analytical and numerical results. Moreover, the curves drawn in full lines feature a strong nonlinear behaviour and it can be observed (like in the elastic case) that the clamped plate requires a higher pressure to be deformed, while the pressure is of the same order of magnitude in the two other cases.

The curves plotted in Fig. 5 and Fig. 6 represent the stress distributions in the thickness, both for a deflection of 2 mm. The longitudinal stress σ_{yy} and shear stress σ_{yz} are presented in Fig. 5 and Fig. 6, respectively. The value of σ_{yy} is taken in the middle of the plate while σ_{yz} is taken on the symmetry side EFGH near the edge, i.e. where it reaches its highest value. It can be observed that the variation of σ_{yy} along the thickness follows a third order symmetric curve and that this value is not too different in all cases. Such a small difference is due to the fact that the deformation state in the center of the plate is identical for all cases (as the deformed shapes are the same, see Fig. 7), since this region is far from the edges. It can be expected that for an infinite plate, these three curves will merge together. Conversely, the shear stress depends strongly on the boundary conditions, the value of σ_{yz} being much higher in the case of the clamped plate compared to the other cases when the same central deflection is considered. The clamped plate having the higher stiffness, the load must be increased to

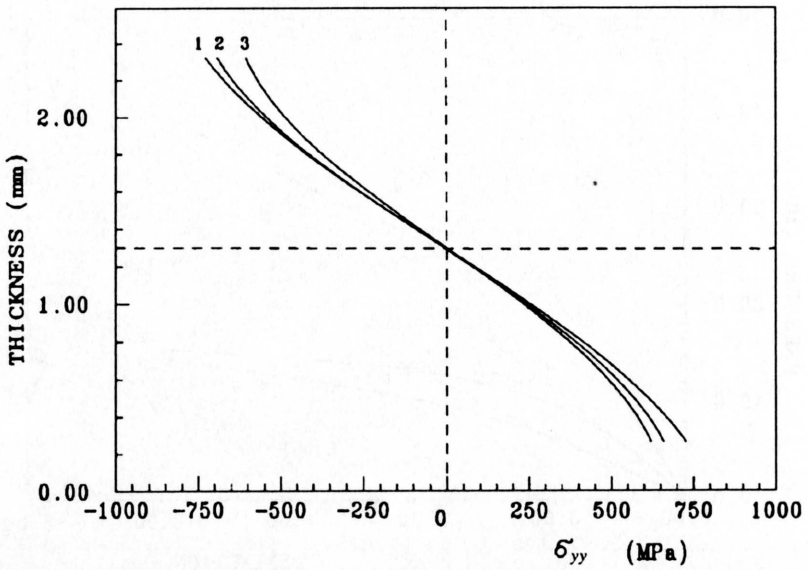

FIG. 5. Longitudinal stress distribution σ_{yy} obtained between points F and G, along the thickness for a 2 mm central deflection, for a clamped plate (1), a simply supported plate (2), and a sliding simply supported plate (3).

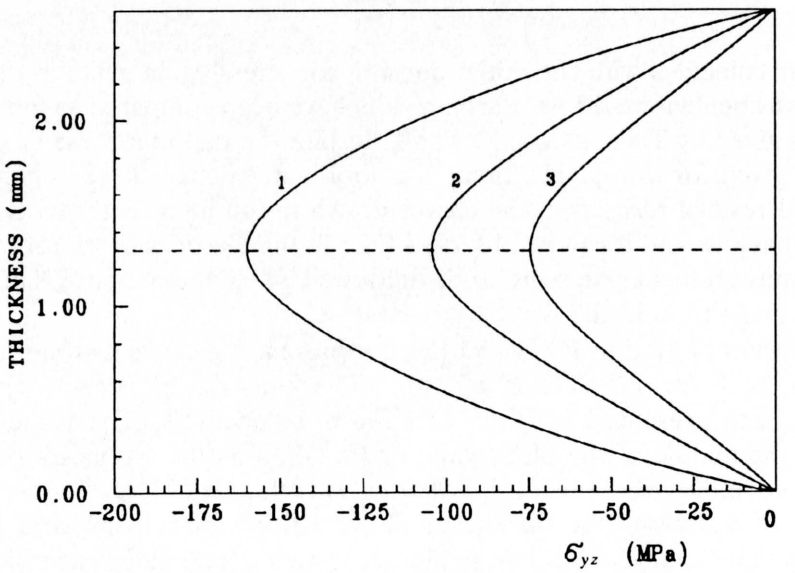

FIG. 6. Shear stress distribution σ_{yz} obtained between points E and H, along the thickness for a 2 mm central deflection, for a clamped plate (1), a simply supported plate (2), and a sliding simply supported plate (3).

obtain the same central deflection, which lead naturally to a higher shear stress level. Moreover, all curves have a classical symmetric shape with respect to the mid-plane.

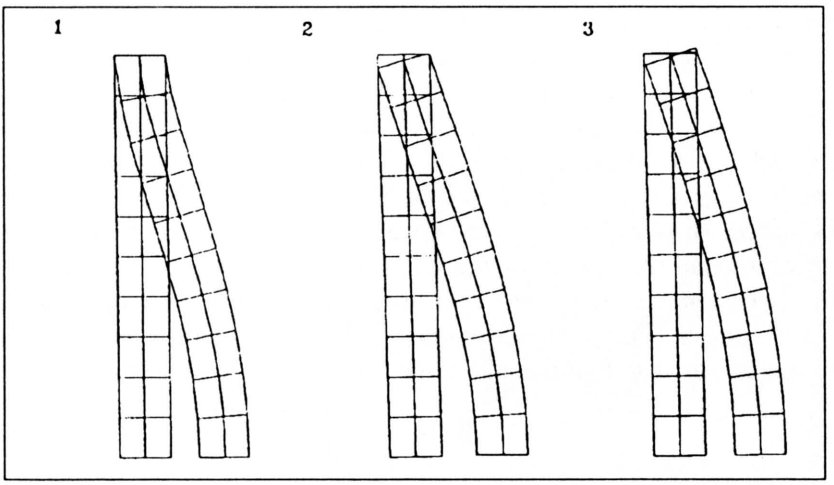

FIG. 7. Initial and deformed shape of the symmetry side EFGH of the plate for a deflection of 2 mm. Meshes correspond to a clamped plate (1), a simply supported plate (2), and a sliding simply supported plate (3).

3.2. Influence of the mesh

The influence of the mesh on the numerical results has been studied on the clamped square plate (see also subsection 3.3 for details about the material parameters). The pressure-deflection loading curves obtained for $n = 4$, 6, 8 and 10 quadratic elements on the lateral sides, respectively, are presented in Fig. 8. It can

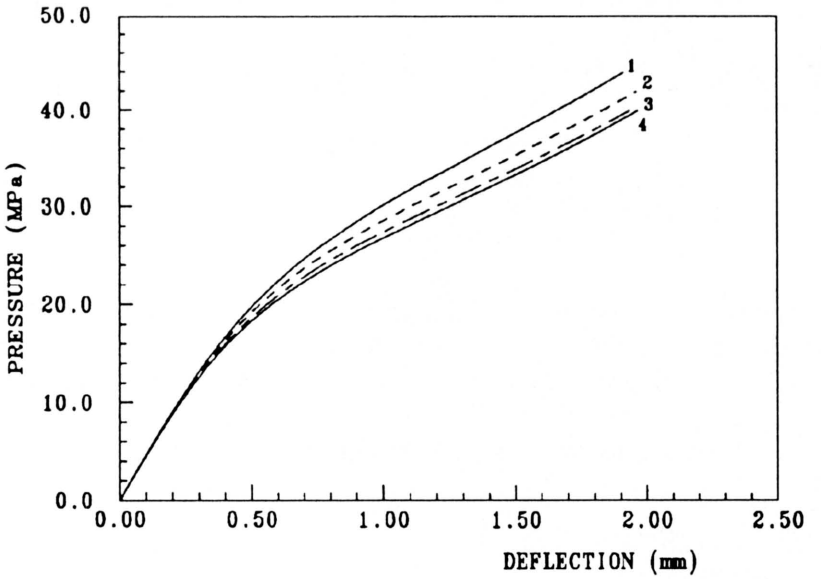

FIG. 8. Pressure-deflection loading curves obtained on a square plate for $n = 4$ (1), $n = 6$ (2), $n = 8$ (3) and $n = 10$ (4) quadratic elements on each lateral side of the plate, respectively. The mesh contains 2 elements in the thickness.

be observed that the number of elements on the edge side has a great influence on the numerical results, especially when this number is rather small. As it could be expected, a small number of elements leads to an overestimation of the bending rigidity. When this number increases, the calculations converge to a stable solution which seems to be reached for $n = 10$, for the gap between curves 3 and 4 is rather small. The curves presented in Fig. 9 represent the pressure-deflection curves obtained for $n = 1$, 2 and 3 quadratic elements in the thickness. It can be seen that for a small number of elements ($n = 1$), the rigidity of the plate is again overestimated in the range of small strains, but also that it tends to saturate for larger deformations. For a higher number of elements, the difference between curves obtained for $n = 2$ and 3 elements becomes quasi-negligible.

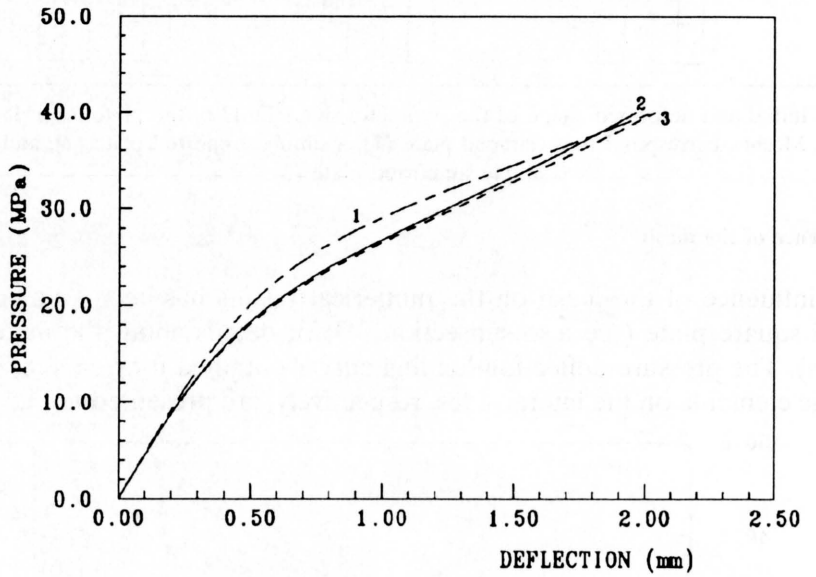

FIG. 9. Pressure-deflection loading curves obtained on a square plate for $n = 1$ (1), $n = 2$ (2) and $n = 3$ (3) quadratic elements in the thickness of the plate, respectively. The mesh contains 10 elements on each lateral side.

As a whole, a mesh of $n = 10$ elements on each lateral side and of $n = 2$ elements in the thickness offers a good compromise between the accuracy, the reliability of the mesh and the calculation time. This mesh is used for all the other calculations; indeed, one observes that the convergence is stable in all tests, no locking phenomenon appears and the solution always converges to a stable shape.

3.3. Shape memory alloy behaviour

Concerning the study of SMA, the material parameters have been identified on a NiTi alloy from the experimental results obtained in simple shear by MANACH [13]. The determination of these parameters has already been detailed

in MANACH *et al.* [23]. The values are given in Table 1 (in MPa) and are considered as temperature-independent.

Table 1. Material parameters of the elastohysteresis constitutive law.

	k_r	μ_r	μ_∞	μ_h	S_0
Austenitic state	425000	22500	2500	7500	100
Martensitic state	425000	22500	2500	7500	200

The evolution of Q_r as a function of the temperature has been determined to follow a linear relation such as: $Q_r = 5\sqrt{2}(T - 313)$ MPa [23] for $T > 313$ K, and 0 MPa otherwise. In the austenitic state, the test is performed at $T = 353$ K and in the martensitic state at $T = 313$ K. The numerical simple shear stress-strain curves obtained using these parameters are presented in Fig. 10 and Fig. 11 for the austenitic and martensitic states, respectively. Moreover, loops and subloops have been performed on these simulated curves in order to feature the main characteristics of the elastohysteresis model. The results obtained on the pressure-deflection loading-unloading curves in the middle of the plate are presented in Fig. 12 in the austenitic (A) and in the martensitic (M) state, respectively.

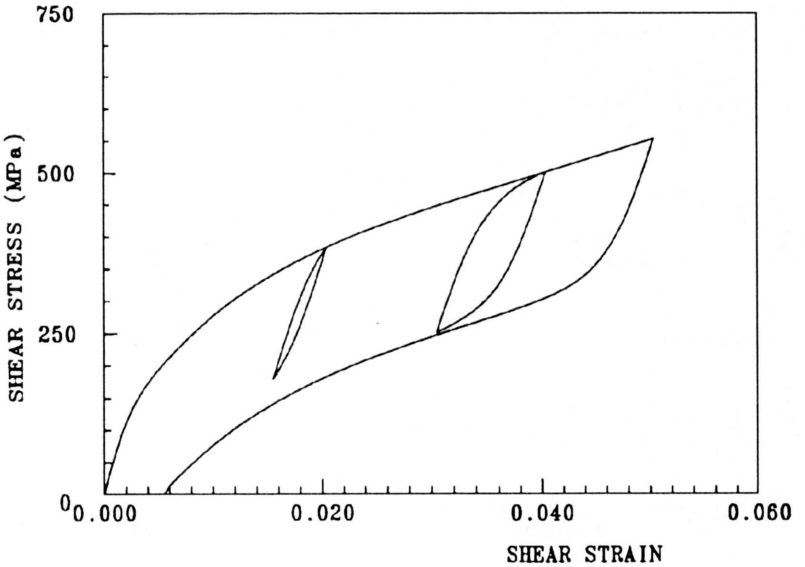

FIG. 10. Numerical stress-strain curve obtained in simple shear on a NiTi alloy from the parameters identified by the experimental results of Manach [13] in the austenitic state at $T = 353$ K.

It is now well known that the deformation mode of materials presenting a thermoelastic martensitic transformation is highly influenced by the temperature at which the deformation takes place. Two mechanisms of deformation can

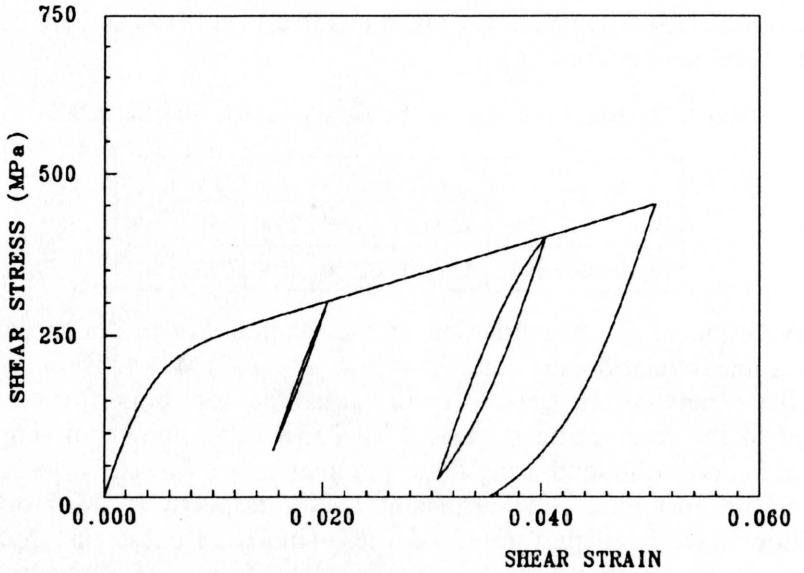

FIG. 11. Numerical stress-strain curve obtained in simple shear on a NiTi alloy from the parameters identified by the experimental results of Manach [13] in the martensitic state at $T = 313$ K.

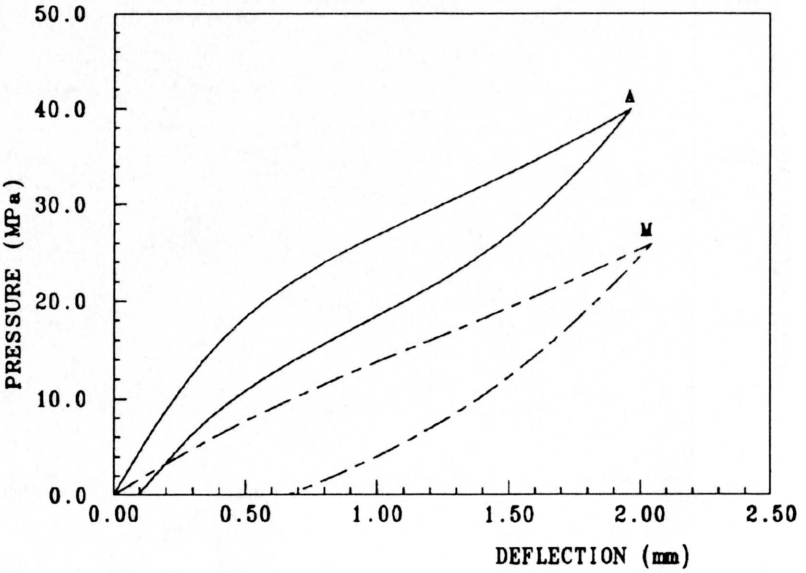

FIG. 12. Pressure-deflection loading-unloading curve obtained for the bending of a NiTi clamped square plate in the austenitic (A) and in the martensitic (M) state, respectively.

occur, i.e. the reorientation of the martensite variants when the material is in the martensitic state, and the stress-induced martensitic transformation when the

material is in the austenitic state. Qualitatively, the curves presented in Fig. 12 exhibit the typical mechanical behaviours of SMA related to these two previous phenomena, i.e. the superelastic effect of the austenitic phase and the rubber-like behaviour of the martensitic phase. Then for curve (M), the deformation is produced by the motion of internal defects such as martensite-martensite interfaces or martensite twins. The loading curve corresponds to the development of the martensite variant reorientation, while the unloading curve is characterized by a partial reorientation of the martensite variants, producing then a greater reverse deformation than the classical elastic deformation. For curve (A), the main mechanism of deformation is produced by the stress-induced martensitic transformation during loading and its quasi-total reversion during unloading, e.g. [25].

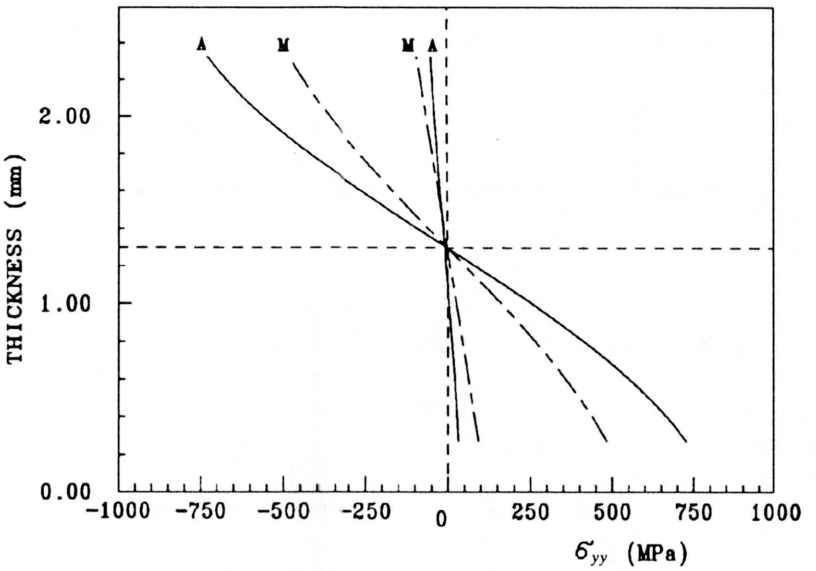

FIG. 13. Longitudinal stress distribution σ_{yy} obtained between points F and G, along the thickness, for a 2 mm central deflection, for a clamped plate at the end of the loading and unloading in the austenitic (A) and in the martensitic (M) state, respectively.

The stress distributions in the thickness are presented in Fig. 13 and Fig. 14 for the longitudinal stress σ_{yy} and for the shear stress σ_{yz}, respectively. Comparisons are made for the same central deflection of 2 mm. It can be observed that the residual stresses are of the same order of magnitude, the longitudinal stress σ_{yy} being greater in the martensitic state (which is more deformed) while the shear stress σ_{yz} is similar for both cases, which is coherent with consideration of subsection 3.1. It can also be pointed out that those stress distributions are in agreement with the analytical solutions given by Kirchhoff for an elastic clamped square plate.

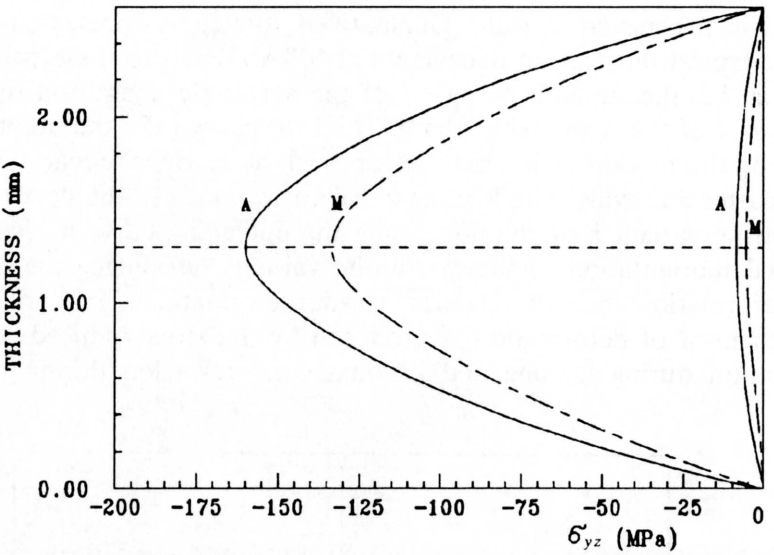

FIG. 14. Shear stress distribution σ_{yz} obtained between points E and H, along the thickness for a 2 mm central deflection, for a clamped plate at the end of the loading and unloading in the austenitic (A) and in the martensitic (M) state, respectively.

4. Conclusions

A new three-dimensional finite element model of the unusual deformation of shape memory alloys has been developed. The validity of this model has been analyzed in the case of the bending behaviour of NiTi alloy. The formulation of this model is written in the case of large geometrical transformations including large deformations. In this context, a general 3D kinematics has been studied. The constitutive behaviour is defined using an elastohysteresis tensorial scheme and finally, the equilibrium equations are deduced using the principle of virtual power which is solved by the finite element method.

The modelling ability of the formulation has been presented in the case of three-dimensional plate behaviour, the numerical study concerning the bending behaviour of a NiTi square plate under several boundary conditions. The behaviour of the plate under several boundary conditions features a good agreement, at the beginning of the loading, between the numerical and analytical elastic results, while the influence of the mesh has also been analyzed. Furthermore, this study shows that the behaviour of SMA is well modelled by the elastohysteresis constitutive law and that the main effects observed numerically are consistent with those observed experimentally on such shape memory alloys.

Acknowledgements

The authors are grateful to the Service Technique des Programmes Aéronautiques of the French Ministry of Defence for financial support. The authors also wish to thank P. GUÉLIN and P. PÉGON for useful discussions.

References

1. P. SCHMIDT-MENDE and G. BLOCK, *Applications of NiTi-based shape memory alloys*, [in:] Proc. European Conference on Martensitic Transformations in Science and Technology, p. 245, Bochum, Germany 1989.
2. D. STÖCKEL, *Industrial applications of NiTi shape memory alloys*, [in:] Proc. European Conference on Martensitic Transformations in Science and Technology, p. 223, Bochum, Germany 1989.
3. I. MÜLLER and K. WILMANSKI, *A model for phase transition in pseudoelastic bodies*, Il Nuevo Cimento, 57B, p. 283, 1980.
4. F. FALK, *Model free energy, mechanics and thermodynamics of shape memory alloys*, Acta Metall., **28**, p. 1773, 1980.
5. L. LÜ, E. AERNOUDT, P. WOLLANTS, J. VAN HUMBEECK and L. DELAEY, *Simulation of transformation hysteresis*, Zeitschrift für Metallkunde, 81, p. 613, 1990.
6. J. ORTIN, *Partial hysteresis cycles in shape memory alloys: experiments and modelling*, [in:] Proc. European Symposium on Martensitic Transformation and Shape Memory Properties, p. C4-13, Aussois, France 1991.
7. K. TANAKA, S. KOBAYASHI and Y. SATO, *Thermomechanics of transformation pseudoelasticity and shape memory effect in alloys*, Intern. J. Plast., 2, p. 59, 1986.
8. E. PATOOR, A. EBERHARDT and M. BERVEILLER, *Potentiel pseudoélastique et plasticité de transformation martensitique dans les mono et polycristaux métalliques*, Acta Metall., **35**, p. 2779, 1987.
9. M. FREMOND, *Mécanique des milieux continus: matériaux à mémoire de forme*, C.R. Académie des Sciences de Paris, 304, p. 239, 1987.
10. L.C. BRINSON and R. LAMMERING, *Finite element analysis of the behavior of shape memory alloys and their applications*, Intern. J. Solids and Structures, **30**, p. 3261, 1993.
11. D. FAVIER, *Contribution à l'étude théorique de l'élastohystérésis à température variable: application aux propriétés de mémoire de forme*, Thèse d'Etat, Institut National Polytechnique de Grenoble, Grenoble, France, 1988.
12. D. FAVIER, P. GUÉLIN and P. PÉGON, *Thermomechanics of hysteresis effects in shape memory alloys*, [in:] Proc. Intern. Conference on Martensitic Transformation, p. 559, Sydney, Australia 1989.
13. P.Y. MANACH, *Etude du comportement thermomécanique d'alliages à mémoire de forme NiTi*, Thèse de Doctorat, Institut National Polytechnique de Grenoble, Grenoble, France 1993.
14. P. GUÉLIN, *Notes on the Cauchy tensors* $g^i \otimes g^j \, {}^t_R\sigma_{ij}$ *and* $g_i \otimes g^j \, {}^t_R\sigma^i_{\cdot j}$ *expressing the discrete memory concept*, [in:] Summer School in Two-phase Medium Mechanics, p. 57, Gdańsk, Poland 1983.
15. P. PÉGON and P. GUÉLIN, *Finite strain plasticity in convected frames*, Intern. J. Numerical Methods in Engng., 22, p. 521, 1986.
16. G. RIO, B. TATHI and F. HORKAY, *Introducing bending rigidity in a finite element membrane sheet metal forming model*, [in:] Proc. Intern. Seminar Mecamat'91, p. 449, Fontainebleau, France 1991.
17. H. VERGUTS, L. DELAEY, E. AERNOUDT and W. VERMEERSCH, *On hysteresis effects in shape memory alloys*, [in:] Proc. Euromech Colloquium 171, p. 214, Warszawa, Poland 1983.
18. D. FAVIER, P. GUÉLIN and R. CAMMARANO, *Application of a phenomenological elastohysteresis theory to the modelling of magnetisation*, [in:] Proc. Intern. Symposium on Magnetic Anisotropy and Coercivity in Rare-Earth Transition Metal Alloys, p. 137, Canberra, Australia 1992.
19. P. GUÉLIN, *Remarques sur l'hystérésis mécanique: les bases d'un schéma thermomécanique à structure héréditaire*, J. Mécanique, **19**, p. 217, 1980.
20. B. WACK, J.M. TERRIEZ and P. GUÉLIN, *A hereditary type, discrete memory, constitutive equation with applications to simple geometries*, Acta Mech., **50**, p. 9, 1983.
21. P. PÉGON, *Contribution à l'étude de l'élastohystérésis élastoplastique*, Thèse d'Etat, Institut National Polytechnique de Grenoble, Grenoble, France 1988.

22. P. PÉGON, P. GUÉLIN, D. FAVIER, B. WACK and W.K. NOWACKI, *Constitutive scheme of discrete memory form for granular materials*, Arch. Mech., **43**, p. 3, 1991.

23. P.Y. MANACH and D. FAVIER, *Comparison between isothermal tensile and shear tests on a NiTi shape memory alloy*, [in:] Proc. Intern. Conference on Martensitic Transformations, p. 941, Monterey, USA, 1992.

24. S. TIMOSHENKO and S. WOINOWSKY-KRIEGER, *Théorie des plaques et des coques*, Dunod, Paris 1961.

25. S. MIYAZAKI, K. OTSUKA and Y. SUZUKI, *Transformation pseudoelasticity and deformation behavior in a Ti–50.6at %Ni alloy*, Scripta Metall., **15**, p. 287, 1981.

UNIVERSITÉ DE BRETAGNE OCCIDENTALE
LABORATOIRE DE GÉNIE MÉCANIQUE ET MATÉRIAUX, GUIDEL
and
UNIVERSITÉ JOSEPH FOURIER
LABORATOIRE SOLS-SOLIDES-STRUCTURES, GRENOBLE, FRANCE.

Received November 28, 1994.

Arch. Mech., 47, 3, pp. 557–576, Warszawa 1995

Development of ground liquefaction due to surface waves (*)

A. SAWICKI and R. STAROSZCZYK (GDAŃSK)

EXPLOSIVE-INDUCED GROUND motions cause a number of complex phenomena in the water-saturated subsoil. For example, pore pressures are generated as a result of ground motions leading to a progressive weakening of saturated soil and to soil's liquefaction. The phenomena of pore pressure generation and liquefaction seem to be the main reasons which initiate underwater slides. It is assumed that these phenomena are induced by the passage of Rayleigh waves caused by explosions. The process of pore pressure generation is described by the compaction and liquefaction theory of saturated granular materials. The theory is applied in order to study the behaviour of water-saturated half-space, the motion of which is induced by the passage of Rayleigh waves. Numerical computations were performed by means of Finite Element Method. They show the history of pore pressure generation, development of liquefaction zones and changes of displacement amplitudes in the subsoil. The analysis was carried out for both harmonic in time and transient Rayleigh waves.

1. Introduction

THE PRESENT PAPER has been inspired by a field experiment ADFEX (Arctic Delta Failure Experiment) designed by the Canadian and Norwegian researchers in order to study submarine slides. There is an urgent need for predicting the behaviour of natural underwater slides for risk assessment of offshore structures, underwater pipelines, communication cables etc. One of important problems that appears to be insufficiently recognized deals with the submarine slide initiation, SYVITSKI and SCHAFER [29], cf. also FRYDMAN and TALESNICK [9].

Experimental slides were artificially triggered using explosives. Explosive-induced ground motions cause a number of complex phenomena in the water-saturated subsoil. For example, pore pressures are generated as a result of ground motions leading to a progressive weakening of saturated soil, and to soil's liquefaction in the extreme case. The phenomena of pore pressure generation and liquefaction, caused by the passage of surface waves, seem to be the main reasons which initiate slides.

The aim of the present paper is to study the behaviour of water-saturated half-space subjected to the passage of both harmonic in time and transient Rayleigh waves. Saturated sand is treated as a two-phase mixture, with the solid grains as one constituent and the pore water as the second one. The phenomenon of pore pressure generation in such a mixture is described within the framework of the theory originally developed by MORLAND and SAWICKI [18, 19], cf. some further modifications of that theory, SAWICKI [24], MORLAND *et al.* [20].

(*) Paper presented at 30th Polish Solid Mechanics Conference, Zakopane, September 5–9, 1994.

In the case of surface waves harmonic in time, the plane strain problem has been transformed into the one-dimensional problem in space by applying the method of LYSMER [14]. In the case of transient surface waves the solution is built on the basis of the solution for the time-harmonic case by applying the Fast Fourier Transform technique.

Numerical results show the history of pore pressure generation, development of liquefaction zones and changes of displacement amplitudes within the sandy subsoil. An effect of pore pressure dissipation is also taken into account.

The results obtained indicate that the surface waves may lead to the pore pressure generation in a saturated subsoil, and subsequently to liquefaction. The other original feature of the present paper seems to be a presentation of a relatively simple method of dealing with the problem of surface waves propagated over a half-space, in which such phenomena as pore pressure generation and liquefaction occur.

2. Wave motions and liquefaction

Mechanics of fluid-saturated granular media has been studied in various branches of science and engineering, including geophysics and civil engineering, depending on the objectives of investigations. Particular attention, especially in recent years, has been devoted to the mechanics of saturated soils in which, under certain conditions, the phenomena of pore pressure generation and soil's liquefaction take place. Several, both empirical and theoretical, models for soils have been developed and applied to various problems of practical importance. Extensive reviews of existing literature can be found in ZIENKIEWICZ *et al.* [32], FINN [7], MARTIN and SEED [16], ISHIHARA and TOWHATA [12].

Pore pressure generation in saturated soils, and subsequent liquefaction, is caused mainly by cyclic loads, although the same phenomena can arise under monotonic loading, cf. MARTIN *et al.* [15]. An extensive research has been devoted to study the behaviour of fluid-saturated sand layers subjected to earthquake-induced motions. The most elementary model for predicting earthquake effects is the one-dimensional wave propagation problem for such a layer subjected to a cyclic horizontal acceleration at its base, ISHIHARA and TOWHATA [12], ZIENKIEWICZ *et al.* [32], SAWICKI and MORLAND [23]. The primary source of the layer motion is the upward shear wave propagation from the underlying vibrating rock. Elaborated models allow the prediction of pore pressure generation in the soil column and the development of liquefaction zones.

The model of upwards shear wave propagation is a simplification of a complex loading situation during earthquakes. It is known that the major part of energy released during earthquakes is transmitted in the form of surface waves propagating in the Earth's crust, cf. EWING *et al.* [6], ACHENBACH [1], GAZETAS and YIEGIAN [10]. The surface waves are also generated by underground and surface

explosions (cf. DAS [5]. Thus, when studying the influence of seismic loads on pore pressures in saturated sands it is necessary to take into account some effects caused by surface waves.

The authors of this paper have not found in available literature any study devoted to the influence of surface waves on pore pressure generation in a saturated subsoil and soil's liquefaction. It is thus hoped that the present paper will contribute a little to this important problem.

The importance of blast-induced liquefaction was recognized by geotechnical engineers long time ago. KUMMENEJE and EIDE [13] report about some Norwegian investigations on blasting tests performed in order to study the influence of explosions on settlements and changes in soil strength, as well as liquefaction. It seems that from that time no significant progress in understanding the phenomena associated with the influence of wave motions on soil's liquefaction has been achieved, cf. a reference search by RAWLINGS [22]. In the opinion of FRAGASZY and VOSS [8], there was no generally accepted theory to explain the blast-induced liquefaction mechanism, or to predict the occurrence and effects of that phenomenon.

The above opinion is supported by more recent investigations. For example, RAJU and GUDEHUS [21] describe a field experiment performed in the Lausitz region of Germany, but they even do not attempt to propose any theoretical model of the phenomena observed. Another paper of VEYERA and CHARLIE [30] deals with the laboratory study of compressional liquefaction. They present a new experimental apparatus that has been developed to study the behaviour of saturated soils subjected to compressional stress-wave loading. Their results indicate that it is possible to liquefy sand under such conditions. However, they do not propose any theoretical description of the problem, cf. VEYERA and CHARLIE [30].

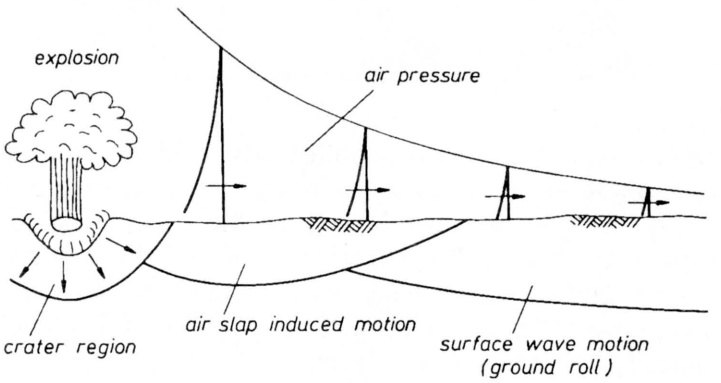

FIG. 1. Regions of ground's motion due to explosion, after STUDER and KOK [28].

STUDER and KOK [28] present some considerations about the influence of explosions on the ground liquefaction. According to their opinion, there is hardly any experience in liquefaction as a result of a non-contained explosion. They sug-

gest that the uncommonly flat craterforms after several nuclear-weapon experiments performed in the Pacific could be explained by liquefaction phenomena, although there are no detailed observations and measurement results available because that phenomenon was not found to be of interest in the past. Studer and Kok have distinguished some regions within a subsoil in which different phenomena caused by a non-contained explosion occur (cf. Fig. 1).

It is seen from Fig. 1 that at some distance from the source of explosion the surface wave motion of the ground dominates. Such a long-distance effects are of interest to civil engineers and will be considered in this paper.

3. Formulation of the problem

The plane strain problem of the motion of water-saturated sand half-space is studied. The motions of the subsoil are generated by Rayleigh surface waves propagating in the x direction (Fig. 2). The analysis is carried out for both harmonic in time and transient waves.

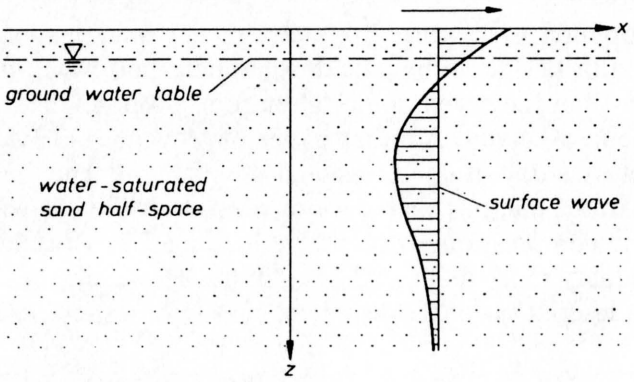

FIG. 2. Coordinate system (plane strain problem).

In the problem considered we deal with loads which act in a relatively short period of time, ranging from a fraction of a second in the case of blasts, to few seconds in the case of earthquakes. Moreover, the phenomena of our interest, as pore pressure generation and liquefaction, occur only in saturated sands characterized by a rather low permeability. Accordingly, one can assume that the relative motion between the soil grains and the pore fluid is negligibly small, and, hence, the following relation can be written:

$$\mathbf{u}^s = \mathbf{u}^f = \mathbf{u}, \tag{3.1}$$

where $\mathbf{u}$ denotes the displacement vector, and the respective superscripts distinguish either the soil skeleton (s) or the pore fluid (f). The assumption of common displacement field $\mathbf{u}$ of both constituents of the two-phase medium allows

for adopting a simplified model of saturated soil, corresponding to the so-called "undrained conditions". Such a model leads to a rather simple description of the phenomenon of pore pressure generation. The relative motion of both phases is caused by the phenomenon of filtration which depends on real time. The influence of filtration on pore pressure generation depends on both the duration of the applied loads and the subsoil's permeability. That influence will be taken into account in a numerical procedure applied in order to solve a boundary value problem. It is assumed that within each step of computations the subsoil properties do not change and the assumption of undrained conditions is valid. In the next step of computation the state of excess pore pressures is "frozen", and assumed as an initial condition for the problem of pore pressure dissipation. Then the dissipation problem is solved giving an initial state for subsequent step of computation of excess pore pressure, cf. SAWICKI and ŚWIDZIŃSKI [26]. The equations of motion of saturated sand, treated as a single-phase medium, are of the following form (ACHENBACH, [1]):

$$\sigma_{ij,j} + \varrho\, g_i = \varrho \frac{\partial^2 u_i}{\partial t^2}, \tag{3.2}$$

where σ_{ij} denotes the total stress tensor, ϱ is the soil density, g_i are the components of the external body force density, and t denotes time.

The total stress in the two-phase medium is a sum of partial stresses in respective constituents:

$$\sigma_{ij} = \sigma_{ij}^{s} + \sigma_{ij}^{f}, \tag{3.3}$$

with σ_{ij}^{s} and σ_{ij}^{f} denoting the stress tensor components in the soil skeleton and pore fluid, respectively. The non-viscous liquid does not carry shearing stresses, so we can express the fluid stress tensor components by

$$\sigma_{ij}^{f} = -\delta_{ij} \cdot n \cdot {}^{E}p^{f}, \tag{3.4}$$

where δ_{ij} is the Kronecker delta, n denotes the volume porosity and ${}^{E}p^{f}$ stands for the intrinsic pore pressure. The behaviour of the saturated soil depends to great extent upon the so-called effective stresses σ'_{ij}, defined by the equation

$$\sigma'_{ij} = \sigma_{ij} + \delta_{ij} \cdot {}^{E}p^{f}. \tag{3.5}$$

In this paper we have adopted the solid mechanics sign convention, i.e. positive values of the stress tensor components σ_{ij} mean tension, while positive fluid pressures ${}^{E}p^{f}$ mean compression.

The soil mass density ϱ is related to the respecive intrinsic skeleton and pore fluid densities ${}^{E}\varrho^{s}$ and ${}^{E}\varrho^{f}$ by the formula:

$$\varrho = (1 - n)\, {}^{E}\varrho^{s} + n\, {}^{E}\varrho^{f}. \tag{3.6}$$

When analysing the deformation of the soil it is useful to distinguish two kinds of it. The first one includes reversible (elastic) changes of dynamic origin, generated by propagating wave; and the second kind includes both static (elastic due to the own weight of soil) and irreversible (inelastic related to the sand compaction) variations. Thus, it is convenient to decompose the displacement, strain and stress fields as follows:

$$\begin{aligned} u_i &= u_i^R + u_i^I, \\ e_{ij} &= e_{ij}^R + e_{ij}^I, \\ \sigma_{ij} &= \sigma_{ij}^R + \sigma_{ij}^I, \end{aligned} \tag{3.7}$$

with the strain tensor components e_{ij} defined by:

$$e_{ij} = \frac{1}{2}(u_{i,j} + u_{j,i}), \tag{3.8}$$

and the superscripts R and I referring to the reversible and irreversible parts of relevant quantity. Decomposition of the stress tensor, and consequent decomposition of the equation of motion, have been introduced for the sake of simplicity. Note that the irreversible part of the stress tensor is caused by the gravity and remains constant during the analysed processes of pore pressure generation and dissipation.

Substitution of Eq. (3.7) into Eqs. (3.2), under the assumption that the time derivatives of irreversible parts of displacements u_i^I are small in comparison with the reversible (dynamic) ones, leads to the following two equations:

$$\sigma_{ij,j}^R = \varrho \frac{\partial^2 u_i^R}{\partial t^2} \tag{3.9}$$

for reversible, and

$$\sigma_{ij,j}^I + \varrho g_i = 0 \tag{3.10}$$

for irreversible variations. Eq. (3.9) governs the motions of subsoil due to dynamic loads, while Eq. (3.10) describes the stress state due to static loads.

It is assumed that the motions of the subsoil are excited by the passage of Rayleigh surface waves. Harmonic in time and transient waves are studied. Since the solution for a wave of arbitrary time dependence will be built on the basis of time-harmonic solution by applying the Fourier superposition method, we confine our attention to the variations harmonic in time, which can be expressed in the following form:

$$\begin{aligned} u_i^R &= U_i \exp(i\omega t), \\ e_{ij}^R &= E_{ij} \exp(i\omega t), \\ \sigma_{ij}^R &= T_{ij} \exp(i\omega t), \end{aligned} \tag{3.11}$$

with U_i, E_{ij} and T_{ij} being the amplitudes of respective functions. Assuming the surface wave to propagate in the positive x direction, the general solution of Eq. (3.9), describing the soil displacements generated by the wave, can be expressed by the formulae:

$$
\begin{aligned}
u_x^R &= A(z)\exp[i(\omega t - kx)], \\
u_z^R &= B(z)\exp[i(\omega t - kx)],
\end{aligned}
\tag{3.12}
$$

where u_x^R and u_z^R denote the horizontal and vertical displacements of the subsoil, respectively, k is the wavenumber of the surface wave, ω is the angular frequency of oscillations, and $i = \sqrt{-1}$ is the imaginary unit. The functions $A(z)$ and $B(z)$ are to be determined from the boundary conditions, which at the free surface ($z = 0$) are of the form

$$
\sigma_{zz}^R(x,0,t) = \sigma_{xz}^R(x,0,t) = 0. \tag{3.13}
$$

In addition, the functions u_x^R and u_z^R, together with their first space derivatives, should vanish for infinite values of depth z.

As concerns the transient wave motion, the elastic changes in the subsoil are determined by employing the solution for the waves harmonic in time. In the present work the transient wave is defined by a function describing the time variation of σ_{xx} at the free surface. This function is expanded in the Fourier series and the corresponding free surface displacement amplitude is determined for each stress harmonic. These displacement amplitudes are then used to normalise each component wave, and, finally, a superposition of all harmonic modes is carried out in order to describe the transient wave pattern. In this analysis the discrete Fourier series are applied, and all calculations are performed by means of the Fast Fourier Transform.

In order to determine the displacement, strain and stress fields in the soil due to the Rayleigh wave passage, it is necessary to supplement Eqs. (3.9) with the appropriate stress-strain relations. In the present investigation we have assumed that, within the range of strains analysed (less than 10^{-3}), the elastic response of the soil to the applied loads is governed by the Hooke's law

$$
\sigma_{ij}^R = \lambda\delta_{ij}e_{kk}^R + Ge_{ij}^R, \tag{3.14}
$$

with λ and G denoting Lamé's elastic constants. Both elastic parameters are assumed to be stress-dependent (they vary during the process of pore pressure generation). Amongst many factors influencing the elastic properties of soils, the most significant role is played by the magnitude of the effective stress in the soil skeleton. In the literature of the subject most attention has been paid to the shear modulus G. In the present analysis we adopt one of the simplest approaches being, however, in good agreement with the results of experimental tests (SILVER and SEED [27]; HARDIN and DRNEVICH [11]), i.e.

$$
G = G_0 + G_1\sqrt{p'}, \tag{3.15}
$$

where G_0 and G_1 are constants which should be determined empirically, and p' (which has to be substituted into (3.14) in units 10^5 Pa) denotes the mean effective pressure in the soil:

$$p' = -\frac{1}{3}\sigma_{kk}^s - {}^E p^f , \tag{3.16}$$

where the first term on RHS denotes the mean total pressure due to static loads. No experimental data regarding the influence of the stress level on Lamé's constant λ have been available so far. Therefore we have assumed this quantity to vary in such a way that the Poisson's ratio ν remains constant throughout the whole deformation process (such an approximation is widely applied in geomechanics). Consequently, there is

$$\lambda(p') = \frac{2\nu}{1-2\nu} G(p'). \tag{3.17}$$

Irreversible strains consist of two parts:

$$e_{ij}^I = e_{ij}^s + e_{ij}^c . \tag{3.18}$$

The static part of the strain tensor e_{ij}^s represents the settlement of the subsoil due to its own weight. The strains e_{ij}^s, together with the stresses σ_{kk}^s, can be easily determined by using standard methods of the classical soil mechanics.

The tensor e_{ij}^c, appearing in Eq. (3.18), represents inelastic strains developing in the soil due to the shearing. In order to determine these strains we make use of the model formulated by MORLAND [17] and MORLAND *et al.* [20], which is an extension of the earlier developed compaction theory of granular media (MORLAND and SAWICKI [18, 19]). In the model adopted the compaction, meant as a decrease in sand volume due to irreversible rearrangement of a granular structure, is governed by an evolutionary law. That law describes the rate of compaction as a function of the current inelastic strain state (compaction) and a certain scalar measure of the current deviatoric state. Following MORLAND [17], the constitutive equation describing the soil compaction is adopted in the following form:

$$\frac{d e^c}{d \xi} = \alpha \cdot R(e^c) \cdot S(J_1), \tag{3.19}$$

where e^c denotes compaction ($e^c = -e_{kk}^c$), and $e^c > 0$ means volume decrease. The variable ξ is a time-independent loading parameter, which is increasing as shearing takes place, but remains constant during purely isotropic straining. This variable, representing the accumulating deviatoric strain, is defined by

$$d\xi = \sqrt{\frac{1}{2} d\hat{e}_{ij} \, d\hat{e}_{ij}} , \tag{3.20}$$

where $\hat{e}_{ij}$ is a deviatoric part of the strain tensor,

$$d\hat{e}_{ij} = de_{ij} - \frac{1}{3}\delta_{ij}\, de_{kk}\,. \tag{3.21}$$

The parameter α, entering Eq. (3.19), is a material constant ($0 < \alpha < \sqrt{3}$), and R and S are material functions. These functions have been determined experimentally from an oedometric test. After MORLAND *et al.* [20], the model functions R and S have been assumed in the following forms:

$$\begin{aligned} R(e^c) &= \exp\left\{-\sum_{n=1}^{N} r_n (e^c)^n\right\}, \\ S(J_1) &= 1 + \sum_{n=1}^{N} s_n \left(\sqrt{3J_1}\right)^n, \end{aligned} \tag{3.22}$$

where

$$J_1 = \frac{1}{2}\,\hat{e}_{ij}\,\hat{e}_{ij} \tag{3.23}$$

denotes the second deviatoric strain invariant. The polynomial coefficients r_n and s_n, appearing in Eqs. (3.22), were calculated by correlating the experimental data with the assumed polynomial curves used for the construction of the material functions R and S (for details see MORLAND *et al.*, [20]).

The above constitutive relations can be applied for both monotonic and cyclic loads. However, in the case of cyclic (not necessarily time-harmonic) motions of the subsoil, the analysis can be considerably simplified by applying an approach, denoted as an engineering compaction theory, formulated by SAWICKI [24]. In this approach the behaviour of the compacting sand is averaged over each cycle of loading, and the interest is restricted to the mean trend only, i.e. the local oscillations imposed on this trend are excluded from the analysis. Therefore the constitutive relation governing the sand compaction has the form:

$$\frac{d\Phi}{dN} = D_1 J_2 \exp(-D_2\Phi), \tag{3.24}$$

where Φ is a measure of compaction, defined by

$$\Phi = \frac{1-n}{n}\, e^c, \tag{3.25}$$

and N is a number of cycles (treated as a continuous variable), and J_2 is the second invariant of the deviatoric part of strain amplitudes tensor E_{ij}:

$$J_2 = \frac{1}{2}\,\hat{E}_{ij}\cdot\hat{E}_{ij}\,, \tag{3.26}$$

with

$$\hat{E}_{ij} = E_{ij} - \frac{1}{3}\delta_{ij} E_{kk} . \tag{3.27}$$

The parameters D_1 and D_2 are material constants for a given sand, and can be determined experimentally (cf. SAWICKI [24]).

The constitutive relations (3.19) and (3.24) describe the behaviour of dry sands, or saturated ones in free draining conditions, in which the pore water can easily flow through porous soil skeleton. When, however, the saturated sand is subjected to shearing in either no draining or partially draining conditions, rearrangements in the soil structure are resisted by the pore water and, consequently, pore fluid pressures are generated. The phenomena of compaction in free draining conditions, and pore pressure generation in undrained conditions, can be quantitatively related to each other by the following formula, deduced on the empirical basis by MARTIN *et al.* [15]:

$$\frac{ds}{d\xi} = \frac{1}{\kappa} \frac{de^c}{d\xi} \tag{3.28}$$

for monotonic, and

$$\frac{ds}{dN} = \frac{1}{\kappa} \frac{de^c}{dN} \tag{3.29}$$

for cyclic loads, with s denoting the generated pore pressure and κ being the soil skeleton compressibility.

In the problem considered a free drainage of the pore water across the upper surface of the saturated half-space can occur, resulting in dissipation of the generated pore pressures. A method of dealing with the problem of pore pressure dissipation was briefly described at the beginning of this Chapter. The equation governing this process, assuming incompressibility of pore fluid, is of the following form (VERRUIJT [31]):

$$\frac{\partial s}{\partial t} = \beta \nabla^2 s , \tag{3.30}$$

where the coefficient β is defined by

$$\beta = \frac{k_f}{E \varrho^f \kappa} , \tag{3.31}$$

and ∇^2 denoting the Laplace operator. The filtration equation (3.30) should be solved with the boundary conditions

$$s(x, h_w, t) = 0 \tag{3.32}$$

and

$$\lim_{z\to\infty} \frac{\partial s}{\partial z} = 0, \tag{3.33}$$

where h_w is the depth of ground water table (see Fig. 1). Equation (3.32) means that the pore fluid can freely move through the surface $z = h_w$, while Eq. (3.33) means that no pore fluid motion takes place at the infinite depth z.

Simultaneous solution of the set of three differential equations: (3.19) or (3.24), (3.28) or (3.29) and (3.30) enables the calculation of current values of generated pore pressures s due to the wave-induced loads. The increase of pore pressures leads to redistribution of the total stresses between the soil skeleton and the pore fluid and, due to decrease in the mean effective stress p', to progressive weakening of the soil (cf. Eq. (3.15) and (3.17)). Denoting by p'_0 the initial (static) mean effective pressure, and assuming that at the beginning of dynamic loading $s = 0$, the changes in the mean effective pressures during the dynamic loading process can be described by the relation

$$p' = p'_0 - s. \tag{3.34}$$

When the mean effective stress $p' = 0$, the shear modulus G reaches its minimum, residual value G_0. At this moment the soil resistance to relative motions of the skeleton grains becomes negligibly small and the soil is said to be liquefied (for $G_0 \to 0$ the saturated sand behaves macroscopically like a liquid).

The constitutive relations describing the behaviour of liquefied soil have not been available yet, so we have assumed in this study that since the onset of liquefaction the mechanical properties of the medium do not change (i.e. they are described by residual values of Lamé's constants).

4. Remarks on numerical solution to the problem

The problem has been solved by applying an incremental step-by-step in time method and the finite element method in space variables. The semi-infinite domain has been replaced by a layer of finite depth H (see Fig. 3). A rectangular finite elements grid has been imposed on this layer. The discrete model consists of a system of n sublayers, each of constant elastic properties for a given time step. The thickness b_j of each sublayer can be different, while a horizontal spacing a is assumed to be constant throughout the discrete system.

The plane, harmonic in time, wave propagation problem has been transformed to the one-dimensional in space problem by employing the method formulated by LYSMER [14]. This method is based on the following formulae, relating the displacement amplitudes at the neighbouring nodes, situated at the same depth z:

$$\begin{aligned} U_l(x - a, z) &= U_l(x, z)\exp(ika), \\ U_l(x + a, z) &= U_l(x, z)\exp(-ika), \end{aligned} \tag{4.1}$$

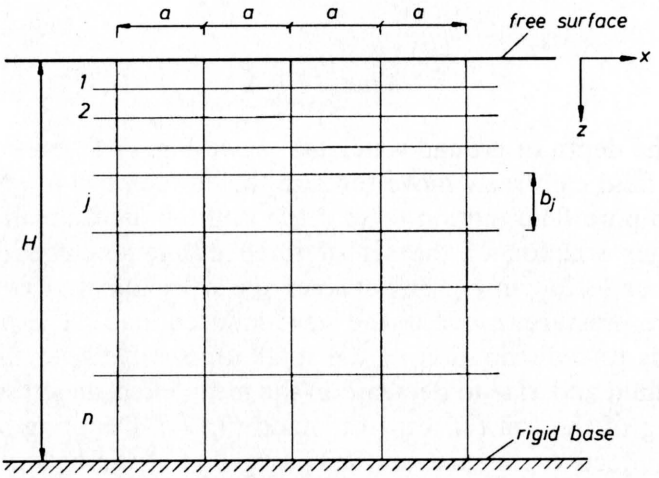

FIG. 3. Discrete model of the problem.

with $l = x, z$, for amplitudes of horizontal and vertical displacements, respectively. By applying Eq. (4.1) we are able to express the displacement amplitudes at any nodal point of the same depth z by means of the amplitude at one chosen node (x_0, z). Hence, the wave pattern in the whole layer is completely described by displacement amplitudes at the nodes situated along the chosen line $x = x_0$. In effect, we deal with the one-dimensional problem, with sublayer stiffness and inertia matrices describing the properties of the discrete system. The elements of these matrices depend on elastic constants G_j and λ_j, mass density ϱ_j, the wavenumber k, and the mesh sizes a and b_j. In order to achieve a better approximation of the continuous medium by the discrete system we assume the horizontal spacing a to be infinitesimally small. That is, we calculate the so-called limit sublayer stiffness and mass matrices. Then, by assembling all the sublayer matrices into global ones, we arrive at the generalised eigenvalue problem, with complex-valued stiffness matrix and real, tri-diagonal inertia matrix. Next, by performing some matrix manipulations, the eigenvalue problem is reduced first – to the one in real variables, and then – to the standard eigenproblem for a real and symmetric matrix. By solving this problem, we obtain a set of eigenvectors, from which we choose the one corresponding to the lowest eigenvalue (the remaining vectors are omitted, because of considering the layer of finite depth instead of the half-space). The fundamental, Rayleigh wave mode, is then normalised with respect to the chosen wave parameter, e.g. free surface displacement or acceleration amplitude, the total wave energy, etc. Having determined the surface wave mode (which describes the displacements within the vertical profile of the soil layer), we are able to determine current strain and stress fields, and, hence, deviatoric invariants J_1 or J_2, appearing in the constitutive relations (3.19) and (3.24). Next, solving simultaneously the differential equations (3.19) or (3.24), (3.28) or

(3.29) and (3.30), we can calculate current values of the generated excess pore pressures s, effective pressures p' and, finally, the modified values of elastic constant: G and λ. The whole procedure is repeated for each step of calculations until the prescribed number of cycles (or the time) are reached.

5. Numerical results

Some numerical computations have been performed for both the time-harmonic and transient surface waves. The material parameters, describing the sand compaction, were determined experimentally by SAWICKI and ŚWIDZIŃSKI [25] – for the case of cyclic, and MORLAND *et al.* [20] – for the case of monotonic loading. The parameters for different sands have been used in the two cases considered. The surface waves parameters, used in the computations, have been chosen on the basis of data published in STUDER and KOK [28]. In both cases the ground water table was assumed to lie 2 m below the free surface of the subsoil. The thickness of the soil layer in the FEM model is $H = 200$ m. The model consists of 40 discrete sublayers, the upper 20 ones of thickness 2 m each.

5.1. Waves harmonic in time

The calculations have been carried out for material parameters corresponding to the medium dense Ottawa sand: $G_0 = 10$ MPa, $G_1 = 70$ MPa, Poisson's ratio $\nu = 0.25$, earth pressure coefficient $K_0 = 0.5$ (needed to calculate the pressure due to the own weight of the soil), the intrinsic sand density ${}^E\varrho^s = 2650\,\text{kg/m}^3$, initial porosity $n = 0.4$, the compaction parameters $D_1 = 1740$ and $D_2 = 115$. It has been assumed that the motion of the subsoil is induced by the Rayleigh wave of angular frequency $\omega = 12.57\,\text{s}^{-1}$ (wave period $T = 0.5$ s), and the initial horizontal acceleration amplitude at the free surface equal to 0.1 g ($0.91\,\text{m/s}^2$).

Figure 4 displays the time history of pore pressure generation within the upper 50 m (filtration coefficient $k_f = 10^{-9}$ m/s). One can see that the excess pore pressures are generated most rapidly in the two regions: near the free surface of the sand deposit and at the depth of about 30 m. Consequently, two liquefaction zones develop (see also Fig. 5). The first one appears at the instant $N = 10.6$ ($t = 5.3$ s) under the ground water table, where the soil is the weakest (the latter because of small values of static effective pressures, which considerably influence both Lamé's constants). The second zone of liquefied soil appears at $N = 27.6$ ($t = 13.8$ s), at the depth of about 24 m, where the magnitudes of generated pressures are much greater (in this region the shear stress amplitudes produced by the Rayleigh wave reach maximum values). The second liquefaction zone spreads out very quickly, and after the time of 1.7 s the two regions of liquefied soil merge. From that moment ($t > 31$ s), the process of pore pressure generation develops at much smaller rate and affects the relatively small domain that lies directly under the zone of the already liquefied soil.

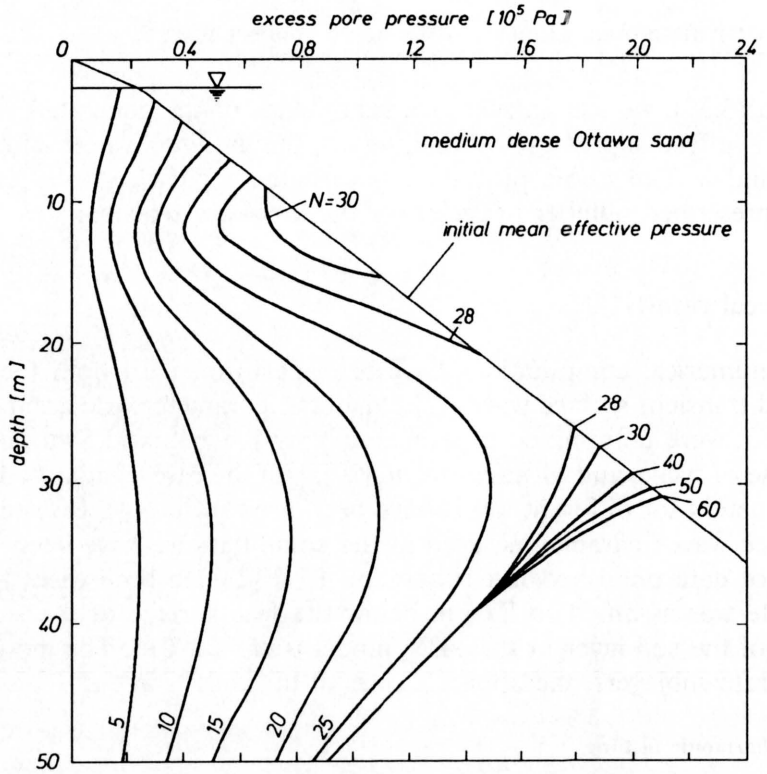

FIG. 4. Pore pressure generation history for surface waves harmonic in time.

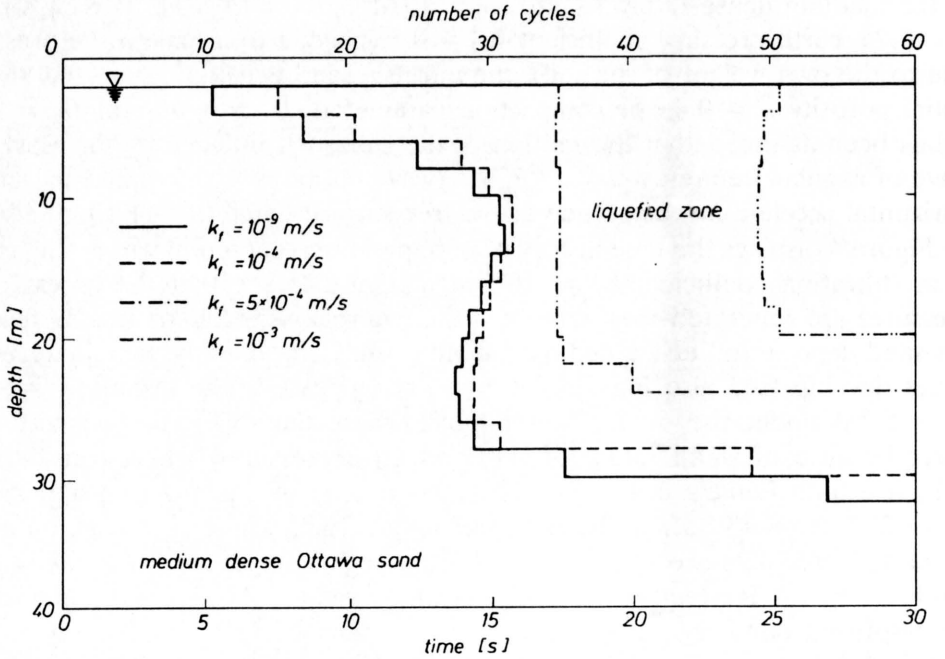

FIG. 5. Influence of the filtration coefficient k_f on development of liquefaction due to surface waves harmonic in time.

Figure 5 illustrates the influence of soil permeability on the rate and range of the liquefaction process. It is seen that the liquefaction due to seismic loads can develop not only in soils characterised by low permeability, but also in sands considered as highly permeable. For the numerical data applied, the phenomenon of liquefaction develops even for the filtration coefficient as high as $k_f = 10^{-3}$ m/s. Only very permeable sands ($k_f \gtrsim 5 \times 10^{-3}$ m/s), are not susceptible to liquefaction (the phenomena of pore pressure generation and dissipation balance each other). On the other hand, it follows from Fig. 5 that all sands characterised by the filtration coefficient $k_f \lesssim 10^{-4}$ m/s behave similarly and can be regarded (at least when considering seismic loads) as practically impermeable.

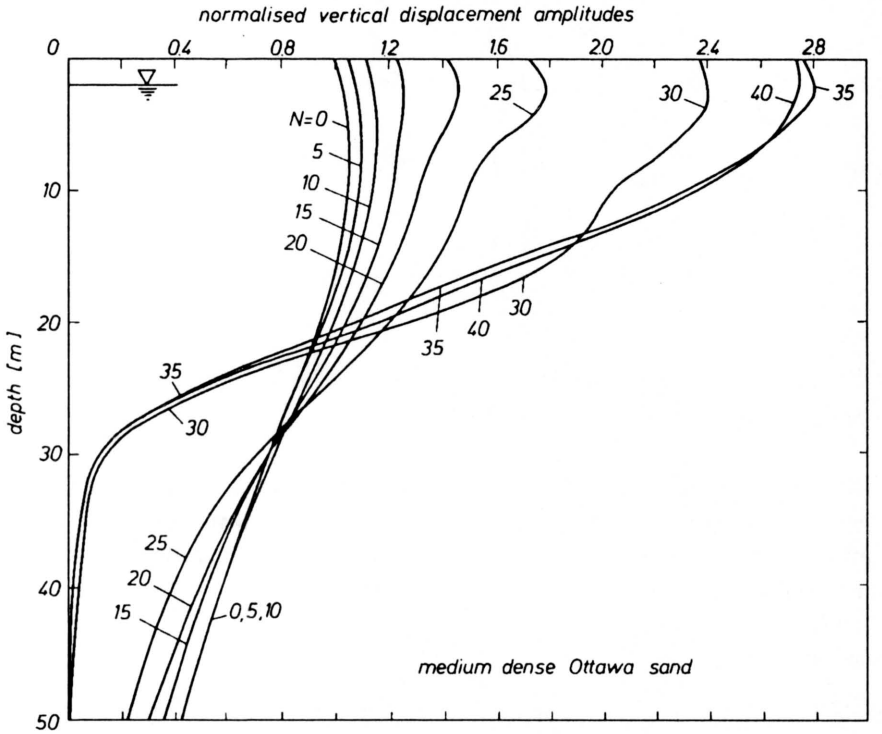

FIG. 6. Changes in vertical displacement amplitudes with increasing number of cycles N of surface waves.

The variations in displacement field in the subsoil as a function of the number of cycles N are shown in Figs. 6 and 7. For the sake of convenience, the vertical and horizontal amplitudes plotted in these figures are normalised with respect to the initial free surface vertical displacement amplitude. The most considerable changes in displacement field occur in the period preceding the onset of the second (deeper) zone of liquefaction. The formation of the first, near-free surface liquefaction zone, affects the wave pattern in a relatively small degree. Only the weakening (due to increasing pore pressures) of deeper layers of the

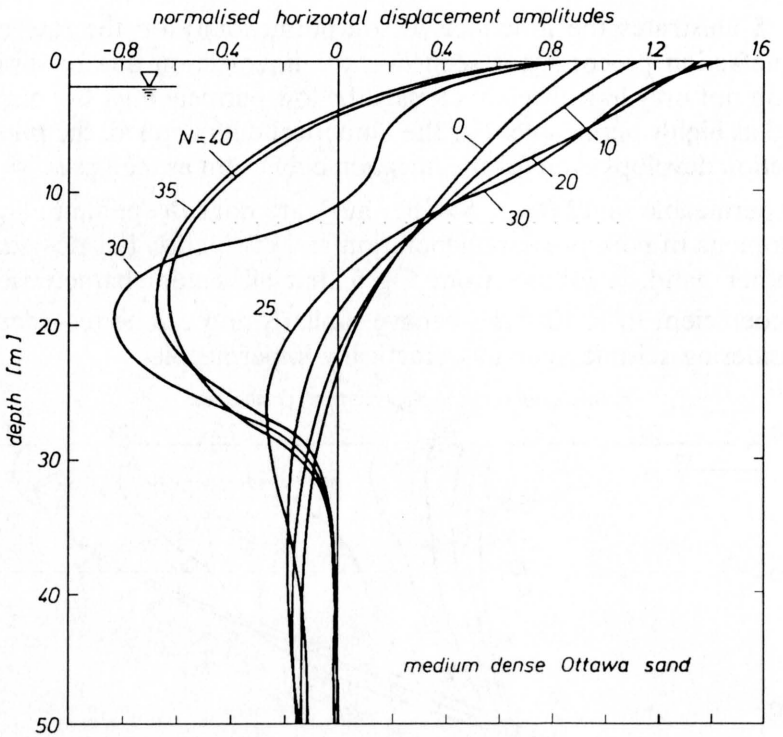

FIG. 7. Changes in horizontal displacement amplitudes with increasing number of cycles N of surface waves.

subsoil leads to significant increase in displacement amplitudes. For instance, at the free surface, the maximum vertical displacement amplitudes are almost 2.8 times greater than the initial ones; as concerns horizontal motions, the increase in amplitudes is less dramatic – it does not exceed the value of 1.6.

5.2. Transient wave

The following parameters, corresponding to the loose Leighton Buzzard sand, have been used in computations: $G_0 = 8.25\,\text{MPa}$, $G_1 = 50\,\text{MPa}$, Poisson's ratio $\nu = 0.25$, the initial porosity $n = 0.40$, the skeleton intrinsic mass density ${}^E\varrho^s = 2650\,\text{kg/m}^3$, the filtration coefficient $k_f = 10^{-4}\,\text{m/s}$. The material functions, describing the compaction of sand, have been assumed after MORLAND *et al.* [20]. It has been assumed that the motions of the subsoil have been induced by the surface wave which produces, at a chosen point of the free surface, the horizontal stress distribution of a triangular shape in temporal domain (cf. Fig. 8). The total duration od excitement is $T_0 = 0.1\,\text{s}$, with the maximum value of the stress $\sigma_{xx}^{\max} = 10^5\,\text{Pa}$ reached at the instant $t_0 = 0.02\,\text{s}$.

Figure 8 illustrates the development of liquefaction zone (dotted area) during the passage of the surface wave ($t \leq 0.1\,\text{s}$), and subsequent resolidification of

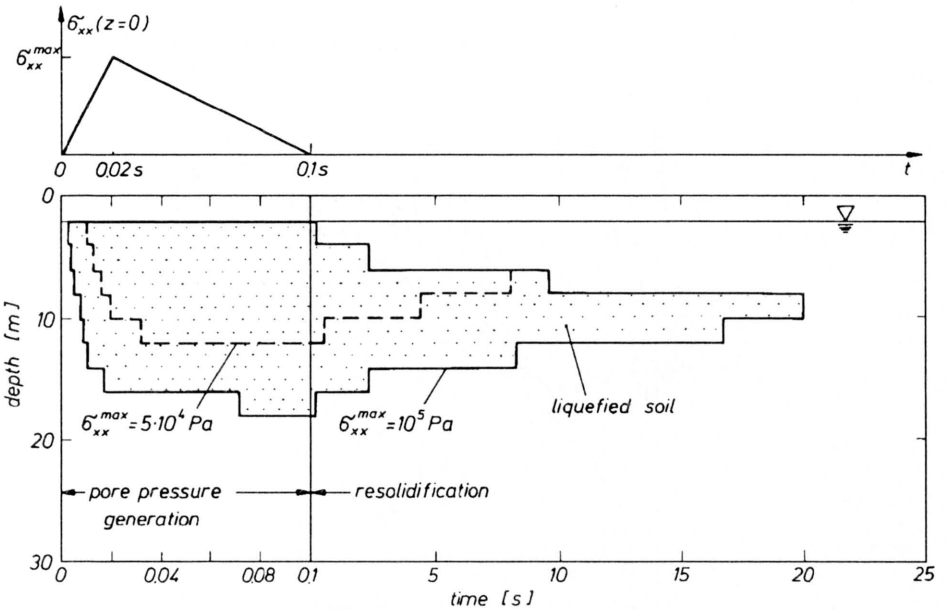

FIG. 8. Development of liquefaction ($t \leq 0.1$ s) and resolidification ($t > 0.1$ s) in saturated sand deposit due to transient surface wave.

the soil deposit after the passage of the wave ($t > 0.1$ s). It is seen that the liquefaction zone spreads out monotonically from the near-ground water table region towards deeper layers of the subsoil. The process of liquefaction develops almost entirely during the first loading phase ($t < 0.02$ s). During the unloading phase the liquefaction zone increases its range as well. For comparison, in the same figure the range of liquefaction for smaller maximum stress level ($\sigma_{xx}^{\max} = 5 \times 10^4$ Pa) is depicted with a dashed line. After the passage of the wave the phenomenon of pore pressure generation stops, and the process of dissipation of pore pressures starts. Consequently the soil begins to resolidificate. For the value of $k_f = 10^{-4}$ m/s this process takes only about 20 s due to a high sand permeability; but for less permeable soils this period can be measured in days or weeks.

Finally, Fig. 9 shows the histories of pore pressure generation (a) and dissipation (b). As it follows from the plots, the most rapid increase in the generated pore pressures occurs in the loading phase ($t \leq 20$ ms), while during the unloading the rate of excess pore pressure increase falls down significantly. In Fig. 9b the changes in pore pressures distribution due to their dissipation are displayed for 0.1 s $\leq t \leq$ 1000 s. One can notice that during the first period the excess pore pressures decrease only in the upper part of the layer, while in its lower part (directly under the liquefied zone) an increase is observed. Only after some period of time ($t \gtrsim 500$ s), a uniform decrease in pore pressures throughout the whole sand deposit takes place.

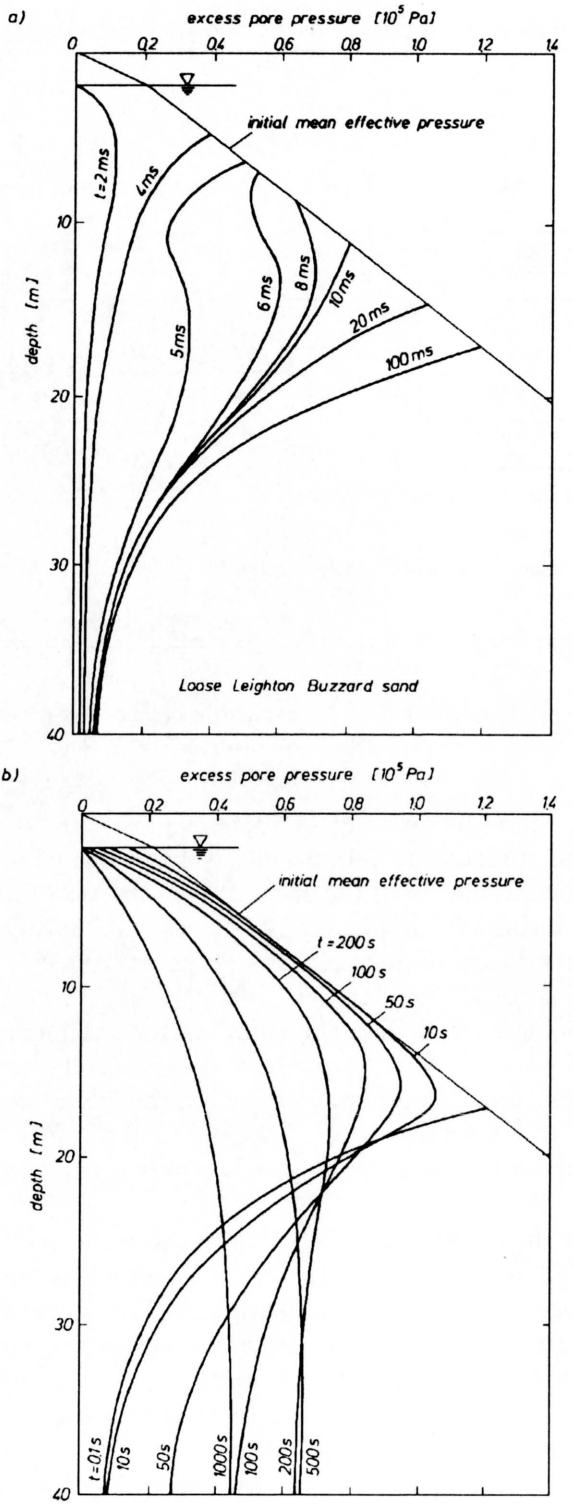

FIG. 9. a) Pore pressure generation during the passage of surface wave ($t \leq 0.1$ s); b) Pore pressure dissipation after the passage of surface wave ($t > 0.1$ s).

6. Conclusions

An original method of dealing with the problem of surface waves propagation over a half-space, in which such phenomena as pore pressure generation and liquefaction occur, is presented in this paper. The method is based on the constitutive theory of saturated granular materials that takes into account the above mentioned phenomena, and a numerical algorithm based on the Finite Element Method. Numerical computations, performed for real data, show that the surface waves propagating over a saturated subsoil may lead to the pore pressure generation and the subsequent ground's liquefaction indeed, as it has been observed in practice.

Mechanisms of development of liquefaction zones in the subsoil are illustrated by numerical examples, as well as some detailed conclusions are drawn. The main conclusion which follows from the present paper is that the method proposed can serve as a theoretical tool in the analysis of pore pressure generation and subsequent liquefaction of a subsoil subjected to the passage of surface waves. Further work, both theoretical and experimental, is necessary in order to develop more precise methods of dealing with the problems analysed in this paper.

References

1. J.D. ACHENBACH, *Wave propagation in elastic solids*, North-Holland, Amsterdam 1973.
2. K.-J. BATHE, *Finite element procedures in engineering analysis*, Prentice Hall, Englewood Cliffs, New Jersey 1982.
3. E. BODEWIG, *Matrix calculus*, North-Holland, Amsterdam 1959.
4. R.M. BOWEN, *Compressible porous media models by use of the theory of mixtures*, Int. J. Engng. Sci., **20**, 6, 697–735, 1982.
5. B.M. DAS, *Fundamentals of soil dynamics*, Elsevier, New York – Amsterdam – Oxford 1983.
6. W.M. EWING, W.S. JARDETZKY and F. PRESS, *Elastic waves in layered media*, McGraw–Hill, New York 1957.
7. W.D.L. FINN, *Dynamic response analyses of saturated sands*, [in:] Soil Mechanics – Transient and Cyclic Loads, PANDE and ZIENKIEWICZ [Eds.], John Wiley and Sons, 105, 1982.
8. R.J. FRAGASZY and M.E. VOSS, *Laboratory modelling of blast-induced liquefaction*, Proc. Soil Dynamics and Earthquake Engng. Conf., Southampton, pp. 873–886, 1982.
9. S. FRYDMAN and M. TALESNICK, *Analysis of seismically triggered slides of Israel*, Environ. Geol. Water Sci, **11**, 1, pp. 21–26, 1988.
10. G. GAZETAS and M.K. YEGIAN, *Shear and Rayleigh waves in soil dynamics*, ASCE J. Geotech. Engng. Div., **105**(GT12), pp. 1455–1470, 1979.
11. R.D. HARDIN and V.P. DRNEVICH, *Shear modulus and damping in soils: measurement and parameter effects*, ASCE J. Soil Mech. Found. Div., **98**(SM6), pp. 603–624, 1972.
12. K. ISHIHARA and I. TOWHATA, *Dynamic response analysis of level ground based on the effective stress method*, [in:] Soil Mechanics – Transient and Cyclic Loads, PANDE and ZIENKIEWICZ [Eds.], John Wiley and Sons, 133, 1982.
13. O. KUMMENEJE and O. EIDE, *Investigation of loose sand deposits by blasting*, Proc. 5th Int. Conf. on Soil Mech. Found. Eng., Paris, Vol. 1, paper No. 45, pp. 1–7, 1961.
14. J. LYSMER, *Lumped mass method for Rayleigh waves*, Bull. Seism. Soc. Am., **60**, 1, 89–104, 1970.
15. G.R. MARTIN, W.D.L. FINN and H.B. SEED, *Fundamentals of liquefaction under cyclic loadings*, ASCE J. Geotech. Engng. Div., **101**(GT5), 423–428, 1975.

16. P.P. MARTIN and H.B. SEED, *One-dimensional dynamic ground response analyses*, ASCE J. Geot. Engng. Div., **108**(GT7), 935, 1982.
17. L.W. MORLAND, *Compaction and shear settlement of granular materials*, J. Mech. Physics Solids, **41**, 507–530, 1993.
18. L.W. MORLAND and A. SAWICKI, *A mixture model for the compaction of saturated sand*, Mech. Mat., **2**, 217–231, 1983.
19. L.W. MORLAND and A. SAWICKI, *A model for compaction and shear hysteresis in saturated granular materials*, J. Mech. Physics Solids, **33**, 1, 1–24, 1985.
20. L.W. MORLAND, A. SAWICKI and P.C. MILNE, *Uni-axial compaction of a granular material*, J. Mech. Physics Solids, **41**, 11, 1755–1779, 1993.
21. V.R. RAJU and G. GUDEHUS, *Compaction of loose sand deposits using blasting*, Proc. 13th ICSMFE, New Delhi, pp. 1145–1150, 1994.
22. C.G. RAWLINGS, *Blast induced liquefaction of soils – A reference search*, NGI Reports 52209-1, March, Oslo 1987.
23. A. SAWICKI and L.W. MORLAND, *Pore pressure generation in a saturated sand layer subjected to a cyclic horizontal acceleration at its base*, J. Mech. Physics Solids, **33**, 6, 545–559, 1985.
24. A. SAWICKI, *An engineering model for compaction of sand under cyclic loading*, Engng. Trans., **35**, 4, 677–693, 1987.
25. A. SAWICKI and W. ŚWIDZIŃSKI, *Compaction curve as one of basic characteristics of granular soils*, Proc. French-Polish Seminar on Soil Mechanics, Grenoble, 103–115, 1987.
26. A. SAWICKI and W. ŚWIDZIŃSKI, *Pore pressure generation, dissipation and resolidifaction in a saturated soil*, Soils and Foundations, **29**, 4, 1–18, 1989.
27. M.L. SILVER and H.B. SEED, *Deformation characteristics of sand under cyclic loading*, ASCE J. Soil Mech. Found. Div., **97**(SM9), 1171–1182, 1971.
28. J. STUDER and L. KOK, *Blast-induced excess porewater pressure and liquefaction. Experience and application*, Proc. Int. Symp. on Soils under Cyclic and Transient Loading, Swansea, A.A.Balkema, 581–593, 1980.
29. J. SYVITSKI and C. SCHAFER, *ADFEX – Environmental Impact Statement*, Geological Survey of Canada, Dartmouth 1990.
30. G.E. VEYERA and W.A. CHARLIE, *Liquefaction of shock-loaded saturated sand*, [in:] Soil Dynamics and Liquefaction, A.S. CAKMAK [Ed.], Elsevier/Computational Mechanics Publications, 205–219, 1987.
31. A. VERRUIJT, *Elastic storage of aquifers*, [in:] Flow Through Porous Media, R.J.M. DE WIEST [Ed.], Academic Press, New York 1969.
32. O.C. ZIENKIEWICZ, C.T. CHANG and T. HINTON, *Nonlinear seismic response and liquefaction*, Int. J. Num. Anal. Methods in Geomechanics, **2**, 381–404, 1978.

POLISH ACADEMY OF SCIENCES
INSTITUTE OF HYDROENGINEERING, GDAŃSK.

Received October 28, 1994.

Arch. Mech., 47, 3, pp. 577–599, Warszawa 1995

Shear band localization in saturated porous media (*)

B. A. SCHREFLER, C. E. MAJORANA
and L. SANAVIA (PADOVA)

A COMPUTATIONAL ANALYSIS of dynamic strain localization in multiphase solids is presented in this paper. The governing equations are obtained by means of averaging theories based on spatial averaging operators. Continuum wave propagation is used for the study of localization. The directions of localization are obtained by means of an eigenvalue analysis of the acoustic tensor. The investigation of the development of localized bands is carried out by means of a finite element code. The influence on localization of coupling between the constituents is studied. Several examples are shown.

Notation

s	solid phase,
f	fluid phase,
g	gaseous phase,
l	liquid phase,
$\mathbf{a}$	solid acceleration,
$\mathbf{a}^f$	fluid acceleration,
$\mathbf{b}$	body force vector,
$\mathbf{B}$	acoustic tensor,
c	acceleration wave speed,
C_s	specific moisture content,
$\mathbf{C}_T$	tangential constitutive tensor,
$\mathbf{D}$	Eulerian strain rate tensor,
d/dt	material time derivative with respect to the moving solid,
e	void ratio,
$f_{,i}$	$\partial f/\partial x_i$,
$f_{/i}$	$\partial f/\partial X_i$,
$\overline{g}$	gravity acceleration,
$\mathbf{E}$	deformation tensor,
$\mathbf{F}$	deformation gradient tensor,
$\mathbf{G}$	dynamic seepage matrix,
$\mathbf{H}$	permeability matrix,
$\mathbf{I}$	identity matrix 3×3,
K_s	solid grain bulk modulus,
K_T	overall skeleton bulk modulus,
K_l	fluid phase bulk modulus,
k_{rl}	liquid phase relative permeability,
$\mathbf{k}_{\alpha l}$	absolute permeability tensor,
$\mathbf{k}_l = \mathbf{k}_{\alpha l} k_{rl} \frac{\varrho_l \overline{g}}{\mu}$	permeability tensor,
$\mathbf{K}_T$	tangential stiffness tensor,

(*) Paper presented at 30th Polish Solid Mechanics Conference, Zakopane, September 5–9, 1994.

$\mathbf{K}_\sigma$ initial stress tensor,
$\mathbf{L}$ velocity gradient tensor,
$\mathbf{M}$ mass matrix,
$\mathbf{m}$ $[1\ 1\ 1\ 0\ 0\ 0]^T$,
p_g gas pressure,
p_l water pressure,
$\mathbf{P}$ equivalent force vector,
$\mathbf{Q}$ coupled matrix,
$\mathbf{q}$ average relative water velocity,
q average relative gas velocity,
$\mathbf{R}$ rotation tensor,
$\mathbf{S}$ compressibility matrix,
S water saturation,
$(1 - S) = S_g$ gas saturation,
t time variable,
$\mathbf{t}$ surface traction tensor,
$\mathbf{u}$ solid displacements,
$\mathbf{U}$ right stretch tensor,
$\mathbf{v}$ solid velocity,
$\mathbf{v}^f$ fluid velocity,
$\mathbf{v}^r$ relative velocity,
$\mathbf{V}$ left stretch tensor,
$\mathbf{W}$ spin tensor,
α Biot's coefficient,
β_1, β_2, Θ Newmark's parameters,
ε linear elastic strain tensor,
$\boldsymbol{\Theta}$ material rotation rate tensor,
η^i normal jump of the spatial velocity gradient,
μ liquid dynamic viscosity,
ϱ porous medium density,
ϱ_s solid grain density,
ϱ_l water density,
ϱ_g gas density,
σ Cauchy stress tensor,
$^J\dot{\sigma}$ Jaumann stress rate tensor,
σ'' effective stress tensor,
ϕ porosity.

Variable with overbar refers to the nodal values.

1. Introduction

GEOMATERIALS EXHIBIT, both in laboratory experiments and in field situations strain accumulations in well defined narrow zones. In such shear bands, material behaviour is inelastic, while the remaining zones are elastic, with infinitesimal strains. The triggering mechanisms for the formation of shear bands are inhomogeneities in the material and stress concentrations. Typical examples can be found in brittle geomaterials such as concrete and rocks, where progressive damage produces strain softening, or in soil as for instance in case of slope instability

or foundation failure. When the frictional properties of the material are more critical than the cohesive properties, we have Mode II (shear banding) dominated processes which may be simulated by plasticity models.

The analysis of strain localization is of importance in engineering practice because localization is a precursor to failure. In this work we present the theoretical framework of localization in geomaterials and the results of the first developments of computational investigations. Geomaterials are considered as multiphase materials in fully saturated conditions. The final aim however is to develop a model applicable both to fully saturated and partially saturated conditions.

It will be shown that the role of the fluid in localization is fundamental, since shear band formation preceding failure is affected by the interaction between solids and fluids, in terms of time sequence of band formation and the way of shear band development.

The topic of strain localization has been analysed in recent years by many authors, in particular in connection with single-phase solids [14]. The problem of dynamic localization in single phase solids has been investigated, e.g., by SLUYS [19]. Strain localization in multi-phase materials received less attention. Quasi-static cases were studied by RICE [16] and RUDNICKI [17] and dynamic cases by VARDOULAKIS [22]. A finite element analysis of dynamic strain localization of saturated porous media was first presented by LORET and PREVOST [10].

In the present paper we also use the dynamics of wave propagation [2] to investigate localization. Loret et Prevost applied a uniform axial compressive velocity jump along the top and bottom of a specimen, while Sluys used compressive impact loading. In both cases high frequency situations are studied where localization is initiated when the elastic loading wave hits the symmetry line (or immediately after). Here we show that dynamic localization may also be initiated by ramp loading which is more common in practical engineering situations. Localization starts here well after the first wave front hits the symmetry line but, as in the above cases, no weak element is needed to trigger off the formation of a shear band. This means that at least in fluid saturated media, propagating waves are not negligible even if a relatively small number of low frequencies govern the response.

The acoustic tensor is used as a search algorithm to determine the inclination angle of the shear band and as a check of the obtained numerical solution. This information may be used for mesh alignment. Coupling phenomena between solid skeleton and pore fluid are investigated in detail and the influence of permeability in fully saturated situations is pointed out. Pore pressure localization is also shown.

Since we aim to extend the model to partially saturated conditions, we treat the porous medium as a three-phase continuum, with the pores filled by water and air.

The fully saturated case, dealt with here, is only a subcase of the more general model. This model is explained next, following [12].

2. Mechanics of porous materials

2.1. Mathematical framework

2.1.1. Kinematics. The kinematics needed in the following is briefly recalled first.

Strain behaviour is locally defined by the deformation gradient tensor **F** [11, 12]. The polar decomposition theorem allows to express pure straining by the right stretch tensor **U** or the left stretch tensor **V**, while the rigid body rotation is described by the skew-symmetric tensor **R**:

$$F_{ij} = x_{i,j} = R_{ik} U_{kj} = V_{ik} R_{kj} . \tag{2.1}$$

The deformation process is described by the velocity gradient tensor **L**, which, referred to spatial coordinates, is given by

$$L_{ij} = v_{i,j} = \left(\dot{R}_{im} U_{mk} + R_{im} \dot{U}_{mk} \right) (R_{mk} U_{mj})^{-1}. \tag{2.2}$$

Its symmetric part is the Eulerian strain rate tensor **D**, related to pure straining component according to:

$$D_{ij} = \frac{1}{2}(L_{ij} + L_{ji}) = \frac{1}{2} R_{ik} \left[\dot{U}_{kn} (U_{nm})^{-1} + (U_{kn})^{-1} \dot{U}_{nm} \right] R_{jm} , \tag{2.3}$$

while its skew-symmetric component is the spin tensor **W**. This is commonly associated with the material rotation rate tensor $\Theta = \dot{\mathbf{R}} \mathbf{R}^T$ [13] (giving the angular velocity of the material [4]), even if it differs from it according to the following expression:

$$W_{ij} = \frac{1}{2}(L_{ij} - L_{ji}) = \dot{R}_{ik} R_{jk} + \frac{1}{2} R_{ik} \left[\dot{U}_{kn} (U_{nm})^{-1} - (U_{kn})^{-1} \dot{U}_{nm} \right] R_{jm} . \tag{2.4}$$

The approach adopted here to study the overall behaviour of multiphase media is an updated Lagrangian formulation, where the reference configuration is the last converged step. This description is properly Lagrangian only for the solid phase, while it is Eulerian in nature for the fluids: their relative flows are of importance here, hence their motion is referred to the actual configuration assumed by the solid skeleton.

The velocity and acceleration of each fluid particle can then be written with reference to the ones of the corresponding solid points, once the relative velocity, $\mathbf{v}^r$, is introduced. Assuming that kinematics variables not explicitly marked refer to the solid phase motion, we can write:

$$v_i^f = v_i + v_i^r , \qquad a_i^f = a_i + \frac{dv_i^r}{dt} + v_j^r (v_i + v_i^r)_{/j} , \tag{2.5}$$

where d/dt is the material time derivative with respect to the moving solid.

An average relative fluid velocity is obtained through averaging technique over a representative volume element dV. This velocity component is indicated by q_i for the liquid phase [18]:

$$v_i^{ls} = q_i = \frac{dV_f}{dV}\frac{dV_i}{dV_f}\langle v_i{}^r\rangle_l^l = \phi S\,\langle v_i{}^r\rangle_l^l \tag{2.6}$$

and by q_i for the gaseous phase.

$$v_i^{gs} = \mathrm{q}_i = \frac{dV_f}{dV}\frac{dV_g}{dV_f}\langle v_i^r\rangle_g^g = \phi(1-S)\langle v_i^r\rangle_g^g\,. \tag{2.7}$$

The averaging symbol $\langle\ \rangle$ is omitted in the following.

2.1.2. Balance equations. The macroscopic balance equations of mass and momentum are also obtained by means of systematic application of averaging procedures [7–9, 18] to the relevant balance equations of the constituents at microscopic level. The ensuing macroscopic balance equations coincide under appropriate assumptions with those of the classical mixture theories, integrated by the concept of volume fractions [6].

In the following, deviatoric stress components are not considered in fluids and compressive pore pressure is defined as positive. At the macroscopic level, the effects due to deviatoric stress components are accounted for through Darcy's law, by viscous drag forces exerted on the solid phase. Isothermal conditions and no phase changes are assumed and the phases are immiscible and chemically non-reacting.

The linear momentum balance equation for the whole mixture may be locally written in its Eulerian form [12] as:

$$\begin{aligned}\varrho b_i + \sigma_{ij/j} - \varrho a_i - \phi\varrho_f(a_i{}^f - a_i)\\ = \varrho b_i + \sigma_{ji/j} - \varrho a_i - \varrho_f\left[\phi\frac{dv_i{}^r}{dt} + q_j{}^f\left(v_{i/j} + v_{i/j}^r\right)\right] = 0.\end{aligned} \tag{2.8}$$

When this local condition is written for one phase alone, a specific term must be introduced to take into account the mechanical interactions occurring at the real interfaces with the other phases. These surfaces differ, in fact, from the boundary of the representative volume element over which the quantities are averaged. The external momentum supply represents the dissipative part of fluid-solid exchange,

$$\mathcal{S}_i^{s\leftrightarrow f} = \phi\varrho_f a_i^f - \phi p_{f/i} - \phi\varrho_f b_i\,. \tag{2.9}$$

The mass conservation equation is introduced in its local form for the mixture water plus solid:

$$v_{i/i} + \frac{(1-\phi)}{\varrho_s}\frac{d\varrho_s}{dt} + \frac{\phi}{\varrho_l}\frac{d\varrho_l}{dt} + \frac{\phi}{S}\frac{dS}{dt} + \frac{q_{i/i}}{S} + \frac{q_i}{S\,\varrho_l}(\varrho_l)_{/i} = 0, \tag{2.10}$$

and for the mixture gas plus solid:

$$v_{i/i} + \frac{(1-\phi)}{\varrho_s}\frac{d\varrho_s}{dt} + \frac{\phi}{\varrho_g}\frac{d\varrho_g}{dt} + \frac{\phi}{(1-S)}\frac{d(1-S)}{dt} + \frac{\mathrm{q}_{i/i}}{(1-S)} + \frac{\mathrm{q}_i}{(1-S)\varrho_g}(\varrho_g)_{/i} = 0. \tag{2.11}$$

According to the updated Lagrangian formulation applied, the convective components of acceleration must be considered only for the relative velocity of the fluids. Effective stress with the correction for multiphase flow, where saturations are used as weights, and with the further correction [24] for the deformability of the grains (with $\alpha = 1 - K_T/K_S$), is now introduced in the linear momentum balance equation. The equilibrium condition for the whole mixture can be written in its weak form as virtual velocity equation:

$$\int_V \left[\sigma''_{ij} - \alpha\delta_{ij}(Sp_l + (1-S)p_g)\right] D_{ij}dV - \int_A f_i v_i\, dA - \int_V \varrho b_i v_i\, dV - \int_V \varrho\frac{dv_i}{dt}v_i\, dV + \int_V \phi\left[\varrho_l S\frac{d}{dt}\left(\frac{q_i}{\phi S}\right) + \varrho_g(1-S)\frac{d}{dt}\left(\frac{\mathrm{q}_i}{\phi(1-S)}\right)\right] v_i\, dV + \int_V \phi\left[\varrho_l q_j\left(\frac{q_i}{\phi S}\right)_{/j} + \varrho_g \mathrm{q}_j\left(\frac{\mathrm{q}_i}{\phi(1-S)}\right)_{/j}\right] v_i\, dV = 0. \tag{2.12}$$

The weak form of the continuity equations is obtained by integrating over the porous media volume the local conditions weighted with functions δp_α, which have continuity up to their first derivatives and satisfy the boundary conditions. The equation for water plus solid becomes [12]:

$$\int_V \delta p_l \left\{\alpha S v_{i,i} + C_{ll}\dot{p}_l + C_{lg}\dot{p}_g + \left[\frac{C_{lg}}{(1-S)}(p_l - p_g) + \phi\right]\dot{S}\right\} dV + \int_V \delta p_l q_i \frac{(\varrho_l)_{/i}}{\varrho_l} dV + \int_V (\delta p_l)_{/i} q_i\, dV + \int_A \delta p_l q_i n_i\, dA = 0 \tag{2.13}$$

and for the mixture gas plus solid:

$$\int_V \delta p_g \left\{\alpha(1-S)v_{i,i} + C_{gg}\dot{p}_g + C_{lg}\dot{p}_g - \left[\frac{C_{lg}}{S}(p_g - p_l) + \phi\right]\dot{S}\right\} dV + \int_V \delta p_g \mathrm{q}_i \frac{(\varrho_g)_{/i}}{\varrho_g} dV + \int_V (\delta p_g)_{/i}\mathrm{q}_i\, dV + \int_A \delta p_g \mathrm{q}_i n_i\, dA = 0 \tag{2.14}$$

(see Appendix for the coefficients C_{gg}, C_{lg} and C_{ll}).

2.1.3. Constitutive relationships. A hypoelastic constitutive relationship is here adopted. When dealing with large deformation effects, involving also large rotations, care must be taken in the material frame invariance of the law itself. This can be obtained by expressing the constitutive law as a function of objective fields, which here are chosen as the objective Eulerian strain rate **D** (Eq. (2.3)) and the associated objective stress rate measure defined by Jaumann [12], which is related to the Cauchy stress rate by the non-objective spin tensor, **W** (Eq. (2.4) through:

$$(2.15) \qquad {}^{J}\dot{\sigma}_{ij} = \dot{\sigma}_{ij} - \sigma_{ik}W_{jk} - \sigma_{mj}W_{im} = \dot{\sigma}_{ij} - {}^{R}\dot{\sigma}_{ij}$$

$$\text{with} \quad {}^{R}\sigma_{ij} = \dot{\sigma}_{ik}W_{jk} + \sigma_{jk}W_{ik}\,.$$

The constitutive law taking into account the modified effective stress principle mentioned above can thus be written in incremental form as:

$$(2.16) \qquad \dot{\sigma}_{ij} = C_{ijkl}D_{kl} - \alpha\delta_{ij}\left(S\,\dot{p}_l + (1-S)\,\dot{p}_g\right) + {}^{R}\dot{\sigma}_{ij}\,.$$

The Jaumann stress rate tensor can be properly used as a co-rotational measure associated with **D** in an updated Lagrangian approach with the strain increments kept small enough in each step of the analysis. In this hypothesis not only **D** gives a suitable description of the strain rate, but also **W** is an accurate approximation of the local angular velocity. This approach can also be used for elasto-plastic analyses, and leads to a good approximation in the hypothesis of small elastic components of deformation [12].

As far as the fluid phases are concerned, the constitutive equation governing the momentum exchange among different phases can be expressed as a function of average relative velocity, $\mathbf{q}^f$, once its frame invariance is proved. The latter variable depends on volume fractions, which are objective being scalar, and on the relative velocity, $\mathbf{v}^r$, which is also frame indifferent [12].

A thermodynamically consistent constitutive equation is then introduced for the dissipative part of fluid-solid exchange of momentum, which is related to fluid relative average velocity through the resistivity tensor $\Re^f$

$$(2.17) \qquad \mathcal{S}^{s\leftrightarrow f} = \phi\Re^f_{ij}q_j\,.$$

This relationship leads in fully saturated conditions to the generalised Darcy's law, which can be written in the following form:

$$(2.18) \qquad q_i = (k_{\alpha l})_{ij}\left[-(p_l)_{/j} + \varrho_l(b_j - a_j)\right].$$

For partially saturated conditions, the absolute permeability tensor $\mathbf{k}_{\alpha l}$ must be multiplied by the relative permeability k_{rl}, given as function of p_l [18]. A similar relationship has to be written for the gas phase.

The symmetric tensor $\mathbf{k}_{\alpha l}$, when the permeability is distributed in an anisotropic way, is updated according to $\mathbf{k}'_{\alpha l} = \mathbf{R}^T \mathbf{k}_{\alpha l} \mathbf{R}$.

In finite deformations this permeability tensor should be further updated if it is assumed to be a function of void ratio e, defined as the ratio between the void volume over the solid one. Being e_o in the initial configuration,

$$e_o = \frac{dV_o^l}{dV_o^s} = \frac{dV_o - dV_o^s}{dV_o^s} = \frac{\phi_o}{1 - \phi_o} \tag{2.19}$$

we have in the actual configuration

$$e = \frac{\phi}{1 - \phi} = \frac{dV}{dV_s} - 1 = \frac{dV}{dV_o} \frac{dV_o}{dV_o^s} \frac{dV_o^s}{dV^s} - 1 = J(1 - e_o) J_s^{-1} . \tag{2.20}$$

Using an updated Lagrangian approach with time step increments small enough to have in each of them only a negligible contribution from the second order strain component, volume strain is satisfactorily approximated by the trace of the linear strain tensor. The current void ratio can then be evaluated by neglecting the specific contribution of proper grain deformation to the overall volume strain, which leads to

$$e = (1 + e_o)(1 + \operatorname{tr}\varepsilon) - 1 = e_o + (1 + e_o)\operatorname{tr}\varepsilon. \tag{2.21}$$

2.1.4. Simplified governing equations. The numerical formulation actually implemented is developed assuming the gas phase at atmospheric pressure ($p_g = 0$).

Convective components of pressure and fluid density variation, which are seen to be not significant, are neglected and air density is assumed to be zero. In this case the mass balance of the mixture gas plus solid gives only the air flow and needs not to be considered.

Another simplification arises when acceleration frequencies are low, as is the case in earthquake motion: all the terms involving the relative component of fluid acceleration can then be ignored [24], being:

$$\left| a_i^l - a_i \right| = \left| \frac{d}{dt} \left(\frac{q_i}{\phi S} \right) + q_j \left(\frac{q_i}{\phi S} \right)_{/j} \right| \ll |a_i|. \tag{2.22}$$

This allows for reducing the primary variables to solid displacements and fluid pressure, and the final system to be solved consists of the momentum balance condition for the whole mixture and the continuity equation for the mixture water plus solid:

$$\int_V \sigma''_{ij} D_{ji} \, dV - \int_V \alpha \delta_{ij} S p_l D_{ji} \, dV - \int_A f_i v_i \, dA - \int_V \varrho b_i v_i \, dV - \int_V \varrho \, \dot{v}_i v_i \, dV = 0, \tag{2.23}$$

$$\int_V \delta p_l \left(\alpha S v_{i,i} + \frac{1}{Q}\dot{p}_l\right) dV + \int_V (\delta p_l)_{/i} \left\{(k_{\alpha l})_{ij} \frac{k_{rl}}{\mu_l}\left[-(p_l)_{/j} + \varrho_l(b_j - a_j)\right]\right\} dV + \int_A \delta p_l q_i n_i \, dA = 0, \tag{2.24}$$

where, in the hypothesis of an isotropic medium, Darcy's law has been introduced in its generalised form.

The incremental solution of our problem can be obtained once the incremental form of the constitutive equation is given:

$$d\sigma_{ij} = C_{ijkl} D_{kl} \, dt - \alpha \delta_{ij} S \, dp + d^R \sigma_{ij} \tag{2.25}$$

together with the saturation relationships

$$p = S p_l \qquad S = S(p_l), \qquad k_{rl} = k_{rl}(p_l), \qquad C_S = \phi \frac{dS}{dp_l}, \tag{2.26}$$

and the initial

$$u_i = u_{0i}, \qquad \dot{u}_i = \dot{u}_{0i}, \qquad p = p_{l0}, \tag{2.27}$$

and the boundary conditions are introduced:

$$\begin{array}{lllll} \text{a) imposed displacements} & u_i = \bar{\bar{u}}_i & \text{on } \Gamma_u & \text{for } t \geq 0, \\ \text{b) imposed tractions} & t_i = \bar{\bar{t}}_i & \text{on } \Gamma_t & \text{for } t \geq 0, \\ \text{c) imposed pressures} & p_l = \bar{\bar{p}}_l & \text{on } \Gamma_{pl} & \text{for } t \geq 0, \\ \text{d) imposed flows} & q_i = \bar{\bar{q}}_i & \text{on } \Gamma_q & \text{for } t \geq 0. \end{array} \tag{2.28}$$

2.1.5. Spatial and time discretization. For a quantitative solution, Eqs. (2.23) and (2.24) are discretised in space by finite elements using Galerkin's procedure, and in time by Newmark's scheme [26]. The unknown field variables are expressed in the whole domain by global shape function matrices, $\mathbf{N}$ and $\mathbf{N}_p$, as functions of nodal value vectors $\bar{\mathbf{u}}$ and $\bar{\mathbf{p}}_l$:

$$\mathbf{u} = \mathbf{N}\bar{\mathbf{u}}, \qquad p_l = \mathbf{N}_p \bar{\mathbf{p}}_l . \tag{2.29}$$

In the updated Lagrangian approach adopted, the strain operator, $\mathbf{B}_o$, which relates the strain rate vector with the vector of nodal velocities, is referred to the last known configuration

$$\bar{\mathbf{D}} = \mathbf{B}_o \bar{\mathbf{v}} . \tag{2.30}$$

Once the coupling matrix $\mathbf{Q}$, the mass matrix $\mathbf{M}$ and the external load vector $\mathbf{f}^u$ are introduced (see Appendix), the equilibrium equation (2.23) can be written as

$$\int_V \mathbf{B}_o^T \sigma'' \, dV - \mathbf{Q}\bar{\mathbf{p}}_l + \mathbf{M}\ddot{\bar{\mathbf{u}}} = \mathbf{f}^u . \tag{2.31}$$

The continuity Eq. (2.24) becomes:

$$\mathbf{H}\,\bar{\mathbf{p}}_l + \mathbf{G}\,\ddot{\bar{\mathbf{u}}} + \mathbf{Q}^T\,\dot{\bar{\mathbf{u}}} + \mathbf{S}\,\dot{\bar{\mathbf{p}}}_l = \mathbf{f}^p, \tag{2.32}$$

where **H** is the permeability matrix, **G** the dynamic seepage matrix, **S** the compressibility matrix and $\mathbf{f}^p$ the flow vector (see Appendix). Since the effect of the dynamic seepage forcing term is negligible [23], the coupled system at time t_{n+1} is:

$$\begin{aligned} \mathbf{M}_{n+1}\,\ddot{\bar{\mathbf{u}}}_{n+1} + \bar{\mathbf{P}}_{n+1} - \mathbf{Q}_{n+1}\bar{\mathbf{p}}_{n+1} &= \mathbf{f}^u_{n+1}, \\ \mathbf{Q}_{n+1}\,\dot{\bar{\mathbf{u}}}_{n+1} + \mathbf{H}_{n+1}\bar{\mathbf{p}}_{n+1} + \mathbf{S}_{n+1}\,\dot{\bar{\mathbf{p}}}_{n+1} &= \mathbf{f}^p_{n+1}, \end{aligned} \tag{2.33}$$

where $\bar{\mathbf{P}}_{n+1}$ is the equivalent nodal force vector. The Newmark scheme adopted for time integration, with the lowest allowable order for each variable, permits to write the variables and their derivatives at t_{n+1} as functions of their values at t_n:

$$\begin{aligned} \dot{\bar{\mathbf{u}}}_{n+1} &= \dot{\bar{\mathbf{u}}}_n + \ddot{\bar{\mathbf{u}}}_n\,\Delta t + \beta_1 \Delta\ddot{\bar{\mathbf{u}}}\,\Delta t = \dot{\bar{\mathbf{u}}}^{\,p}_{n+1} + \beta_1 \Delta\ddot{\bar{\mathbf{u}}}_n\,\Delta t, \\ \bar{\mathbf{u}}_{n+1} &= \bar{\mathbf{u}}_n + \dot{\bar{\mathbf{u}}}_n \Delta t + \frac{\ddot{\bar{\mathbf{u}}}_n\,\Delta t^2}{2} + \frac{\beta_2 \Delta\ddot{\bar{\mathbf{u}}}_n\,\Delta t^2}{2} = \bar{\mathbf{u}}^p_{n+1} + \frac{\beta_2 \Delta\ddot{\bar{\mathbf{u}}}_n\,\Delta t^2}{2}, \\ \bar{\mathbf{p}}_{n+1} &= \bar{\mathbf{p}}_n + \dot{\bar{\mathbf{p}}}_n \Delta t + \Theta \Delta\dot{\bar{\mathbf{p}}}_n \Delta t = \bar{\mathbf{p}}^p_{n+1} + \Theta \Delta\dot{\bar{\mathbf{p}}}_n \Delta t, \end{aligned} \tag{2.34}$$

where $\dot{\bar{\mathbf{u}}}^{\,p}_{n+1}$, $\bar{\mathbf{u}}^p_{n+1}$ and $\bar{\mathbf{p}}^p_{n+1}$ are predicted values from known parameters at time t_n.

Insertion of Eqs. (2.34) into (2.33) allows the coupled system to be written in the form

$$\begin{aligned} \Psi^u_{n+1} &= \mathbf{M}_{n+1}\Delta\ddot{\bar{\mathbf{u}}}_n + \bar{\mathbf{P}}_{n+1} - \mathbf{Q}_{n+1}\Theta\Delta t\Delta\dot{\bar{\mathbf{p}}}_n - \mathbf{F}^u_{n+1} = 0, \\ \Psi^p_{n+1} &= \mathbf{Q}^T_{n+1}\beta_1\Delta t\Delta\ddot{\bar{\mathbf{u}}}_n + \mathbf{H}_{n+1}\Theta\Delta t\Delta\dot{\bar{\mathbf{p}}}_n + \mathbf{S}_{n+1}\Delta\dot{\bar{\mathbf{p}}}_n - \mathbf{F}^p_{n+1} = 0. \end{aligned} \tag{2.35}$$

At the beginning of each time step $\bar{\mathbf{P}}_{n+1}$ must be evaluated by integration of the constitutive law, the stress field at the previous step being known. Relative permeability and specific capacity (Eq. (2.26)) must be updated as well as void ratio and absolute permeability.

The nonlinear coupled system (2.35) is solved by an iterative procedure. If a Newton-Raphson scheme is adopted to linearize the problem, the Jacobian matrix of transformation, **J**, at the i-th-iteration is:

$$\mathbf{J} = \left.\frac{\partial\Psi}{\partial x}\right|_{x=x_i} = \begin{pmatrix} \dfrac{\partial\Psi^u}{\partial\left(\Delta\ddot{\bar{\mathbf{u}}}\right)} & \dfrac{\partial\Psi^u}{\partial\left(\Delta\dot{\bar{\mathbf{p}}}\right)} \\ \dfrac{\partial\Psi^p}{\partial\left(\Delta\ddot{\bar{\mathbf{u}}}\right)} & \dfrac{\partial\Psi^p}{\partial\left(\Delta\dot{\bar{\mathbf{p}}}\right)} \end{pmatrix} = \begin{pmatrix} \mathbf{M} + \dfrac{1}{2}\mathbf{K}_T\beta_2\Delta t^2 & -\mathbf{Q}\Theta\Delta t \\ \mathbf{Q}^T\beta_1\Delta t & \mathbf{H}\Theta\Delta t + \mathbf{S} \end{pmatrix}. \tag{2.36}$$

The tangent stiffness matrix in Eq. (2.36) has been derived in [12] as

$$d\mathbf{P} = \int_V \left[\mathbf{B}_o^T \overline{\overline{\mathbf{C}}} \mathbf{B}_o + \mathbf{G}_\tau^T \hat{\sigma} \mathbf{G}_\tau\right] d\bar{\mathbf{u}}\, dV = (\mathbf{K} + \mathbf{K}_\sigma)\, d\bar{\mathbf{u}} = \mathbf{K}_T\, d\bar{\mathbf{u}}. \tag{2.37}$$

$\mathbf{K}_T$ is the sum of two terms: the matrix $\mathbf{K}$, corresponding to the linear elastic stiffness matrix, but referred to the constitutive matrix $\overline{\overline{\mathbf{C}}}$, modified by Cauchy stresses at time t, as:

$$\overline{\overline{\mathbf{C}}} = \mathbf{C} - \sigma_{d1} + \sigma_{d2} = \mathbf{C} - \sigma_d \tag{2.38}$$

and the initial stress matrix $\mathbf{K}_\sigma$, respectively equal to:

$$\mathbf{K} = \int_V \mathbf{B}_o^T \overline{\overline{\mathbf{C}}} \mathbf{B}_o\, dV, \qquad \mathbf{K}_\sigma = \int_V \mathbf{G}_\tau^T\, \hat{\sigma}\, \mathbf{G}_\tau\, dV. \tag{2.39}$$

Since the matrix σ_{d2} lacks in symmetry (see Appendix), $\mathbf{K}_T$ is also not symmetric, but this fact is usually negligible [13].

The system to be solved can then be written in the following form, which is symmetric provided the tangent stiffness matrix itself is symmetric:

$$\begin{pmatrix} \mathbf{M} + \frac{1}{2}\mathbf{K}_T \beta_2 \Delta t^2 & -\mathbf{Q}\Theta\Delta t \\ -\mathbf{Q}^T\Theta\Delta t & -\frac{\Theta}{\beta_1}(\mathbf{H}\Theta\Delta t + \mathbf{S}) \end{pmatrix} \begin{pmatrix} \Delta\, \ddot{\bar{\mathbf{u}}} \\ \Delta\, \dot{\mathbf{p}} \end{pmatrix} = \begin{pmatrix} -\Psi^u \\ -\frac{\Theta}{\beta_1}\Psi^p \end{pmatrix}. \tag{2.40}$$

Since the Newton–Raphson method requires the Jacobian matrix to be evaluated and inverted at each iteration, also other modified schemes are used to achieve convergence with less computational effort. In particular, the use of secant updates, like Davidon's and Broyden–Fletcher–Goldfarb–Shanno's (BFGS) methods are found advantageous in nonlinear analyses.

3. Dynamic localization theory in saturated porous solids

The finite strain localization theory is here based on the analysis of wave propagation in continuous solids. The first fundamental investigations on this subject are due to Duhem and Hadamard (1903). A presentation of the theory in general form and systematic literature references can be found in TRUESDELL and NOLL [20], TRUESDELL and TOUPIN [21] and in CHEN [2].

Let Σ be the wave front (here considered as a Riemannian manifold in motion, through which the acceleration and the velocity gradient can be discontinuous functions); $\mathbf{n}$ is the normal directed outward from the above manifold. Denoting

$$\eta^i = \operatorname{grad} \dot{\mathbf{x}}^i \tag{3.1}$$

the normal jump of the spatial velocity gradient of the i-phase along this manifold ($i = s, l$), Hadarmard's compatibility conditions can be written as

$$\left\| \dot{\mathbf{E}}^i \right\| = \frac{1}{2} \left(\eta^i \otimes \mathbf{n} + \mathbf{n} \otimes \eta^i \right), \tag{3.2}$$

$$\left\| \ddot{\mathbf{x}}^i \right\| = -c\eta^i, \tag{3.3}$$

where $\mathbf{E}^i$ is the deformation tensor of the i-phase, $\| \dots \|$ denotes the jump of the quantity inside the symbol, c represents the velocity of the manifold Σ with respect to the material frame of the analysed solid and $\otimes$ is, as usual, the dyadic or tensor product. Consequently, momentum equilibrium equations impose the condition

$$\| \dot{\sigma}^i \| \cdot \mathbf{n} = \varrho^i c^2 \eta^i . \tag{3.4}$$

Expressing the constitutive relationship in incremental form, LORET and PREVOST have shown in [10] that for the saturated case, c^2, squares of the wave propagation velocities coincide with the eigenvalues of the acoustic tensor $\mathbf{B}$, expressed by:

$$\mathbf{B} = \begin{pmatrix} \mathbf{B}^{ss} & \mathbf{B}^{sl} \\ (\mathbf{B}^{sl})^T & B^{ll} \end{pmatrix}, \tag{3.5}$$

where $B^{ll} = \dfrac{1}{\varrho^l} \dfrac{K}{\phi} > 0$ is a positive scalar quantity, $\mathbf{B}^{sl} = \dfrac{1}{\sqrt{\varrho^s \varrho^l}} \dfrac{1-\phi}{\phi} K_l \mathbf{n}$ is a vector and $\mathbf{B}^{ss} = \dfrac{1}{\varrho} \mathbf{n} \cdot \mathbf{A}^{ss} \cdot \mathbf{n}$ is a second order tensor containing the tensor of the solid moduli.

The hyperbolicity condition of the problem, implying an effective wave propagation, requires real values of the propagation velocity c. Consequently the eigenvalues of the tensor $\mathbf{B}$ must be real and positive. $\mathbf{B}$ inherits the symmetry properties of the solid moduli tensor and is hence symmetric for associative plasticity. In this case the eigenvalues are real and loss of hyperbolicity occurs in form of a stationary wave. In [10] it has been shown that the loss of hyperbolicity cannot occur for a positive plastic modulus. In case of non-associative plasticity $\mathbf{B}$ is no longer symmetric and loss of hyperbolicity may occur in form of flutter instability [10], where two square wave speeds become complex conjugate. In the following we assume associative plasticity and monitor the loss of hyperbolicity checking the sign of $\det \mathbf{B}$ in the Gauss points.

Developing the determinant of $\mathbf{B}$ matrix, it can be observed that the global result is related to the evolution of the constitutive parameters of the solid skeleton and the analysis of strain localization is reduced to the study of the sign of $\mathbf{n} \cdot \mathbf{A}'^{ss} \cdot \mathbf{n}$ [10].

In the two-dimensional case, $n_1 = \cos\vartheta$, $n_2 = \sin\vartheta$ hold; if one poses $x = \tan\vartheta$, the following expression is obtained

$$\det \mathbf{B}(\mathbf{n}) = P(x) = a_4x^4 + a_3x^3 + a_2x^2 + a_1x + a_0;$$

hence conditions for the onset of finite strain localization is transformed into a problem of searching the roots of a fourth degree polynomial or to find its minima by studying their signs (to find physically meaningful solutions).

4. Numerical examples

The two-dimensional domain of fully saturated porous material is discretised by means of isoparametric triangular or quadrilateral finite elements. Linear finite elements have been chosen because of their computational efficiency in nonlinear analysis and their low distortional characteristics.

The finite elements used for discretising the problem have not been intentionally oriented along particular lines (unbiased mesh).

The performed analyses show in particular:

i) the necessity of softening in the constitutive law (associative plasticity) to have shear band formation,

ii) the influence of permeability on band growth,

iii) particular patterns of stresses, pressures and strains with respect to the corresponding ones in hardening plasticity or elasticity,

iv) a weak mesh dependence of the results.

4.1. Quadrilateral sample

The onset and growth of localized bands in a soil sample of rectangular shape made of saturated material of dimensions 25×35 m are analysed (Fig. 1). The sample is subject to axial compression by means of uniformly distributed loads both on the upper and lower surfaces, as also indicated in Fig. 1.

The solid and fluid domains are not subject to any initial stress state (hence gravitational effects or hydrostatic pressures are not accounted for). In the fluid discretization the top and bottom surfaces are considered impermeable.

In the considered model, homogeneous and isotropic solid and fluid phases are taken into account. The constitutive relationship of the solid skeleton is of Mohr-Coulomb type, with a linear displacement-strain relationship.

It can be noted that plastic strains are concentrated in narrow bands of finite amplitude where high strain gradients occur (Fig. 2). In Fig. 3 localization directions are shown as found with the procedure based on the analysis of the acoustic tensor.

Figure 4 shows that in case of plasticity with hardening no band formation appears.

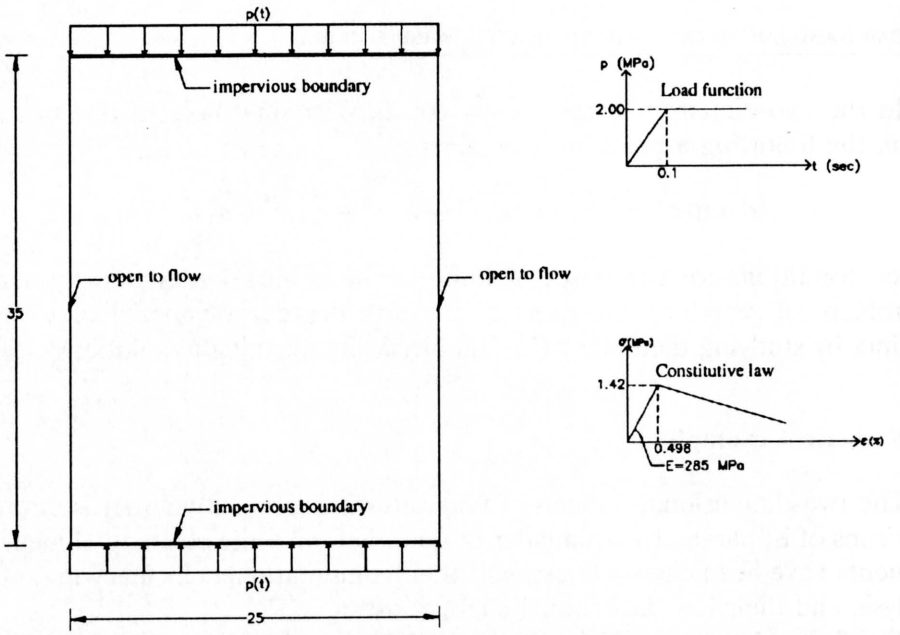

FIG. 1. Description of the geometrical and material characteristics of the reference example. Young's modulus $E = 285\,\text{MPa}$, Poisson's ratio $\nu = 0.4285$, solid grain density $\varrho_s = 2000\,\text{Kg/m}^3$, liquid density $\varrho_l = 1000\,\text{Kg/m}^3$, apparent cohesion $c_o = 1.42\,\text{MPa}$, hardening modulus $H = -40\,\text{MPa}$, angle of internal friction $\varphi = 20°$, volumetric liquid modulus $K_l = 200\,\text{MPa}$, volumetric solid modulus $K_s = 678\,\text{GPa}$, initial porosity $\phi_o = 0.2$.

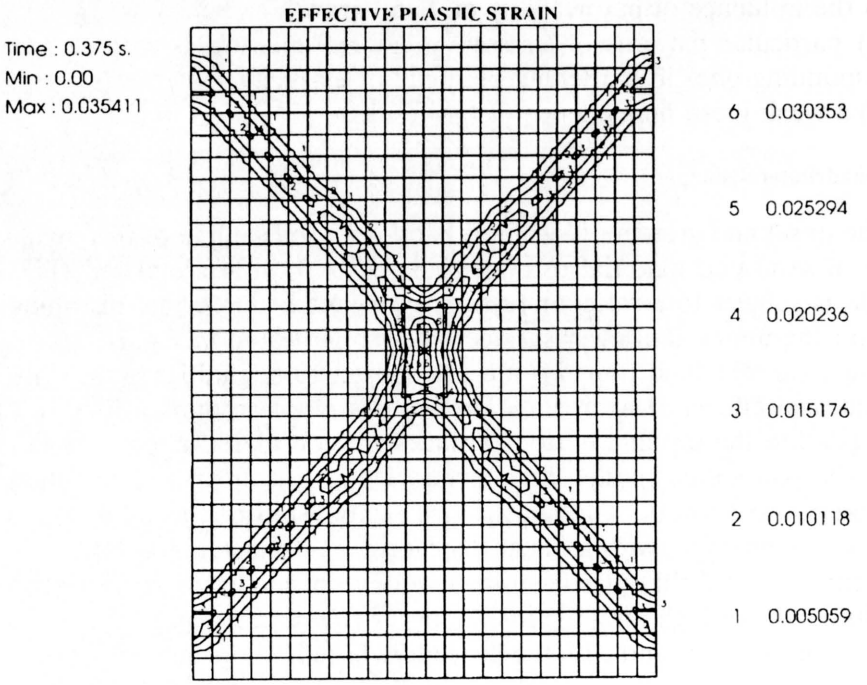

FIG. 2. Effective plastic strain at $t = 0.375\,\text{s}$ with a permeability of 0.25 m/s.

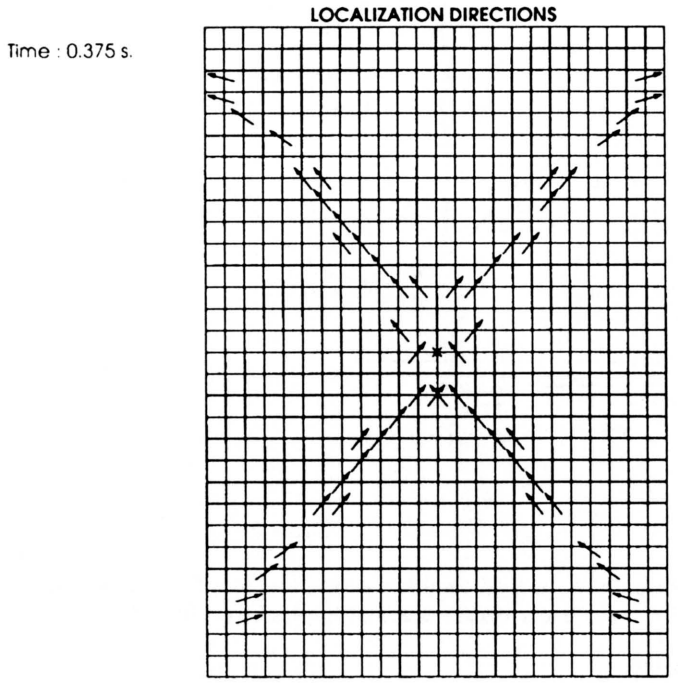

FIG. 3. Localization directions which follow from the analysis of the acoustic tensor.

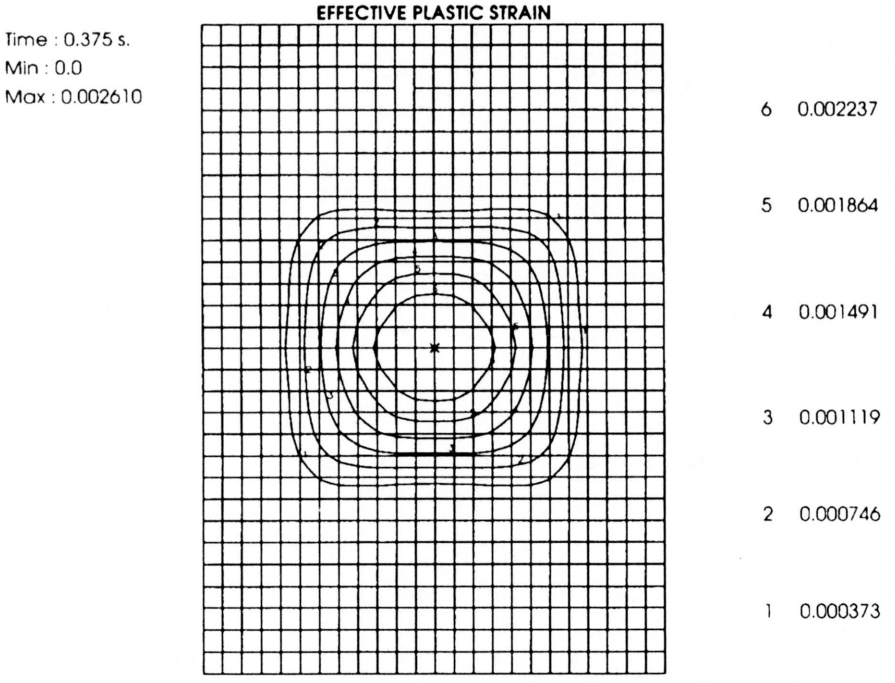

FIG. 4. Effective plastic strain at $t = 0.375$s in plasticity with hardening.

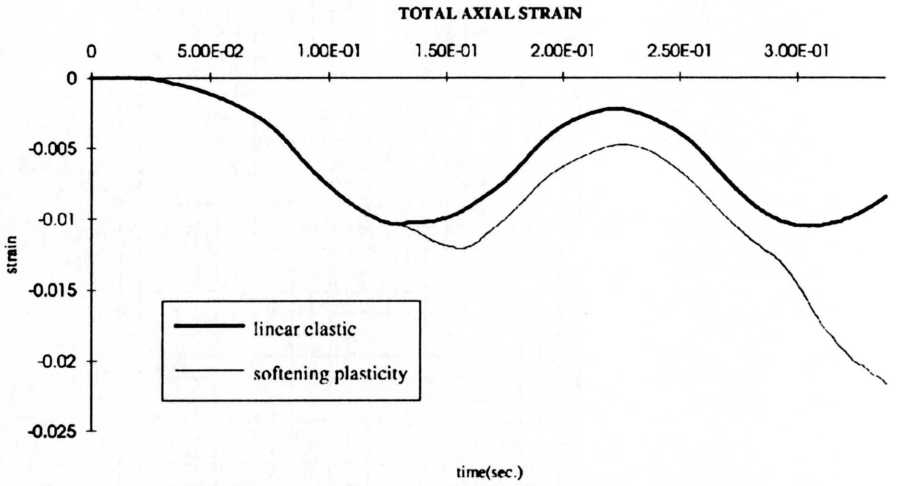

FIG. 5. Comparison between total axial strains vs. time in a Gauss point close to the centre, in the linear elastic case and in plasticity with softening.

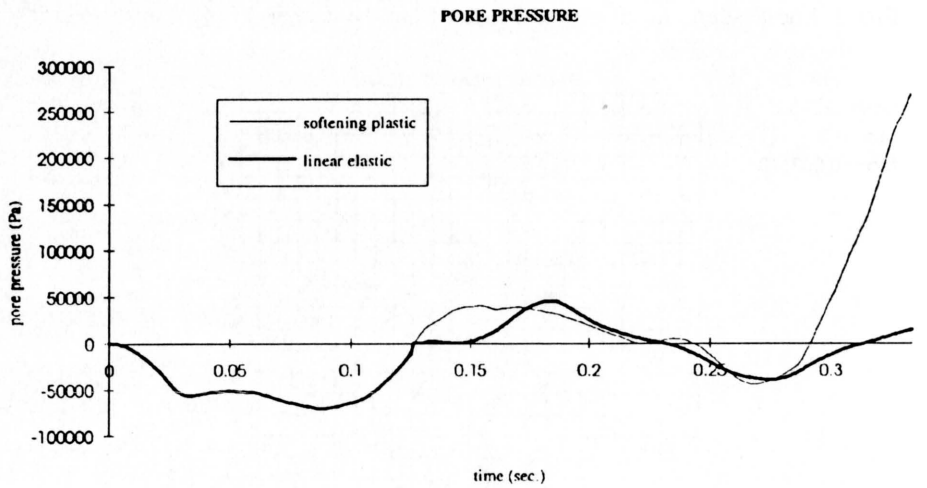

FIG. 6. Comparison between pressures vs. time in the central node in the linear elastic case and in plasticity with softening.

The time transients of strains (Fig. 5) and pressures (Fig. 6) are characterized by a wave form, with a marked regularity up to the onset of the shear band formation ($t < 0.3$ s), since the plastic effect is yet limited. Plastic strain shows a different pattern, characterized by a plateau (Fig. 7). For $t > 0.3$ s loss of periodicity can be noted in Fig. 5, as well as a sudden development of pore water tractions (Fig. 6).

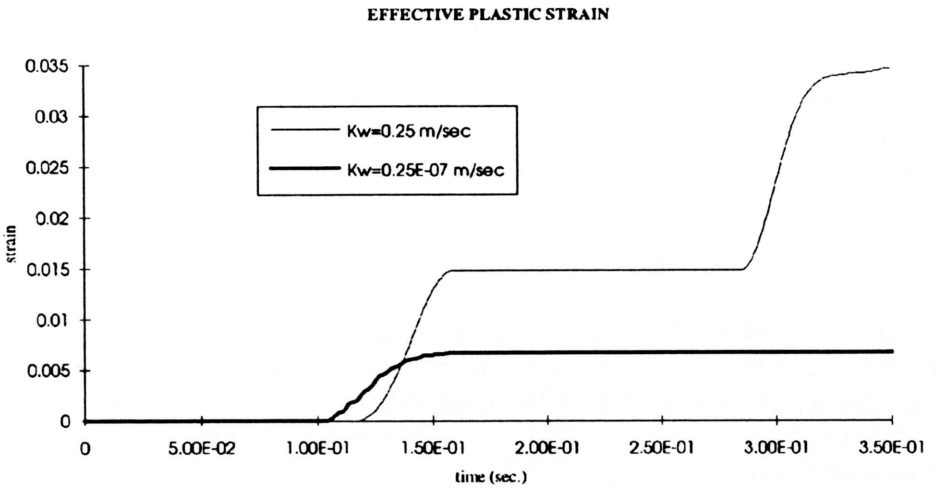

FIG. 7. Comparison between effective plastic strains vs. time in a Gauss point nearest the centre, for different permeabilities.

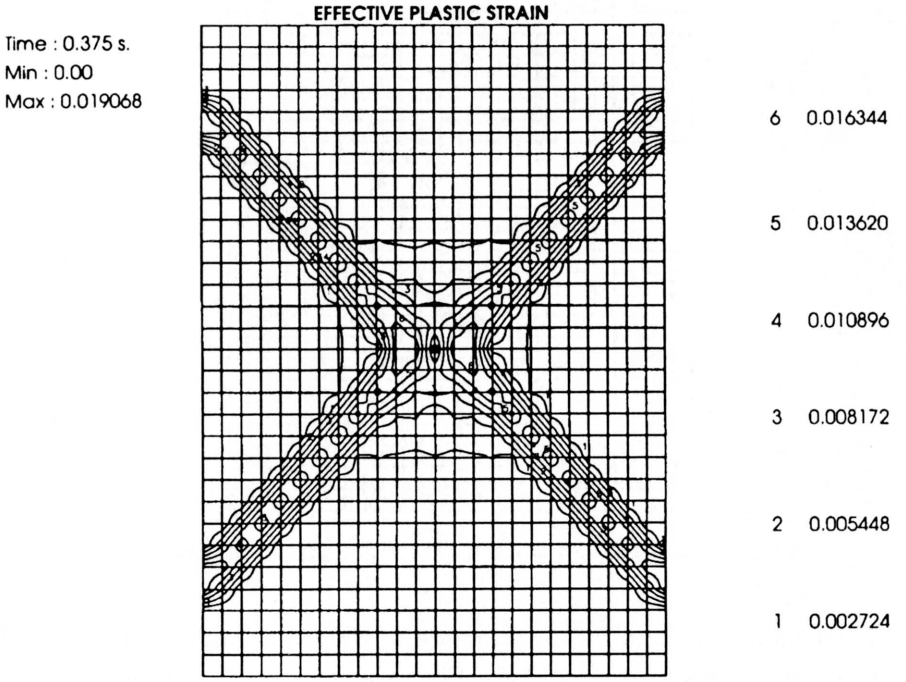

FIG. 8. Effective plastic strains at $t = 0.375$ s with a permeability of $0.25E - 03$ m/s.

It should be noted that the material properties for the Mohr-Coulomb model chosen are those of a sand which dilates because of shear. The shear band has hence higher porosity, which implies transient flow into it. In the example, water cannot flow fast enough, hence pore water traction develops in the shear band as can be clearly seen in Figs. 6 and 10.

4.2. Influence of permeability

The permeability affects the degree of coupling between the two phases and presents a significant role in the development of localization. The lower is its value, the higher is the part of the load increment assumed by water and the slower is the transfer to the solid skeleton. Hence coupling effects increase as the permeability decreases.

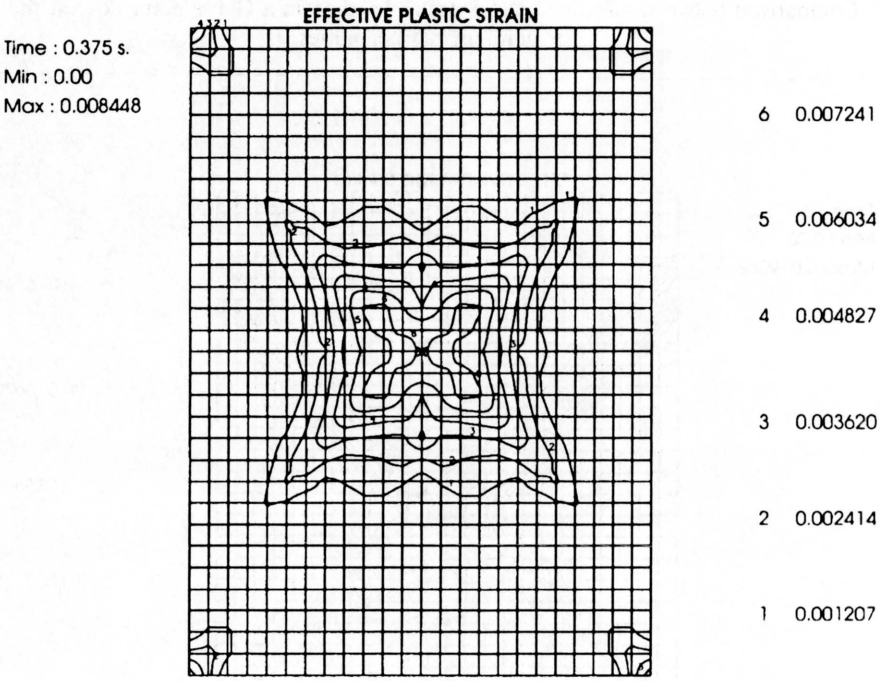

FIG. 9. Effective plastic strains at $t = 0.375$ s with a permeability of $0.25E - 10$ m/s.

In localization this implies the variation of the plastic strain levels (Fig. 7), the change of band dimension (compare Figs. 2 and 8) up to the disappearance of their formation (Fig. 9). For a permeability of $0.25E - 03$ m/s, pore water pressure localization develops as shown in Fig. 10. As noted previously, we have pore water tractions in the shear band. For a permeability value of 0.25 m/s, no such pore pressure localization has been observed.

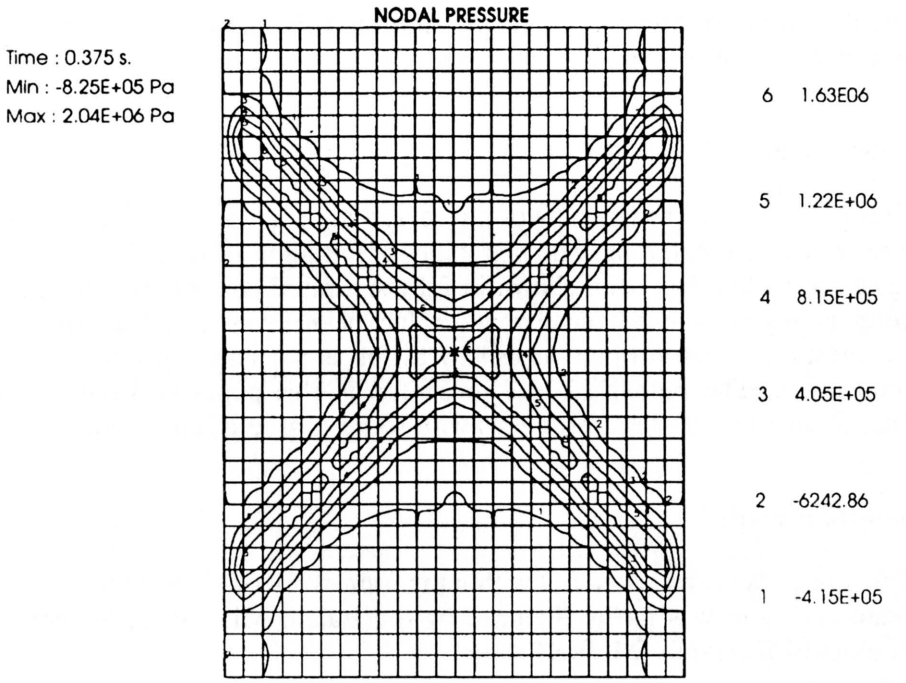

FIG. 10. Nodal pressures at $t = 0.375$ s with a permeability of $0.25E - 03$ m/s.

4.3. Dependence on spatial discretization

Using in a single phase material a rate or gradient-independent material model, the localization is strongly dependent on the chosen discretization, and the numerical solution cannot have a physical meaning. This is connected with the presence of a softening branch in the constitutive relationship, responsible for the loss of hyperbolicity in the equations of motion. The wave propagation disappears because either a wave with zero velocity or two waves with imaginary velocities (stationary jump) appear. Such statement can be easily demonstrated in the one-dimensional case, where the wave velocity is equal to $\pm\sqrt{D_{ep}/\varrho}$, D_{ep} being the elastoplastic modulus (negative in the softening branch). Hence the system of differential equations becomes ill-posed, i.e. is strongly dependent on the initial and boundary conditions. The absence of a scale parameter in the constitutive law leads to the dependence of the band width on the element dimension. Such an internal length scale may be introduced either by using a model with polar constituents, see e.g. PASTOR *et al.* [15], gradient-dependent plasticity [6] or rate-dependent plasticity.

The tests carried out with program Swandyne [23, 12] have shown that for a multiphase material the situation is not so dramatic, because of the natural presence of a Laplacian (Eqs. (2.10) and (2.18)). The use of rate-dependent plasticity,

e.g. of the model of Duvaut-Lions [5], improves the performance only slightly. This topic will however be further pursued.

5. Conclusions

This paper shows early results of a research in progress on localization in two or three-phase geomaterials. The possibility of initiation of shear band formation using ramp loading has been shown in fully saturated conditions. The influence of permeability on shear band formation has been investigated in some detail. Many questions are still open, especially as far as partially saturated conditions are concerned. The numerical tool presented in this paper is however a good starting point to solve these problems with some degree of confidence.

Acknowledgements

This work has been carried out within the framework of HCM project "ALERT geomaterials" and was partly financed by the Italian Ministry of Scientific and Technological Research (MURST 40%).

Appendix

$$\text{coupling matrix} \quad \mathbf{Q} = \int_V \mathbf{B}_o^T S \mathbf{m} \mathbf{N}_p \, dV,$$

$$\text{mass matrix} \quad \mathbf{M} = \int_V \mathbf{N}_u^T [\varrho_s (1-\phi) + \varrho_l \phi S] \mathbf{N}_u \, dV,$$

$$\text{permeability matrix} \quad \mathbf{H} = \int_V (\nabla \mathbf{N}_p)^T \mathbf{k}_l \nabla \mathbf{N}_p \, dV,$$

$$\text{dynamic seepage matrix} \quad \mathbf{G} = \int_V (\nabla \mathbf{N}_p)^T \mathbf{k}_l \varrho_l \mathbf{N}_u \, dV,$$

$$\text{compressibility matrix} \quad \mathbf{S} = \int_V \mathbf{N}_p^T \frac{1}{Q} \mathbf{N}_p \, dV,$$

$$\text{external load vector} \quad \mathbf{f}^u = \int_V \mathbf{N}_u^T [\varrho_s (1-\phi) + \varrho_l \phi S] \mathbf{b} \, dV + \int_A \mathbf{N}_u^T \mathbf{t} \, dA,$$

$$\text{flow vector} \quad \mathbf{f}^p = \int_V (\nabla \mathbf{N}_p)^T \mathbf{k}_l \varrho_l \mathbf{b} \, dV - \int_A \mathbf{N}_p^T \mathbf{q}^T \mathbf{n} \, dA,$$

$$\text{equivalent force vector} \quad \mathbf{P} = \int_V \mathbf{B}_o^T \sigma'' \, dV,$$

$$\mathbf{F}^u_{n+1} = \mathbf{f}^u_{n+1} - \mathbf{M}_{n+1}\,\ddot{\overline{\mathbf{u}}}_n + \mathbf{Q}_{n+1}\left(\overline{\mathbf{p}}_n + \Delta t\,\dot{\overline{\mathbf{p}}}\right),$$

$$\mathbf{F}^p_{n+1} = \mathbf{f}^p_{n+1} - \mathbf{Q}^T_{n+1}\left(\dot{\overline{\mathbf{u}}}_n + \Delta t\,\ddot{\overline{\mathbf{u}}}_n\right) - \mathbf{H}_{n+1}\left(\overline{\mathbf{p}}_n + \Delta t\Delta\,\dot{\overline{\mathbf{p}}}_n\right) - \mathbf{S}_{n+1}\,\dot{\overline{\mathbf{p}}}_n,$$

$$C_{ll} = \frac{(\alpha-\phi)}{K_s}S^2 + \frac{\phi S}{K_l},$$

$$C_{lg} = \frac{(\alpha-\phi)}{K_s}S(1-S),$$

$$C_{gg} = \frac{(\alpha-\phi)}{K_s}(1-S)^2 + \frac{\phi(1-S)}{K_g},$$

$$\frac{1}{Q} = C_{ll} + \frac{C_{lg}}{S_g}\frac{C_s}{\phi}p_l + C_s = C_s + \frac{\phi S}{K_l} + \frac{(\alpha-\phi)}{K_s}S\left(S + \frac{C_s}{\phi}p_l\right),$$

$$\mathbf{B}^T_{0i} = \begin{bmatrix} \dfrac{\partial N_i}{\partial x_1} & 0 & 0 & 0 & \dfrac{\partial N_i}{\partial x_3} & \dfrac{\partial N_i}{\partial x_2} \\ 0 & \dfrac{\partial N_i}{\partial x_2} & 0 & \dfrac{\partial N_i}{\partial x_3} & 0 & \dfrac{\partial N_i}{\partial x_1} \\ 0 & 0 & \dfrac{\partial N_i}{\partial x_3} & \dfrac{\partial N_i}{\partial x_2} & \dfrac{\partial N_i}{\partial x_1} & 0 \end{bmatrix},$$

$$\mathbf{G}^T_r = \left(\frac{\partial N_i}{\partial x_1}\mathbf{I}, \frac{\partial N_i}{\partial x_2}\mathbf{I}, \frac{\partial N_i}{\partial x_3}\mathbf{I},\right),$$

$$\hat{\sigma} = \begin{pmatrix} \hat{\sigma}_{11} & \hat{\sigma}_{12} & \hat{\sigma}_{13} \\ \hat{\sigma}_{21} & \hat{\sigma}_{22} & \hat{\sigma}_{23} \\ \hat{\sigma}_{31} & \hat{\sigma}_{32} & \hat{\sigma}_{33} \end{pmatrix} \qquad \text{with} \quad \hat{\sigma}_{ij} = \sigma_{ij}\mathbf{I},$$

$$\sigma_{d2} = \begin{pmatrix} \sigma_{11} & \sigma_{11} & \sigma_{11} & 0 & 0 & 0 \\ \sigma_{22} & \sigma_{22} & \sigma_{22} & 0 & 0 & 0 \\ \sigma_{33} & \sigma_{33} & \sigma_{33} & 0 & 0 & 0 \\ \sigma_{23} & \sigma_{23} & \sigma_{23} & 0 & 0 & 0 \\ \sigma_{13} & \sigma_{13} & \sigma_{13} & 0 & 0 & 0 \\ \sigma_{12} & \sigma_{12} & \sigma_{12} & 0 & 0 & 0 \end{pmatrix},$$

$$\sigma_{d1} = \begin{pmatrix} 2\sigma_{11} & 0 & 0 & 0 & \sigma_{13} & \sigma_{12} \\ 0 & 2\sigma_{22} & 0 & \sigma_{23} & 0 & \sigma_{21} \\ 0 & 0 & 2\sigma_{33} & \sigma_{32} & \sigma_{31} & 0 \\ 0 & \sigma_{32} & \sigma_{23} & \overline{\overline{\sigma}}_{23} & \sigma_{21} & \sigma_{31} \\ \sigma_{31} & 0 & \sigma_{13} & \sigma_{12} & \overline{\overline{\sigma}}_{13} & \sigma_{32} \\ \sigma_{21} & \sigma_{12} & 0 & \sigma_{13} & \sigma_{23} & \overline{\overline{\sigma}}_{12} \end{pmatrix} \qquad \text{with} \quad \overline{\overline{\sigma}}_{ij} = \frac{\sigma_{ij} - \sigma_{ji}}{2}.$$

References

1. N. BICÀNIC and A. SELMAN, *On mesh dependence of failure mode predictions for strain softening analyses*, 1993 [in press].
2. P.J. CHEN, *Growth and decay of waves in solids*, Mechanics of Solids, vol. III, C. TRUESDELL [Ed.], Springer-Verlag, Berlin, Heidelberg 1973.
3. O. COUSSY, *Mécanique des milieux poreux*, Editions Technip, Paris 1991.
4. J.K. DIENES, *On the analysis of rotation and stress rate in deforming bodies*, Acta Mech., **32**, 217–232, 1979.
5. G. DUVAUT and J.L. LIONS, *Les inéquations en mécanique et en physique*, Dunod, Paris 1972.
6. W. EHLERS, *Toward finite theories of liquid-saturated elasto-plastic porous media*, Int. J. Plasticity, **7**, 433–475, 1991.
7. M. HASSANIZADEH and W.G. GRAY, *General conservation equations for multi-phase system. 1. Averaging technique*, Adv. Water Res., **2**, 131–144, 1979.
8. M. HASSANIZADEH and W.G GRAY, *General conservation equations for multi-phase system. 2. Mass, momenta, energy and entropy equations*, Adv. Water Res., **2**, 191–201, 1979.
9. M. HASSANIZADEH and W.G. GRAY, *General conservation equations for multi-phase system. 3. Constitutive theory for porous media flow*, Adv. Water Res., **3**, 25–40, 1980.
10. B. LORET and J.H. PREVOST, *Dynamic strain localization in fluid-saturated porous media*, J. Engng. Mech., **11**, 907–922, 1991.
11. J.E. MARSDEN and T.J.R. HUGHES, *Mathematical foundation of elasticity*, Prentice-Hall, Englewood Cliffs, NJ, 1983.
12. E.A. MEROI, B.A. SCHREFLER and O.C. ZIENKIEWICZ, *Large strain static and dynamic semisaturated soil behaviour*, Int. J. Num. Anal. Meth. Geomech., **19**, 2, 81–106, 1995.
13. F. MOLENKAMP, *Limits to the Jaumann stress rate*, Int. J. Num. Anal. Meth. Geomech., **10**, 151–176, 1986.
14. D.R.I. OWEN, E. ONATE and E. HINTON, Proc. of the third International Conf. on Computational Plasticity; Section 3. Localisation and material instabilities, (Barcelona, 6-10 April, 1992), Pineridge Press, Swansea 1992.
15. M. PASTOR, J.P. VILLOTTE, O.C. ZIENKIEWICZ *et al., Numerical analysis of failure and localization in soils*, Euro-Greco project 4, Strains Localization in Geomaterials, 32–38, 1992.
16. J.R. RICE, *On the stability of dilatant hardening for saturated rock masses*, J. Geophys. Res., **80**, 11, 1531–1536, 1975.
17. J.W. RUDNICKI, *Effect of dilatant hardening on the development of concentrated shear-deformation in fissured rock masses*, J. Geophys. Res., **89**, B11, 9259–9270, 1984.
18. B.A. SCHREFLER, L. SIMONI, K. XI and O.C. ZIENKIEWICZ, *Mechanics of partially saturated porous media*, [in:] Num. Meth. and Const. Mod. in Geom., CISM, **311**, C.S. DESAI and G. GIODA [Ed.], Springer-Verlag, Wien, New York 1993.
19. L.J. SLUYS, *Wave propagation, localization and dispersion in softening solids*, Ph.D. Thesis, Civil Engineering Department of Delft University of Technology, 1992.
20. C. TRUESDELL and W. NOLL, *The non-linear field theories of mechanics*, S. FLÜGGE [Ed.], Handbuch der Physik, vol. III/3, Springer-Verlag, Berlin 1965.
21. C. TRUESDELL and R. TOUPIN, *The classical field theories*, Handbuch der Physik, vol. III/1, Springer-Verlag, Berlin 1960.
22. I. VARDOULAKIS, *Dynamic stability analysis of undrained simple shear on water-saturated granular soils*, Int. J. Numer. Anal. Meth. Geomech., **10**, 2, 177–190, 1986.

23. Y.M. XIE, *Finite element solution and adaptive analysis for static and dynamic problems of saturated-unsaturated porous media*, Ph.D. thesis, Department of Civil Engineering, Swansea University, U.K. 1990.

24. O.C. ZIENKIEWICZ, A..C. CHAN, M. PASTOR, D.K. PAUL and T. SHIOMI, *Static and dynamic behaviour of soils: a rational approach to quantitative solutions. I. Fully saturated problems*, Proc. R. Soc. Lond., A 429, 285–309, 1990.

25. O.C. ZIENKIEWICZ and T. SHIOMI, *Dynamic behavior of saturated porous media: the generalised Biot formulation and its numerical solution*, Int. J. Num. Anal. Meth. in Geom., 8, 71–96, 1984.

26. O.C. ZIENKIEWICZ and R.L. TAYLOR, *The finite element method*, Vol. 2, McGraw-Hill Book Company, London 1991.

UNIVERSITÀ DEGLI STUDI DI PADOVA
FACOLTÀ DI INGEGNERIA
ISTITUTO DI SCIENZA E TECNICA DELLE COSTRUZIONI, PADOVA, ITALY.

Received November 3, 1994.

Arch. Mech., 47, 3, pp. 601–615, Warszawa 1995

Misfit dislocations and anisotropic coarsening in superalloys (*)

J. L. VALLÉS, D. J. ARRELL and J. BRESSERS (PETTEN)

THE HIGH TEMPERATURE coarsening of the hardening precipitates in single crystal nickel-base superalloys is analysed in the light of the interfacial dislocation networks which develop to relieve the lattice mismatch. A criterion based on the ratio of interfacial energies in the principal directions is applied to the prediction of anisotropy in the microstructural morphology under different stress and temperature conditions. The new criterion is shown to represent a clear improvement with respect to previous approaches. The range of stress-temperature prediction diagrams constructed for a number of real alloys shows good agreement with experimental behaviour. The prediction diagrams are also used to illustrate how the ratio of elastic moduli and the intrinsic lattice mismatch are the two relevant parameters in governing the evolution of the morphology.

1. Introduction

THE EXCELLENT high temperature structural properties of nickel-base superalloys rely on their special two-phase microstructure, consisting of ordered γ' cuboidal precipitates in a γ matrix. The γ' particles, whose faces are aligned with the $\{100\}$ axes of the γ phase, act as precipitation-hardening agents via dislocation pinning and Orowan loop formation. For applications such as turbine blades, single crystals of superalloys are grown, in which the mechanical properties are further enhanced by the removal of grain boundary-based failure mechanisms. Precipitate morphology in these alloys is known to exhibit anisotropy under applied loads at elevated temperatures. Under uniaxially applied stresses, needles parallel to the load axis or plates perpendicular to it have been identified experimentally. This phenomenon, known as anisotropic coarsening or more commonly rafting, is the subject of much interest, since it appears to have a significant effect on the high temperature mechanical properties.

Previous attempts to explain the rafting behaviour have concentrated on applying the theory of the elastic energy of inclusions. Recently, a novel approach has been developed [1], in which the strain energy associated to the lattice parameter mismatch between the γ and γ' phases is considered in terms of an interfacial network of misfit dislocations. This lattice mismatch, inherent in systems with semi-coherent precipitates, is modified anisotropically by an external load. A new criterion based on these ideas improves the prediction of the rafting response, also accounting for the temperature dependence. This new approach allows for the clarification of a number of issues which were not fully understood [2]. In particular, we analyse the significance of the changes with respect to temperature of

(*) Paper presented at 30th Polish Solid Mechanics Conference, Zakopane, September 5–9, 1994.

the ratio of the elastic moduli of the two phases, which are shown to be more relevant for the formation of a needle- or plate-type morphology than the inherent interfacial misfit, the parameter which has been generally used to predict rafting.

2. Prediction of precipitate morphology

Since the first reports of anisotropic coarsening over twenty years ago [3], considerable attention has been directed towards characterising and quantifying its effects on the mechanical properties of superalloys. Though opinions still differ as to whether the process of rafting is beneficial or detrimental [4, 5 and 6], the phenomenon is clearly worthy of study.

The classical method for the prediction of the direction of anisotropic coarsening developed by PINEAU [7], was based on the theory of the elastic energy of inclusions. Specifically, the most energetically favourable morphology was identified, for each given set of elastic constants, within a set of shapes consisting of spheres, infinitely long needles and infinite plates. It was assumed for simplicity that interaction with neighbouring particles was negligible.

The approach of using discrete non-interacting particles, such as those found in low γ' volume-fraction alloys, was also followed by KHACHATURYAN and co-workers [8] to study more complex particle morphologies. This idea has been further extended by THOMSON and VOORHEES [9], in a consideration of the lowest energy shape for individual non-interacting particles. Experimental and theoretical studies have shown that under certain conditions particle splitting can be favoured, in contrast to the usual particle coalescence behaviour [10]. Some recent studies by Johnson and co-workers have also analysed how the elastic strain energy in the matrix can produce a driving force to bring particles closer together, which results in the coalescence of particles. However, this has only been explored for simplified elastically isotropic systems in the absence of external stresses [11].

Purely elastic methodologies present an obvious shortcoming in that for non-trivial inclusion shapes it is necessary to treat the energy as a distributed field, whose intricate description inhibits a prediction of the behaviour in real systems. Moreover, dealing with particles with more complex shapes requires the use of finite element methods [9, 12]. A way to circumvent these problems would be using a microstructural approach which also involves the localisation of the energy. Ideally, the new criterion should allow for a simple incorporation into simulation procedures to model the rafting behaviour [13].

3. Anisotropic distribution of misfit dislocations

During ageing of superalloys at elevated temperatures the elastic strain caused by a mismatch

$$\delta = \frac{2(a_{\gamma'} - a_{\gamma})}{(a_{\gamma'} + a_{\gamma})} \tag{3.1}$$

between the lattice parameters a_γ and $a_{\gamma'}$ of the γ and γ' phases, respectively, is relieved by the formation of misfit dislocations. These [110]⟨111⟩-type edge dislocations form networks which transform the coherent interfaces between the two phases into semi-coherent ones. The significance of this is that it relieves the elastic strains present, which inhibit the growth and coalescence of the γ' particles.

Experimental work [14] has shown that, in [001]-oriented single crystals, when a uniaxial stress is applied there is a tetragonal distortion of both phases, such that the lattice parameters increase in the direction of an applied tensile stress and decrease in the perpendicular directions. This behaviour inverts under compressive stresses. By calculating the number of dislocations required to relieve the unconstrained misfit on a unit length of $\gamma - \gamma'$ interface, we can determine its interfacial energy. The tetragonal distortion occurs in both the matrix and the precipitate, but since the elastic moduli of the two phases are different, their expansions will differ, and the mismatch between the lattice parameters of the two phases will change, and will do so anisotropically. The number of dislocations required to relieve these strains will thus be unequal in those two principal directions, due to both the direct strain along the load axis [14 and 15] and the Poisson strain in the axes perpendicular to it, as shown schematically in Fig. 1.

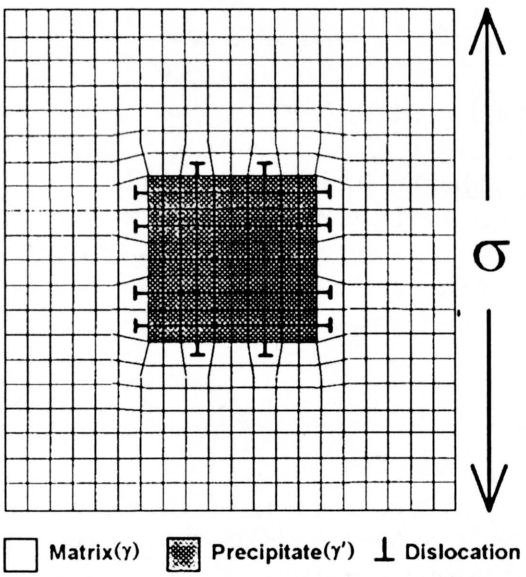

FIG. 1. Schematic of the anisotropy of dislocation formation under an applied tensile stress.

Thus, once the energy of a dislocation has been calculated, by determining the number of dislocations on a given interface we can find the total energy. The value calculated for this energy in the unstressed state is found to be in agreement with experimentally measured $\gamma - \gamma'$ surface energies [1]. By evaluating the interfacial

energies in the directions parallel and perpendicular to the stress axis, one can determine the degree of anisotropy in the interfacial energy. Since the tendency to reduce the surface energy of the system will lead to the growth of the lower energy surfaces at the expense of the higher ones, the value of this energy anisotropy can be used to predict anisotropic coarsening.

4. Criterion based on the energy ratio

We can incorporate these ideas into a quantitative criterion to predict the precipitate morphology if we consider the energy associated to the distribution of the misfit dislocations. In order to relieve the interfacial stresses produced by the lattice misfit at the $\gamma - \gamma'$ interface, a regular distribution of non-interacting dislocations develops, whose density is given by the difference in the number of crystal planes per unit length in the two phases, $N = |a_\gamma - a_{\gamma'}|/|a_\gamma \cdot a_{\gamma'}|$. The total interfacial energy (per unit length of interface and unit length of dislocation) is then given by the product of this density multiplied by the energy per unit length of each dislocation, $U_{\text{disloc}} = \alpha \cdot G_\gamma \cdot a_\gamma^2$ (with G_γ, the shear modulus proportional to E_γ, the elastic modulus) and can be expressed by [1]

$$U = N U_{\text{disloc}} = K \frac{a_\gamma}{a_{\gamma'}} |a_{\gamma'} - a_\gamma| E_\gamma , \tag{4.1}$$

where K is a numerical constant.

When an external stress is applied along one of the principal lattice directions of the single crystal, different strains will be produced in the γ and γ' phases, according to their different elastic moduli. As a consequence, the misfit between the two phases, and thus the number of dislocations required to relieve the strain produced, will be controlled by the stress applied. If we explicitly incorporate this dependence, along the load axis

$$U^{\text{para}} = K(1 + \sigma/E_\gamma) \frac{a_\gamma^0}{a_{\gamma'}^0} \left| a_{\gamma'}^0 - a_\gamma^0 \frac{1 + \sigma/E_\gamma}{1 + \sigma/E_{\gamma'}} \right| E_\gamma , \tag{4.2}$$

where a_γ^0 and $a_{\gamma'}^0$ are the lattice parameters in the absence of an applied stress. In contrast, the strains due to the Poisson effect will govern the stress dependence in the perpendicular directions, giving

$$U^{\text{perp}} = K(1 - \nu\sigma/E_\gamma) \frac{a_\gamma^0}{a_{\gamma'}^0} \left| a_{\gamma'}^0 - a_\gamma^0 \frac{1 - \nu\sigma/E_\gamma}{1 + \nu\sigma/E_{\gamma'}} \right| E_\gamma . \tag{4.3}$$

The ratio R of these two energies can be used as a measure of the driving force for the interfaces in one direction to grow at the expense of those in the

other one, resulting in a reduction in the total energy of the system. This ratio can be expressed as

$$R = \frac{U^{\text{para}}}{U^{\text{perp}}} = \frac{(1 + \sigma/E_\gamma)}{(1 - \nu\sigma/E_\gamma)} \left| \frac{a^0_{\gamma'} - a^0_\gamma \dfrac{1 + \sigma/E_\gamma}{1 + \sigma/E_{\gamma'}}}{a^0_{\gamma'} - a^0_\gamma \dfrac{1 - \nu\sigma/E_\gamma}{1 - \nu\sigma/E_{\gamma'}}} \right| \tag{4.4}$$

and provides a criterion to predict the morphology in a superalloy undergoing coarsening. In essence, when $R = 1$ the energies U^{para} and U^{perp} are equal, and thus there will be no interfacial energy or precipitate shape anisotropy. When $R > 1$, the energy at the interfaces parallel to the stress axis exceeds that of the perpendicular interfaces. As a result of this, there will be a tendency to reduce the higher energy interfaces, and thus the γ' precipitates will oblate and, for high precipitate volume fractions, coalesce forming extended plates perpendicular to the load axis. Conversely, when $R < 1$, the coalescence takes place parallel to the stress axis, and needles develop. Since the value of R contains information not only about the preferential coarsening direction but also on the degree of anisotropy of the interfacial energy, a quantitative prediction of the changes in precipitate morphology is also possible.

It is important to point out that since the material properties used to compute R, such as the lattice parameters and the elastic moduli of the two phases, vary with temperature, what the criterion really provides is a prediction of the rafting behaviour for a material at a given stress and temperature.

5. Classical morphology prediction map

The classical representation used to predict the rafting morphology in a superalloy is a plot of the shape giving the minimum elastic energy for different conditions of applied stresses and elastic moduli of the two phases. The best known diagram produced in this way was developed by PINEAU [7], and took only three extreme shapes into account: infinite large plates, infinitely long needles and spheres. In Fig. 2a, the most energetically favourable of these three configurations is plotted versus two nondimensional variables encompassing the stress level and the elastic properties of the alloy, namely $X = \sigma/(E_\gamma \cdot \delta)$, the longitudinal strain measured in units of the misfit, and $Y = E_{\gamma'}/E_\gamma$, the ratio of the elastic moduli. A similar diagram can be constructed using the new criterion based on the energy ratio by reformulating the expression for R in Eq. (4.4) as a function of the same nondimensional parameters, i.e.

$$R(X, Y, \nu, \delta) = \frac{1 + X\delta}{1 - \nu X\delta} \cdot \frac{\dfrac{2 + \delta}{2 - \delta} - \dfrac{1 + X\delta}{1 + X\delta/Y}}{\dfrac{2 + \delta}{2 - \delta} - \dfrac{1 - \nu X\delta}{1 - \nu X\delta/Y}}. \tag{5.1}$$

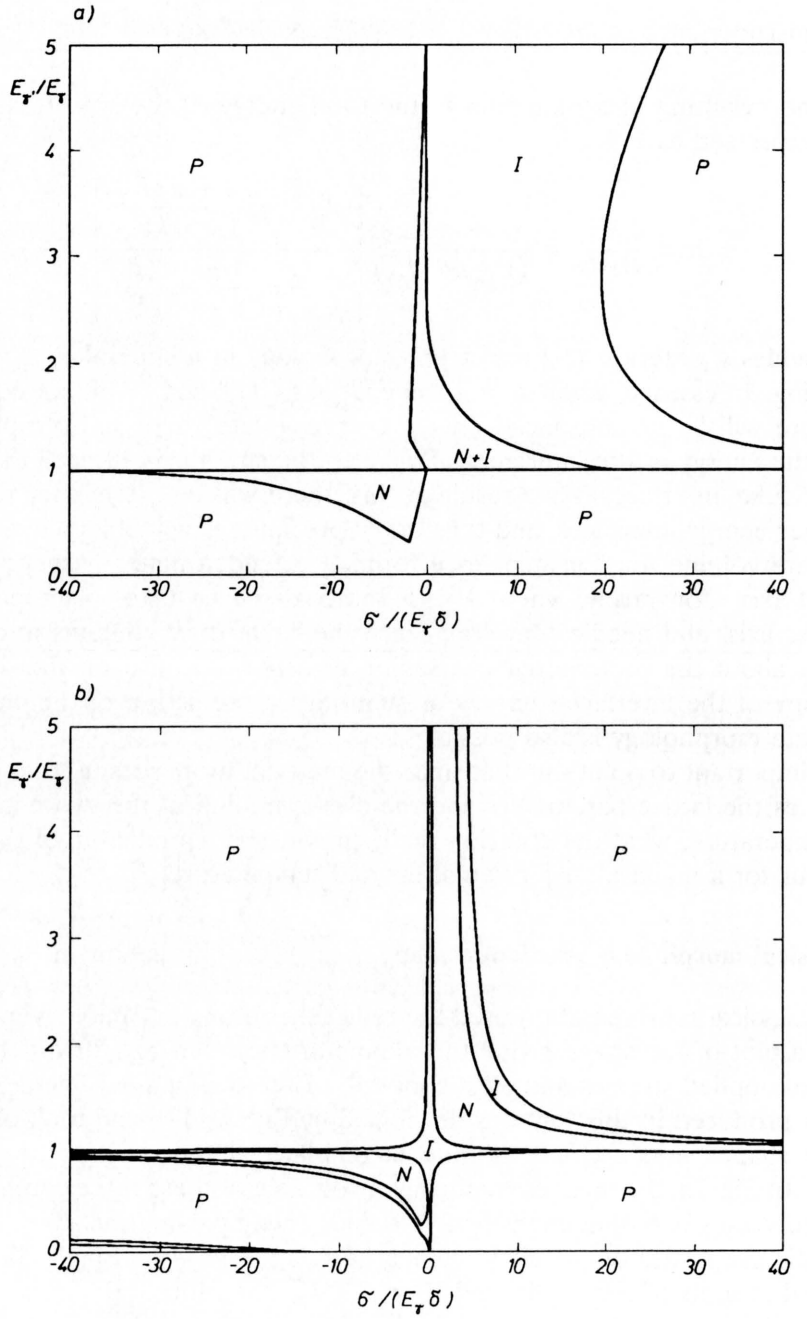

FIG. 2. a) Classical morphology prediction map based on the elastic energy criterion [7]. The symbols P, N and I represent Plate, Needle and Isotropic coarsening, respectively. b) Morphology prediction map based on the new dislocation-based criterion. The boundaries between the regions are at $R = 0.9$ and $R = 1.1$, and the symbols describing the regions are as in Fig. 2a.

A contour map of R, as given by Eq. (5.1), has been plotted in Fig. 2b, using a value of $\nu = 0.3$, the one used by Pineau, and a typical value for the lattice mismatch (Eq. (3.1)) of $\delta = -0.0014$, which is the room temperature misfit for superalloy SRR99 [16].

When one compares the diagrams produced using Pineau's work (Fig. 2a) and the new criterion (Fig. 2b), a close similarity can be observed. However, there are some important differences. As the calculations performed in [7] were limited to a small number of points in the diagram, some details which are apparent in the new diagram are found to be missing in Fig. 2a. Specifically, one would expect that between the regions in which plates are predicted and those in which needles are the most favoured structure, an intermediate region of isotropic structures would be found. This is seen to be the case with the new criterion. A second limitation in Pineau's classical analysis is that there are large uncertainties in the energy determination, due to the graphical method used. Owing to this, some regions of the diagram could only be identified as regions in which two particle morphologies are energetically equivalent.

The construction of the classical prediction diagram itself also exhibits certain shortcomings. Specifically, the location of the point corresponding to the desired data requires some calculation, and the effects of individual parameters, such as temperature, are not easily visualised. In fact, for a specific superalloy when only one horizontal line in the classical map is required to show the stress dependence of the rafting behaviour at a given temperature, a complex curve may be required in order to visualise the behaviour over a temperature range. It is important to point out that these diagrams are plotted for specific values of material parameters, and thus to perform realistic predictions alloy specific maps are required. Given these limitations, we have chosen to produce prediction maps for each specific alloy in which R contours are plotted versus axes of applied stress and temperature.

6. Temperature-stress maps for real superalloys

For each real superalloy, a temperature-stress map can be constructed to predict the microstructural morphology if the thermal expansion coefficient and the temperature dependence of the elastic modulus are known for both phases. The use of these alloy-specific diagrams clearly shows how two parameters in particular, strongly affect the rafting behaviour of superalloys. It is generally considered that the magnitude of the inherent mismatch between the γ and γ' phases is the most significant factor controlling the degree of rafting produced by an applied stress. Experimental work [17, 18, 19] has shown how the degree of rafting of a variety of alloys can be correlated with the mismatch. However, relatively little research has been devoted to the effect that a change in the ratio of the elastic moduli of the two phases produces. The $T - \sigma$ maps considered below show that more emphasis should be put on the study of this latter parameter.

6.1. Superalloy NASAIR 100

The micromechanical properties of NASAIR 100 are typical of modern single crystal superalloys, which generally have a negative value for the lattice mismatch and a high volume fraction of γ' phase at operation temperatures. This is also the case, for example, for MAR-M200, CMSX-6 or AM1. At high temperatures, the alloy NASAIR 100 has been found to exhibit plate forming behaviour during tensile creep [2, 4] and needle formation under compressive loads.

In order to construct the temperature-stress diagram based on the R criterion, knowledge of the temperature dependence of the material properties is required. The plots of the lattice mismatch versus temperature and the elastic moduli versus temperature for NASAIR 100, which we show in Figs. 3 and 4, respectively, have

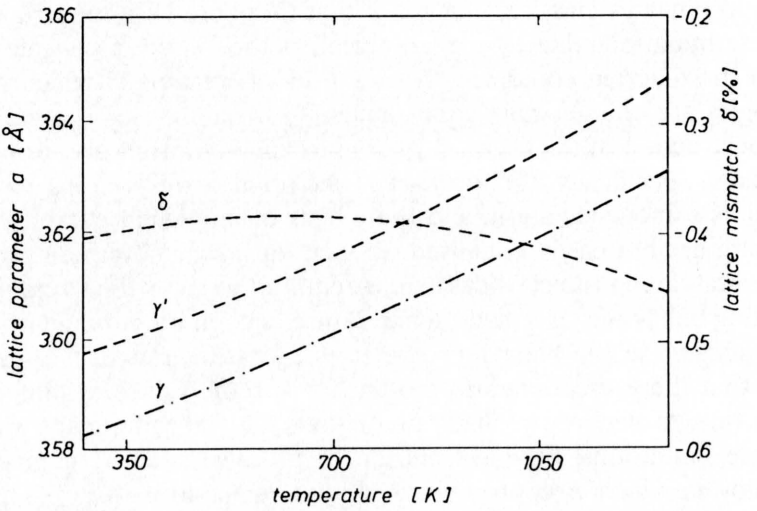

FIG. 3. Temperature dependence of lattice parameters and lattice mismatch in NASAIR 100, after Nathal [21].

been produced using literature data [20 and 21]. In Fig. 3, the interfacial misfit is seen to change by a relatively small amount, from -0.00386 to -0.00454, when temperature increases from 273 K to 1273 K. In contrast, the elastic modulus of γ', which at low temperatures is smaller than that of the γ phase (i.e. $E_{\gamma'}/E_{\gamma} < 1$), shows a shallower decline with temperature, and γ' becomes stiffer than γ at approximately 850 K. Thus, the change in the ratio of $E_{\gamma'}/E_{\gamma}$ from 0.83 to 1.12 over the same temperature range, as shown in Fig. 4, proves to be more significant. This alloy is therefore a good example of why the elastic modulus ratio should be considered to be the most significant variable in the prediction of the anisotropic coalescence of superalloys.

The most important characteristic of the diagram in Fig. 5 is the point at which the predicted direction of rafting inverts when temperature changes. At this point, which corresponds to equal elastic moduli of the γ and γ' phases, according to

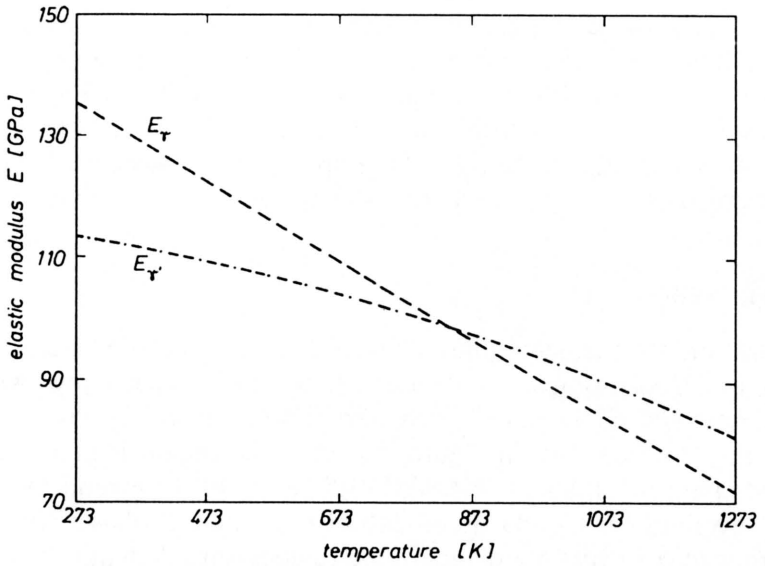

FIG. 4. Temperature dependence of elastic modulus in NASAIR 100 [20].

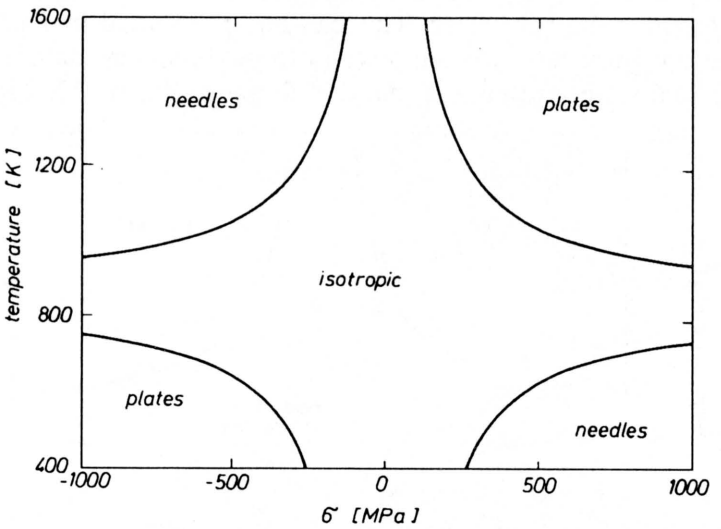

FIG. 5. $T - \sigma$ diagram for NASAIR 100 produced with contours at $R = 0.9$ and $R = 1.1$.

elasticity theory an applied stress would have no effect on the misfit between the two phases, and thus would not produce anisotropy. In our approach, R deviates slightly from one, with a change of the same order as the strain produced, but this is not large enough to affect the isotropic morphology significantly. The existence of this modulus ratio threshold ($E_\gamma = E_{\gamma'}$) is important in explaining the creep behaviour of superalloys. For example, it has been reported [22] that in CMSX-4, at some temperatures high enough for coarsening to occur at an

appreciable rate, coarsening can occur isotropically even under applied loads. At higher temperatures, under similar stress conditions anisotropy is detected. This behaviour manifests itself in the diagram for NASAIR 100 in Fig. 5 as the horizontal boundary between isotropic and plate or needle formation. The diagram also shows that a change in the sign of the applied stress switches the microstructural morphology from plates perpendicular to the stress axis to needles parallel to it or *vice versa*.

6.2. Superalloy SRR99

The diagram for this superalloy (Fig. 6) has been included here in order to show that the R criterion is subtle enough to predict that alloys with broadly similar microstructural responses to external stresses will behave in ways that are noticeably different. In the figure, the isotropic region is predicted to be at a higher temperature than for NASAIR 100, and also to extend over a smaller range. Since values for the elastic moduli of the γ and γ' phases were not available, in order to construct the diagram, the temperature dependence of NASAIR 100 was extrapolated using the elastic modulus for bulk SRR99 [23]. Whilst this method only provides an approximate prediction, the correlation with experimental data is found to be very good. This can be appreciated in Fig. 7, where we superimpose our prediction for the plate-isotropic boundary onto a summary of the experimental rafting responses found in literature [5, 16, 17, 24].

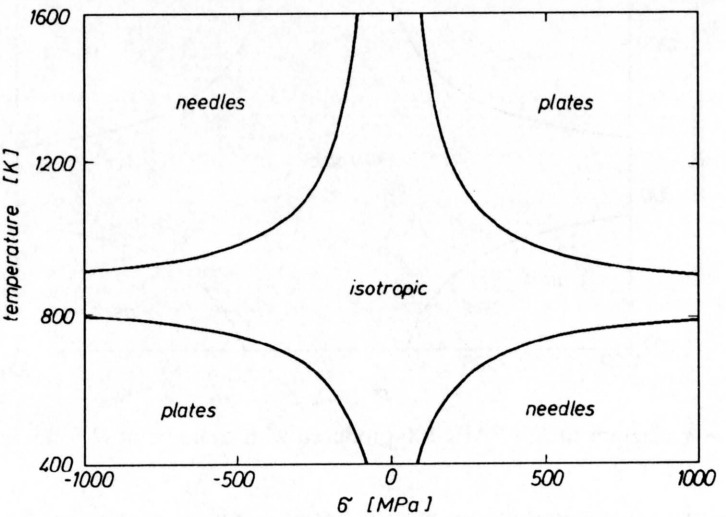

FIG. 6. $T - \sigma$ diagram for SRR99 produced with contours at $R = 0.9$ and $R = 1.1$.

6.3. Superalloy CMSX-2

The second factor controlling the rafting behaviour of superalloys is the inherent misfit between the two phases, though its significance varies strongly from

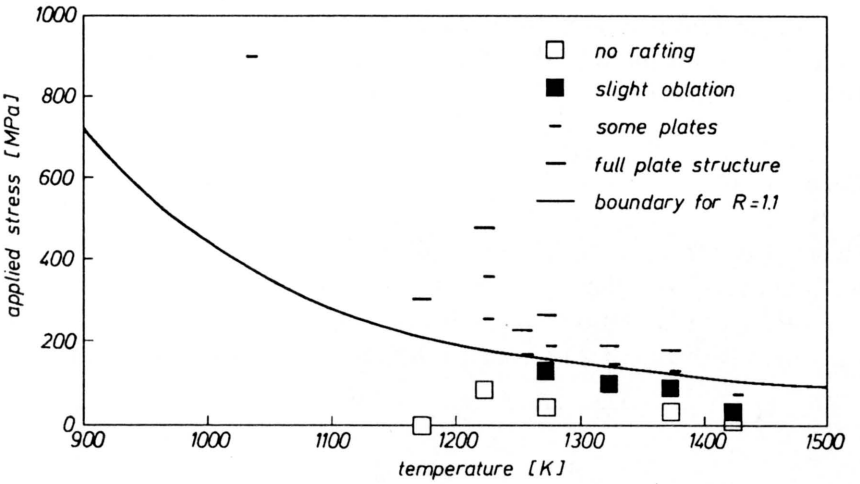

FIG. 7. Comparison of experimental and predicted plate-isotropic boundary in SRR99.

one alloy to another. Several alloys, including CMSX-2, have a positive misfit at low temperatures and a negative one at high temperatures [25 and 26]. Thus, their behaviour follows that of NASAIR 100 (Fig. 5) and SRR99 (Fig. 6) at high temperatures, but deviates markedly at low temperatures, where a second inversion in the rafting behaviour takes place when the sign of the misfit changes. The temperature at which the mismatch becomes zero depends on the external stresses, as can be seen in Fig. 8, where the inversion point is found to increase in temperature when the applied stress becomes less compressive or more tensile. In

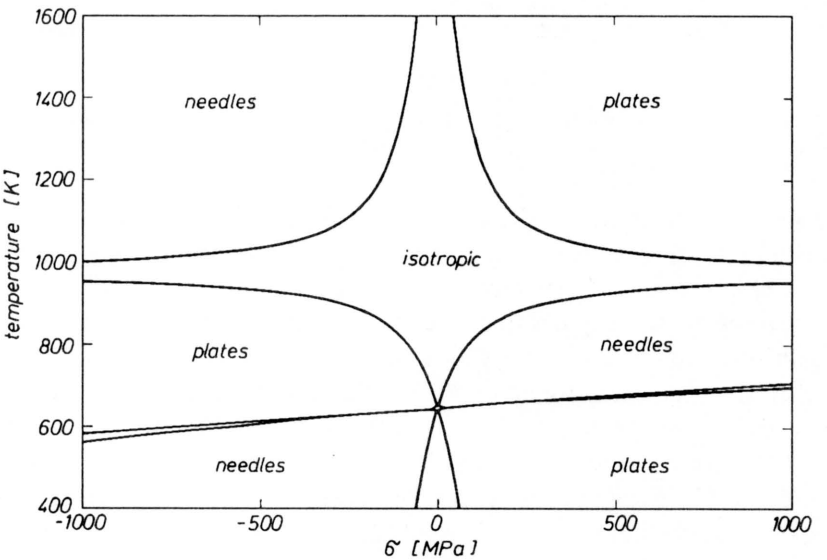

FIG. 8. $T - \sigma$ diagram for CMSX-2 produced with contours at $R = 0.9$ and $R = 1.1$.

CMSX-2, this second inversion takes place at temperatures which are too low for diffusion to be significant, and thus this cannot be confirmed by experimentation. However, in principle this may occur at higher temperatures for other alloys.

6.4. Model binary alloy

We have also studied a model binary alloy with a composition of Ni-15 at.% Al [27], which in contrast to the alloys discussed above, exhibits both a positive misfit and an elastic modulus ratio that is always larger than one. The corresponding diagram, which is distinctly different to the previous ones, is shown in Fig. 9. As

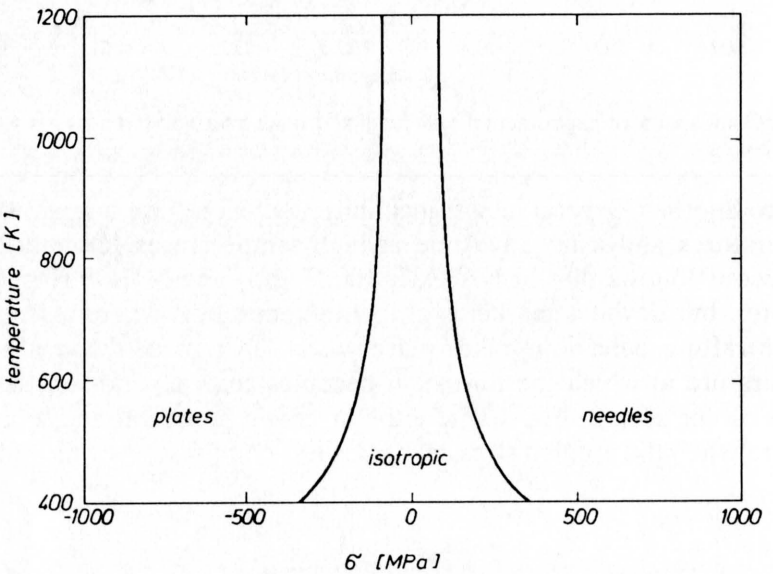

FIG. 9. $T - \sigma$ diagram for the model binary alloy Ni-15at.% Al produced with contours at $R = 0.9$ and $R = 1.1$.

would be expected from the positive lattice misfit, the diagram predicts that needles form under tensile stresses and plates are produced under compressive ones. What is more interesting is the fact that there is no region in which the elastic moduli converge to the same value, and thus there is no minimum temperature at which anisotropy ceases to be thermodynamically possible. Consequently, in contrast with the materials discussed above, the minimum temperature for rafting to occur is entirely controlled by kinetics. This is in agreement with experimental evidence [27] showing anisotropic coalescence in this alloy at temperatures as low as 1023 K (750° C), a temperature at which only isotropic coalescence is found in most modern superalloys [22]. The ability to predict the disparate behaviour of the materials discussed above is clear evidence of the wide applicability of the dislocation-based criterion.

7. Outlook

The inherent simplicity of the R based criterion facilitates its incorporation into a lattice model, where Monte Carlo conserved dynamics is able to simulate the evolution of coalescence processes in superalloys [13]. In this way, the evolution of the $\gamma - \gamma'$ microstructure has been simulated under a wide range of temperatures and applied tensile and compressive stresses. These simulations have reproduced the behaviour found experimentally regarding aspect ratios and other relevant properties, and have allowed us to determine a relationship between the simulation time, temperature and stress parameters and the experimental ones. The lattice model can be further refined by explicitly incorporating the kinetic effects associated with diffusion through the dislocation cores. Thus, the criterion based on the anisotropy of the distribution of misfit dislocations is shown to be useful not only to construct prediction maps but also to simulate the evolution of the coarsening morphology.

We envisage further development in different directions. Firstly, we intend to extend the criterion by producing a three-dimensional formulation. This will allow us to model the effects of multiaxial stress systems on the rafting behaviour. One application which is of particular interest within the framework of our research program is the effect of coating-induced stresses on the microstructural morphology. Our final aim is to be able to use these micromechanical simulations to determine stress histories in a material exposed to complex temperature and stress cycles, such as those occurring under thermomechanical fatigue (TMF).

8. Conclusions

The anisotropy in the distribution of interfacial dislocations has been shown to provide a better criterion for prediction of precipitate morphology in single crystal nickel-base superalloys under load and at elevated temperatures than is currently possible using classical elasticity-based methods.

Contour plots of the interfacial energy ratio R, which has been reformulated as a function of the nondimensional parameters involved in Pineau's classical prediction map, provide the most favourable morphology for the different stress and temperature conditions. These temperature-stress diagrams have been proven to be more informative than the classical prediction map, and have allowed direct comparison with experimental morphologies.

To illustrate the effects of the individual nondimensional parameters we have constructed T-σ diagrams for a range of real alloys, which show markedly different characteristics. Using these diagrams we have shown that the ratio of the elastic moduli is the most significant parameter, due to its temperature dependence, which in the commercial alloys considered led to an inversion in microstructural morphology. The sign of the lattice mismatch is shown to be important, but its magnitude is found to be of less significance.

9. Acknowledgement

This work has been performed within the Specific Research and Development Programme of the European Commission.

References

1. D.J. ARRELL and J.L. VALLÉS, *Interfacial dislocation based criterion for the prediction of rafting behavior in superalloys*, Scripta Metall. Mater., **30**, 149–153, 1994.
2. M.V. NATHAL, R.A. MACKAY and R.G. GARLICK, *Temperature dependence of $\gamma - \gamma'$ lattice mismatch in nickel-based superalloys*, Mater. Sci. Engng., **75**, 195–205, 1985.
3. J.K. TIEN and S.M. COPLEY, *The effect of uniaxial stress on the periodic morphology of coherent gamma prime precipitates in nickel-base superalloy crystals*, Metall. Trans., **2**, 215–219, 1971.
4. M.V. NATHAL, R.A. MACKAY and R.V. MINER, *Influence of precipitate morphology on intermediate temperature creep properties of a nickel-base superalloy single crystal*, Metall. Trans., **20A**, 133–141, 1989.
5. M. FELLER-KNIEPMEIER and T. LINK, *Correlation of microstructure and creep stages in the $< 100 >$ oriented superalloy SRR99 at 1253 K*, Metall. Trans., **20A**, 1233–1238, 1989.
6. D. AYRAULT, A. FREDHOLM and J.-L. STRUDEL, [in:] High Temperature Alloys, Their Exploitable Potential, J.B. MARRIOT *et al.* [Eds.], p. 71, Elsevier Applied Science, Amsterdam 1987.
7. A. PINEAU, *Influence of uniaxial stress on the morphology of coherent precipitates during coarsening – elastic energy considerations*, Acta Metall., **24**, 559–564, 1976.
8. A.G. KHACHATURYAN and V.N. HAIRAPETYAN, *Elastic energy and shape of new phase coherent inclusions*, Phys. Stat. Sol., **57**, 801–813, 1973.
9. M.E. THOMPSON, C.S. SU and P.W. VOORHEES, *The equilibrium shape of a misfitting precipitate*, Acta Metall. Mater., **42**, 2107–2122, 1994.
10. A.G. KHACHATURYAN, S.V. SEMENOVSKAYA and J.W. MORRIS Jr, *Theoretical analysis of strain-induced shape changes in cubic precipitates during coarsening*, Acta Metall., **36**, 1563–1572, 1988.
11. T.A. ABINANDANAN and W.C. JOHNSON, *Coarsening of elastically interacting coherent particles*, Acta Metall. Mater., **41**, 17–39, 1993.
12. J. GAYDA and D.J. SROLOVITZ, *A Monte Carlo-Finite Element model for strain energy controlled microstructural evolution: "Rafting" in superalloys*, Acta Metall., **37**, 641–650, 1989.
13. J.L. VALLÉS and D.J. ARRELL, *Monte Carlo simulation of anisotropic coarsening in nickel-base superalloys*, Acta Metall. Mater., **42**, 2999–3008, 1994.
14. D. BELLET and P. BASTIE, *Temperature dependence of the lattice parameter of the γ and γ' phases in the nickel-based superalloy CMSX-2. Part I. Observation of a tetragonal distortion of the γ' phase at high temperature by γ-ray diffractometry*, Philos. Mag. B., **64**, 135–141, 1991.
15. A. HAZOTTE *et al.*, *On the contribution of internal stresses to the high-temperature broadening of gamma-ray diffraction peaks in a Ni-based single crystal*, Philos. Mag. Lett., **66**, 189–196, 1992.
16. H.A. KUHN *et al.*, *An X-ray study of creep-deformation induced changes of the lattice mismatch in the γ'-hardened monocrystalline nickel-base superalloy SRR99*, Acta Metall. Mater., **39**, 2783, 1991.
17. H.M. TAWANCY, N.M. ABBAS and A.I. AL-MANA, *Thermal stability of advanced Ni-base superalloys*, J. Mater. Sci., **29**, 2445–2458, 1994.
18. N. LOUAT, K. SADANANDA and M.A. IMAM, *Morphological stability of γ' precipitates in nickel-base superalloys*, Published in the Proceedings of TMS-AIME Fall Meeting, Toronto, Canada, 299–315, 1985.
19. M.V. NATHAL and L.J. EBERT, *The influence of cobalt, tantalum and tungsten on the microstructure of single crystal nickel-base superalloys*, Metall. Trans., **16A**, 1849–1862, 1985.
20. J. GAYDA and R.A. MACKAY, *Analysis of γ' shape changes in a single crystal Ni-base superalloy*, Scripta Metall., **23**, 1835–1838, 1989.
21. M.V. NATHAL, R.A. MACKAY and R.G. GARLICK, *Temperature dependence of $\gamma - \gamma'$ lattice mismatch in Nickel-base superalloys*, Mater. Sci. Engng., **75**, 195–205, 1985.
22. T.M. POLLOCK and A.S. ARGON, *Directional coarsening in nickel-base single crystals with high volume fractions of coherent precipitates*, Acta Metall. Mater., **42**, 1859–1874, 1992.

23. D.J. ARRELL and J.L. VALLÉS, [in:] Localized Damage II – Computer-Aided Assessment and Control, M.H. ALIABADI [Ed.], Computational Mechanics Publications, Southampton, pp. 279–285, 1994.

24. D.G. GOODALL, Private communication.

25. A. HAZOTTE *et al.*, *On the contribution of internal mismatch stresses to the high-temperature broadening of gamma-ray diffraction peaks in a Ni-based single crystal*, Philos. Mag. Lett., **66**, 189–196, 1992.

26. D. BELLET and P. BASTIE, *Temperature dependence of the lattice parameter of the γ and γ' phases in the nickel-based superalloy CMSX-2. Part II. Neutron diffraction study of the lattice parameter mismatch*, Philos. Mag. B, **64**, 143–152, 1991.

27. T. MIYAZAKI, K. NAKAMURU and H. MORE, *Experimental and theoretical investigations on morphological changes of γ' precipitates in Ni-Al single crystals during uniaxial stress-annealing*, J. Mater. Sci., **14**, 1827–1837, 1979.

JOINT RESEARCH CENTRE
INSTITUTE FOR ADVANCED MATERIALS, PETTEN, THE NETHERLANDS.

Received November 15, 1994.

Arch. Mech., 47, 3, pp. 617–633, Warszawa 1995

Finite deformation analysis of motion of granular material in a silo (*)

Z. WIĘCKOWSKI (ŁÓDŹ) and M. KLISIŃSKI (LULEÅ)

MOTION OF a granular material during silo discharging is analysed in the paper. The mechanical behaviour of the granular material is described using the model of elastic-perfectly plastic solid with the yield condition of the Drucker-Prager type. The phenomenon of friction between the stored material and silo walls is taken into account – the Coulomb model of friction is utilized in the analysis. The large displacement, large strain problem is described using the updated Lagrangian formulation, and solved with the help of the finite element method. The plane strain and axisymmetric problems are investigated.

1. Introduction

THE MAIN AIMS of the analysis of motion of granular materials in silos are to determine the loads acting on the silo walls during the different stages of its operation, and flow pattern during discharging the silo. Three stages of the operation process are interesting from the engineering point of view: filling the silo, storing the material, and discharging the silo.

In the past, it used to be a common practice to decouple the theoretical predictions of stresses and deformations within the bulk material, although it is obvious that such an approach means the disregarding of constitutive equations. The existing design rules employ semi-empirical expressions for the stress distribution, such as those suggested by WALTERS [1] and ENSTAD [2]. Velocity distribution can be obtained for simple geometries using idealized constitutive assumptions, as described by JENIKE and SHIELD [3].

Recently, significant improvements have been made in formulating the fundamental governing equations based on continuum mechanics. The appropriate relations are used to describe the behaviour of the bulk material. The resulting initial-boundary value problems are solved using numerical techniques, in particular the finite element method. It should be emphasised that the important pioneering work has been carried out by EIBL, ROMBACH and HÄUSSLER (see e.g. [4–5]).

Two approaches have been used to describe the motion of the material inside a silo. In the first approach, the granular material is treated as the non-classical fluid [4–7], whereas in the second one, the material is treated as the solid body [7]. Two different ways of description of motion are used in these two approaches: the Eulerian description, and the Lagrangian one, respectively.

(*) Paper presented at 30th Polish Solid Mechanics Conference, Zakopane, September 5–9, 1994.

This work concerns the solid approach to the modelling of motion of a granular material in a silo. The material behaviour is described by the elastic-plastic model. The paper contains the formulation of the problem being under consideration, the description of the method used to solve the problem, and some numerical results.

2. Setting of the problem

Let us consider a time interval $I = [0, T]$, where $T > 0$. Let $\Omega^t \subset \mathcal{R}^3$ denote the region occupied by the body at time $t \in I$, the boundary $\partial\Omega^t$ of which consists of three parts Γ_u^t, Γ_σ^t, and Γ_f^t such that

$$\overline{\Gamma_u^t} \cup \overline{\Gamma_\sigma^t} \cup \overline{\Gamma_f^t} = \partial\Omega, \qquad \Gamma_u^t \cap \Gamma_\sigma^t = \Gamma_u^t \cap \Gamma_f^t = \Gamma_f^t \cap \Gamma_\sigma^t = \emptyset.$$

Although two-dimensional problems are solved in the paper, the general 3-dimensional case is considered throughout this section.

2.1. Boundary conditions

We assume that the displacements are known on the boundary part Γ_u^t

$$u_i = U_i^t \qquad \text{on} \quad \Gamma_u^t, \tag{2.1}$$

and that for the second boundary part Γ_σ^t the following relation is satisfied

$$\sigma_{ji}^t n_j^t = t_i^t \qquad \text{on} \quad \Gamma_\sigma^t, \tag{2.2}$$

where σ_{ji}^t is the tensor of Cauchy stresses, $\mathbf{n}^t$ is the unit vector outwardly normal to the boundary $\partial\Omega^t$, t_i is the given Cauchy stress vector. It is assumed that, on the part Γ_f^t, the contact boundary conditions exist, governed by the Coulomb friction law. Let g_N denote the following distance function

$$g_N(\mathbf{x}) = \left(P_i^{\Gamma_w}(\mathbf{x}) - x_i\right) n_i,$$

where $\mathbf{x} \in \Gamma_f^t$, $\mathbf{P}^{\Gamma_w}$ is the operator of projection onto the surface Γ_w of obstacle body (silo wall) defined as follows

$$\|\mathbf{P}^{\Gamma_w}(\mathbf{x}) - \mathbf{x}\| \leq \|\mathbf{y} - \mathbf{x}\| \qquad \forall \mathbf{y} \in \Gamma_w, \tag{2.3}$$

$\mathbf{n}$ is the unit vector inwardly normal to the surface Γ_w with the beginning at the point $\mathbf{P}^{\Gamma_w}(\mathbf{x})$. In (2.3), $\|\cdot\|$ denotes the Euclidean norm of vector $\|\mathbf{z}\| = \sqrt{z_i z_i}$.

The frictional contact conditions can be described by the following set of relations (e.g. [8])

$$\begin{aligned} &g_N \geq 0, \qquad \sigma_N \leq 0, \qquad \dot{u}_N \sigma_N = 0, \\ &f(\sigma_N, \boldsymbol{\sigma}_T) \leq 0, \qquad \dot{u}_{Ti} \sigma_{Ti} \leq 0, \end{aligned} \tag{2.4}$$

where the Coulomb friction condition is applied

$$f(\sigma_N, \boldsymbol{\sigma}_T) = -\mu|\sigma_N| + \|\boldsymbol{\sigma}_T\| \leq 0, \tag{2.5}$$

σ_N and $\boldsymbol{\sigma}_T$ denote the normal and tangential components of the Cauchy stress vector, respectively, $\sigma_N = \sigma_{ij} n_i n_j$, $\sigma_{Ti} = \sigma_{kj} n_k (\delta_{ij} - n_i n_j)$, μ is the friction coefficient, u_N and $\mathbf{u}_T$ are the normal and tangential components of the relative displacement between the closest points of two bodies

$$u_N = \left(u_i(\mathbf{P}^{\Gamma_w}(\mathbf{x}^s)) - u_i(\mathbf{x}^s)\right) n_i,$$
$$u_{Ti} = \left(u_j(\mathbf{P}^{\Gamma_w}(\mathbf{x}^s)) - u_j(\mathbf{x}^s)\right) (\delta_{ij} - n_i n_j).$$

The variational formulation of the contact problem for deformable bodies leads to the implicit variational inequality, some terms of which are non-differentiable functionals (see e.g. [8–9]), what makes the problem difficult to solve. To overcome these troubles, the penalty regularization method can be used for the frictional constraints (2.4), (2.5) (e.g. [10]).

In the regularized form of the friction law, the relation between the normal components of the force rate and the relative velocity has the form

$$\dot{\sigma}_N = \begin{cases} -c_N \dot{u}_N & \text{if } g_N \geq 0, \\ 0 & \text{if } g_N < 0. \end{cases} \tag{2.6}$$

The tangential component of the relative velocity (slip) is expressed as the sum of two parts $\dot{\mathbf{u}}_T^{\mathrm{e}}$ and $\dot{\mathbf{u}}_T^{\mathrm{i}}$, called elastic and inelastic, which satisfy the constitutive relations similar to the elastic-plastic relations [11, 12]

$$\dot{u}_{Ti} = \dot{u}_{Ti}^{\mathrm{e}} + \dot{u}_{Ti}^{\mathrm{i}}, \tag{2.7}$$

$$\dot{u}_{Ti}^{\mathrm{e}} = -\frac{1}{c_T} \dot{\sigma}_{Ti}, \qquad \dot{u}_{Ti}^{\mathrm{i}} = -\dot{\lambda} \frac{\partial f}{\partial \sigma_{Ti}}, \qquad \dot{\lambda} \geq 0, \tag{2.8}$$

where c_N and c_T are the penalty parameters.

It should be noted that the surfaces Γ_u^t, Γ_σ^t, and Γ_f^t vary in time. This means that the boundary conditions of type (2.2)

$$\sigma_{ji}^t n_j^t = 0 \qquad \text{on } \Gamma_\sigma^t,$$

are valid for the part of the body surface Ω^t located below the outlet of a silo, and for the upper free surface, the points of which are candidates to be in contact with a wall of the silo.

For points located on a symmetry axis (if it exists), the following boundary conditions are applied

$$u_N = 0, \qquad \boldsymbol{\sigma}_T = \mathbf{0}$$

which correspond to the bilateral boundary conditions for a smooth wall.

2.2. Equation of virtual work

Let V_U^t be the set of kinematically admissible fields of displacements, which means that every $u_i \in V_U^t$ satisfies the displacement boundary conditions (2.1), and is a sufficiently regular field on Ω^t so that all the mathematical operations used have sense. Using the kinematic and static variables referred to the configuration Ω^t, we can write the principle of virtual work as follows (e.g. [15])

$$\int_{\Omega^t} \sigma_{ij}^t \, \delta\varepsilon_{ij}^t \, dx^t = \int_{\Omega^t} \varrho^t (f_i^t - \ddot{u}_i) \, \delta u_i \, dx^t + \int_{\Gamma_\sigma^t} t_i^t \, \delta u_i \, ds^t + \int_{\Gamma_f^t} \sigma_{ji}^t \, n_j \, \delta u_i \, ds^t, \tag{2.9}$$

where σ_{ij} is the Cauchy stress tensor, $\varepsilon_{ij}^t = \frac{1}{2}\left(\partial u_i/\partial x_j^t + \partial u_j/\partial x_i^t\right)$ is the tensor of small strains, f_i^t and t_i^t are the body and surface forces, respectively, referred to the configuration Ω^t, ϱ^t is the mass density of the material measured in the configuration Ω^t, dx^t and ds^t are the volume and surface elements, respectively. The relation (2.9) is fulfilled for every $\delta u_i \in V_0^t$, where V_0^t denotes the space of displacements fields satisfying the homogeneous boundary conditions $\delta u_i = 0$ on Γ_u^t.

2.3. Constitutive relations

The elastic-plastic material model with the Drucker-Prager yield condition, and the non-associated flow rule is applied to describe the behaviour of the bulk material. It is assumed that the plastic strains have zero dilatation, that is to say, the material is plastically incompressible [6].

Let B denote the convex set of plastically admissible stresses $B = \{\sigma_{ij} : f(\sigma_{ij}) \leq 0\}$, where the Drucker-Prager yield condition is used for the Cauchy stress tensor

$$f(\sigma_{ij}) = q + mp. \tag{2.10}$$

In (2.10), $m = 18\sin\varphi/(9 - \sin^2\varphi)$ is the number depending on the angle of internal friction φ, $p \equiv \frac{1}{3}\sigma_{ii}$, and $q \equiv \sqrt{\frac{3}{2} s_{ij} s_{ij}}$ are stress invariants, where s_{ij} denotes the deviatoric part of the stress tensor, $s_{ij} = \sigma_{ij} - p\,\delta_{ij}$.

The constitutive relations have the following form:

$$d_{ij} = d_{ij}^{\mathrm{e}} + d_{ij}^{\mathrm{p}}, \tag{2.11}$$

$$\overset{\nabla}{\sigma}_{ij} = C_{ijkl} \, d_{kl}^{\mathrm{e}}, \tag{2.12}$$

$$d_{ij}^{\mathrm{p}} = \begin{cases} \dot{\lambda} \dfrac{\partial g}{\partial \sigma_{ij}} & \text{if} \quad f(\sigma_{ij}) = 0, \\ 0 & \text{if} \quad f(\sigma_{ij}) < 0, \end{cases} \tag{2.13}$$

where $\dot{\lambda} \geq 0$, and g is the plastic potential defined here by the relation $g = q$. The notation used in (2.11)–(2.13) is as follows: $d_{ij} = \frac{1}{2}(\dot{u}_{i,j} + \dot{u}_{j,i})$ is the tensor of deformation rate, d^{e}_{ij} and d^{p}_{ij} are its elastic and plastic parts, respectively,

$$\overset{\nabla}{\sigma}_{ij} = \dot{\sigma}_{ij} - \sigma_{ik}\,\dot{\omega}_{kj} - \sigma_{jk}\,\dot{\omega}_{ki} \tag{2.14}$$

is the Jaumann stress rate tensor, $\dot{\omega}_{ij} = \frac{1}{2}(\dot{u}_{j,i} - \dot{u}_{i,j})$ denotes the spin tensor, $C_{ijkl} = \left(\kappa - \frac{2}{3}\mu\right)\delta_{ij}\,\delta_{kl} + \mu(\delta_{ik}\,\delta_{jl} + \delta_{il}\,\delta_{jk})$ is the tensor of elastic constants, where κ and μ are the bulk and shear moduli, respectively.

The constitutive model of a granular material, used in the paper, is simple, and such important effects like plastic hardening and dependence of elastic constants on the current stress state is not taken into account. It should be treated as the first step in the analysis of silo discharging. More accurate material models like that known from literature, the elastic-plastic model of LADE [13], and the generalized hypoelastic model proposed by KOLYMBAS [14] must be studied.

2.4. Initial conditions

The following initial conditions are applied: $u_i(0) = u^{\mathrm{s}}_i$, $\dot{u}_i(0) = 0$, $\sigma_{ij}(0) = \sigma^{\mathrm{s}}_{ij}$, where u^{s}_i is the static deformation of the bulk material caused by the gravity forces, and σ^{s}_{ij} denotes the corresponding field of stresses.

3. Finite element solution

The solution of the problem can be found, using the incremental procedure with the updated Lagrangian approach, for finite number of time instants $t_1, t_2, \ldots, t_n, \ldots, t_N$ $(0 < t_1 < t_2 < \ldots < t_n < \ldots < t_N = T)$. Assuming that the solution of the problem is known for the time $t \equiv t_n$, the equation of virtual work can be written for the instant $t + \Delta t \equiv t_{n+1}$ as follows (e.g. [15]):

$$\int_{\Omega^t} S^{t+\Delta t}_{ij}\,\delta E_{ij}\,dx^{\mathrm{t}} = \int_{\Omega^t} \varrho^{\mathrm{t}}(f^{t+\Delta t}_i - \ddot{u}_i)\,\delta u_i\,dx^{\mathrm{t}} + \int_{\Gamma^{t+\Delta t}_\sigma} t^{t+\Delta t}_i \delta u_i\,ds^{t+\Delta t} + \int_{\Gamma^{t+\Delta t}_f} \sigma^{t+\Delta t}_{ji}\,n_j\,\delta u_i\,ds^{t+\Delta t}, \tag{3.1}$$

where $u_i \equiv u^{t+\Delta t}_i = u^t_i + \Delta u_i$, $S^{t+\Delta t}_{ij} \equiv S^t_{ij} + C^t_{ijkl}\,\Delta E_{kl}$, S_{ij} and E_{ij} are the second Piola-Kirchhoff stress and the Green-Lagrange strain tensors, respectively, both measured in the configuration Ω^t.

3.1. Finite element discretization

Using the Galerkin approximation for the increment of displacements

$$\Delta \mathbf{u} = \mathbf{N}(\mathbf{x})\,\mathbf{U},$$

where $\mathbf{N}$ is the matrix of interpolation functions of class $C^0(\Omega^t)$, and $\mathbf{U}$ is the vector of degrees of freedom, we can obtain, from the equation of virtual work (3.1), the following set of nonlinear differential equations

$$\mathbf{M}\,\ddot{\mathbf{U}} + \mathbf{F}_{t+\Delta t} = \mathbf{R}_{t+\Delta t}, \tag{3.2}$$

where $\mathbf{M}$ is the mass matrix, $\mathbf{F}$ is the vector of nodal internal forces, and $\mathbf{R}$ is the vector of nodal external and nodal contact forces. The problem of finite deformations has been formulated following [16]. The 3- and 6-node, isoparametric, triangular elements have been used in both the plane strain and axisymmetric problems.

3.2. Solution of dynamic problem

To solve the dynamic problem (3.2), the methods of Newmark and Wilson have been implemented [16]. Assuming that the solution of the system is known for the time t, the unknown variables and their time derivatives are approximated for the instant $t + \Theta\Delta t$ using the following relations

$$\begin{aligned}
\dot{\mathbf{U}}_{t+\Theta\Delta t} &= \dot{\mathbf{U}}_t + \Theta\,\Delta t\,\left((1-\delta)\,\ddot{\mathbf{U}}_t + \delta\,\ddot{\mathbf{U}}_{t+\Theta\Delta t}\right), \\
\mathbf{U}_{t+\Theta\Delta t} &= \mathbf{U}_t + \Theta\,\Delta t\,\dot{\mathbf{U}}_t + (\Theta\,\Delta t)^2\left(\left(\frac{1}{2}-\alpha\right)\ddot{\mathbf{U}}_t + \alpha\,\ddot{\mathbf{U}}_{t+\Theta\Delta t}\right),
\end{aligned} \tag{3.3}$$

where $\Theta = 1$, $0 \le \delta \le 1$, $0 \le \alpha \le \frac{1}{2}$ for the Newmark method, and $\Theta \ge 1$, $\delta = \frac{1}{2}$, $\alpha = \frac{1}{6}$ for the Wilson method. After using the relations (3.3), the system (3.2) can be rewritten as the following set of nonlinear algebraic equations

$$\begin{aligned}
&\frac{1}{\alpha\,(\Theta\,\Delta t)^2}\,\mathbf{M}\,\mathbf{U}_{t+\Theta\Delta t} + \mathbf{F}_{t+\Theta\Delta t} \\
&\qquad = \mathbf{R} + \frac{1}{\alpha\,(\Theta\,\Delta t)^2}\,\mathbf{M}\left(\mathbf{U}_t + \Theta\,\Delta t\,\dot{\mathbf{U}}_t + (\Theta\,\Delta t)^2\left(\frac{1}{2}-\alpha\right)\ddot{\mathbf{U}}_t\right),
\end{aligned}$$

which has been solved using the iterational method of the Newton-Raphson type.

3.3. Time-integration of constitutive relations

Using the forward-Euler rule of integration to the relation (2.14), we can write

$$\frac{1}{\Delta t}(\sigma_{ij}^{t+\Delta t} - \sigma_{ij}^{t}) = \overset{\nabla}{\sigma}_{ij} + \sigma_{ik}^{t}\,\dot{\omega}_{kj} + \sigma_{jk}^{t}\,\dot{\omega}_{ki},$$

and obtain stresses at time $t + \Delta t$ as the projection of elastic (trial) stresses

$$\sigma_{ij}^{e} = \sigma_{ij}^{t} + C_{ijkl}\,\Delta\varepsilon_{kl} + \sigma_{ik}^{t}\,\Delta\omega_{kj} + \sigma_{jk}^{t}\,\Delta\omega_{ki}, \tag{3.4}$$

where $\Delta\varepsilon_{ij} = \Delta t\, d_{ij}$, $\Delta\omega_{ij} = \Delta t\,\dot{\omega}_{ij}$, onto the set of plastically admissible stresses B [6]

$$\sigma_{ij}^{e} \in B \Rightarrow \sigma_{ij}^{t+\Delta t} = \sigma_{ij}^{e},$$

$$\sigma_{ij}^{e} \notin B \Rightarrow \begin{cases} \sigma_{ii} < 0 \Rightarrow \sigma_{ij}^{t+\Delta t} = p^{e}\,\delta_{ij} - \dfrac{m\,p^{e}}{q^{e}}\,s_{ij}^{e}, \\ \sigma_{ii} \geq 0 \Rightarrow \sigma_{ij}^{t+\Delta t} = 0. \end{cases}$$

For small gradients of displacements, it follows from the relation [15]

$$\frac{dE_{ij}}{dt} = \frac{\partial x_k}{\partial x_i^t}\frac{\partial x_l}{\partial x_j^t}\,d_{kl}$$

that the tensor $\Delta\varepsilon_{ij}$, occuring in (3.4), can be approximated by the Green–Lagrange strain tensor, $\Delta\varepsilon_{ij} \approx E_{ij}$.

3.4. Solution of contact problem

The problem of contact boundary conditions has been solved using the concept of contact elements described in [12]. In the two-dimensional case considered here, the geometry of the contact element consists of a node and a straight segment of the boundary of an obstacle body. In the two-dimensional case, the element tangent matrix $\mathbf{K}_T^e$ and the element vector of contact forces $\mathbf{R}_f^e$ are represented, in the local coordinate system $(\mathbf{n}, \mathbf{t})$ (where $\mathbf{n}$ and $\mathbf{t}$ are the unit vectors, normal and tangential to the line Γ_w, respectively), as follows:

$$\mathbf{K}_T^e = \begin{bmatrix} c_N & 0 \\ 0 & c_T \end{bmatrix} \qquad \text{in case of stick,}$$

$$\mathbf{K}_T^e = \begin{bmatrix} c_N & 0 \\ -\mu c_N \operatorname{sign}(q_T^{t+\Delta t}) & 0 \end{bmatrix} \qquad \text{in case of slip,}$$

$$\mathbf{R}_f^e = \begin{bmatrix} q_N^{t+\Delta t} \\ q_T^{t+\Delta t} \end{bmatrix},$$

when the contact takes place ($g_N \leq 0$), and $\mathbf{K}_T^e = \mathbf{0}$, $\mathbf{R}_f^e = \mathbf{0}$ otherwise, where

$$q_N^{t+\Delta t} = q_N^t - c_N \Delta u_N,$$
$$q_T^{t+\Delta t} = q_T^t - c_T(\Delta u_T + \Delta\lambda \operatorname{sign}(q_T^{t+\Delta t})),$$

$$\Delta\lambda = \begin{cases} 0 & \text{if } f(q_N^{t+\Delta t}, q_T^e) \leq 0, \\ \dfrac{1}{c_T}\left(-\mu |q_N^{t+\Delta t}| + q_T^e \operatorname{sign}(q_T^{t+\Delta t})\right) & \text{otherwise,} \end{cases}$$

$$q_T^e = q_T^t - c_T \Delta u_T,$$

Δu_N and Δu_T are the normal and tangential increments of nodal displacements.

4. Mesh rezoning

During the deformation process, elements become distorted so significantly that the mesh rezoning is necessary. The element mesh is regenerated when the following condition is violated at any integration point within a silo

$$\sqrt{\left(\frac{E_{11} - E_{22}}{2}\right)^2 + (E_{12})^2} \leq E_{\text{sh}}^{\max}, \tag{4.1}$$

where $E_{\text{sh}}^{\max}$ is the given number, $E_{\alpha\beta}$ ($\alpha, \beta = 1, 2$) is the Green-Lagrange strain tensor measuring the deformation of the element at an integration point relevant to the transformation from the reference to real element.

The nodal variables, like velocities, related to the new element mesh, are calculated using the interpolation formula

$$\mathbf{v}(x_P, y_P) = \mathbf{N}(\xi_P, \eta_P)\, \mathbf{v}_e,$$

where $\mathbf{N}(\xi_P, \eta_P)$ are the values of shape functions calculated for reference coordinates of the element (belonging to the old mesh), in which the new node is located, $\mathbf{v}_e$ is the vector of nodal values of the old element.

The state variables, like stresses and mass density, defined at integration points, are transformed from the old mesh to the new one, using the collocation method. The method is applied to the reference space of the old element. For example, the new values of stress components are calculated using the formula

$$\sigma_{ij}(\xi_P, \eta_P) = \mathbf{P}^{\mathrm{T}}(\xi_P, \eta_P) \begin{bmatrix} \mathbf{P}^{\mathrm{T}}(\xi_1, \eta_1) \\ \mathbf{P}^{\mathrm{T}}(\xi_2, \eta_2) \\ \vdots \end{bmatrix}^{-1} \boldsymbol{\sigma}_{ij},$$

where $\mathbf{P}(\xi, \eta) = [1\ \xi\eta\ \xi^2\eta^2\ \xi\eta\ \ldots]^{\mathrm{T}}$ is the polynomial basis, $\boldsymbol{\sigma}_{ij}$ is the vector of stress values at integration points of an element.

Mapping from an old mesh to a new one violates the consistency of the fields. It means that stresses do not satisfy the plastic yield condition, boundary tractions do not satisfy the friction condition, and the equations of motion are not fulfilled. Numerical experiences show that the largest inconsistency appears in the relatively thin layer located along the part of the boundary of the body where the contact boundary conditions exist. To avoid large inconsistency of the state fields, a certain procedure of recovery of consistency is required.

5. Overall algorithm

The numerical procedure, used to solve the considered dynamic problem is outlined below.

1. Read the following initial values obtained from the static solution: coordinates of nodes, values of stresses, and the determinant of deformation gradient at integration points from a disk file.

2. Calculate nodal values of gravity forces **R**, and reactions of silo walls.

3. Calculate accelerations from Eq. (3.2) (written for $t = 0$) if $t = 0$, or read them from a disk file, otherwise.

4. Loop over all time steps.

5. Initiate displacements

$$\mathbf{U}^{(0)}_{t+\Theta\Delta t} = \mathbf{0}.$$

6. Calculate the auxiliary matrix **A** dependent on the quantities corresponding to the previous time step t

$$\mathbf{A}_t = -\left(\frac{1}{\alpha\,\Theta\,\Delta t}\,\dot{\mathbf{U}}_t + \left(\frac{1}{2\alpha} - 1\right)\ddot{\mathbf{U}}_t\right).$$

7. Loop over iterations (set k := 1)

8. Assemble the stiffness, and mass matrices: $\mathbf{K}_t$ and **M**.

9. Calculate the nodal internal forces $\mathbf{F}^{(k-1)}_{t+\Theta\Delta t}$.

10. Add the contribution of contact forces to the global matrices $\mathbf{K}_t$, and $\mathbf{F}^{(k-1)}_{t+\Theta\Delta t}$.

11. Calculate the inertial forces

$$\mathbf{D}^{(k-1)} = \mathbf{M}\left(\mathbf{A}_t + \frac{1}{\alpha\,(\Theta\,\Delta t)^2}\,\mathbf{U}^{(k-1)}_{t+\Theta\Delta t}\right).$$

12. Calculate the improvement of displacements solving the system of linear algebraic equations

$$\mathbf{K}_t\,\Delta\mathbf{U}^{(k)} = \overline{\mathbf{F}}^{(k-1)} \equiv \mathbf{R}_{t+\Theta\Delta t} - \mathbf{F}^{(k-1)}_{t+\Theta\Delta t} - \mathbf{D}^{(k-1)}.$$

13. Update displacements

$$\mathbf{U}^{(k)}_{t+\Theta\Delta t} = \mathbf{U}^{(k-1)}_{t+\Theta\Delta t} + \Delta\mathbf{U}^{(k-1)}.$$

14. Check if some nodes have left the silo walls or have moved from one segment of the wall to the other. If so, modify the boundary conditions for these nodes.

15. Check the accuracy of the solution. If

$$\frac{\|\Delta\mathbf{U}^{(k)}\|}{\|\mathbf{U}^{(k)}_{t+\Theta\Delta t}\|} \leq \varepsilon$$

go to 17.

16. End of loop over iterations (set k := k + 1, and go to 8).

17. Check if mesh-rezoning is necessary using the criterion (4.1). If so, generate the new mesh, evaluate the new data for nodes and integration points, and restart the calculation process from the beginning. If the criterion (4.1) is satisfied, go to 18. The criterion (4.1) is checked only at integration points located currently inside the silo. If the criterion has not been checked for any point, it means that all the integration points are found below the silo outlet, and the calculations may be stopped.

18. Evaluate accelerations, velocities, and displacements for the instant $t + \Delta t$ using the equations

$$\begin{aligned}
\ddot{\mathbf{U}}_{t+\Delta t} &= \ddot{\mathbf{U}}_t + \frac{1}{\Theta}(\ddot{\mathbf{U}}_{t+\Theta\Delta t} - \ddot{\mathbf{U}}_t),\\
\ddot{\mathbf{U}}_{t+\Theta\Delta t} &= \frac{1}{\alpha(\Theta\,\Delta t)^2}\mathbf{U}_{t+\Theta\Delta t} + \mathbf{A}_t,\\
\dot{\mathbf{U}}_{t+\Delta t} &= \dot{\mathbf{U}}_t + \Delta t\left((1-\delta)\,\ddot{\mathbf{U}}_t + \delta\,\ddot{\mathbf{U}}_{t+\Delta t}\right),\\
\mathbf{U}_{t+\Delta t} &= \mathbf{U}_t + \Delta t\,\dot{\mathbf{U}}_t + (\Delta t)^2\left(\left(\frac{1}{2}-\alpha\right)\ddot{\mathbf{U}}_t + \alpha\,\ddot{\mathbf{U}}_{t+\Delta t}\right).
\end{aligned}$$

19. Update stresses, and values of the determinant of deformation gradient at integration points.

20. Update reactions for contact nodes.

21. Update coordinates of nodes

$$\mathbf{X}_{t+\Delta t} = \mathbf{X}_t + \mathbf{U}_t\,.$$

22. End of loop over time steps.

23. Save the solution on a disk file if required.

24. Stop the calculation process.

6. Numerical results

6.1. Plane strain problem – smooth walls

Let us consider a silo of the shape presented in Fig. 1. The dimensions are measured in metres. The plane strain problem is considered in the example. Calculations have been made for three variants of material data specified in Tab. 1. The problem has been solved assuming frictionless bilateral constraints on the silo walls.

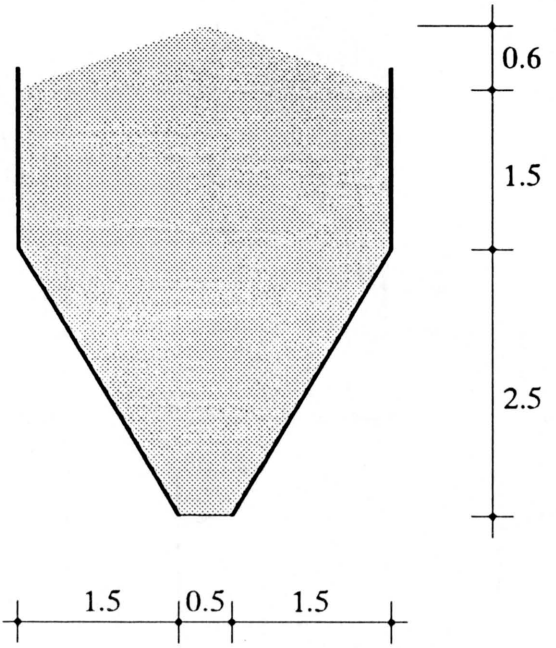

FIG. 1. Example of a silo – plane strain problem.

Table 1. Exemplary material data – plane strain problem.

material constant	unit	variant		
		I	II	III
ϱ	kg/m^3	1500	1500	1500
E	Pa	$1 \cdot 10^6$	$1 \cdot 10^6$	$2 \cdot 10^6$
ν		0.3	0.3	0.3
φ	°	25	35	25

The maximum size of an element has been set as 0.2 m, for which the mesh consisting of 923 nodes and 432 6-node triangular elements has been generated initially. Because of the symmetry of the problem, half of the region is discretised.

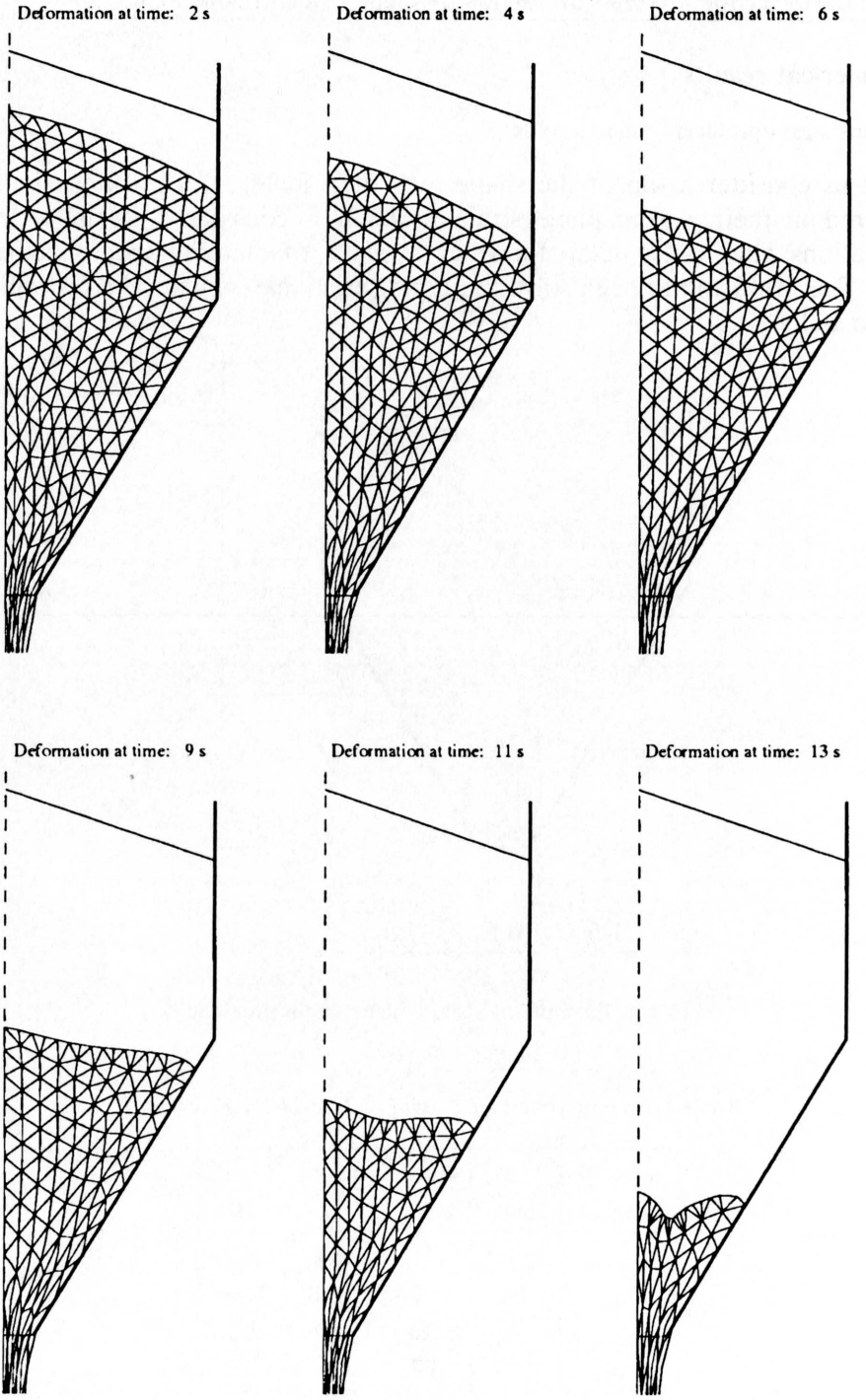

FIG. 2. Deformation process – plane strain problem.

The problem has been solved with the accuracy of 0.005 in the static case, and 0.01 in the dynamic one, using the modified Newton-Raphson algorithm, where the matrix of finite element equations is recalculated for the first and second iterations. The dynamic problem has been solved using the Newmark method with the parameters $\delta = 0.5$, $\alpha = 0.25$, and time increments 0.005 s at the beginning of the process and 0.02 s later on. In the dynamic analysis, $E_{12}^{\max} = 1$ has been used as the limit for admissible element distortion.

The number of mesh-rezonings needed for each variant of data is shown in Tab. 2. The times of discharging processes and times of computer calculations performed on the work-station Sun IPX (40 MHz) with Sparc Power up (Weitek 80 MHz) are also shown in the table.

Table 2. Main results of calculations – plane strain problem.

variant	I	II	III
number of mesh rezonings	4	6	5
time of discharging [s]	11.35	14.36	13.05
time of calculation [h:mm:ss]	1:52:00	2:18:02	2:06:03

Some states of deformation for the variant II of material data are shown in Fig. 2.

6.2. Axisymmetric problem – walls with friction

The axisymmetric problem of discharging the silo, presented in Fig. 3, is considered in the second example. The only conical part of the silo is filled with a bulk material. Calculations have been made for three variants of material data specified in Tab. 3, where φ denotes the internal friction angle, and φ_w is the angle of friction between a bulk material and a silo wall.

Table 3. Exemplary material data – axisymmetric problem.

material constant	unit	variant		
		I	II	III
ϱ	kg/m^3	1500	1500	1500
E	Pa	$1 \cdot 10^6$	$1 \cdot 10^6$	$1 \cdot 10^6$
ν		0.3	0.3	0.3
φ	°	25	25	25
φ_w	°	20	10	0

The maximum size of an element has been set at 0.1 m, but the size of elements located near the silo wall has been reduced to 0.05 m. Under these conditions,

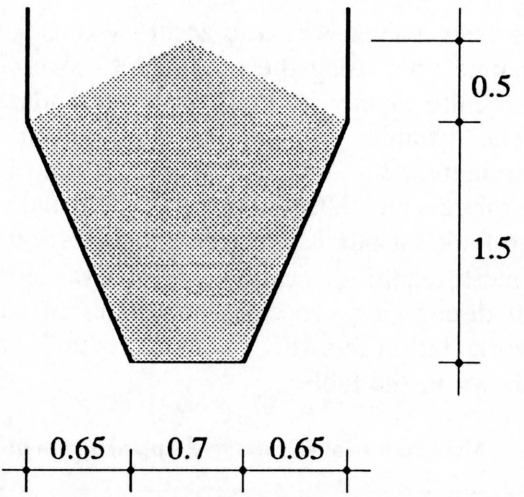

FIG. 3. Example of a silo – axisymmetric problem.

the mesh consisting of 1478 nodes and 701 6-node triangular elements has been generated.

The problem has been solved to within the accuracy of 0.005 in the static case, and 0.01 in the dynamic one, using the Newton-Raphson algorithm with an unsymmetric matrix of finite element equations. The dynamic problem has been solved using the Newmark method with the parameters $\delta = 0.5$, $\alpha = 0.25$, and time increments 0.0025 s at the beginning of the process and 0.01 s later on. The whole process of discharging the silo has been analysed with the same element mesh.

The duration of discharging processes and times of computer calculations performed on the computer mentioned above are shown in Table 4.

Table 4. Main results of calculations – axisymmetric problem.

variant	I	II	III
time of discharging [s]	6.53	4.54	3.75
time of calculation [h:mm:ss]	4:12:40	3:06:11	2:45:02

The discharging process is illustrated in Fig. 4, for the value of friction angle $\varphi_w = 20°$. The distribution of the wall tractions is shown in Fig. 5 for the same value of friction angle. The diagrams of normal and tangential stresses are drawn in thick and thin lines, respectively.

Large values of the boundary tractions, near the silo outlet, can be observed in the last figure, for some instants, when the discharging process is developed. It seems that they are determined inaccurately. This is caused by the significant distortion of elements, which is the largest in the neighbourhood of the outlet.

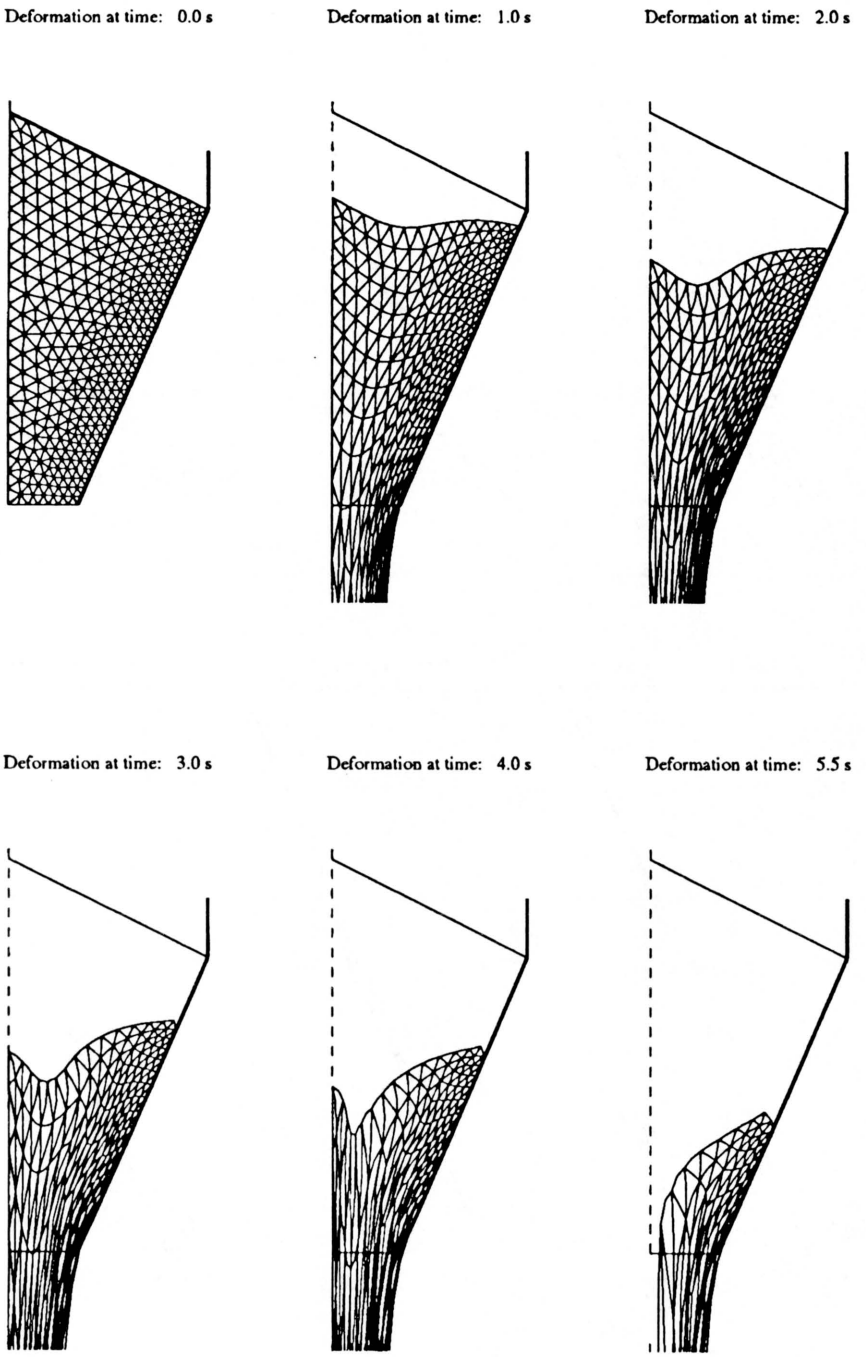

FIG. 4. Deformation process – axisymmetric problem.

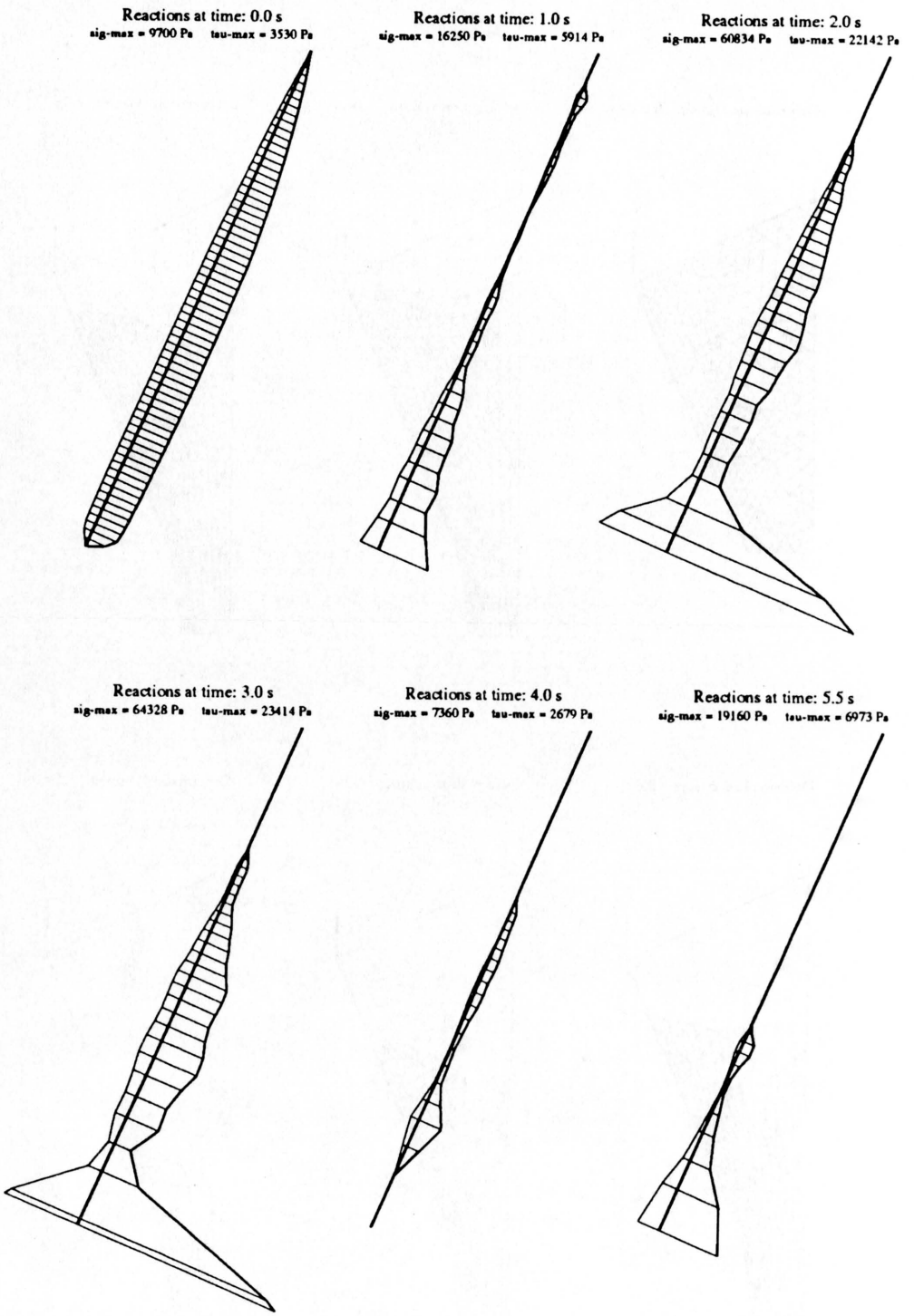

FIG. 5. Wall tractions – axisymmetric problem.

Acknowledgement

The work was supported by Nordisk Industrifond and TFR and done during the visit of the first author at Division of Structural Mechanics, Luleå University of Technology in the period of September 1992–August 1994.

References

1. J. K. WALTERS, *A theoretical analysis of stresses in axially-symmetric hoppers and bunkers*, Chemical Engng. Science, **28**, p. 779, 1997.
2. G.G. ENSTAD, *A novel theory of the arching and doming in mass flow hoppers*, Ph. D. Dissertation, University of Trondheim, 1981.
3. A.W. JENIKE and R.T. SHIELD, *On the plastic flow of Coulomb solids beyond original failure*, J. Applied Mech., **26**, 599–602, 1959.
4. J. EIBL and G. ROMBACH, *Numerical investigation on discharging silos*, Proc. 6th Int. Conf. on Numerical Methods in Geomechanics, A. SWOBODA [Ed.], Balkema, 317–320, 1988.
5. U. HÄUSSLER and J. EIBL, *Numerical investigation on discharging silos*, J. Engng. Mech., ASCE, **110**, 957–971, 1984.
6. K. RUNESSON and L. NILSSON, *Finite element modelling of the gravitational flow of a granular material*, Int. J. Bulk Solids Handling, **6**, 877–884, 1986.
7. M. KLISIŃSKI, K. RUNESSON, Z. WIĘCKOWSKI and E. HERMANSSON, *Modelling of flow of bulk materials in silos*, Proc. of Conf. "Reliable Flow of Particulate Solids II", Oslo, August 1993.
8. G. DUVAUT and J.L. LIONS, *Les inéquations en mécanique et en physique*, Dunod, Paris 1972.
9. N. KIKUCHI and J.T. ODEN, *Contact problems in elasticity: A study of variational inequalities and finite element methods*, SIAM, Philadelphia 1988.
10. T.A. LAURSEN and J.C. SIMO, *A continuum-based finite element formulation for the implicit solution of multibody, large deformation frictional contact problems*, Int. J. Numer. Meth. Engng., **36**, 3451–3485, 1993.
11. R. MICHAŁOWSKI and Z. MRÓZ, *Associated and nonassociated sliding rules in contact friction problems*, Arch. Mech., **30**, 259–276, 1970.
12. P. WRIGGERS, T. VU VAN and E. STEIN, *Finite element formulation of large deformation impact-contact problem with friction*, Comp. Struct., **37**, 319–331, 1990.
13. V.P. LADE, *Elastic-plastic stress-strain theory for cohesionless soil with curved yield surface*, Int. J. Solids Structures, **13**, 1019–1033, 1989.
14. D. KOLYMBAS, *Generalized hypoelastic constitutive equation*, [in:] Constitutive Equations for Granular Non-Cohesive Solids, A. SAADA and B. BIANCHINI [Eds.], Balkema, 349–359, 1988.
15. L.E. MALVERN, *Introduction to the mechanics of a continuous medium*, Prentice-Hall, Englewood Cliffs, 1969.
16. K.-J. BATHE, E. RAM and E.L. WILSON, *Finite element formulations for large deformation dynamic analysis*, Int. J. Num. Meth. Engng., **9**, 353–386, 1975.

ŁÓDŹ UNIVERSITY OF TECHNOLOGY, ŁÓDŹ
and
LULEÅ UNIVERSITY OF TECHNOLOGY, LULEÅ, SWEDEN.

Received October 3, 1994.

Arch. Mech., 47, 3, pp. 635–643, Warszawa 1995

On the description of consolidation processes in saturated reinforced subsoils (*)

M. WOŹNIAK (ŁÓDŹ)

IN THIS PAPER, a certain averaged model of periodically reinforced saturated porous media is proposed. The characteristic feature of this model is that it describes the effect of the microstructure length on the macro-behaviour of the medium. It is shown that in nonstationary processes this effect plays an important role and cannot be neglected.

1. Introduction

THIS PAPER DEALS with consolidation processes in periodically reinforced fully saturated subsoils, in which the maximum length of the unit cell is much smaller than the minimum characteristic length of the region occupied by the medium under consideration. As it is known, a periodic material structure of this kind is usually modelled by a certain homogeneous equivalent medium, the properties of which are called the effective moduli. These moduli describe in an averaged manner the periodic inhomogeneous material structure of the body, [1–4].

In this paper it will be shown that in nonstationary processes the aforementioned effective moduli models can lead to incorrect results, since they neglect the influence of the size of the unit cell on the dynamic behaviour of the medium. To this end we propose a refined averaged model of a periodically reinforced subsoil which describes the microstructure length scale effect on the consolidation process. The proposed approach takes into account a procedure used in micro-elastodynamics of composites leading to what is called the refined macro-dynamics of periodic structures, [5, 6]. The obtained results are similar to those derived from the averaged formulation of nonstationary problems for stratified porous media, [7]. For the sake of simplicity, the basis of our investigations is the simplified linear consolidation theory for fully saturated linear-elastic porous media, [8–10]. A more general approach is reserved for a separate study.

Notations

The subscripts i, j, k, l run over 1, 2, 3 and are related to the orthogonal Cartesian coordinate system $0x_1x_2x_3$ in the physical space. The non-tensorial superscripts a, b, ...and A, B, ...run over 1, ..., n and 1, ..., N, respectively. Summation convention holds for all kinds of the aforementioned indices. The

(*) Paper presented at 30th Polish Solid Mechanics Conference, Zakopane, September 5–9, 1994.

region occupied by the periodically reinforced saturated porous medium in its initial configuration is denoted by Ω. The unit cell of the periodic structure under consideration is given by $Y \equiv (0, l_1) \times (0, l_2) \times (0, l_3)$. The value $l \equiv [(l_1)^2 + (l_2)^2 + (l_3)^2]^{1/2}$ is referred to as the microstructure length parameter, and is assumed to be sufficiently small as compared to the minimum characteristic length of Ω. The points in the physical space are denoted by $\mathbf{x} \equiv (x_1, x_2, x_3)$ and t is the time coordinate $t \in [0, t_f)$. For an arbitrary Y-periodic integrable function f we introduce the averaging operator $\langle f \rangle$

$$\langle f \rangle \equiv \frac{1}{l_1 l_2 l_3} \int_Y f(\mathbf{x})\, dv, \qquad dv \equiv dx_1 dx_2 dx_3.$$

The remaining notations related to the direct description of the periodic inhomogeneous medium under consideration are:

u_i displacements from the initial configuration,
s_{ij} stresses,
s_i boundary tractions,
b_i body forces,
ϱ mass density,
C_{ijkl} elastic moduli,
p excess of a pore fluid pressure,
q_i pore fluid discharge,
q fluid outflow across the boundary,
β fluid compressibility modulus,
η porosity,
k_{ij} permeability moduli,
e pore fluid dilatational strain,
n_i unit normal outward to the boundary $\partial\Omega$ of the region Ω.

The components of the heterogeneous medium under consideration (saturated soil and reinforcement) are assumed to be homogeneous and isotropic; hence

$$C_{ijkl} = \left[K(\mathbf{x}) - \frac{2}{3}G(\mathbf{x})\right]\delta_{ij}\delta_{kl} + G(\mathbf{x})(\delta_{ik}\delta_{jl} + \delta_{il}\delta_{jk}), \qquad \varrho = \varrho(\mathbf{x}), \qquad k_{ij} = \delta_{ij}k,$$

where the compression modulus $K(\mathbf{x})$, shear modulus $G(\mathbf{x})$, mass density $\varrho(\mathbf{x})$ are Y-periodic functions assuming positive constant values in the saturated soil and in the reinforcement, and k is a constant soil permeability coefficient. Moreover, by $\zeta = \zeta(\mathbf{x})$, $\mathbf{x} \in \Omega$, we denote a Y-periodic function defined by: $\zeta(\mathbf{x}) = 1$ if the point $\mathbf{x}$ is occupied by the saturated soil (in the initial state of the medium), and $\zeta(\mathbf{x}) = 0$ otherwise.

2. Physical foundations

In order to describe the behaviour of the reinforced subsoil we apply the simplified consolidation theory, [8–10]. We introduce, for the time being, the

inertial terms due to the motion of the reinforcement and the soil, neglecting the inertial effects related to the outflow of the pore liquid which is supposed to be very slow. We also assume perfect bonding between the reinforcement and the soil. Under the aforementioned restrictions, the balance laws proposed in [9, 10] can be written in the form of conditions

$$\begin{aligned} \int_{\Omega} s_{ij}\delta u_{i,j}\,dv &= \oint_{\partial\Omega} s_i\delta u_i\,da + \int_{\Omega} \varrho(b_i - \ddot{u}_i)\delta u_i\,dv, \\ \int_{\Omega} q_i\delta p_{,i}\,dv &= \oint_{\partial\Omega} q\delta p\,da + \int_{\Omega} (\zeta\,\dot{u}_{i,i} - \eta\,\dot{e})\delta p\,dv, \end{aligned} \tag{2.1}$$

together with the known constitutive relations, [9, 10]:

$$\begin{aligned} s_{ij} &= C_{ijkl}u_{(k,l)} + \delta_{ij}\zeta p\,, \\ q_i &= \zeta k_{ij}p_{,j}\,, \\ e &= \zeta\beta p. \end{aligned} \tag{2.2}$$

If there are no constraint conditions imposed on displacements $u_i = u_i(\mathbf{x}, t)$ and the pore pressure excess $p = p(\mathbf{x}, t)$, then Eqs. (2.1), (2.2) lead to a system of partial differential equations for u_i and p with highly oscillating (piecewise constant) coefficients. As it is known, this system is inconvenient in applications to the analysis of special problems. This is why Eqs. (2.1), (2.2) will be used here only as a starting point for the modelling procedure, leading to certain averaged models of the medium under consideration.

3. Modelling approach

The modelling approach will be based on the concepts of a regular macro-field and that of micro-shape functions, [5, 6]. The system of Y-periodic, sufficiently regular linear independent real-valued functions h^a, $a = 1, \ldots, n$ can be taken as the micro-shape function system if: $\langle h^a \rangle = 0$, $h^a(\mathbf{x}) \in \mathcal{O}(l)$, $h^a{}_{,i}(\mathbf{x}) \in \mathcal{O}(1)$, $a = 1, \ldots, n$. We also assume that $\langle \varrho h^a \rangle = 0$, $\langle \zeta H^A \rangle = 0$. In the sequel we shall introduce two systems: h^a, $a = 1, \ldots, n$ and H^A, $A = 1, \ldots, N$. At the same time it is assumed that for every point x_0 such that $Y(\mathbf{x}_0) \equiv \mathbf{x}_0 + Y \subset \Omega$, linear combinations $c^a{}_i h^a(\mathbf{x})$ and $C^A H^A(\mathbf{x})$, $\mathbf{x} \in Y(\mathbf{x}_0)$, (where $c^a{}_i$, C^A are arbitrary constants) describe the disturbances in displacements and in pressure, respectively, caused by the inhomogeneity of the medium. Moreover, a sufficiently regular field defined on Ω will be called macro-field if the increments of this field and all its derivatives within an arbitrary but fixed cell $Y(\mathbf{x}_0)$, $Y(\mathbf{x}_0) \subset \Omega$ can be neglected from the computational viewpoint. Let λ_F be the known calculation accuracy of values of a certain function F. Hence, the continuous field $F(\mathbf{x})$, $\mathbf{x} \in \Omega$, will be

called the macro-field (related to the known unit cell V and the accuracy parameter λ_F) if $|\mathbf{x}' - \mathbf{x}''| < l$ implies $|F(\mathbf{x}') - F(\mathbf{x}'')| < \lambda_F$ for every $\mathbf{x}', \mathbf{x}'' \in \Omega$. If similar conditions hold also for all derivatives of F, then F is called the regular macro-field. For the details the reader is referred to [5, 6]. Generalizing the approach proposed in [7] we introduce three modelling hypotheses:

MACRO-CONSTRAINT HYPOTHESIS

In the periodically reinforced saturated medium under consideration, the distribution of displacements $u_i(\mathbf{x}, t)$ and of the pore pressure $p(\mathbf{x}, t)$ can be expected to be of the form

$$
\begin{aligned}
u_i(\mathbf{x}, t) &= U_i(\mathbf{x}, t) + h^a(\mathbf{x}) V_i{}^a(\mathbf{x}, t), \\
p(\mathbf{x}, t) &= \zeta(\mathbf{x})[P(\mathbf{x}, t) + H^A(\mathbf{x}) R^A(\mathbf{x}, t)], \qquad \mathbf{x} \in \Omega, \quad t \in [0, t_f),
\end{aligned} \tag{3.1}
$$

where $U_i(\cdot, t)$, $V_i{}^a(\cdot, t)$, $P(\cdot, t)$, $R^A(\cdot, t)$, for every $t \in [0, t_f)$ are arbitrary regular macro-fields constituting the new basic unknowns, and h^a, H^A are systems of the micro-shape functions which have to be assumed *a priori* in every problem under consideration.

Fields U_i and P are called macro-displacement and macro-pore pressure excess fields, respectively. According to the sense of the micro-shape functions and bearing in mind that the macro-fields are approximately constant in every cell $V(\mathbf{x}_0)$, $V(\mathbf{x}_0) \subset \Omega$, it can be seen that the terms $h^a V^a{}_i$ and $H^A R^A$ describe possible oscillations of the displacements and of the pore pressure, respectively, caused by periodic inhomogeneity of the medium. Hence, the unknown fields $V^a{}_i$, R^A will be called *inhomogeneity internal variables or correctors*, cf. [5–7].

MACRO-BALANCE HYPOTHESIS

The balance equations (2.1) are assumed to hold for every

$$
\begin{aligned}
\delta u_i(\mathbf{x}) &= \delta U_i(\mathbf{x}) + h^a(\mathbf{x}) \delta V^a{}_i(\mathbf{x}), \\
\delta p(\mathbf{x}) &= \delta P(\mathbf{x}) + H^A(\mathbf{x}) \delta R^A(\mathbf{x}), \qquad \mathbf{x} \in \Omega,
\end{aligned} \tag{3.2}
$$

where δU_i, $\delta V^a{}_i$, δP, δR^A are arbitrary linearly independent regular macro-fields.

The meaning of the aforementioned hypothesis is implied by the form of the constraint conditions (3.1).

MACRO-APPROXIMATION ASSUMPTION

In the balance equations obtained by combining Eqs. (2.1), (2.2), (3.1) and (3.2), terms $\mathcal{O}(\lambda_F)$ are neglected as compared to terms $F(\mathbf{x})$ for an arbitrary macro-field F.

This assumption is strictly related to the meaning of a regular macro-field. The micro-structure parameter l is not treated here as a small parameter and all terms $\mathcal{O}(l)$ will be retained.

Substituting the right-hand sides of Eqs. (3.1) into (2.2) and then substituting the obtained form of constitutive equations into the balance conditions (2.1), taking into account Eqs. (3.2), and using the Macro-Approximation Assumption, after rather lengthy manipulations we arrive at the variational condition involving exclusively certain averaged constants and macro-fields. Since δU_i, δP, $\delta V^a{}_i$, δR^A are linearly independent fields, we arrive finally at the system of partial differential equations for macro-displacements U_i, macro-pore pressure excess P and inhomogeneity internal variables (correctors) $V^a{}_i$, R^A. The obtained results represent what will be called the micro-structural model of the reinforced saturated subsoil under consideration. The governing equations of this model will be presented in the subsequent section.

4. Micro-structural model

The micro-structural model of the medium under consideration is governed by the Macro-Balance Equations which hold in Ω for every $t \in [0, t_f)$

$$
\begin{aligned}
S_{ij,j} - \langle \varrho \rangle \ddot{U}_i + \langle \varrho \rangle b_i &= 0, \\
\langle \varrho h^a h^b \rangle \ddot{V}^b{}_i + S^a{}_i &= 0, \\
\eta\beta \langle \zeta \rangle \dot{P} - Q_{i,i} - \langle \zeta \rangle \dot{U}_{i,i} &= 0, \\
\eta\beta \langle \zeta H^A H^B \rangle \dot{R}^B + Q^A &= 0,
\end{aligned}
\tag{4.1}
$$

where S_{ij}, $S^a{}_i$, Q_i and Q^A are determined by the following Macro-Constitutive Equations:

$$
\begin{aligned}
S_{ij} &= \langle C_{ijkl} \rangle U_{k,l} + \langle C_{ijkl} h^a{}_{,l} \rangle V^a{}_k + \delta_{ij} \langle \zeta \rangle P, \\
S^a{}_i &= \langle C_{ijkl} h^a{}_{,j} \rangle U_{k,l} + \langle C_{ijkl} h^a{}_{,j} h^b{}_{,l} \rangle V^b{}_k, \\
Q_i &= k_{ij} \langle \zeta \rangle P_{,j} + k_{ij} \langle \zeta H^A{}_{,j} \rangle R^A, \\
Q^A &= k_{ij} \langle \zeta H^A{}_{,j} \rangle P_{,i} + k_{ij} \langle \zeta H^A{}_{,i} H^B{}_{,j} \rangle R^B.
\end{aligned}
\tag{4.2}
$$

At the same time, on the boundary $\partial\Omega$ for every $t \in [0, t_f)$, under extra assumptions $\delta u_i = \delta U_i$, $\delta p = \delta P$, the following natural macro-boundary conditions hold:

$$
S_{ij} n_j = s_i, \qquad Q_i n_i = q. \tag{4.3}
$$

Combining Eqs. (4.1), (4.2) we obtain the system of $4 + 3n + N$ equations for the basic unknowns U_i, P, $V^a{}_i$, R^A. This is a system of differential equations

with constant coefficients representing the computational model of the periodically reinforced saturated elastic subsoil. It has to be emphasized that equations for the extra unknowns $V^a{}_i$, R^A are ordinary differential equations involving exclusively time-derivatives of these unknowns and hence, they are independent of the boundary conditions. Moreover, for homogeneous medium $\langle C_{ijkl}h^a{}_{,j}\rangle = C_{ijkl}\langle h^a{}_{,j}\rangle = 0$, $\langle \zeta H^A{}_{,j}\rangle = \zeta\langle H^A{}_{,j}\rangle = 0$, and under homogeneous initial conditions for $V^a{}_i$, R^A we obtain that $V^a{}_i = 0$, $R^A = 0$ for every $\mathbf{x} \in \Omega$, $t \in [0, t_f)$. That is why the extra unknown fields $V^a{}_i$, R^A were called the inhomogeneity internal variables. The characteristic feature of the obtained micro-structural model of reinforced saturated subsoils is that it takes into account the effect of the size of the unit cell on the global behaviour of the medium. This effect is described by terms: $\langle \varrho h^a h^b\rangle \ddot{V}^b{}_i$, $\langle \zeta H^A H^B\rangle \dot{R}^B$ in Eqs. (4.1) which are of the order of l^2, l being the microstructure length parameter defined in Sec. 1. In stationary processes the aforementioned terms are equal to zero and hence, the steady-state behaviour of the medium is independent of the scale of the microstructure in the framework of the proposed model. Similar conclusions were also formulated in [7] where the micro-structural model of saturated multilayered media was investigated.

It has to be emphasized that for the micro-structural model, all terms involving the micro-structure lenght parameter l are retained. On the other hand, for the effective modulus model given below, all terms of the order l will be neglected.

5. Effective modulus model

Scaling the microstructure down, by neglecting terms involving $\langle \varrho h^a h^b\rangle$ and $\langle \zeta H^A H^B\rangle$ in Eqs. (4.1) we obtain that $S^a{}_i = 0$ and $Q^A = 0$. Using Eqs. (4.2) we arrive at the two independent systems of linear algebraic equations for $V^a{}_i$ and R^A:

$$\langle C_{ijkl}h^a{}_{,j}h^b{}_{,l}\rangle V^b{}_k = -\langle C_{ijkl}h^a{}_{,j}\rangle U_{k,l}\,,$$
$$k_{ij}\langle \zeta H^A{}_{,i}H^B{}_{,j}\rangle R^B = -k_{ij}\langle \zeta H^A{}_{,j}\rangle P_{,i}\,.$$

It can be shown that the linear transformations $\mathbf{R}^{3n} \to \mathbf{R}^{3n}$ and $R^N \to R^N$ given by $\langle C_{ijkl}h^a{}_{,j}h^b{}_{,l}\rangle$ and $k_{ij}\langle \zeta H^A{}_{,i}H^B{}_{,j}\rangle$, respectively, are invertible. Hence, denoting by $D^{ab}{}_{ij}$, E^{AB} the appropriate inverse transformations we obtain

$$V^a{}_i = -D^{ab}{}_{ij}\langle C_{jklm}h^b{}_{,k}\rangle U_{l,m}\,,$$
$$R^A = -E^{AB}k_{ij}\langle \zeta H^B{}_{,j}\rangle P_{,i}\,.$$

Thus, after introducing the notations

$$C^{\text{eff}}{}_{ijkl} \equiv \langle C_{ijkl}\rangle - \langle C_{ijmn}h^a{}_{,n}\rangle D^{ab}{}_{mp}\langle C_{prkl}h^b{}_{,l}\rangle,$$
$$k^{\text{eff}}{}_{ij} \equiv k_{ij}\langle \zeta\rangle - k_{ik}\langle \zeta H^A{}_{,k}\rangle E^{AB}k_{jl}\langle \zeta H^B{}_{,l}\rangle \tag{5.1}$$

we obtain the system of equations

$$
\begin{aligned}
S_{ij} &= C^{\text{eff}}{}_{ijkl} U_{k,l} + \delta_{ij} \langle \zeta \rangle P, \\
Q_i &= k^{\text{eff}}{}_{ij} P_{,j} .
\end{aligned}
\tag{5.2}
$$

Eqs (5.2) together with the macro-balance equations $(4.1)_{1,3}$:

$$
\begin{aligned}
S_{ij,j} - \langle \varrho \rangle \ddot{U}_i + \langle \varrho \rangle b_i &= 0, \\
\eta \beta \langle \zeta \rangle \dot{P} - Q_{i,i} - \langle \zeta \rangle \dot{U}_{i,i} &= 0,
\end{aligned}
\tag{5.3}
$$

and the natural macro-boundary conditions (4.3), represent the asymptotic approximation $l \to 0$ of the micro-structural model of the medium under consideration. Material constants $C^{\text{eff}}{}_{ijkl}$, $k^{\text{eff}}{}_{ij}$ in Eqs. (5.2) are called the effective moduli and hence, Eqs. (5.2), (5.3) describe what will be called the effective modulus model of the reinforced saturated medium under investigation. It has to be emphasized that in the general asymptotic homogenization approach, the effective moduli in Eqs. (5.2) can be calculated by special procedures; in this sense formulae (5.1) represent only certain approximations of the effective moduli, depending on a choice of micro-shape functions. Obviously, this model neglects the effect of the microstructure length parameter l on the macro-behaviour of the medium.

6. Evaluation of the scale length effects

In this section it will be shown that in non-stationary problems the effective modulus model, governed by Eqs. (5.2), (5.3), (4.3), can lead to incorrect results and hence, we have to take the micro-structural model as a basis of our investigations. To this end we consider a reinforced soil layer bounded by planes $x_1 = \pm L$. For the sake of simplicity it is assumed that the reinforcement of the layer can be treated as periodic in x_1-axis direction and constant in directions of x_2- and x_3-coordinate axes. In this case we shall introduce only one micro-shape function $h = h(x_1)$, setting $h^1 = h$, $H^1 = h$ and $n = N = 1$. This function can be assumed in the form $h = l \sin(2\pi x_1/l)$, where micro-structure length parameter l satisfies the condition $l \ll L$. In this case there exist four inhomogeneity internal variables which will be denoted by: $V_i \equiv V^1{}_i$, $R \equiv R^1$. We shall also neglect body forces b_i in equations of motion. Let the layer under consideration have the impervious boundaries subjected to the normal constant compressive forces. Hence, the natural macro-boundary conditions have the form $S_{11} = s$, $S_{12} = S_{13} = 0$, $Q_1 = 0$ and holds for $x_1 = \pm L$, $(x_2, x_3) \in \mathbf{R}^2$ and $t \in [0, t_f)$, where $s = \text{const}$. The initial conditions (for $t = 0$) will be assumed in the form: $U_1 = cx_1$, $U_2 = U_3 = 0$, $\dot{U}_i = 0$, $P = P_0$ and $V_i = \dot{V}_i = 0$, $R = 0$, where c and P_0 are constants (initial conditions for V_i and R can be imposed only in the framework of the microstructural model).

The aforementioned boundary and initial conditions, together with Eqs. (4.1), (4.2), represent the boundary-value problem for functions U_i, P, V_i, R, considered in the framework of the micro-structural model. Let us define

$$\kappa^2 = \frac{\langle C_{1111}(h_{,1})^2\rangle(\langle\zeta\rangle + \eta\beta\langle C_{1111}\rangle) - \eta\beta\langle C_{1111}h_{,1}\rangle^2}{\langle\varrho(h)^2\rangle(\langle\zeta\rangle + \eta\beta\langle C_{1111}\rangle)},$$

(6.1)

$$K = \frac{\langle C_{1111}h_{,1}\rangle}{\langle C_{1111}\rangle}(\langle\zeta\rangle P_0 - s),$$

where it can be shown that $\kappa^2 > 0$. The approximate solution to this problem, satisfying the first of Eqs. (4.1) (for $i = 1$ and $b_i = 0$) in the averaged form

$$\int_{-L}^{L} \left(S_{1j,j} - \langle\varrho\rangle \ddot{U}_1\right) dx_1 = 0,$$

is given by

$$U_1(\mathbf{x}, t) = -\frac{\langle\zeta\rangle P_0 - s}{\langle C_{1111}\rangle} x_1 - \frac{\eta\beta\langle C_{1111}h_{,1}\rangle}{\langle\zeta\rangle + \eta\beta\langle C_{1111}\rangle} \frac{K}{\kappa^2}[1 - \cos(\kappa t)]x_1,$$

(6.2)

$$U_2(\mathbf{x}, t) = U_3(\mathbf{x}, t) = 0,$$

$$P(\mathbf{x}, t) = P_0 - \frac{\langle C_{1111}h_{,1}\rangle}{\langle\zeta\rangle + \eta\beta\langle C_{1111}\rangle} \frac{K}{\kappa^2}[1 - \cos(\kappa t)],$$

$$t \in [0, t_f), \quad x_1 \in [-L, L].$$

At the same time, the inhomogeneity internal variables are

$$V_1(\mathbf{x}, t) = \frac{K}{\kappa^2}[1 - \cos(\kappa t)], \qquad V_2(\mathbf{x}, t) = V_3(\mathbf{x}, t) = 0,$$

$$R(\mathbf{x}, t) = 0, \qquad t \in [0, t_f).$$

In the framework of the effective modulus model we obtain

$$U_1(\mathbf{x}, t) = -\frac{\langle\zeta\rangle P_0 - s}{C^{\text{eff}}_{1111}}, \qquad U_2(\mathbf{x}, t) = U_3(\mathbf{x}, t) = 0, \qquad P(\mathbf{x}, t) = P_0. \tag{6.3}$$

In this case the inhomogeneity internal variables do not enter the system of governing equations.

Comparing Eqs. (6.2) and (6.3) it can be easily seen that the effective modulus model is not capable of describing time-dependent oscillations in macro-displacements and macro-pore pressure caused by the inhomogeneity of the medium under consideration. This phenomenon is strictly related to the size of the microstructure (the value of the microstructure length parameter l) which

is described by the term $\langle \varrho(h)^2 \rangle \in \mathcal{O}(l^2)$ included in the definition of the constant κ^2 in Eqs. (6.1). The final conclusion is that in nonstationary problems of reinforced saturated subsoils, the effect of the size microstructure length on the behaviour of the medium cannot be neglected and hence, the effective modulus models can lead to incorrect results. The microstructural model, proposed in this contribution, can be applied to describe this effect.

References

1. A. BENSOUSSAN, J.L. LIONS and G. PAPANICOLAOU, *Asymptotic analysis of periodic structures*, North-Holland, Amsterdam 1980.
2. N.S. BAKHVALOV and G.P. PANASENKO, *Averaging of processes in periodic media* [in Russian], Nauka, Moskva 1984.
3. R. JONES, *Mechanics of composite materials*, McGraw-Hill, New York, St.Louis, London 1975.
4. S. NEMAT-NASSER and M. HORI, *Micromechanics: overall properties of heterogeneous materials*, North-Holland, Amsterdam 1993.
5. CZ. WOŹNIAK, *Refined micro-dynamics of periodic structures*, Arch. Mech., **45**, 3, 295–304, 1993.
6. CZ. WOŹNIAK, M. WOŹNIAK and S. KONIECZNY, *A note on dynamic modelling of periodic composites*, Arch. Mech., **45**, 6, 779–783, 1993.
7. M. WOŹNIAK, *Averaged formulation of non-stationary problems for stratified porous media*, [in press in J. Theor. Appl. Mech., 2, 1995].
8. M.A. BIOT, *General theory of three-dimensional consolidation*, J. Appl. Phys., **12**, 155–164, 1941.
9. DE JOSSELIN DE JONG, *Three-dimensional consolidation* [in Dutch], L.G.M.- Mededelingen, 7, 57–73, 1963.
10. A. VERRUIJT, *Generation and dissipation of pore water pressure*, Finite Elements in Geomechanics, John Wiley and Sons, 293–317, New York 1977.

ŁÓDŹ UNIVERSITY OF TECHNOLOGY
DEPARTMENT OF GEOTECHNICAL AND STRUCTURE ENGINEERING, ŁÓDŹ.

Received November 3, 1994.